7-6-2022 2:00 PM

Extrinsic And Intrinsic Factors Influencing Homeostasis And Repair In Oral Tissues

Georgia Nikoloudaki, *The University of Western Ontario*

Supervisor: Hamilton, Douglas W., *The University of Western Ontario*

A thesis submitted in partial fulfillment of the requirements for the Doctor of Philosophy degree in Anatomy and Cell Biology

Abstract

The oral tissues, including gingiva and buccal mucosa, heal rapidly with minimal scar formation. Although in the oral cavity, the palatal mucosa is associated with excessive scarring in response to injury. In this thesis, first, I investigated the complex relationship between cells and their microenvironment using wound healing models in which extracellular matrix composition and mechanical stiffness affect cellular responses during acute wound repair. I also determined how intrinsic differences of cells recruited during healing contribute to wound resolution.

In Chapter 2, I first investigated cell-extrinsic factors, specifically the influence of the pro-fibrotic matricellular protein periostin on palatal healing. Using a genetic deletion strategy, it was determined that in the palate periostin modulates myofibroblast differentiation and fibronectin synthesis in a manner dependent on the stiffness of the microenvironment surrounding the cells.

In chapter 3, I focused on the role of extracellular periostin on periodontal ligament (PDL) fibroblast phenotype using in vitro assays and gene-expression analyses. These findings suggest that the influence of periostin is context dependent; matrix-bound periostin does not promote or inhibit mineralization of the PDL, but the addition of exogenous periostin to isolated PDL fibroblasts resulted in increased mineralization concomitant with changes in gene expression.

In chapter 4, to explore cell-intrinsic differences, a lineage tracing approach was used to trace populations of cells derived from embryonic Foxd1- and NG2- expressing progenitors during development, homeostasis, and excisional wound healing. I show in the palate that Foxd1-lineage progeny associate with blood vessels in development and adult tissues, after injury, they expand but remain associated with neovascular structures. In contrast, NG2-lineage progeny associate with fibroblasts in healthy adult tissues and post-injury contribute to myofibroblast populations.

In conclusion, the studies in this thesis have further defined the complex interactions that exist between resident cells and their micro-environment using the palate as a model system. The data from this thesis provides important information for the design of future therapeutics for oral wounds, and also contributes to a growing understanding of fibroblast

heterogeneity and how divergent populations contribute to different processes during wound repair.

Keywords

Extracellular Matrix (ECM), Fibroblasts, Foxd1, NG2, Lineage Tracing, Matricellular Proteins, Myofibroblasts, Palate, Periodontal ligament, Periostin, Tissue Repair, Wound Healing

Lay Abstract

In Canada, approximately 400-500 babies are born each year with cleft palate (1 in 790 live births, among the highest in the world). This condition occurs when tissues in the baby's face and mouth do not fuse properly during pregnancy, leaving an opening (cleft) in the roof of the mouth (palate). Surgery is required during infancy or childhood in order to close the opening. Due to the specific characteristics of the palate, healing after surgery typically results in the formation of a scar. This scar is very rigid and prevents proper development of the face and mouth, which can dramatically affect a child's appearance, speech, teeth, eating, and the ability to develop socially. My research focuses on periostin, a protein playing a prominent role during scar formation in human skin and in skin wound repair. I found that this protein, as well as the stiffness of the hard palate, play a significant role in the function of cells that participate in the healing process. This protein is also found in the supporting structures around the tooth. Here, I showed that the role of periostin in the periodontium is to support the maintenance of these structures. Lastly, I investigated what types of cells are recruited during palatal healing and I found two distinct populations that have unique roles: one population is primarily involved in the formation of new vessels in the wound, and the other is involved in the formation of matrix that supports the growing cells. In conclusion, studies in this thesis have further defined the complex interactions that exist between cells and their environment using the palate as a model system. The data from this thesis provides important information for the design of future therapeutics for oral wounds, cleft palate reconstruction, and also contributes to a growing understanding of fibroblast heterogeneity and how divergent populations contribute to different processes during wound repair

Co-Authorship Statement

Chapter 1

Georgia Nikoloudaki wrote the chapter. Douglas W. Hamilton contributed to the design of the introduction and provided critical feedback during preparation of this chapter. A part of this chapter has been published in AJP Cell Physiology: Nikoloudaki G., Kreber C., Hamilton DW. Wound Healing and Fibrosis: A Contrasting Role for Periostin in Skin and the Oral Mucosa, 2020 May; 318(6), https://doi.org/10.1152/ajpcell.00035.2020.

Chapter 2

Georgia Nikoloudaki performed the experiments, data analysis, and prepared the figures. Douglas W. Hamilton conceived the initial study models, contributed to the ongoing experimental design and direction of the study, acquired ethical approval for animal work. Georgia Nikoloudaki wrote the chapter with Douglas W. Hamilton providing critical feedback. A version of this chapter has been published in Matrix Biology: Nikoloudaki G., Snider P., Simmons O., Conway SJ, Hamilton DW. Periostin and Matrix Stiffness Combine to Regulate Myofibroblast Differentiation and Fibronectin Synthesis During Palatal Healing, https://doi.org/10.1016/j.matbio.2020.07.002.

Chapter 3

Georgia Nikoloudaki performed the experiments, data analysis, and prepared the figures. Douglas W. Hamilton contributed to the design and direction of the study, acquired ethical approval for collection of human teeth. Dr. Eli Sone, University of Toronto, performed the ex-vivo mineralization assay. Georgia Nikoloudaki wrote the chapter with Douglas W. Hamilton providing critical feedback. This chapter is in preparation for manuscript submission.

Chapter 4

Georgia Nikoloudaki performed the experiments, data analysis, and prepared the figures. Douglas W. Hamilton contributed to the design and direction of the study, acquired ethical

approval for animal work. Georgia Nikoloudaki wrote the chapter with Douglas W. Hamilton providing critical feedback. This chapter is in preparation for manuscript submission.

Chapter 5

Georgia Nikoloudaki wrote the chapter. Douglas W. Hamilton provided critical feedback during preparation of this chapter.

Acknowledgments

I am grateful to all those who have provided me with the possibility of completing this research, as well as the Department of Anatomy and Cell Biology at Western University. This has been a rewarding and invaluable experience.

First and foremost, I would like to express my deepest gratitude to my supervisor and mentor, Dr. Douglas W. Hamilton, for his support and allowing me to pursue research in cell biology. When I first started working in the lab, I did not have a lot of experience in the experimental methods used in a wet lab. Dr. Hamilton guided me to adopt a systematic approach in conducting research: from forming a solid, testable hypothesis to design experiments, collect, analyze and interpret research data. With his guidance and mentorship, I have achieved goals that I previously thought that there were unimaginable, and without a doubt his mentoring style has helped me to develop the skills to become an independent researcher and has prepared me very well for a career in academia.

I am also grateful to my advisory committee members Dr. Dale Laird and Dr. Mark Darling for providing critical feedbacks on my research in the committee meetings. They have provided direction and kept my thesis on course and focused. I have benefited greatly from their expertise and the time that they have provided over the years.

Thank you to all of the animal care staff, veterinary technicians, and veterinarians who made all of the animal work possible.

I would like to thank all the members of Hamilton laboratory for their support and precious friendships. It has been a privilege to work with such a dedicated group of people who I learned a lot from and formed life-long friendships. Special thanks to Sarah Brooks, Shawna Kim, Karrie McLeod and Yoon Chi, for our adventures in and outside of the lab! Your commitment and encouragement made this a really enjoyable journey for me. I am thankful for the technical training provided by John Walker throughout my degree. Through our scientific discussions, he helped me think more critically, and he his dedication further motivated me.

Last but not least, I would like to express appreciation to my family, especially my parents, Manolis and Frida, and my sister Maria. Thanks for your unconditional love and support, and for always believing in me and my dreams.

Finally, I would like to thank my husband Pavlos for his endless motivation and support during this degree. While completing his graduate studies at Western, his perseverance and commitment to academic excellence have been a wonderful inspiration. I couldn’t have done it without your support.

There is no way I could have completed my PhD without all of you. I am truly blessed.

Table of Contents

List of Tables

List of Figures

List of Appendices

List of Abbreviations

ADAM	A disintegrin and metalloproteinase
AGE	Advanced glycation end-products
bFGF	Basic fibroblast growth factor
BMP	Bone morphogenic protein
BSP	Bone sialoprotein
CCN	Connective tissue growth factor family member
CD	Cluster of differentiation
CRD	Carbohydrate recognition domain
CXCL12	C-X-C motif chemokine 12
DAMP	Damage associated molecular pattern
DIGE	Drug-induced gingival enlargement
DEGs	Differentially expressed genes
DMP-1	Dentin matrix protein- 1

DT	Diphtheria Toxin
E	Embryonic day
ECM	Extracellular matrix
EGFR	Epidermal growth factor receptor
EMT	Epithelial to mesenchymal transition
ERK	Extracellular signal-regulated kinase 1
FACS	Fluorescence-activated cell sorting
FAK	Focal adhesion kinase
FAS-1	Fasciclin-1
FBS	Fetal bovine serum
FLN	Foxd1 lineage-negative
FLP	Foxd1 lineage-positive
Foxd1	Forkhead box D1
GEFs	Guanide-exchange factors
GFP	Green fluorescence protein
IBMX	3-isobutyl-1-methylxanthine
IGF	Insulin-like growth factor
IL	Interleukin
iNOS	Inducible nitric oxide synthase

ISH	In situ hybridization
JNK	c-Jun N-terminal Kinase
KO	Knockout
LOX	Lysyl Oxidase
LTBP	Latent TGFβ binding protein
lsl	Loxp-STOP-Loxp
MLC	Myosin light chain
MMP	Matrix metalloproteinase
MSC	Mesenchymal stem/stromal cell
MPs	Matricellular proteins
mPFBS,	Murine palatal fibroblasts
NG2	Neuron-glial antigen 2
NIGE	Nifedipine-induced gingival enlargement
NCP	Non-collagenous protein
OPG	Osteoprotegerin
OPN	Osteopontin
OSF-2	Osteoblast specific factor 2
PBS	Phosphate buffered saline
PDGF	Platelet derived growth factor

PDGFR	Platelet derived growth factor receptor
PDL	Periodontal ligament
PSTN	Periostin
P75NTR	p75 neurotrophin receptor
ROCK	Rho-associated protein kinase
RT-qPCR	Real-time quantitative polymerase chain reaction
SLRPs	small leucine-rich proteoglycans
SOX10	SRY-Box Transcription Factor 10
SPARC	Secreted protein acidic and rich in cysteine
TCP	Tissue culture plastic
tdTomato	Tandem dimer Tomato red fluorescent protein variant
TGFβ	Transforming growth factor beta
TGFβR	Transforming growth factor beta receptor
TGFBI/βigh3	Transforming growth factor-β-induced gene product-h3
TIMP	Tissue inhibitor of metalloproteinase
TLR	Toll-like receptor
TNFα	Tumor necrosis factor alpha
TNX	Tenascin-X
TSP	Thrombospondin

VEGF	Vascular endothelial growth factor
vWF	Von Willebrand Factor
WT	wild type
αSMA	Alpha- smooth muscle actin
μ-CT	micro-computed topography

Chapter 1

1 Rationale, Literature Review and Thesis Overview

1.1 Rationale, Hypothesis and Objectives

Wound healing in soft connective tissues, such as skin and oral mucosal tissue, is defined as a coordinated series of overlapping events leading to resolution of the injury or defect. Passing through the phases of hemostasis, inflammation, proliferation and remodeling, concomitant with re-epithelialization, barrier function is re-established (Karamanos et al., 2019). However, different healing profiles have been described for different tissues. In particular, wound healing in the oral mucosa is known to exhibit reduced scarring compared with cutaneous injuries; injuries to the oral mucosa, including gingival tissue, heal rapidly with minimal scar formation (Pereira & Sequeira, 2021; Politis et al., 2016; Toma et al., 2021). However, while still part of the oral environment, the palatal mucosa is associated with excessive scarring in response to injury (Larjava et al., 2011; Pereira & Sequeira, 2021; Wijdeveld et al., 1987, 1991). Unlike skin and gingival connective tissue, palatal soft tissue is a rigid mucoperiosteum; mucosa and the periosteum are merged and tightly attached to the palatal bone (Nanci, 2013)

The outcome of the healing process is dependent on several different factors: extrinsic and cell intrinsic factors. Extrinsic factors include the matrix stiffness surrounding the cells, signaling molecules such as TGFβ1, or ECM components such as matricellular proteins, e.g. Periostin, (Hinz, 2007; Serini et al., 2002a). In this thesis we build on previous work from our lab to further explore the contrasting tissue-specific effects of periostin bioactivity that could be partially responsible for the distinct healing patterns evident when skin, gingiva and the palatal mucoperiosteum are compared (Nikoloudaki et al., 2020) and could provide deeper understanding of how differences in molecular composition and physical properties of these tissues lead to the different healing outcomes.

In addition to the above mentioned extrinsic factors, recent evidence also suggests that resident cell-specific intrinsic differences can alter how they respond to extrinsic stimuli, as well as the downstream effect of that response (Driskell et al., 2013; Jiang & Rinkevich, 2021.). While the majority of evidence emerges from studies done in skin, liver and other organs, there are only few reports about the presence of embryonically distinct cell populations within the oral environment (Byrd et al., 2019; Jiang & Rinkevich, 2021). The discovery of distinct cell subpopulations in the oral cavity through lineage-tracing techniques, and the understanding of their specific roles could provide new insights in the differences between oral and skin fibroblasts in wound healing. Here, we build upon previous work from our lab in order to further the understanding of how cell intrinsic and extrinsic properties influence palatal healing, with a focus on fibroblast activation, and differentiation into myofibroblasts, for the purpose of guiding the development of future biomaterial development for wound healing applications.

This thesis explores the ***overarching hypothesis*** that fibroblast activation and differentiation into myofibroblasts during an acute healing response in the palate relies on cell-intrinsic differences stemming from a population's embryonic lineage, and cell-extrinsic factors present within the extracellular matrix (ECM). Specifically, it was first hypothesized that modifying the ECM by deletion of the gene coding for the ECM protein periostin would impair granulation tissue formation and cellular contraction during palatal wound healing (*Aim 1*). Secondly, we hypothesized that periostin protein would inhibit mineralization of the surrounding collagenous matrix in vivo and osteogenic differentiation of periodontal ligament fibroblasts in vitro (*Aim 2*). Finally, we hypothesized that embryonic progenitors that express Foxd1 would contribute to myofibroblast progenitors within the palatal mucoperiosteum, and that binary expression of Foxd1 and NG2 could be used to stratify palatal fibroblasts to identify unexplored embryonic lineages of myofibroblast progenitors present within the palatal mucoperiosteum of mice (*Aim 3*).

These were explored through the following three specific Aims:

1. To identify the expression profile of periostin in murine palate during development, homeostasis and excisional wound healing and investigate the effect of genetic deletion of periostin on palatal wound repair.

2. To investigate the role of periostin in the maintenance and inhibition of mineralization of the periodontal ligament.

3. To assess Foxd1 expression in palatal progenitor populations during development, and to determine how cells derived from Foxd1- and NG2- expressing progenitors contribute to wound repair.

1.2 Wound Healing

Traumatic injury initiates a well-orchestrated cascade of cell and molecular events that leads to repair. This wound healing process can be divided into distinct but overlapping phases: hemostasis, inflammatory, proliferative and tissue remodeling/maturation phase, with each part characterized by specific cellular and molecular events (Cañedo-Dorantes & Cañedo-Ayala, 2019). Initially, hemostasis occurs to control blood loss and reduce the risk of systemic infection. During this phase, the traumatized lining of blood vessels, the platelet aggregation, and the activation of the coagulation cascade provide molecular signals that initiate tissue repair (Cañedo-Dorantes & Cañedo-Ayala, 2019; Reinke & Sorg, 2012). The inflammatory phase is characterized first by neutrophil infiltration, with a primary role in targeting infection through their innate immune function. Temporally, macrophages migrate into the wound, debriding damaged tissue, phagocytosing neutrophils, and stimulating transition into the proliferative phase through the release of growth factors such as transforming growth factor-β1 (TGFβ1), platelet derived growth factor (PDGF), and vascular endothelial growth factor (VEGF) (Chazaud, 2014). During the proliferative phase, fibroblasts, which are the primary effectors of tissue repair, migrate into the wound, proliferate, and begin producing a temporary matrix called granulation tissue (Martin & Nunan, 2015; Sorg et al., 2017). Finally, in the remodeling phase, fibroblasts turn over the granulation tissue into a type I collagen rich scar (Cañedo-Dorantes & Cañedo-Ayala, 2019; Reinke & Sorg, 2012; Sorg et al., 2017)

Hemostasis is a rapid process that leads to cessation of bleeding from a blood vessel, while at the same time it initiates the wound repair response (Cañedo-Dorantes & Cañedo-Ayala, 2019; Martin & Nunan, 2015). Vessel injury and disruption of the endothelial layer leads to platelet activation due to their exposure to the underlying matrix and tissue factor. The matrix releases cytokines and inflammatory markers that lead to adhesion of the platelets and their aggregation at that site which leads to the formation of a temporary platelet plug. The platelet adhesion is a complex process mediated by interactions between various receptors and proteins including tyrosine kinase receptors, glycoprotein receptors, other G-protein receptors as well as the von Willebrand Factor (vWF). The von Willebrand Factor functions via binding to the Gp 1b-9 within the platelets (Periayah et al., 2017). Adhered and

aggregated platelets release their cytoplasmic granules that include ADP, thromboxane A2, serotonin, platelet-derived growth factor (PDGF), vascular endothelial growth factor (VEGF), serotonin, and coagulation factors. (Etulain, 2018; Periayah et al., 2017). Platelets were also shown to produce a positive effect on mouse skin wound healing by enhancing the angiogenic potential of mesenchymal stem cells (Levoux et al., 2021). If the platelet plug is not enough to stop the bleeding, the third stage of hemostasis begins, which is the activation of the coagulation cascade. Prothrombin, thrombin, and fibrinogen are the main factors involved in the outcome of the coagulation cascade. Traumatized vessels and activated platelets release prothrombin activator, which in turn activates the conversion of prothrombin into thrombin. Thrombin then facilitates the conversion of a soluble plasma protein fibrinogen into long, insoluble fibers of fibrin, which polymerizes and forms a fibrin polymer mesh and results in a cross-linked fibrin clot that further stabilizes the clot. Platelets in the clot then begin to shrink, tightening the clot and causing vasoconstriction (thromboxane A2) to initiate the process of wound healing. Platelets also undergo a transformation of their shape into a pseudopodal shape which in-turn leads to release reactions of various chemokines (Periayah et al., 2017). Platelet aggregation and degranulation also assist the recruitment of circulating neutrophils and monocytes through cytokine and growth factor release, inducing their presentation of adhesion molecules to promote cellular homing to the site of injury(Etulain, 2018; Greaves et al., 2013; Martin & Nunan, 2015). Moreover, many of the factors released by platelets have been reported to have direct antimicrobial effects (Etulain, 2018; Y.-Q. Tang et al., 2002; Yeaman, 2010)

The inflammatory response is further supported by resident macrophages and dendritic cells. In response to tissue damage and platelet degranulation, neutrophils are next to populate the wound bed, followed by the recruitment of circulating monocytes, which differentiate into macrophages (Greaves et al., 2013; Reinke & Sorg, 2012). Neutrophils and macrophages participate in the innate immune response through their release of inflammatory mediators and bactericidal factors. They also release proteases and enzymes for the debridement of the inflamed tissue and they are removing bacteria and cellular debris from the damaged tissue via phagocytosis (Ellis et al., 2018; Wang, 2018). Finally, neutrophils and macrophages innate immune response through their release of

inflammatory mediators, advancing the wound beyond the inflammatory phase (Mahdavian Delavary et al., 2011; Rodero & Khosrotehrani, 2010).

In tissues such as skin or oral mucosa that are covered by epithelium, keratinocytes begin to migrate laterally between the non-viable, dried fibrin clot, and the viable fibrin rich layer infiltrated by the fibroblasts to cover the wound bed and maturing granulation tissue (Arora et al., 2016; Rousselle et al., 2019). Injured keratinocytes also contribute to the inflammatory response during healing by releasing high-mobility group box protein 1 (HMGB1), heat shock protein (HSP), antimicrobial peptides (defensins, cathelicidin, calgranulin A/B), cytokines (IL-1a, IL-33) and chemokines (IL-8)(Juráňová et al., 2017; Piipponen et al., 2020). These endogenous molecules are considered to be a subgroup of host-derived damage-associated molecular patterns (DAMPs) that signal tissue and cell injury via Toll-like receptors (TLRs), which in turn initiate immune responses (Juráňová et al., 2017; Piipponen et al., 2020; Xiao et al., 2020).

Following the inflammatory response, the proliferation phase of wound healing is initiated to restructure the wound site towards repair or regeneration. During the proliferation phase, fibroblasts deposit ECM, which initially is mainly collagen III, forming highly vascularized granulation tissue that replaces the fibrin clot (Rognoni et al., 2018). This vascularized tissue results from endothelial cell and perciyte migration into the wound bed in response to the release of pro-angiogenic stimuli, such as VEGF and bFGF, released by keratinocytes, platelets, fibroblasts, and inflammatory cells (Cañedo-Dorantes & Cañedo-Ayala, 2019; Martin & Nunan, 2015; Tonnesen et al., 2000). These newly formed blood vessels contribute in the further maturation of the granulation tissue and provide nutrition in addition to oxygen for cell infiltration into the wound space (Tonnesen et al., 2000). Fibroblasts and other mesenchymal populations including pericytes are recruited to the developing granulation tissue in response to chemotactic stimuli, including platelet-derived growth factor (PDGF) and basic fibroblast growth factor (bFGF) where they assume a matrix secreting, contractile phenotype known as a myofibroblast, primarily in response to TGFβ1(Hinz, 2007, 2010a). More specifically, fibroblasts transition to the myofibroblast

phenotype is associated with α-smooth muscle actin (α-SMA) expression and its incorporation to stress fibers, concomitant with extracellular matrix production, and wound contraction (Hinz, 2007, 2007, 2015a). Wound contraction initiates a positive feedback mechanism through which increased matrix stiffness enhances myofibroblast differentiation through both mechano-sensing and activation of latent TGFβ1(Hinz, 2015b).

The final and longest phase of wound repair, the remodeling phase, takes place from months to years following the initial injury (Velnar et al., 2009). During this phase secretion of MMPs from fibroblasts, macrophages and endothelial cells contributes to the remodeling of type III collagen to type I collagen by fibroblasts (Martins et al., 2013). The wound bed becomes less cellular as cells like fibroblasts and macrophages undergo apoptosis (Dg, 1998). The previous provisional ECM transitions from loose fibronectin tissue networks to larger and denser collagen bundles (Glim et al., 2015; Politis et al., 2016; Toma et al., 2021). Large networks of blood vessels start to develop and the fibrillar network of the ECM becomes more aligned and organized (Velnar et al., 2009). Temporally, resident cells including keratinocytes and macrophages continue to remodel the remaining permanent ECM as the repaired tissue return to homeostasis (Velnar et al., 2009; Xue & Jackson, 2015).

During the different phases of wound healing, it is known that several different factors affect the healing outcome, including growth factors, the composition of the ECM, cellular origin, and spatiotemporal recruitment of different cell populations during these phases. The focus of this thesis is to investigate how cell-extrinsic factors, such as ECM composition, and cell intrinsic factors regulate the wound healing process in the oral cavity.

1.3 Soft Tissue Healing: Compare and contrast skin and oral tissues

While cutaneous and oral tissues follow a similar macroscopic healing process, it has been demonstrated that they in fact exhibit many variations at the cellular and molecular level in relation to processes resulting in the restoration of tissue architecture and function. Wounds in the oral mucosa heal significantly faster, with minimal scar formation in comparison to skin wounds (Glim et al., 2013.; Iglesias-Bartolome et al., 2018; D. Pereira & Sequeira, 2021; Wong et al., 2009). This difference has been attributed to several factors, including the presence of saliva in the oral cavity, the embryonic origin of the cells involved, the elicited inflammatory response, variable presence of growth factors, phenotypic differences between oral and cutaneous fibroblasts, differences in ECM composition, as well as the presence of bacteria that stimulate wound healing (Figure 1.1) (Häkkinen et al., 2000; Iglesias-Bartolome et al., 2018; Lepekhin et al., 2002; Pereira & Sequeira, 2021).

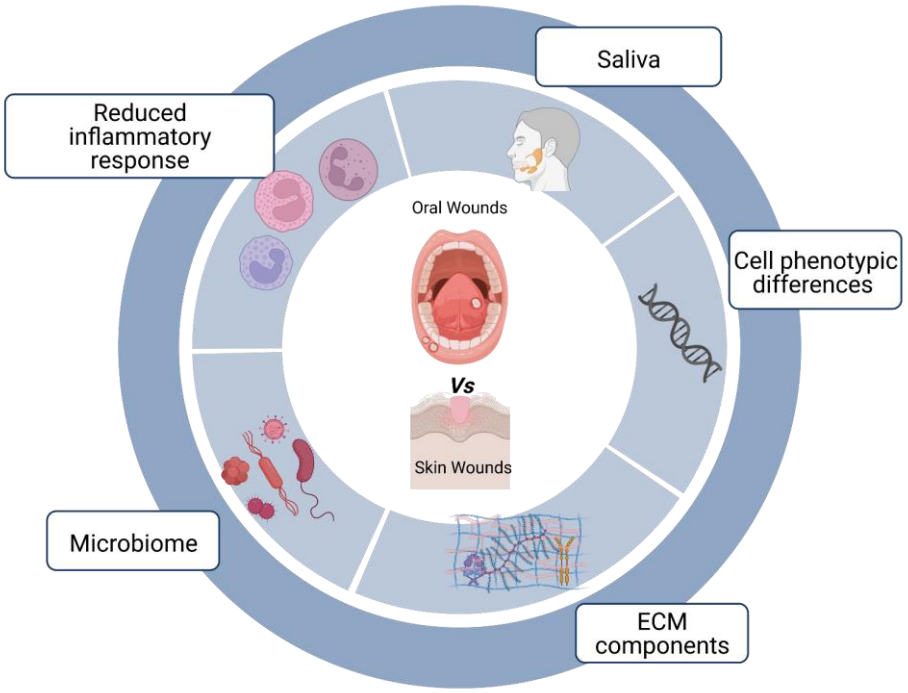

Figure 1-1 Schematic diagram of factors affecting the wound healing in the oral environment

One of the most notable differences between skin and tissues in the oral cavity is that the latter are in constant contact with saliva and the oral microbiome (Bodner et al., 1993; Hutson et al., 1979; Y. Su et al., 2018). Saliva could contribute to the wound repair process by providing a pool of growth factors such as epidermal growth factor (EGF), VEGF and FGF, and compound and peptides with antimicrobial function, such as mucins, lactoferrin, lysozyme, lactoperoxidase, statherin, histatins and antibodies (secretory immunoglobin A, sIgA) (Hof et al., 2014; Lynge Pedersen & Belstrøm, 2019). Saliva components are also responsible for improved oral keratinocyte and fibroblast migration (Boink et al., 2016). Experimentally reduced and arrested salivary gland activity in animals resulted in

prolonged inflammatory response and delayed wound healing, with saliva modulating aspects of oral wound healing by regulating the inflammatory response and myofibroblast recruitment (Bodner et al., 1993; Dayan et al., 1992; Oudhoff et al., 2008). The oral microbiome is essential for the oral cavity homeostasis. Healthy oral biofilm was found to result in an increased expression of antimicrobial peptides and improved barrier function in reconstituted human gingiva (Shang et al., 2018). Altered microbiome was found to negatively impact wound healing and gingival mesenchymal stem cell functions through secretion of lipopolysaccharides and subsequent stimulation of miRNA-21/Sp1/telomerase reverse transcriptase pathway (Y. Su et al., 2018).

In mucosal and cutaneous injury, after hemostasis, granulation tissue forms and matures through the inflammatory phase (Cañedo-Dorantes & Cañedo-Ayala, 2019; Pereira & Sequeira, 2021). In the oral mucosa, during the inflammatory phase of the healing process reduced recruitment of neutrophils, macrophages, and T-cells is observed when compared to cutaneous wounds (Dipietro, 2003; Häkkinen et al., 2000; Wong et al., 2009). The reduced numbers of immune cells observed in oral wounds is associated with reduced levels of inflammatory cytokines, such as interleukin (IL)-23, IL-24, IL-6, IL-8, tumor necrosis factor alpha (TNF-α) and pro-fibrotic cytokines (TGF-β1), leading to decreased recruitment of inflammatory cells, and elevated anti-fibrotic cytokine TGF-β3(L. Chen et al., 2010; Glim et al., 2013.; Schrementi et al., 2008; Szpaderska et al., 2003). The reduced inflammation observed in the oral tissues during wound healing might be an indication of a more efficient mechanism or response (Caetano et al., 2021; Moutsopoulos & Konkel, 2018; Williams et al., 2021).

At the end of the inflammatory stage, proliferation and migration of keratinocytes and fibroblasts occurs into the wound bed (Cañedo-Dorantes & Cañedo-Ayala, 2019; Pereira & Sequeira, 2021). Fibroblasts secrete extracellular matrix and remodel the granulation tissue, while keratinocytes restore barrier function to the damaged tissue. In the oral cavity epithelial cells start migrating and proliferating 24h post-wounding and, for excisional wounds up to 5 mm, a complete re-epithelialization is reached by day 2 to 3 in oral mucosa,

while in skin it could take up to 7 days (Bodner et al., 1993; L. Chen et al., 2010; Harrison & Jurosky, 1991a, 1991b; Iglesias-Bartolome et al., 2018; Larjava, 2013; Szpaderska et al., 2003).

Following the inflammatory response, the proliferation phase of wound healing commences, to restructure the wound site towards repair or regeneration. In cutaneous wounds it starts from 2 to 10 days after injury and can last for up to 3 weeks, depending on the location and the type/extent of injury. In contrast, in oral mucosa wounds the inflammation peaks at days 2 to 3, but it is resolved by day 6 (Bodner et al., 1993; Harrison & Jurosky, 1991a; Iglesias-Bartolome et al., 2018; Szpaderska et al., 2003). Fibroblasts and mesenchymal stem cells play a central role during the proliferating phase of wound healing. Strong evidence suggests that multiple fibroblast phenotypes exist within one tissue (Giannopoulou & Cimasoni, 1996; Moulin et al., 1998), but it also has been shown that cellular phenotypes can be substantially variable among the same tissues but in different anatomical regions (Gabbiani, 1996; Giannopoulou & Cimasoni, 1996). Moreover, it is now becoming evident that not all fibroblasts in a tissue arise from the same embryonic origin (Driskell et al., 2013; Rinkevich et al., 2015a, 2015c; Sriram et al., 2015). From a developmental perspective, dorsal skin and oral mucosal fibroblasts have different origins, which could partially explain the phenotypic differences between oral and cutaneous fibroblasts: while the non-cranial dorsal skin dermis has an *Engrailed1*-lineage-positive somitic origin, the oral mucosa lamina propria and cranial skin dermis originates from *Wnt1*-lineage-positive neural crest cells (Ishii et al., 2012; Janebodin et al., 2011; Rinkevich et al., 2015b). Mah and colleagues found that $CD26^+$ skin fibroblasts associate with higher expressions of profibrotic genes and transforming growth factor-β persist in hypertrophic-like scars formed after skin wound healing, whereas in gingiva $CD26^+$ fibroblasts are only residually present (Mah et al., 2017). Oral mucosal fibroblasts express higher levels of hepatocyte growth factor (HGF) compared to dermal fibroblasts (Stephens, Hiscox, et al., 2001), therefore the former might more effectively resist to TGF-β1-driven myofibroblast differentiation when compared to dermal fibroblasts (Dally et al., 2017).

Several studies have investigated how different fibroblast lineages contribute to oral and to skin wound healing (Jiang et al., 2020; Jiang & Rinkevich, 2021; Rinkevich et al., 2015b) Apart from the *Engrailed1*-lineage-positive fibroblast subpopulation, the study from Rinkevich and colleagues reports a *Wnt1*-lineage-positive population in the oral dermis tightly linked to the non-fibrotic healing that characterizes the oral mucosa. A reciprocal transplantation of these oral mucosal- and skin-derived fibroblast populations performed in mice revealed that the cells mimic the response of their tissue of origin. The grafting of *Wnt1*-lineage-positive oral fibroblasts in skin resulted in decreased scar tissue formation while skin fibroblasts contributed to a scar-like tissue formation in the oral wound site, proving that the oral fibroblast lineage is a determinant for the scarless healing of the oral mucosa (Rinkevich et al., 2015b), Mah et al. investigated the relation between the distinct phenotypes of gingival fibroblasts and skin fibroblasts and their different wound healing patterns, in 3D cell cultures. Of significance, they observed that gingival fibroblasts proliferate faster and express higher levels of molecules involved in modulation of inflammation and ECM remodeling (MMP-1, -3, -10, TIMP-4) compared to dermal fibroblasts (Mah et al., 2014). In contrast, dermal fibroblasts exhibited significantly higher expression of fibrillar (collagens and elastin) and non-fibrillar (SLRPs and matricellular proteins) ECM proteins, as well as molecules involved in TGF-β induction of the myofibroblast phenotype and cell contractility (TGF-β1, TGF-β2, TGF-β3, Smad, α-SMA, CXCL12, Cadherin-2, -11). Their findings are indicative that gingival fibroblasts display a phenotype that may promote faster resolution of inflammation and ECM remodeling, which is associated with reduced scar formation, while skin fibroblasts have a profibrotic, scar-prone phenotype (Mah et al., 2014). Faster invasion of granulation tissue in vivo could increase the maturation of the defect, which secondarily could also enable faster re-epithelialization by providing an appropriate ECM for epithelial migration (Shannon et al., 2006).

Oral fibroblasts have also been reported to be highly responsive to TGFβ-1, the major profibrotic cytokine expressed during healing, with TGFβ-1 increasing proliferation rates as well as collagen synthesis, when compared to dermal fibroblasts (H. G. Lee & Eun, 1999). The ECM composition of oral wounds is different than in cutaneous wounds: ECM

composition have been quantified between oral mucosa and skin, with the former showing increased expression of fibronectin, fibronectin ED-A, hyaluronic acid and chondroitin sulphate, and decreased expression of elastin (Glim et al., 2014). It has been shown that Fibronectin ED-A, an alternative spliced isoform de novo which is expressed during wound healing and fibrotic changes, is highly upregulated in myofibroblasts (Zent & Guo, 2018a). Earlier reports from Serini et al. (Serini et al., 2002b) suggested that fibronectin ED-A acts as a necessary ECM component for TGFβ induction of myofibroblast differentiation. Additional evidence for the role of fibronectin ED-A in myofibroblast activation has been demonstrated via the latent TGFβ binding protein-1 (LTBP-1)/EDAFN/ integrin interaction network, where fibronectin immobilizes LTBP-1 and thus stores TGF-β1 in the ECM (Klingberg et al., 2018).

During the remodeling phase, MMPs mediate the reorganization and turnover of the ECM, and in turn are regulated by TIMPs, the balance of which has been found to affect the outcome of wound healing process (Caley et al., 2015; Martins et al., 2013). In oral wounds MMP tissue inhibitors (TIMP-1 and TIMP-2) production is reduced, therefore allowing for increased MMP-2 activity in the remodeling phase of oral wound healing(Glim et al., 2013.; Stephens et al., 2001). Other differences in the wound ECM between the two tissues include the collagen III to collagen I ratio, which is increased in oral wounds (Glim et al., 2013.), and the pro-fibrotic matricellular protein periostin. Our lab has shown that periostin is involved in regulation of ECM synthesis in gingival wound healing, while in skin it appears as a mediator of myofibroblast differentiation through β1 integrin-focal adhesion kinase (FAK) signaling (Elliott et al., 2012a; Kim, Nikoloudaki, Michelsons, et al., 2019; Nikoloudaki et al., 2020).

Focusing on oral keratinocytes, more recent methods involving transcriptomic analysis have uncovered molecular differences between skin and oral mucosal wound healing (Iglesias-Bartolome et al., 2018). Sox2 and Pitx1 transcription factors were shown to be the master regulators of the oral mucosal wound healing response in the keratinocytes when compared to skin keratinocytes (Iglesias-Bartolome et al., 2018).

To conclude, the ability of the oral mucosa to heal without scarring cannot be attributed to a single feature but to several extrinsic and intrinsic factors present in the different stages of the wound healing process, which are crucial to the final non-scar outcome. Interestingly, while still part of the oral environment, the palatal mucosa is associated with excessive scarring after cleft palate reconstructive surgery (Larjava et al., 2011; Wijdeveld et al., 1987, 1991). Unlike skin and gingiva, palatal soft tissue is a rigid mucoperiosteum with the mucosal tissue and periosteum merged and tightly attached to the palatal bone (Nanci, 2013). The investigation of distinct healing patterns among skin, gingiva and the palatal mucoperiosteum could provide deeper understanding of how differences in molecular composition and physical properties of these tissues lead to the different healing outcomes.

1.4 Extracellular Matrix and Matricellular proteins

In recent years a plethora of research has demonstrated that the extracellular matrix (ECM) composition is an important determinant of soft tissue healing (Wells et al., 2016). In particular, matricellular proteins have seen increasing attention due to their role in the direct modification of cell behaviour. Defined by Paul Bornstein in 1995 (Bornstein, 1995), matricellular proteins were classified initially on their ability to modify cell adhesion to the ECM. Surprisingly, initial analysis of matricellular proteins through genetic deletion, revealed that many of the mice lacking individual matricellular proteins developed normally and exhibited no major phenotypes in adulthood (Murphy-Ullrich & Sage, 2014; H. F. Rios et al., 2008). However, when challenged in injury models, these same mice lacking specific matricellular proteins exhibited significant defects in healing, which highlighted a potentially important role for matricellular proteins in wound healing processes.

While fibrin, collagen and fibronectin are required to provide structural support to tissues during healing, matricellular proteins typically are upregulated in the granulation tissue where they modulate the adhesion, migration, proliferation and differentiation of pericytes,

fibroblasts and epithelial cells up to 15 days post-wounding (Kyriakides & Bornstein, 2003; Midwood et al., 2004). As a class of proteins, matricellular proteins specifically modulate cell-matrix interactions and cell function (adhesion, spreading, migration, proliferation and differentiation) (Bornstein & Sage, 2002a) by interacting with cell-surface receptors (e.g., integrins) and other bioeffector molecules, as well as with structural matrix proteins such as collagens. Certain matricellular proteins exhibit affinity for binding TGF-β1, a growth factor which is important for fibroblast recruitment and differentiation during wound repair (Barrientos et al., 2008; Hinz, 2007, 2016). In general, matricellular proteins act in a temporal and spatial manner to control different aspects of wound repair (Basu et al., 2001; Hamilton, 2008a; Jackson-Boeters et al., 2009; Kyriakides & Bornstein, 2003; Midwood et al., 2004; Puolakkainen et al., 2005; Zhou et al., 2010).

Due to the relative ease of creating experimental skin injuries, much of the research on the role of matricellular proteins in the regulation of healing have focused on skin, rather than tissues such as gingiva. Over the last 12 years, Dr. Hamilton's lab has investigated how matricellular proteins, and in particular periostin, regulate processes underlying the healing of soft connective tissues. Periostin was explored previously by the Hamilton lab as an important modulator of mesenchymal cell behavior during the proliferative and remodeling phases of soft tissue healing. More specifically, the contrasting effects of periostin on dermal and gingival fibroblasts demonstrate the specificity of matricellular protein bioactivity in relatively homologous tissues (Elliott et al., 2012a; Kim, Nikoloudaki, Michelsons, et al., 2019; Nikoloudaki et al., 2020; J.-Y. Su et al., 2021).

1.5 Periostin as a Modulator of Cell-ECM interactions

Matricellular proteins are transiently-expressed non-structural proteins (Bornstein & Sage, 2002b). First described in 1995, periostin (POSTN) was identified as an 811 amino acid protein secreted by murine osteoblasts that is required for cell adhesion (Takeshita et al., 1993). Originally termed osteoblast specific factor 2 (OSF-2), due to it localization to the periodontal ligament and periosteum of mice, it was renamed periostin in 1999 and subsequently classified as a matricellular protein in 2007 by Norris and colleagues (Litvin

et al., 2004). Structurally, periostin is a secreted 90 kDa N terminus-glycosylated protein containing four tandem fasciclin domains (A. Kudo, 2011), with several different isoforms described (Bai et al., 2010; Cai et al., 2019; Gadermaier et al., 2018; Morita & Komuro, 2016). The physiological significance of periostin expression in adult systems has been mainly identified in collagen-rich biomechanically active tissues (Hamilton, 2008b) such as the skin, bone, and heart, periodontium, periodontal ligament and within developing teeth (Kruzynska-Frejtag et al., 2004), highlighting a subtle, but complex role for periostin in tissue homeostasis, healing and pathology.

Like many matricellular proteins, periostin has been defined as a non-structural ECM component, although as research has continued, evidence has accumulated demonstrating that it can modify the biomechanical properties of collagenous based tissues (Conway et al., 2014; Norris et al., 2007). The multi-domain structure of periostin allows for numerous interactions with extracellular/secretory proteins (Kii & Ito, 2017). Specifically, periostin has been shown to modulate cross-linking and stabilization of the extracellular matrix, including through regulation of collagen fibrillogenesis and cross-linking (Hwang et al., 2014; Norris et al., 2007). Periostin is also known to act as a scaffold for assembly of several extracellular matrix proteins (type I collagen, fibronectin, tenascin-C, and laminin γ2) as well as accessory proteins (BMP-1 and CCN3) (Amizuka et al., 2009; Elliott & Hamilton, 2011; A. Kudo & Kii, 2018; Maruhashi et al., 2010; Rogers et al., 2008), although the binding site for collagens has not been yet identified (Kii & Ito, 2017; Norris et al., 2007) Among the structural domains of periostin, the EMI region has attracted significant scientific interest, as it is involved in cellular signaling and protein–protein interaction (Kii & Ito, 2017). The EMI domain, named after its presence in proteins of the EMILIN family of extracellular matrix glycoproteins, is a cysteine-rich sequence of ∼80 amino acids that is most often found at the amino terminus of extracellular proteins that are forming or are compatible with multimer formation (Callebaut et al., 2003; Doliana et al., 2000). Extracellularly, periostin directly binds to fibronectin through the EMI domain (Kii et al., 2009; Norris et al., 2007). Fibronectin has several sites for interacting with collagens, suggesting that the EMI domain of periostin may indirectly interact with collagens (Fig. 1.2) (Kii & Ito, 2017). Intracellularly, a proximal localization between periostin and

fibronectin in the endoplasmic reticulum of fibroblastic cells has been observed, indicating that the two proteins interact prior to fibronectin's secretion (Kii et al., 2016), and evidence suggests that periostin enhances secretion of fibronectin from the endoplasmic reticulum into the extracellular environment (Kii et al., 2016). In totality, this information demonstrates a critical role for periostin in extracellular matrix homeostasis and the regulation of cell phenotype.

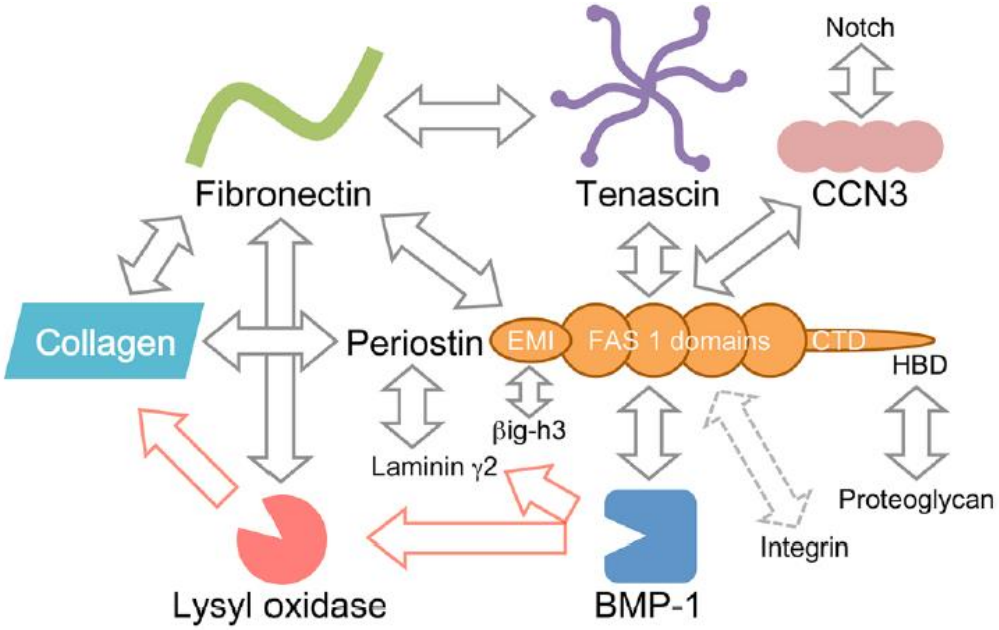

Figure 1-2 Periostin and its interacting proteins.

The known interacting proteins of periostin are depicted based on the multi-domain structure of periostin. CTD carboxyl-terminal domain, HBD heparin-binding domain *(Adapted from Kii et al. 2017).*

1.6 Periostin in the Oral Cavity

Originally described in the oral cavity within the periodontal ligament, periostin has now been shown to also be highly expressed in developing teeth at epithelial-to-mesenchymal interaction sites and the periosteum (H. Rios et al., 2005; Wen et al., 2010). Periostin is also associated with several pathological conditions, including our analysis of the stroma and differentiated odontogenic epithelium of human ameloblastic fibromas, ameloblastic fibro-odontomas and odontomas (Chau et al., 2013), in peripheral and central ossifying fibromas, focal cemento-osseus dysplasia, fibrous dysplasia (Chau et al., 2013) as well as oral squamous-cell carcinoma (Siriwardena et al., 2006).

1.6.1 Periostin in orofacial tissue development

In developing teeth, POSTN mRNA and protein are asymmetrically localized to the lingual/palatal and buccal regions during early epithelial-mesenchymal interaction sites, where it could be linked with deposition and organization of other ECM adhesion molecules (Kruzynska-Frejtag et al., 2004; Romanos et al., 2014). During tooth morphogenesis, at the cap and early bell stage of the tooth germs, periostin is expressed at the interface between the inner enamel epithelium and pre-odontoblasts, as well as in mesenchymal tissues around the cervical loop and dental follicles which then disappear in advance of tooth development. During late bell and mineralization phases of tooth development, periostin is expressed in dental papilla cells and trans-differentiating odontoblasts (Suzuki et al., 2004).

1.6.2 Periostin in postnatal orofacial tissues

In the adult rodent, periostin expression is predominantly identified in the periodontium (Romanos et al., 2014). Immunoelectron microscopic observation of the mature PDL verified the localization of periostin between the cytoplasmic processes of periodontal fibroblasts and cementoblasts and the adjacent collagen fibrils in mice. This finding suggests that periostin participates in various cellular events that are involved in maintaining the integrity of adult teeth, particularly at the sites of hard–soft tissue interface,

serving as adhesive equipment for bearing mechanical forces, including occlusal force and tooth eruption (Romanos et al., 2014; Suzuki et al., 2004). In situ hybridization and immunohistochemical analysis of rodent mandibles revealed the presence of periostin on the alveolar bone surface (Suzuki et al., 2004). The importance of periostin in the maintenance of the PDL integrity is also highlighted by studies using transgenic mice where periostin is genetically deleted. Although periostin knockout (*Postn*$^{-/-}$) mice are viable, the deletion results in defective collagen fibrillogenesis, due to reduction in fibril diameter and defective collagen crosslinking (Norris et al., 2007; Sata et al., 2008), resulting in loss of architecture and functional disruption of several collagenous-based tissues, particularly those subject to constant mechanical loading, such as the PDL, heart, and bone (H. Rios et al., 2005). Micro-computed topography imaging analysis of *Postn*$^{-/-}$ mice skulls revealed the early onset of severe periodontal disease, significant reduction in bone density, structural defects in the incisors resulting in enhanced tooth wear, and showed that orbital bones are completely missing or fail to fuse properly (Hamilton, 2008b). Removal of masticatory forces reduced this damage, showing that the loss of periostin likely impairs the ability of the tissue to withstand mechanical loading (H. F. Rios et al., 2008). Additionally, the PDL of *Postn*$^{-/-}$ mice demonstrated an uneven, irregular distribution of several crucial ECM proteins, such as type-I collagen, fibronectin, and tenascin C (Tabata et al., 2014).

Periostin also plays a role in controlling postnatal tooth formation. In wild-type mice, periostin is expressed in pre-odontoblasts, odontoblasts and ameloblasts, but genetic deletion of periostin in *Postn*$^{-/-}$ mice resulted in a massive increase in dentin formation after mastication and significant enamel defects (H. Rios et al., 2005). Deletion of periostin also resulted in the alteration of expression profiles of many non-collagenous proteins such as dentin sialophosphoprotein (DSPP), dentin matrix protein 1 (DMP1), bone sialoprotein (BSP), and osteopontin (OPN) in incisor dentin (Ma et al., 2011), as well as to morphological changes of the osteocytes (from spindle to round shape) in the jaws as shown by acid-etched scanning electron microscopy (Ren et al., 2015). FAM20C, a member of "Family with sequence similarity 20" also known as DMP4 in mice (Hao et al., 2007), is required for maintenance of healthy periodontal tissues and functions as an

intracellular protein kinase in the secretory pathway (P. Liu et al., 2014). Recently it was shown that FAM20C directly binds to periostin via the Fas-I domain and phosphorylates periostin *in vitro*. In addition, immunohistochemical analysis demonstrated that immunolocalization of FAM20C in murine PDL overlapped with that of periostin (Lin et al., 2020). Taken together, periostin plays a crucial role in the remodeling of collagen matrix and induction of various non-collagenous proteins in dental tissues, showing that periostin is critical for the postnatal tooth and periodontium development, as well as the maintenance of PDL integrity (Du & Li, 2017; Romanos et al., 2014).

1.6.3 Periostin in periodontal inflammation & oral wound healing

Controlled degradation of the ECM is essential in physiological situations involving connective tissue remodeling, such as tissue morphogenesis, repair, and angiogenesis (Petreaca & Martins-Green, 2020). However, excessive breakdown of connective tissue components plays an important role in destruction of overall tissue architecture, *e.g.* the irreversible destruction of periodontal support tissues in periodontitis, such as the alveolar bone, PDL, and root cementum leading to tooth loss (Ravanti et al., 1999). The first to investigate the influence of spatial and temporal periodontal inflammation on the levels of the periostin in an inflammatory-induced periodontal disease model *in vivo* was Padial-Molina and colleagues in a series of animal and clinical studies (Padial-Molina et al., 2012). Using a ligature periodontal inflammatory disease model in rats they found that periostin immunoreactivity is reduced in the presence of inflammation on the PDL and is correlated with detrimental changes to the periodontium over time (Padial-Molina et al., 2012). *In vitro*, human PDL (hPDL) cells had lower periostin protein levels when treated with TNFα and/or bacterial endotoxin. However, these changes were only observed when cells were cultured in a mechanically challenged environment but not in the un-loaded control condition, and the high variability among the groups with an unclear pattern makes it difficult to draw conclusions (Padial-Molina et al., 2013). When exogenous periostin was added to the experimental conditions, hPDL cells exhibited increased proliferation and migration (Padial-Molina et al., 2014). A separate study demonstrated that while IL-4 and IL-13 cytokines significantly induced periostin production in human periodontal ligament

(hPDL) and human gingival fibroblasts (hGF) cultures, no stimulatory effect was observed by TNF-α or bacterial endotoxin on the production of periostin. Additionally, exogenous periostin did not have a significant effect on the production of inflammatory cytokines by hPDL or hGF cells, suggesting that although these cells may be a source of periostin in periodontitis lesions, its role in the inflammatory response or in matrix-protein metabolism might be limited (Nakajima et al., 2014). Tang et al. using human periodontal ligament stem cells (PDLSCs) investigated the role of periostin under inflammatory conditions in the periodontum and found that periostin promoted both the migration and osteogenic differentiation potential of PDLSCs via the JNK signaling pathway with TNFα treatment (Y. Tang et al., 2017).

In clinical studies investigating periostin levels in the gingival crevicular fluid (GCF) (Aral et al., 2016; Balli et al., 2015) and *Postn* mRNA in tissues (Sankardas et al., 2019) at different stages of periodontal disease, it was shown that the total amount and concentration of periostin in the GCF, as well as *Postn* mRNA levels, are reduced with the progression and severity of the disease from healthy controls to chronic periodontitis groups and correlate negatively with clinical parameters of disease (Sankardas et al., 2019). When looking at the expression profile of periostin in GCF/wound fluid over time after periodontal surgery, it was shown that periostin levels increase after surgery, peak at 48 h and are higher in patients with periodontal disease when compared to healthy controls. For both groups periostin levels returned to baseline levels within 2 weeks. This transient local increase of periostin in the GCF after eliminating the chronic inflammatory stimuli and bacterial challenge by periodontal surgery in periodontally affected sites suggests the potential role of periostin in the maturation and stability of the connective tissue (Padial-Molina et al., 2015). Similar results were also reported in healthy patients and patients with chronic periodontitis post non-surgical low-level laser therapy (Kumaresan et al., 2016).

Extracellular matrix molecules are actively remodeled during wound healing and chronic inflammatory diseases, such as periodontitis (Birkedal-Hansen, 1993). Wound healing in soft connective tissues, such as the oral mucosa and the gingival tissue, is defined as a coordinated series of overlapping phases: hemostasis, inflammation, proliferation and

remodeling, concomitant with epithelial barrier formation, which lead to the resolution of the injury (Karamanos et al., 2019).

The oral mucosa and gingival tissues typically heal with minimal scarring, with many similarities evident to the healing described for fetal tissue (Häkkinen et al., 2014; Larjava, 2013). Using a gingivectomy model in rats, it has been shown that periostin regulates ECM synthesis, upregulating fibronectin and collagen synthesis via integrin β1, FAK and JNK, but it is not associated with myofibroblast differentiation during gingival wound healing (Kim, Nikoloudaki, Michelsons, et al., 2019). The low number of myofibroblasts, as shown by the absence of α-smooth muscle immunoreactivity in the wounded tissues, is postulated as an underlying reason for the reduced scar formation in healing of the gingival tissue (Kim, Nikoloudaki, Michelsons, et al., 2019). *In vitro*, treatment with exogenous recombinant human periostin (rhPSTN) to gingival fibroblasts derived from human tissues resulted in increased fibronectin and collagen synthesis, an effect which was attenuated by pharmacological inhibition of FAK and JNK signaling. In support of the *in vivo* observations, the addition of rhPSTN did not induce myofibroblast differentiation or proliferation of gingival fibroblasts, in contrast to its effect on skin and hypertrophic scar fibroblasts as reported by other studies (Crawford et al., 2015; Elliott et al., 2012b; Maeda et al., 2019). In addition, gingival fibroblasts predominantly attach to periostin through β1-integrins (Kim, Nikoloudaki, Michelsons, et al., 2019). The inability of gingival fibroblasts to transition to myofibroblasts even in the presence of periostin may provide a possible explanation of scarless healing that is evident in attached gingiva compared to other tissues, such as skin (Nikoloudaki et al., 2020).

While gingival tissue typically heals without scarring, it is still associated with several fibrotic conditions including drug-induced gingival enlargement (DIGE). DIGE is a pathological condition that develops as a side effect from the systemic administration of the antihypertensive drug nifedipine and anti-seizure drugs, and it is classified as a fibrotic lesion (Brown et al., 1991; Nyska et al., 1994). As such, it is characterized by imbalance in the remodeling and deposition of ECM. Gingival connective tissue from patients with DIGE showed increased immunoreactivity of periostin when compared to healthy

individuals, but absence of α-smooth muscle actin (α-SMA) expressing cells (Kim et al., 2013, 2015). *In vitro*, periostin mRNA and protein levels were up-regulated in response to nifedipine treatment via a TGFβ−dependent mechanism (Kim et al., 2013). Treatment of human gingival fibroblasts *in vitro* with different concentrations of phenytoin also resulted in increased periostin protein levels, which correlated with phospho-Smad3 (p-SMAD3) phosphorylation, suggesting common mechanisms are responsible for DIGE irrespective of the drug (Kim, Nikoloudaki, Darling, et al., 2019). Based on the fact that DIGE is defined as a fibrotic lesion, the molecular pathology is in direct contrast to skin scarring, in that no differentiation or persistence of myofibroblast is associated with the condition.

The palatal mucoperiosteum, even though part of the oral cavity, has been shown to exhibit significant scarring after surgical procedures. It remains critical to fully understand the underlying molecular and cellular mechanisms responsible for ECM accumulation in the palate during the wound healing process. Verstappen et al., using a rat model, found that there are significantly more myofibroblasts in the wounded mucoperiosteum than are evident in skin wounds, which they attributed to the different contractile abilities that these tissues possess and correlated their findings with the different wound healing patterns of these tissues (Verstappen et al., 2012). The investigation of distinct healing patterns among skin, gingiva and the palatal mucoperiosteum could provide deeper understanding of how differences in molecular composition and physical properties of these tissues lead to the different healing outcomes. It would therefore be intriguing to assess the role of periostin in palatal tissues, which - while still in the oral cavity- is strongly associated with scarring after injury.

1.6.4 Periostin in oral pathology

Periostin has also been identified in several pathological, non-neoplastic conditions, including our analysis of the stroma and differentiated odontogenic epithelium of human ameloblastic fibromas, ameloblastic fibro-odontomas and odontomas (Chau et al., 2013), in peripheral and central ossifying fibromas, focal cemento-osseus dysplasia, fibrous dysplasia (Chau et al., 2013), oral lichen planus (Zhang et al., 2018) and ameloblastomas (Kang et al., 2018).

Studies on periostin expression in human cancers have demonstrated an increased expression in a variety of solid tumors where it is associated with their malignant behavior (Extensively reviewed by: (Cui et al., 2017; González-González & Alonso, 2018)). Specifically in oral leukoplakia (Guan et al., 2019) and head and neck squamous cell carcinomas (HNSCCs), increased periostin expression appears to be directly proportional to the invasiveness and aggression of the disease (Y. Kudo et al., 2006; Qin et al., 2016; Siriwardena et al., 2006; Sundar et al., 2018). The serum periostin level in head and neck squamous cell carcinoma patients correlates well with that of VEGF-C and with malignant tumor behavior, including increased tumor stage and lymph node metastasis. Periostin-promoted lymphangiogenesis is mediated by the increased secretion of VEGF-C in cancer cells and by migration and tube formation via Src and Akt activity (Y. Kudo et al., 2012). TGF-β3 signaling promotes periostin expression by cancer-associated fibroblasts (CAFs) resulting in growth, migration and invasion of cancer cells (Qin et al., 2016). Periostin secreted by CAFs also promotes cancer stemness in HNSCCs by activating protein tyrosine kinase 7 (Yu et al., 2018). Furthermore, bone marrow mesenchymal stem cells promoted proliferation, invasion, survival, tumorigenicity and migration of head and neck cancer through periostin-mediated PI3K/Akt/mTOR activation (C. Liu et al., 2018). Based on these findings, periostin could be considered a biomarker with prognostic value of malignant behaviors in HNSCC and a potential target for future therapeutic intervention of HNSCC patients (Yang et al., 2020).

Figure 1-3 Functions of periostin in maintaining health of oral and dental tissues

1.7 Therapeutic Applications of Periostin

The use of neutralizing antibodies against periostin has been mainly investigated in the context of cancer invasion and metastasis. Several reports provide promising results for the potential use of highly-specific anti-periostin antibodies to inhibit metastatic and migratory properties of periostin expressing cells and stroma in ovarian (Zhu et al., 2011) and breast cancer (Van Snick et al., 2016).

More recently, efforts have shifted to the utilization of aptamers as a therapeutic target for periostin. Aptamers are single-stranded oligonucleotides that bind to specific target molecules. Once bound to a specific target, some aptamers are capable of inhibiting its activity (Song et al., 2012). Data from in vivo and in vitro studies demonstrated favorable results for the application of periostin-binding aptamers for the specific inhibition of periostin in peritoneal (Nam et al., 2017) and renal (Um et al., 2017) fibrosis. Local administration of molecules that target and block periostin during wound healing could also be achieved through tissue bioengineering techniques. Biomaterials, such as different types of scaffolds, can be designed to achieve temporal and spatial control over the release of such inhibiting molecules (Rambhia & Ma, 2015), and provide a promising therapeutic solution for cutaneous fibrosis and scarring post-wounding.

1.8 βigh3

TGF-β-induced protein (βigh3) and periostin are considered paralogs because of their structural similarity, as they both contain a single emilin (EMI) and four fasciclin-1 (FAS1) domains (Fig. 1.4). Similar to periostin, βigh3 is also induced by TGFβ signaling in areas of tissue injury and is secreted by activated fibroblasts in the ECM (García-Castellanos et al., 2017). βigh3 binds directly to collagens type I, II and IV (Hashimoto et al., 1997) as well as to proteoglycans, such as biglycan and decorin (Reinboth et al., 2006), where it modulates cell growth, adhesion and migration, tumorigenesis, wound healing, and apoptosis (Mosher et al., 2015). βigh3 is expressed in various tissues, including the bone, cartilage, cornea, heart, liver, and skin (LeBaron et al., 1995; Schwanekamp et al., 2017).

1.8.1 βigh3 in orofacial tissues development

During murine embryogenesis βigh3 is expressed in craniofacial cartilage and growth plates (Ferguson et al., 2003), and the developing tongue (Choi et al., 2009). Han and colleagues found that βigh3 plays a role in chondrocyte and osteoblast differentiation during endochondral ossification (Han et al., 2008). Genetic deletion of βigh3 in *Tgfbi* knockout mice resulted in reduced skeletal size and alterations in cartilage and bone, characterized by matrix degradation (J. M. Lee et al., 2014).

1.8.2 βigh3 in Postnatal tissues

βigh3 is also expressed in human PDL tissues. *In vitro* mineralization assay of hPDL showed that exogenous addition of βigh3 has an inhibitory effect on their mineralization (Ohno et al., 2002). The same research group also showed that during experimental tooth movement of human premolars, βigh3 expression was significantly increased in the PDL (Doi et al., 2003). Recently, βigh3 was also found to be expressed in rat pulp, where it could be associated with reparative dentinogenesis pointing to the potential therapeutic role of βigh3 in the pulpal repair process (Serita et al., 2017).

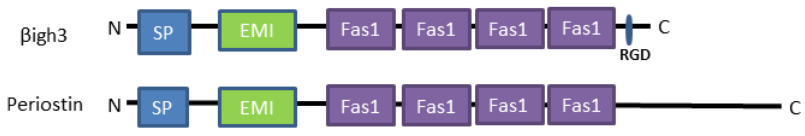

Figure 1-4 Periostin and βigh3 multi-domain structure.
As a matricellular protein, βigh3 is considered a paralog of Postn because of their structural similarity.

1.9 Cell recruitment and origin

During wound healing myofibroblast progenitors proliferate and migrate into the newly formed granulation tissue and differentiate into contractile myofibroblasts that secrete ECM proteins, especially collagens (Hinz, 2007). Different factors have been found to trigger the differentiation of the cells to a myofibroblastic phenotype, including the microenvironmental matrix stiffness, signaling molecules such as TGFβ1, or ECM components such as matricellular proteins, e.g. Periostin, or the ED-A splice variant of fibronectin (Hinz, 2007; Serini et al., 2002a). Apart from the above mentioned extrinsic factors, recent evidence also suggests that myofibroblast progenitor-specific intrinsic differences can alter how they respond to extrinsic stimuli (Driskell et al., 2013; Jiang & Rinkevich, 2021). Extrinsic factors can be inducive to myofibroblast differentiation, but intrinsic cell characteristics can ultimately control the degree to which a myofibroblast progenitor responds, as well as the downstream effect of that response. While the majority of evidence emerges from studies done in skin, liver and other organs, there are only few reports about the presence of embryonically distinct cell populations within the oral environment (Byrd et al., 2019; Jiang & Rinkevich, 2021). The discovery of distinct cell subpopulations within different areas of the oral cavity assessed through lineage-tracing techniques, and the understanding of their specific roles could provide new insights in the differences between oral and skin fibroblasts in wound healing.

Lineage tracing technology has been used to identify several distinct myofibroblast progenitor populations that play a role in skin repair and fibrosis, including fibroblasts, perivascular cells, adipogenic lineages, and bone-marrow derived populations (Driskell et al., 2013; Dulauroy, Carlo, et al., 2012; Jiang & Rinkevich, 2021; LeBleu & Neilson, 2020; Rinkevich et al., 2015b). Potential sources of myofibroblast progenitors include epithelial cells and endothelial cells, derived through a process termed epithelial-mesenchymal (Kalluri & Weinberg, 2009) or endothelial-mesenchymal transition (Zeisberg et al., 2007); circulating bone marrow–derived fibrocytes, tissue-resident fibroblasts, and other mesenchymal cells related to blood vessels, including pericytes, adventitial cells, and

mesenchymal stem cells (Figure 1.5) (MSCs) (Crisan et al., 2008; Di Carlo & Peduto, 2018; Hinz, 2010b; Zent & Guo, 2018b).

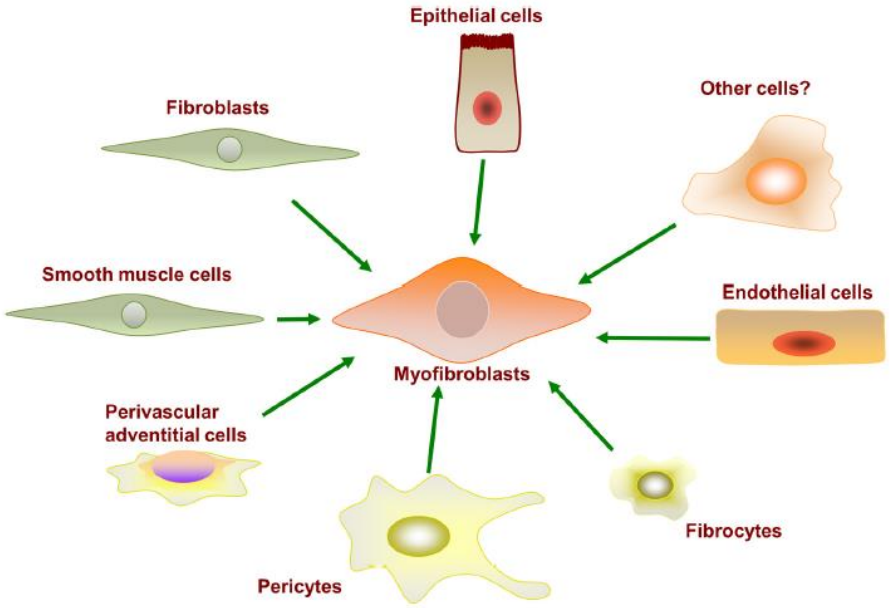

Figure 1-5 Myofibroblasts can differentiate from a variety of precursor cell types
(Schematic adapted from Kendal et al. 2014)

Pericytes are peri-endothelial cells found encircling the endothelial cells of the microvasculature (Greenhalgh et al., 2013), and their contribution in fibrosis of different organs still remains controversial (Guimarães-Camboa et al., 2017b; Kramann et al., 2013; Lemos & Duffield, 2018). Different markers have been used to detect pericytes, such as Rgs5, Pdgfrβ, nestin Tbx18, CD146 and NG2 (Neuron-glial antigen 2, which encodes chondroitin sulfate proteoglycan expressed in oligodendrocytes progenitor, myeloid, and perivascular cells) (Cathery et al., 2018; Yamazaki & Mukouyama, 2018). Lineage tracing experiments have identified cell populations associated with the perivascular space which are activated upon tissue injury and exhibit profibrotic phenotypes, characterized by expression of αSMA and production of fibrillar collagen and other ECM proteins (Dulauroy, Di Carlo, et al., 2012). Genetic fate mapping has shown that resident pericytes

in the liver (hepatic stellate cells) (Mederacke et al., 2013), the kidney (Y.-T. Chen et al., 2011; Humphreys et al., 2010a) and the lungs (Hung et al., 2013) account for the major sources of myofibroblasts post-injury and contribute significantly to fibrotic repair. On the contrary, another study using lineage tracing in a model of murine kidney fibrosis found that pericytes are not a source of myofibroblasts (LeBleu et al., 2013). More specifically, they used lineage tracing of the commonly accepted pericyte markers PDGFRβ and NG2 and found that, upon injury, these cells expanded but contributed to only a small fraction of α-SMA positive myofibroblasts. Moreover, ablation of proliferating PDGFRβ+ or NG2+ cells using a thymidine kinase/ ganciclovir strategy, did not alter matrix deposition following unilateral ureteral obstruction induced kidney fibrosis (LeBleu et al., 2013). In another study, a lineage tracing strategy using expression of the T-box 18 (Tbx18) transcription factor to label smooth muscle cells and pericytes throughout the mouse provided strong evidence that these cell types are not progenitors of myofibroblasts during muscle or cardiac fibrosis (Guimarães-Camboa et al., 2017a). Overall, these studies suggest that various resident cells are likely the major contributors of matrix producing cells during wound healing response, and recent lineage tracing studies highlight that some of the heterogeneity exhibited by adult fibroblast populations arises from distinct embryonic lineages.

Analysis of cell populations through lineage tracing experiments in the oral cavity or the hard palate is sparse in the literature. Utilizing lineage tracing techniques in *Wnt1-Cre;Zsgreen*$^{fl/fl}$ mice it was demonstrated that all the tendons and mesenchyme embedding the soft palate muscles are neural crest-derived, proposing that the posterior attachment of the soft palate to the pharyngeal wall is an interface between the neural crest- and mesoderm-derived mesenchyme in the craniofacial region (Grimaldi et al., 2015). Although regional clonal diversity was also recently demonstrated in the cells of the epithelium that covers the hard palate in mice (Byrd et al., 2019; Jones et al., 2019; Yuan et al., 2019), there is limited analysis of the stromal cells of the palatal mucoperiosteum. Lineage tracing experiments have identified that neural crest-derived cells persist in adult tissues in some areas of the oral mucosa and that Lgr5-lineage-positive cells participate in

the maintenance of the stroma (Boddupally et al., 2016). Exploring the presence and roles of distinct cell subpopulations with different embryologic signatures within the oral tissues may shed light on why some areas in the oral cavity heal with minimal scarring (buccal mucosa, gingiva) when compared to the skin, while others are more prone to scarring after reconstruction surgery, such as the palate.

1.9.1 Foxd1 and NG2 as markers for myofibroblast progenitors

Foxd1 is a transcription factor expressed primarily during development, in paraxial mesoderm-derived populations (Guillaume et al., 2009). Using a Foxd1-Cre knock-in mouse crossed with a Rosa26-loxp-stop-loxp(lsl)-*lacZ* reporter mouse, Humphreys *et al.* (2010) were able to provide evidence for a mesenchymal source of myofibroblasts during kidney fibrosis (Humphreys et al., 2010b). This group used this same model to demonstrate that Foxd1-progenitor– derived pericytes expand after bleomycin lung injury, and activate expression of collagen-I(a)1 and the myofibroblast marker α-SMA in fibrotic foci, showing that 68% of α-SMA-expressing cells in fibrotic lungs are pericyte-derived (Hung et al., 2013). A recent study using a murine cutaneous wounding model showed that Foxd1-lineage progeny cells expand upon injury and contribute to the stromal population and αSMA-positive myofibroblasts, but did not contribute to perivascular and endothelial cells (Walker et al., 2021). In skin, Foxd1-derived progeny account for a subset of dermal fibroblasts and myofibroblasts during wound healing (Walker et al., 2021). In excisional wounds in skin Foxd1-lineage positive (FLP) and Foxd1-lineage negative (FLN) fibroblasts were both found to produce α-SMA contributing to activated myofibroblasts during tissue repair. Interestingly, these cell populations appeared to have unique expression profiles, with FLP cells showing enhanced expression of genes associated with ECM synthesis and remodelling, while FLN populations are associated with signalling/microenvironment, indicating that they have unique specializations and potentially work together in concert during homeostasis and repair (Walker et al., 2021) .

Pericyte function could be tissue-specific as it be influenced by the organ in which the cells reside: In lung two pericyte populations arise from the same Foxd1 progenitor, one of which co-expresses fibroblast and pericyte markers (Col1+ Pdgfrα+ Pdgfrβ+ Ng2+)

(Barron et al., 2016). Type-1 pericytes (Nestin-negative, NG2-positive), produce collagen and contribute to fibrosis in skeletal muscle, but not in the kidney or the heart (Birbrair et al., 2014). In the skin, lineage tracing showed that NG2-positive cells did not give rise to any dermal fibroblast subpopulations during wound healing (Goss et al., 2021), contrary to other perivascular populations (Dulauroy, Carlo, et al., 2012). NG2-positive cells remained associated only with blood vessels, restricted to forming NG2+ blood vessel associated cells, most of which express Pdgfrα and/or Pdgfrβ. (Goss et al., 2021). The same study also showed that NG2-positive perivascular cells were primarily derived from interfollicular papillary and reticular fibroblasts during skin development as well as during regeneration, supporting a potential relationship between pericyte and fibroblast lineages (Goss et al., 2021). This evidence suggests that multiple subpopulations of pericytes may exist within different tissues and differentially contribute to myofibroblast formation and fibrosis. To date, evidence of perivascular cell recruitment and differentiation into myofibroblasts appears to be organ specific (Di Carlo & Peduto, 2018; Gomes et al., 2021; LeBleu & Neilson, 2020; Lemos & Duffield, 2018), and, currently, whether this process occurs within the palatal mucoperiosteum has yet to be tested. Since myofibroblasts contribute to palatal wound healing and are considered largely responsible for fibrotic tissue formation, we investigate their origin and recruitment during palatal wound healing in Chapter 4.

1.10 Thesis Overview

The overall focus of this thesis is to expand upon our understanding of fundamental mechanisms involved in the homeostasis and wound repair in oral tissues, with the ultimate goal of applying the findings to development of novel approaches and biomaterials with specific biochemical and biomechanical properties targeted to accelerate and enhance the healing process, while suppressing fibrosis, after dental and maxillofacial surgical procedures. We provide further evidence for tissue-specific effects of periostin's bioactivity, and cell-intrinsic differences that could provide deeper understanding of how

differences in cellular, molecular composition and physical properties of these tissues lead to the different healing outcomes.

First, the matricellular protein periostin was determined to be associated with fibronectin production, myofibroblast differentiation and infiltration of macrophages in wounded palatal tissues. The effects of periostin on contractile ability and fibronectin synthesis of palatal fibroblasts were also modulated by the stiffness of the microenvironment via integrin-β1/RhoA pathway, providing further evidence that periostin and the stiffness of the ECM act as modulators of matrix synthesis and myofibroblast differentiation during palatal healing. Next, progress is made to determine the role of periostin in the homeostasis of the periodontal ligament under normal and osteogenic conditions, highlighting the diverse and tissue-specific bioactivity of periostin. Finally, a cell lineage tracing strategy previously used to identify profibrotic populations in the kidney, lung and skin was determined to label a vascular cell population in the palatal mucoperiosteum, providing further evidence about the intrinsic differences of cell populations that lead to distinct healing patterns among different tissues.

Through these diverse studies, insights into effects of the ECM microenvironment in the context of palatal repair and the intrinsic cell differences of populations contributing to the healing process have been made. Application of this translatable knowledge could be utilized in the future for development of biomaterials that can be targeted and guided to enhance healing outcomes while inhibiting undesired effects, such as scarring and fibrosis in a tissue-specific manner.

1.11 References

Amizuka, N., Nishiyama, T., Saito, M., Li, M., Matsumoto, K., Kudo, A., & Kii, I. (2009). Incorporation of Tenascin-C into the Extracellular Matrix by Periostin Underlies an Extracellular Meshwork Architecture. *Journal of Biological Chemistry*, *285*(3), 2028–2039. https://doi.org/10.1074/jbc.m109.051961

Aral, C. A., Köseoğlu, S., Sağlam, M., Pekbağrıyanık, T., & Savran, L. (2016). Gingival Crevicular Fluid and Salivary Periostin Levels in Non-Smoker Subjects With Chronic and Aggressive Periodontitis: Periostin Levels in Chronic and Aggressive Periodontitis. *Inflammation*, *39*(3), 986–993. https://doi.org/10.1007/s10753-016-0328-0

Arora, H., Madapusi, B. T., Ramamurti, A., Narasimhan, M., Periasamy, S., & Rao, S. R. (2016). Immunohistochemical localization of epithelial mesenchymal transition markers in cyclosporine a induced gingival overgrowth. *Journal of Clinical and Diagnostic Research*, *10*(8), ZC48–ZC52. https://doi.org/10.7860/JCDR/2016/20808.8271

Bai, Y., Nakamura, M., Zhou, G., Li, Y., Liu, Z., Ozaki, T., Mori, I., & Kakudo, K. (2010). Novel isoforms of periostin expressed in the human thyroid. *Japanese Clinical Medicine*, *1*, 13–20. https://doi.org/10.4137/JCM.S5899

Balli, U., Keles, Z. P., Avci, B., Guler, S., Cetinkaya, B. O., & Keles, G. C. (2015). Assessment of periostin levels in serum and gingival crevicular fluid of patients with periodontal disease. *Journal of Periodontal Research*, *50*(6), 707–713. https://doi.org/10.1111/jre.12254

Barrientos, S., Stojadinovic, O., Golinko, M. S., Brem, H., & Tomic-Canic, M. (2008). PERSPECTIVE ARTICLE: Growth factors and cytokines in wound healing. *Wound Repair and Regeneration*, *16*(5), 585–601. https://doi.org/10.1111/j.1524-475X.2008.00410.x

Barron, L., Gharib, S. A., & Duffield, J. S. (2016). Lung Pericytes and Resident Fibroblasts: Busy Multitaskers. *The American Journal of Pathology*, *186*(10), 2519–2531. https://doi.org/10.1016/j.ajpath.2016.07.004

Basu, A., Kligman, L. H., Samulewicz, S. J., & Howe, C. C. (2001). Impaired wound healing in mice deficient in a matricellular protein SPARC (osteonectin, BM-40). *BMC Cell Biology*, *2*, 15. https://doi.org/10.1186/1471-2121-2-15

Birbrair, A., Zhang, T., Files, D. C., Mannava, S., Smith, T., Wang, Z.-M., Messi, M. L., Mintz, A., & Delbono, O. (2014). Type-1 pericytes accumulate after tissue injury and produce collagen in an organ-dependent manner. *Stem Cell Research & Therapy*, *5*(6), 122. https://doi.org/10.1186/scrt512

Birkedal-Hansen, H. (1993). Role of cytokines and inflammatory mediators in tissue destruction. - Birkedalhansen—1993.pdf. In *Journal of periodontal research*.

Boddupally, K., Wang, G., Chen, Y., & Kobielak, A. (2016). Lgr5 Marks Neural Crest Derived Multipotent Oral Stromal Stem Cells: Lgr5 positive oral stromal stem cells. *STEM CELLS*, *34*(3), 720–731. https://doi.org/10.1002/stem.2314

Bodner, L., Dayan, D., Pinto, Y., & Hammel, I. (1993). Characteristics of palatal wound healing in desalivated rats. *Archives of Oral Biology*, *38*(1), 17–21. https://doi.org/10.1016/0003-9969(93)90149-G

Boink, M. A., van den Broek, L. J., Roffel, S., Nazmi, K., Bolscher, J. G. M., Gefen, A., Veerman, E. C. I., & Gibbs, S. (2016). Different wound healing properties of dermis, adipose, and gingiva mesenchymal stromal cells. *Wound Repair and Regeneration*, *24*(1), 100–109. https://doi.org/10.1111/wrr.12380

Bornstein, P. (1995). Diversity of function is inherent in matricellular proteins: An appraisal of thrombospondin 1. *The Journal of Cell Biology*, *130*(3), 503–506. https://doi.org/10.1083/jcb.130.3.503

Bornstein, P., & Sage, E. H. (2002a). Matricellular proteins: Extracellular modulators of cell function. *Current Opinion in Cell Biology*, *14*(5), 608–616. https://doi.org/10.1016/S0955-0674(02)00361-7

Bornstein, P., & Sage, E. H. (2002b). Matricellular proteins: Extracellular modulators of cell function. *Current Opinion in Cell Biology*, *14*(5), 608–616. https://doi.org/10.1016/S0955-0674(02)00361-7

Brown, R. S., Beaver, W. T., & Bottomley, W. K. (1991). On the mechanism of drug-induced gingival hyperplasia. In *Journal of Oral Pathology & Medicine*. https://doi.org/10.1111/j.1600-0714.1991.tb00419.x

Byrd, K. M., Piehl, N. C., Patel, J. H., Huh, W. J., Sequeira, I., Lough, K. J., Wagner, B. L., Marangoni, P., Watt, F. M., Klein, O. D., Coffey, R. J., & Williams, S. E. (2019). Heterogeneity within Stratified Epithelial Stem Cell Populations Maintains the Oral Mucosa in Response to Physiological Stress. *Cell Stem Cell*, *25*(6), 814-829.e6. https://doi.org/10.1016/j.stem.2019.11.005

Caetano, A. J., Yianni, V., Volponi, A., Booth, V., D'Agostino, E. M., & Sharpe, P. (2021). Defining human mesenchymal and epithelial heterogeneity in response to oral inflammatory disease. *ELife*, *10*, e62810. https://doi.org/10.7554/eLife.62810

Cai, L., Brophy, R. H., Tycksen, E. D., Duan, X., Nunley, R. M., & Rai, M. F. (2019). Distinct expression pattern of periostin splice variants in chondrocytes and ligament progenitor cells. *FASEB Journal : Official Publication of the Federation of American Societies for Experimental Biology*, *33*(7), 8386–8405. https://doi.org/10.1096/fj.201802281R

Caley, M. P., Martins, V. L. C., & O'Toole, E. A. (2015). Metalloproteinases and Wound Healing. *Advances in Wound Care*, *4*(4), 225–234. https://doi.org/10.1089/wound.2014.0581

Callebaut, I., Mignotte, V., Souchet, M., & Mornon, J. P. (2003). EMI domains are widespread and reveal the probable orthologs of the Caenorhabditis elegans CED-1 protein. *Biochemical and Biophysical Research Communications*, *300*(3), 619–623. https://doi.org/10.1016/s0006-291x(02)02904-2

Cañedo-Dorantes, L., & Cañedo-Ayala, M. (2019). Skin Acute Wound Healing: A Comprehensive Review. *International Journal of Inflammation*, *2019*, 3706315. https://doi.org/10.1155/2019/3706315

Cathery, W., Faulkner, A., Maselli, D., & Madeddu, P. (2018). Concise Review: The Regenerative Journey of Pericytes Toward Clinical Translation. *Stem Cells (Dayton, Ohio)*, *36*(9), 1295–1310. https://doi.org/10.1002/stem.2846

Chau, E., Daley, T., Darling, M. R., & Hamilton, D. (2013). The expression and immunohistochemical localization of periostin in odontogenic tumors of mixed epithelial/mesenchymal origin. *Oral Surgery, Oral Medicine, Oral Pathology and Oral Radiology*, *116*(2), 214–220. https://doi.org/10.1016/j.oooo.2013.05.008

Chazaud, B. (2014). Macrophages: Supportive cells for tissue repair and regeneration. *Immunobiology*, *219*(3), 172–178. https://doi.org/10.1016/j.imbio.2013.09.001

Chen, L., Arbieva, Z. H., Guo, S., Marucha, P. T., Mustoe, T. A., & DiPietro, L. A. (2010). Positional differences in the wound transcriptome of skin and oral mucosa. *BMC Genomics*, *11*(1), 471. https://doi.org/10.1186/1471-2164-11-471

Chen, Y.-T., Chang, F.-C., Wu, C.-F., Chou, Y.-H., Hsu, H.-L., Chiang, W.-C., Shen, J., Chen, Y.-M., Wu, K.-D., Tsai, T.-J., Duffield, J. S., & Lin, S.-L. (2011). Platelet-derived growth factor receptor signaling activates pericyte-myofibroblast transition in obstructive and post-ischemic kidney fibrosis. *Kidney International*, *80*(11), 1170–1181. https://doi.org/10.1038/ki.2011.208

Choi, K.-Y., Kim, H.-J., Cho, B.-C., Kim, I.-S., Kim, H.-J., & Ryoo, H.-M. (2009). A TGF-beta-induced gene, betaig-h3, is crucial for the apoptotic disappearance of

the medial edge epithelium in palate fusion. *Journal of Cellular Biochemistry*, *107*(4), 818–825. https://doi.org/10.1002/jcb.22180

Conway, S. J., Izuhara, K., Kudo, Y., Litvin, J., Markwald, R., Ouyang, G., Arron, J. R., Holweg, C. T. J., & Kudo, A. (2014). The role of periostin in tissue remodeling across health and disease. *Cellular and Molecular Life Sciences : CMLS*, *71*(7), 1279–1288. https://doi.org/10.1007/s00018-013-1494-y

Crawford, J., Nygard, K., Gan, B. S., & O'Gorman, D. B. (2015). Periostin induces fibroblast proliferation and myofibroblast persistence in hypertrophic scarring. *Experimental Dermatology*, *24*(2), 120–126. https://doi.org/10.1111/exd.12601

Crisan, M., Yap, S., Casteilla, L., Chen, C.-W., Corselli, M., Park, T. S., Andriolo, G., Sun, B., Zheng, B., Zhang, L., Norotte, C., Teng, P.-N., Traas, J., Schugar, R., Deasy, B. M., Badylak, S., Bűhring, H.-J., Giacobino, J.-P., Lazzari, L., … Péault, B. (2008). A Perivascular Origin for Mesenchymal Stem Cells in Multiple Human Organs. *Cell Stem Cell*, *3*(3), 301–313. https://doi.org/10.1016/j.stem.2008.07.003

Cui, D., Huang, Z., Liu, Y., & Ouyang, G. (2017). The multifaceted role of periostin in priming the tumor microenvironments for tumor progression. *Cellular and Molecular Life Sciences : CMLS*, *74*(23), 4287–4291. https://doi.org/10.1007/s00018-017-2646-2

Dally, J., Khan, J. S., Voisey, A., Charalambous, C., John, H. L., Woods, E. L., Steadman, R., Moseley, R., & Midgley, A. C. (2017). Hepatocyte Growth Factor Mediates Enhanced Wound Healing Responses and Resistance to Transforming Growth Factor-β1-Driven Myofibroblast Differentiation in Oral Mucosal Fibroblasts. *International Journal of Molecular Sciences*, *18*(9), 1843. https://doi.org/10.3390/ijms18091843

Dayan, D., Bodner, L., & Horowitz, I. (1992). Effect of salivary gland hypofunction on the healing of extraction wounds: A histomorphometric study in rats. *Journal of*

Oral and Maxillofacial Surgery, *50*(4), 354–358. https://doi.org/10.1016/0278-2391(92)90397-I

Dg, G. (1998). The role of apoptosis in wound healing. *The International Journal of Biochemistry & Cell Biology*, *30*(9). https://doi.org/10.1016/s1357-2725(98)00058-2

Di Carlo, S. E., & Peduto, L. (2018). The perivascular origin of pathological fibroblasts. *Journal of Clinical Investigation*, *128*(1), 54–63. https://doi.org/10.1172/JCI93558

Dipietro, L. a. (2003). *In Oral Mucosal and Cutaneous Wounds*. 621–626. https://doi.org/10.1177/154405910308200810

Doi, T., Ohno, S., Tanimoto, K., Honda, K., Tanaka, N., Ohno-Nakahara, M., Yoneno, K., Suzuki, A., Nakatani, Y., Ueki, M., & Tanne, K. (2003). Mechanical stimuli enhances the expression of RGD-CAP/βig-h3 in the periodontal ligament. In *Archives of Oral Biology* (Vol. 48, Issue 8, pp. 573–579). https://doi.org/10.1016/S0003-9969(03)00103-1

Doliana, R., Bot, S., Bonaldo, P., & Colombatti, A. (2000). EMI, a novel cysteine-rich domain of EMILINs and other extracellular proteins, interacts with the gC1q domains and participates in multimerization. *FEBS Letters*, *484*(2), 164–168. https://doi.org/10.1016/s0014-5793(00)02140-2

Driskell, R. R., Lichtenberger, B. M., Hoste, E., Kretzschmar, K., Simons, B. D., Charalambous, M., Ferron, S. R., Herault, Y., Pavlovic, G., Ferguson-Smith, A. C., & Watt, F. M. (2013). Distinct fibroblast lineages determine dermal architecture in skin development and repair. *Nature*, *504*(7479), 277–281. https://doi.org/10.1038/nature12783

Du, J., & Li, M. (2017). Functions of Periostin in dental tissues and its role in periodontal tissues' regeneration. *Cellular and Molecular Life Sciences*, *74*(23), 4279–4286. https://doi.org/10.1007/s00018-017-2645-3

Dulauroy, S., Carlo, S. E. D., Langa, F., Eberl, G., & Peduto, L. (2012). Lineage tracing and genetic ablation of ADAM12 + perivascular cells identify a major source of profibrotic cells during acute tissue injury. *Nature Medicine*. https://doi.org/10.1038/nm.2848

Dulauroy, S., Di Carlo, S. E., Langa, F., Eberl, G., & Peduto, L. (2012). Lineage tracing and genetic ablation of ADAM12 + perivascular cells identify a major source of profibrotic cells during acute tissue injury. *Nature Medicine*. https://doi.org/10.1038/nm.2848

Elliott, C. G., & Hamilton, D. W. (2011). Deconstructing fibrosis research: Do pro-fibrotic signals point the way for chronic dermal wound regeneration? *Journal of Cell Communication and Signaling*, *5*(4), 301–315. https://doi.org/10.1007/s12079-011-0131-5

Elliott, C. G., Wang, J., Guo, X., Xu, S. -w., Eastwood, M., Guan, J., Leask, A., Conway, S. J., & Hamilton, D. W. (2012a). Periostin modulates myofibroblast differentiation during full-thickness cutaneous wound repair. *Journal of Cell Science*, *125*(1), 121–132. https://doi.org/10.1242/jcs.087841

Elliott, C. G., Wang, J., Guo, X., Xu, S. -w., Eastwood, M., Guan, J., Leask, A., Conway, S. J., & Hamilton, D. W. (2012b). Periostin modulates myofibroblast differentiation during full-thickness cutaneous wound repair. *Journal of Cell Science*. https://doi.org/10.1242/jcs.087841

Ellis, S., Lin, E. J., & Tartar, D. (2018). Immunology of Wound Healing. *Current Dermatology Reports*, *7*(4), 350–358. https://doi.org/10.1007/s13671-018-0234-9

Etulain, J. (2018). Platelets in wound healing and regenerative medicine. *Platelets*, *29*(6), 556–568. https://doi.org/10.1080/09537104.2018.1430357

Ferguson, J. W., Mikesh, M. F., Wheeler, E. F., & LeBaron, R. G. (2003). Developmental expression patterns of Beta-ig (βIG-H3) and its function as a cell adhesion protein. *Mechanisms of Development*, *120*(8), 851–864. https://doi.org/10.1016/S0925-4773(03)00165-5

Gabbiani, G. (1996). The cellular derivation and the life span of the myofibroblast. *Pathology, Research and Practice*, *192*(7), 708–711. https://doi.org/10.1016/S0344-0338(96)80092-6

Gadermaier, E., Tesarz, M., Suciu, A. A.-M., Wallwitz, J., Berg, G., & Himmler, G. (2018). Characterization of a sandwich ELISA for the quantification of all human periostin isoforms. *Journal of Clinical Laboratory Analysis*, *32*(2). https://doi.org/10.1002/jcla.22252

García-Castellanos, R., Nielsen, N. S., Runager, K., Thøgersen, I. B., Lukassen, M. V., Poulsen, E. T., Goulas, T., Enghild, J. J., & Gomis-Rüth, F. X. (2017). Structural and Functional Implications of Human Transforming Growth Factor β-Induced Protein, TGFBIp, in Corneal Dystrophies. *Structure*, *25*(11), 1740-1750.e2. https://doi.org/10.1016/j.str.2017.09.001

Giannopoulou, C., & Cimasoni, G. (1996). Functional Characteristics of Gingival and Periodontal Ligament Fibroblasts. *Journal of Dental Research* , *75*(3), 895–902. https://doi.org/10.1177/00220345960750030601

Glim, J. E., Beelen, R. H. J., Niessen, F. B., Everts, V., & Ulrich, M. M. W. (2015). The number of immune cells is lower in healthy oral mucosa compared to skin and does not increase after scarring. *Archives of Oral Biology*, *60*(2), 272–281. https://doi.org/10.1016/j.archoralbio.2014.10.008

Glim, J. E., Egmond, M. V., Niessen, F. B., Everts, V., Beelen, R. H. J., Judith, M., & Glim, E. (n.d.). *Detrimental dermal wound healing: What can we learn from the oral mucosa?* https://doi.org/10.1111/wrr.12072

Glim, J. E., Everts, V., Niessen, F. B., Ulrich, M. M., & Beelen, R. H. J. (2014). Extracellular matrix components of oral mucosa differ from skin and resemble that of foetal skin. *Archives of Oral Biology*, *59*(10), 1048–1055. https://doi.org/10.1016/j.archoralbio.2014.05.019

Glim, J. E., Van Egmond, M., Niessen, F. B., Everts, V., Beelen, R. H. J., Judith, M., & Glim, E. (n.d.). *Detrimental dermal wound healing: What can we learn from the oral mucosa?* https://doi.org/10.1111/wrr.12072

Gomes, R. N., Manuel, F., & Nascimento, D. S. (2021). The bright side of fibroblasts: Molecular signature and regenerative cues in major organs. *Npj Regenerative Medicine*, *6*(1), 43. https://doi.org/10.1038/s41536-021-00153-z

González-González, L., & Alonso, J. (2018). Periostin: A matricellular protein with multiple functions in cancer development and progression. *Frontiers in Oncology*, *8*(JUN), 1–15. https://doi.org/10.3389/fonc.2018.00225

Goss, G., Rognoni, E., Salameti, V., & Watt, F. M. (2021). Distinct Fibroblast Lineages Give Rise to NG2+ Pericyte Populations in Mouse Skin Development and Repair. *Frontiers in Cell and Developmental Biology*, *9*, 1240. https://doi.org/10.3389/fcell.2021.675080

Greaves, N. S., Ashcroft, K. J., Baguneid, M., & Bayat, A. (2013). Current understanding of molecular and cellular mechanisms in fibroplasia and angiogenesis during acute wound healing. *Journal of Dermatological Science*, *72*(3), 206–217. https://doi.org/10.1016/j.jdermsci.2013.07.008

Greenhalgh, S. N., Iredale, J. P., & Henderson, N. C. (2013). Origins of fibrosis: Pericytes take centre stage. *F1000Prime Reports*. https://doi.org/10.12703/p5-37

Grimaldi, A., Parada, C., & Chai, Y. (2015). A Comprehensive Study of Soft Palate Development in Mice. *PLOS ONE*, *10*(12), e0145018. https://doi.org/10.1371/journal.pone.0145018

Guan, W.-Q., Li, Q., & Ouyang, Q.-M. (2019). Expression and Significance of Periostin in Tissues and Serum in Oral Leukoplakia and Squamous Cell Carcinoma. *Cancer Biotherapy & Radiopharmaceuticals*, *34*(7), 444–450. https://doi.org/10.1089/cbr.2018.2764

Guillaume, R., Bressan, M., & Herzlinger, D. (2009). Paraxial mesoderm contributes stromal cells to the developing kidney. *Developmental Biology*. https://doi.org/10.1016/j.ydbio.2009.02.034

Guimarães-Camboa, N., Cattaneo, P., Sun, Y., Moore-Morris, T., Gu, Y., Dalton, N. D., Rockenstein, E., Masliah, E., Peterson, K. L., Stallcup, W. B., Chen, J., & Evans, S. M. (2017a). Pericytes of Multiple Organs Do Not Behave as Mesenchymal Stem Cells In Vivo. *Cell Stem Cell*. https://doi.org/10.1016/j.stem.2016.12.006

Guimarães-Camboa, N., Cattaneo, P., Sun, Y., Moore-Morris, T., Gu, Y., Dalton, N. D., Rockenstein, E., Masliah, E., Peterson, K. L., Stallcup, W. B., Chen, J., & Evans, S. M. (2017b). Pericytes of Multiple Organs Do Not Behave as Mesenchymal Stem Cells In Vivo. *Cell Stem Cell*. https://doi.org/10.1016/j.stem.2016.12.006

Häkkinen, L., Larjava, H., & Fournier, B. P. J. (2014). Distinct phenotype and therapeutic potential of gingival fibroblasts. *Cytotherapy*, *16*(9), 1171–1186. https://doi.org/10.1016/j.jcyt.2014.04.004

Häkkinen, L., Uitto, V. J., & Larjava, H. (2000). Cell biology of gingival wound healing. *Periodontology 2000*, *24*, 127–152. https://doi.org/10.1034/j.1600-0757.2000.2240107.x

Hamilton, D. W. (2008a). Functional role of periostin in development and wound repair: Implications for connective tissue disease. In *Journal of Cell Communication and Signaling*. https://doi.org/10.1007/s12079-008-0023-5

Hamilton, D. W. (2008b). Functional role of periostin in development and wound repair: Implications for connective tissue disease. *Journal of Cell Communication and Signaling*, *2*(1–2), 9–17. https://doi.org/10.1007/s12079-008-0023-5

Han, M. S., Kim, J. E., Shin, H. I., & Kim, I. S. (2008). Expression patterns of betaig-h3 in chondrocyte differentiation during endochondral ossification. *Experimental & Molecular Medicine*, *40*(4), 453–460. https://doi.org/10.3858/emm.2008.40.4.453

Hao, J., Narayanan, K., Muni, T., Ramachandran, A., & George, A. (2007). Dentin matrix protein 4, a novel secretory calcium-binding protein that modulates odontoblast differentiation. *The Journal of Biological Chemistry*, *282*(21), 15357–15365. https://doi.org/10.1074/jbc.M701547200

Harrison, J. W., & Jurosky, K. A. (1991a). Wound healing in the tissues of the periodontium following periradicular surgery. I. The incisional wound. *Journal of Endodontics*, *17*(9), 425–435. https://doi.org/10.1016/S0099-2399(07)80131-2

Harrison, J. W., & Jurosky, K. A. (1991b). Wound healing in the tissues of the periodontium following periradicular surgery. 2. The dissectional wound. *Journal of Endodontics*, *17*(11), 544–552. https://doi.org/10.1016/s0099-2399(06)81720-6

Hashimoto, K., Noshiro, M., Ohno, S., Kawamoto, T., Satakeda, H., Akagawa, Y., Nakashima, K., Okimura, A., Ishida, H., Okamoto, T., Pan, H., Shen, M., Yan, W., & Kato, Y. (1997). Characterization of a cartilage-derived 66-kDa protein (RCD-CAP/βig-h3) that binds to collagen. *Biochimica et Biophysica Acta - Molecular Cell Research*. https://doi.org/10.1016/S0167-4889(96)00147-4

Hinz, B. (2007). Formation and Function of the Myofibroblast during Tissue Repair. *Journal of Investigative Dermatology*, *127*(3), 526–537. https://doi.org/10.1038/sj.jid.5700613

Hinz, B. (2010a). The myofibroblast: Paradigm for a mechanically active cell. *Journal of Biomechanics*, *43*(1), 146–155. https://doi.org/10.1016/j.jbiomech.2009.09.020

Hinz, B. (2010b). The myofibroblast: Paradigm for a mechanically active cell. *Journal of Biomechanics*, *43*(1), 146–155. https://doi.org/10.1016/j.jbiomech.2009.09.020

Hinz, B. (2015a). Myofibroblasts. *Experimental Eye Research*, *142*, 56–70. https://doi.org/10.1016/j.exer.2015.07.009

Hinz, B. (2015b). The extracellular matrix and transforming growth factor-β1: Tale of a strained relationship. *Matrix Biology*, *47*, 54–65. https://doi.org/10.1016/j.matbio.2015.05.006

Hinz, B. (2016). Myofibroblasts. *Experimental Eye Research*, *142*, 56–70. https://doi.org/10.1016/j.exer.2015.07.009

Hof, W. van 't, Veerman, E. C. I., Amerongen, A. V. N., & Ligtenberg, A. J. M. (2014). Antimicrobial Defense Systems in Saliva. *Saliva: Secretion and Functions*, *24*, 40–51. https://doi.org/10.1159/000358783

Humphreys, B. D., Lin, S. L., Kobayashi, A., Hudson, T. E., Nowlin, B. T., Bonventre, J. V., Valerius, M. T., McMahon, A. P., & Duffield, J. S. (2010a). Fate tracing reveals the pericyte and not epithelial origin of myofibroblasts in kidney fibrosis. *American Journal of Pathology*, *176*(1), 85–97. https://doi.org/10.2353/ajpath.2010.090517

Humphreys, B. D., Lin, S. L., Kobayashi, A., Hudson, T. E., Nowlin, B. T., Bonventre, J. V., Valerius, M. T., McMahon, A. P., & Duffield, J. S. (2010b). Fate tracing reveals the pericyte and not epithelial origin of myofibroblasts in kidney fibrosis.

American Journal of Pathology, *176*(1), 85–97. https://doi.org/10.2353/ajpath.2010.090517

Hung, C., Linn, G., Chow, Y. H., Kobayashi, A., Mittelsteadt, K., Altemeier, W. A., Gharib, S. A., Schnapp, L. M., & Duffield, J. S. (2013). Role of lung Pericytes and resident fibroblasts in the pathogenesis of pulmonary fibrosis. *American Journal of Respiratory and Critical Care Medicine*, *188*(7), 820–830. https://doi.org/10.1164/rccm.201212-2297OC

Hutson, J. M., Niall, M., Evans, D., & Fowler, R. (1979). Effect of salivary glands on wound contraction in mice. *Nature*, *279*(5716), 793–795. https://doi.org/10.1038/279793a0

Hwang, E. Y., Jeong, M. S., Park, E. K., Kim, J. H., & Jang, S. B. (2014). Structural characterization and interaction of periostin and bone morphogenetic protein for regulation of collagen cross-linking. *Biochemical and Biophysical Research Communications*, *449*(4), 425–431. https://doi.org/10.1016/j.bbrc.2014.05.055

Iglesias-Bartolome, R., Uchiyama, A., Molinolo, A. A., Abusleme, L., Brooks, S. R., Callejas-Valera, J. L., Edwards, D., Doci, C., Asselin-Labat, M.-L., Onaitis, M. W., Moutsopoulos, N. M., Silvio Gutkind, J., & Morasso, M. I. (2018). Transcriptional signature primes human oral mucosa for rapid wound healing. *Science Translational Medicine*, *10*(451), eaap8798. https://doi.org/10.1126/scitranslmed.aap8798

Ishii, M., Arias, A. C., Liu, L., Chen, Y.-B., Bronner, M. E., & Maxson, R. E. (2012). A Stable Cranial Neural Crest Cell Line from Mouse. *Stem Cells and Development*, *21*(17), 3069–3080. https://doi.org/10.1089/scd.2012.0155

Jackson-Boeters, L., Wen, W., & Hamilton, D. W. (2009). Periostin localizes to cells in normal skin, but is associated with the extracellular matrix during wound repair. *Journal of Cell Communication and Signaling*, *3*(2), 125–133. https://doi.org/10.1007/s12079-009-0057-3

Janebodin, K., Horst, O. V., Ieronimakis, N., Balasundaram, G., Reesukumal, K., Pratumvinit, B., & Reyes, M. (2011). Isolation and Characterization of Neural Crest-Derived Stem Cells from Dental Pulp of Neonatal Mice. *PLOS ONE*, *6*(11), e27526. https://doi.org/10.1371/journal.pone.0027526

Jiang, D., Christ, S., Correa-Gallegos, D., Ramesh, P., Gopal, S. K., Wannemacher, J., Mayr, C. H., Lupperger, V., Yu, Q., Ye, H., Mück-Häusl, M., Rajendran, V., Wan, L., Liu, J., Mirastschijski, U., Volz, T., Marr, C., Schiller, H. B., & Rinkevich, Y. (2020). Injury triggers fascia fibroblast collective cell migration to drive scar formation through N-cadherin. *Nature Communications*, *11*(1). https://doi.org/10.1038/s41467-020-19425-1

Jiang, D., & Rinkevich, Y. (2021). Distinct fibroblasts in scars and regeneration. *Current Opinion in Genetics & Development*, *70*, 7–14. https://doi.org/10.1016/j.gde.2021.04.005

Jones, K. B., Furukawa, S., Marangoni, P., Ma, H., Pinkard, H., D'Urso, R., Zilionis, R., Klein, A. M., & Klein, O. D. (2019). Quantitative Clonal Analysis and Single-Cell Transcriptomics Reveal Division Kinetics, Hierarchy, and Fate of Oral Epithelial Progenitor Cells. *Cell Stem Cell*, *24*(1), 183-192.e8. https://doi.org/10.1016/j.stem.2018.10.015

Juráňová, J., Franková, J., & Ulrichová, J. (2017). The role of keratinocytes in inflammation. *Journal of Applied Biomedicine*, *15*(3), 169–179. https://doi.org/10.1016/j.jab.2017.05.003

Kalluri, R., & Weinberg, R. A. (2009). The basics of epithelial-mesenchymal transition. *Journal of Clinical Investigation*, *119*(6), 1420–1428. https://doi.org/10.1172/JCI39104

Kang, Y., Liu, J., Zhang, Y., Sun, Y., Wang, J., Huang, B., & Zhong, M. (2018). Upregulation of Periostin expression in the pathogenesis of ameloblastoma.

Pathology - Research and Practice, *214*(12), 1959–1965. https://doi.org/10.1016/j.prp.2018.08.028

Karamanos, N. K., Theocharis, A. D., Neill, T., & Iozzo, R. V. (2019). Matrix modeling and remodeling: A biological interplay regulating tissue homeostasis and diseases. *Matrix Biology : Journal of the International Society for Matrix Biology*, *75–76*, 1–11. https://doi.org/10.1016/j.matbio.2018.08.007

Kii, I., Amizuka, N., Nishiyama, T., Saito, M., Li, M., Matsumoto, K., & Kudo, A. (2009). Incorporation of Tenascin-C into the Extracellular Matrix by Periostin Underlies an Extracellular Meshwork Architecture. *Journal of Biological Chemistry*, *285*(3), 2028–2039. https://doi.org/10.1074/jbc.m109.051961

Kii, I., & Ito, H. (2017). Periostin and its interacting proteins in the construction of extracellular architectures. *Cellular and Molecular Life Sciences*, *74*(23), 4269–4277. https://doi.org/10.1007/s00018-017-2644-4

Kii, I., Nishiyama, T., & Kudo, A. (2016). Periostin promotes secretion of fibronectin from the endoplasmic reticulum. *Biochemical and Biophysical Research Communications*, *470*(4), 888–893. https://doi.org/10.1016/j.bbrc.2016.01.139

Kim, S. S., Jackson-Boeters, L., Darling, M. R., Rieder, M. J., & Hamilton, D. W. (2013). Nifedipine induces periostin expression in gingival fibroblasts through TGF-beta. *Journal of Dental Research*, *92*(11), 1022–1028. https://doi.org/10.1177/0022034513503659

Kim, S. S., Michelsons, S., Creber, K., Rieder, M. J., & Hamilton, D. W. (2015). Nifedipine and phenytoin induce matrix synthesis, but not proliferation, in intact human gingival connective tissue ex vivo. *Journal of Cell Communication and Signaling*, *9*(4), 361–375. https://doi.org/10.1007/s12079-015-0303-9

Kim, S. S., Nikoloudaki, G., Darling, M., Rieder, M. J., & Hamilton, D. W. (2019). Phenytoin activates smad3 phosphorylation and periostin expression in drug-

induced gingival enlargement. *Histology and Histopathology*. https://doi.org/10.14670/HH-18-015

Kim, S. S., Nikoloudaki, G. E., Michelsons, S., Creber, K., & Hamilton, D. W. (2019). Fibronectin synthesis, but not α-smooth muscle expression, is regulated by periostin in gingival healing through FAK/JNK signaling. *Scientific Reports*, *9*(1), 2708. https://doi.org/10.1038/s41598-018-35805-6

Klingberg, F., Wells, R. G., Walraven, M., Olsen, A. L., Koehler, A., Hinz, B., Chau, G., Chow, M. L., Lodyga, M., Im, M., White, E. S., & Boo, S. (2018). The fibronectin ED-A domain enhances recruitment of latent TGF-β-binding protein-1 to the fibroblast matrix. *Journal of Cell Science*, *131*(5), jcs201293. https://doi.org/10.1242/jcs.201293

Kramann, R., DiRocco, D. P., & Humphreys, B. D. (2013). Understanding the origin, activation and regulation of matrix-producing myofibroblasts for treatment of fibrotic disease: Matrix-producing myofibroblasts for treatment of fibrotic disease. *The Journal of Pathology*, *231*(3), 273–289. https://doi.org/10.1002/path.4253

Kruzynska-Frejtag, A., Wang, J., Maeda, M., Rogers, R., Krug, E., Hoffman, S., Markwald, R. R., & Conway, S. J. (2004). Periostin Is Expressed Within the Developing Teeth at the Sites of Epithelial-Mesenchymal Interaction. *Developmental Dynamics*, *229*(4), 857–868. https://doi.org/10.1002/dvdy.10453

Kudo, A. (2011). Periostin in fibrillogenesis for tissue regeneration: Periostin actions inside and outside the cell. *Cellular and Molecular Life Sciences*, *68*(19), 3201–3207. https://doi.org/10.1007/s00018-011-0784-5

Kudo, A., & Kii, I. (2018). Periostin function in communication with extracellular matrices. *Journal of Cell Communication and Signaling*, *12*(1), 301–308. https://doi.org/10.1007/s12079-017-0422-6

Kudo, Y., Iizuka, S., Yoshida, M., Nguyen, P. T., Siriwardena, S. B. S. M., Tsunematsu, T., Ohbayashi, M., Ando, T., Hatakeyama, D., Shibata, T., Koizumi, K., Maeda, M., Ishimaru, N., Ogawa, I., & Takata, T. (2012). Periostin Directly and Indirectly Promotes Tumor Lymphangiogenesis of Head and Neck Cancer. *PLoS ONE*, *7*(8). https://doi.org/10.1371/journal.pone.0044488

Kudo, Y., Ogawa, I., Kitajima, S., Kitagawa, M., Kawai, H., Gaffney, P. M., Miyauchi, M., & Takata, T. (2006). Periostin promotes invasion and anchorage-independent growth in the metastatic process of head and neck cancer. *Cancer Research*, *66*(14), 6928–6935. https://doi.org/10.1158/0008-5472.CAN-05-4540

Kumaresan, D., Balasundaram, A., Naik, V. K., & Appukuttan, D. P. (2016). Gingival crevicular fluid periostin levels in chronic periodontitis patients following nonsurgical periodontal treatment with low-level laser therapy. *European Journal of Dentistry*, *10*(4), 546–550. https://doi.org/10.4103/1305-7456.195179

Kyriakides, T. R., & Bornstein, P. (2003). Matricellular proteins as modulators of wound healing and the foreign body response. *Thrombosis and Haemostasis*, *90*(6), 986–992. https://doi.org/10.1160/TH03-06-0399

Larjava, H. (2013). Oral Wound Healing: Cell Biology and Clinical Management. In *Oral Wound Healing: Cell Biology and Clinical Management*. https://doi.org/10.1002/9781118704509

Larjava, H., Wiebe, C., Gallant-Behm, C., Hart, D. a., Heino, J., & Häkkinen, L. (2011). Exploring scarless healing of oral soft tissues. *Journal of the Canadian Dental Association*, *77*(C), 1–5.

LeBaron, R. G., Bezverkov, K. I., Zimber, M. P., Pavelec, R., Skonier, J., & Purchio, A. F. (1995). Beta IG-H3, a novel secretory protein inducible by transforming growth factor-beta, is present in normal skin and promotes the adhesion and spreading of dermal fibroblasts in vitro. *The Journal of Investigative Dermatology*, *104*(5), 844–849. https://doi.org/0022202X9500061O [pii]

LeBleu, V. S., & Neilson, E. G. (2020). Origin and functional heterogeneity of fibroblasts. *The FASEB Journal*, *34*(3), 3519–3536. https://doi.org/10.1096/fj.201903188R

LeBleu, V. S., Taduri, G., O'Connell, J., Teng, Y., Cooke, V. G., Woda, C., Sugimoto, H., & Kalluri, R. (2013). Origin and function of myofibroblasts in kidney fibrosis. *Nature Medicine*, *19*(8), 1047–1053. PubMed. https://doi.org/10.1038/nm.3218

Lee, H. G., & Eun, H. C. (1999). Differences between fibroblasts cultured from oral mucosa and normal skin: Implication to wound healing. *Journal of Dermatological Science*, *21*(3), 176–182. https://doi.org/10.1016/S0923-1811(99)00037-7

Lee, J. M., Lee, E. H., Kim, I. S., & Kim, J. E. (2014). Tgfbi deficiency leads to a reduction in skeletal size and degradation of the bone matrix. *Calcified Tissue International*, *96*(1), 56–64. https://doi.org/10.1007/s00223-014-9938-4

Lemos, D. R., & Duffield, J. S. (2018). Tissue-resident mesenchymal stromal cells: Implications for tissue-specific antifibrotic therapies. *Science Translational Medicine*, *10*(426), eaan5174. https://doi.org/10.1126/scitranslmed.aan5174

Lepekhin, E., Gron, B., Berezin, V., Bock, E., & Dabelsteen, E. (2002). Differences in motility pattern between human buccal fibroblasts and periodontal and skin fibroblasts. *European Journal of Oral Sciences*, *110*(1), 13–20. https://doi.org/10.1034/j.1600-0722.2002.00139.x

Levoux, J., Prola, A., Lafuste, P., Gervais, M., Chevallier, N., Koumaiha, Z., Kefi, K., Braud, L., Schmitt, A., Yacia, A., Schirmann, A., Hersant, B., Sid-Ahmed, M., Ben Larbi, S., Komrskova, K., Rohlena, J., Relaix, F., Neuzil, J., & Rodriguez, A.-M. (2021). Platelets Facilitate the Wound-Healing Capability of Mesenchymal Stem Cells by Mitochondrial Transfer and Metabolic Reprogramming. *Cell Metabolism*, *33*(2), 283-299.e9. https://doi.org/10.1016/j.cmet.2020.12.006

Lin, J.-H., Lin, I.-P., Ohyama, Y., Mochida, H., Kudo, A., Kaku, M., & Mochida, Y. (2020). FAM20C directly binds to and phosphorylates Periostin. *Scientific Reports*, *10*(1), 17155. https://doi.org/10.1038/s41598-020-74400-6

Litvin, J., Selim, A.-H., Montgomery, M. O., Lehmann, K., Rico, M. C., Devlin, H., Bednarik, D. P., & Safadi, F. F. (2004). Expression and function of periostin-isoforms in bone. *Journal of Cellular Biochemistry*, *92*(5), 1044–1061. https://doi.org/10.1002/jcb.20115

Liu, C., Feng, X., Wang, B., Wang, X., Wang, C., Yu, M., Cao, G., & Wang, H. (2018). Bone marrow mesenchymal stem cells promote head and neck cancer progression through Periostin-mediated phosphoinositide 3-kinase/Akt/mammalian target of rapamycin. *Cancer Science*, *109*(3), 688–698. https://doi.org/10.1111/cas.13479

Liu, P., Zhang, H., Liu, C., Wang, X., Chen, L., & Qin, C. (2014). Inactivation of Fam20C in cells expressing type I collagen causes periodontal disease in mice. *PloS One*, *9*(12), e114396. https://doi.org/10.1371/journal.pone.0114396

Lynge Pedersen, A. M., & Belstrøm, D. (2019). The role of natural salivary defences in maintaining a healthy oral microbiota. *Journal of Dentistry*, *80*, S3–S12. https://doi.org/10.1016/j.jdent.2018.08.010

Ma, D., Zhang, R., Sun, Y., Rios, H. F., Haruyama, N., Han, X., Kulkarni, A. B., Qin, C., & Feng, J. Q. (2011). A novel role of periostin in postnatal tooth formation and mineralization. *Journal of Biological Chemistry*, *286*(6), 4302–4309. https://doi.org/10.1074/jbc.M110.140202

Maeda, D., Kubo, T., Kiya, K., Kawai, K., Matsuzaki, S., Kobayashi, D., Fujiwara, T., Katayama, T., & Hosokawa, K. (2019). Periostin is induced by IL-4/IL-13 in dermal fibroblasts and promotes RhoA/ROCK pathway-mediated TGF-β1 secretion in abnormal scar formation. *Journal of Plastic Surgery and Hand Surgery*, *53*(5), 288–294. https://doi.org/10.1080/2000656X.2019.1612752

Mah, W., Jiang, G., Olver, D., Cheung, G., Kim, B., Larjava, H., & Häkkinen, L. (2014). Human gingival fibroblasts display a non-fibrotic phenotype distinct from skin fibroblasts in three-dimensional cultures. *PloS One*, *9*(3), e90715. https://doi.org/10.1371/journal.pone.0090715

Mah, W., Jiang, G., Olver, D., Gallant-Behm, C., Wiebe, C., Hart, D. A., Koivisto, L., Larjava, H., & Häkkinen, L. (2017). Elevated CD26 Expression by Skin Fibroblasts Distinguishes a Profibrotic Phenotype Involved in Scar Formation Compared to Gingival Fibroblasts. *The American Journal of Pathology*, *187*(8), 1717–1735. https://doi.org/10.1016/j.ajpath.2017.04.017

Mahdavian Delavary, B., van der Veer, W. M., van Egmond, M., Niessen, F. B., & Beelen, R. H. J. (2011). Macrophages in skin injury and repair. *Immunobiology*, *216*(7), 753–762. https://doi.org/10.1016/j.imbio.2011.01.001

Martin, P., & Nunan, R. (2015). Cellular and molecular mechanisms of repair in acute and chronic wound healing. *The British Journal of Dermatology*, *173*(2), 370–378. https://doi.org/10.1111/bjd.13954

Martins, V. L., Caley, M., & O'Toole, E. A. (2013). Matrix metalloproteinases and epidermal wound repair. *Cell and Tissue Research*, *351*(2), 255–268. https://doi.org/10.1007/s00441-012-1410-z

Maruhashi, T., Kii, I., Saito, M., & Kudo, A. (2010). Interaction between periostin and BMP-1 promotes proteolytic activation of lysyl oxidase. *Journal of Biological Chemistry*, *285*(17), 13294–13303. https://doi.org/10.1074/jbc.M109.088864

Mederacke, I., Hsu, C. C., Troeger, J. S., Huebener, P., Mu, X., Dapito, D. H., Pradere, J.-P., & Schwabe, R. F. (2013). Fate-tracing reveals hepatic stellate cells as dominant contributors to liver fibrosis independent of its etiology. *Nature Communications*, *4*, 2823. https://doi.org/10.1038/ncomms3823

Midwood, K. S., Williams, L. V., & Schwarzbauer, J. E. (2004). Tissue repair and the dynamics of the extracellular matrix. *International Journal of Biochemistry and Cell Biology*, *36*(6), 1031–1037. https://doi.org/10.1016/j.biocel.2003.12.003

Morita, H., & Komuro, I. (2016). Periostin Isoforms and Cardiac Remodeling After Myocardial Infarction: Is the Dispute Settled? In *Hypertension (Dallas, Tex. : 1979)* (Vol. 67, Issue 3, pp. 504–505). https://doi.org/10.1161/HYPERTENSIONAHA.115.06449

Mosher, D. F., Johansson, M. W., Gillis, M. E., & Annis, D. S. (2015). Periostin and TGF- β -induced Protein: Two Peas in a Pod ? *Critical Reviews in Biochemistry and Molecular Biology*, *50*(5), 427–439. https://doi.org/10.3109/10409238.2015.1069791.Periostin

Moulin, V., Castilloux, G., Auger, F. A., Garrel, D., O'Connor-McCourt, M. D., & Germain, L. (1998). Modulated response to cytokines of human wound healing myofibroblasts compared to dermal fibroblasts. *Experimental Cell Research*, *238*(1), 283–293. https://doi.org/10.1006/excr.1997.3827

Moutsopoulos, N. M., & Konkel, J. E. (2018). Tissue-Specific Immunity at the Oral Mucosal Barrier. *Trends in Immunology*, *39*(4), 276–287. https://doi.org/10.1016/j.it.2017.08.005

Murphy-Ullrich, J. E., & Sage, E. H. (2014). Revisiting the matricellular concept. *Matrix Biology : Journal of the International Society for Matrix Biology*, *37*, 1–14. https://doi.org/10.1016/j.matbio.2014.07.005

Nakajima, M., Honda, T., Miyauchi, S., & Yamazaki, K. (2014). Th2 cytokines efficiently stimulate periostin production in gingival fibroblasts but periostin does not induce an inflammatory response in gingival epithelial cells. *Archives of Oral Biology*, *59*(2), 93–101. https://doi.org/10.1016/j.archoralbio.2013.10.004

Nam, B. Y., Park, J. T., Kwon, Y. E., Lee, J. P., Jung, J. H., Kim, Y., Kim, S., Park, J., Um, J. E., Wu, M., Han, S. H., Yoo, T. H., & Kang, S. W. (2017). Periostin-Binding DNA Aptamer Treatment Ameliorates Peritoneal Dialysis-Induced Peritoneal Fibrosis. *Molecular Therapy - Nucleic Acids*, *7*(June), 396–407. https://doi.org/10.1016/j.omtn.2017.05.001

Nanci, A. (2013). Ten Cate's Oral Histology. In *Elsevier: Vol. 8th ed* (p. 166). Elsevier.

Nikoloudaki, G., Creber, K., & Hamilton, D. W. (2020). Wound Healing and Fibrosis: A Contrasting Role for Periostin in Skin and the Oral Mucosa. *American Journal of Physiology-Cell Physiology*. https://doi.org/10.1152/ajpcell.00035.2020

Norris, R. A., Damon, B., Kern, C. B., Wen, X., Forgacs, G., Hoffman, S., Trusk, T., Molkentin, J. D., Goodwin, R. L., Conway, S. J., Norris, R. A., Kasyanov, V., Potts, J. D., Mjaatvedt, C. H., Oka, T., Moreno-Rodriguez, R., Markwald, R. R., Sugi, Y., Davis, J., … Mironov, V. (2007). Periostin regulates collagen fibrillogenesis and the biomechanical properties of connective tissues. *Journal of Cellular Biochemistry*, *101*(3), 695–711. https://doi.org/10.1002/jcb.21224

Nyska, A., Shemesh, M., Tal, H., & Dayan, D. (1994). Gingival hyperplasia induced by calcium channel blockers: Mode of action. *Medical Hypotheses*. https://doi.org/10.1016/0306-9877(94)90061-2

Ohno, S., Doi, T., Fujimoto, K., Ijuin, C., Tanaka, N., Tanimoto, K., Honda, K., Nakahara, M., Kato, Y., & Tanne, K. (2002). RGD-CAP (betaig-h3) exerts a negative regulatory function on mineralization in the human periodontal ligament. *Journal of Dental Research*, *81*(12), 822–825. https://doi.org/10.1177/154405910208101205

Oudhoff, M. J., Bolscher, J. G. M., Nazmi, K., Kalay, H., van't Hof, W., Amerongen, A. V. N., & Veerman, E. C. I. (2008). Histatins are the major wound-closure stimulating factors in human saliva as identified in a cell culture assay. *The FASEB Journal*, *22*(11), 3805–3812. https://doi.org/10.1096/fj.08-112003

Padial-Molina, M., Volk, S. L., & Rios, H. F. (2014). Periostin increases migration and proliferation of human periodontal ligament fibroblasts challenged by tumor necrosis factor -α and Porphyromonas gingivalis lipopolysaccharides. *Journal of Periodontal Research, 49*(3), 405–414. https://doi.org/10.1111/jre.12120

Padial-Molina, M., Volk, S. L., & Rios, H. F. (2015). Preliminary insight into the periostin leverage during periodontal tissue healing. *Journal of Clinical Periodontology, 42*(8), 764–772. https://doi.org/10.1111/jcpe.12432

Padial-Molina, M., Volk, S. L., Rodriguez, J. C., Marchesan, J. T., Galindo-Moreno, P., & Rios, H. F. (2013). Tumor Necrosis Factor-α and Porphyromonas gingivalis Lipopolysaccharides Decrease Periostin in Human Periodontal Ligament Fibroblasts . *Journal of Periodontology*, *84*(5), 694–703. https://doi.org/10.1902/jop.2012.120078

Padial-Molina, M., Volk, S. L., Taut, A. D., Giannobile, W. V., & Rios, H. F. (2012). Periostin is down-regulated during periodontal inflammation. *Journal of Dental Research*, *91*(11), 1078–1084. https://doi.org/10.1177/0022034512459655

Pereira, D., & Sequeira, I. (2021). A Scarless Healing Tale: Comparing Homeostasis and Wound Healing of Oral Mucosa With Skin and Oesophagus. *Frontiers in Cell and Developmental Biology*, *9*, 682143. https://doi.org/10.3389/fcell.2021.682143

Periayah, M. H., Halim, A. S., & Mat Saad, A. Z. (2017). Mechanism Action of Platelets and Crucial Blood Coagulation Pathways in Hemostasis. *International Journal of Hematology-Oncology and Stem Cell Research, 11*(4), 319–327.

Petreaca, M., & Martins-Green, M. (2020). Chapter 6—The dynamics of cell–extracellular matrix interactions, with implications for tissue engineering. In R. Lanza, R. Langer, J. P. Vacanti, & A. Atala (Eds.), *Principles of Tissue Engineering (Fifth Edition)* (pp. 93–117). Academic Press. https://doi.org/10.1016/B978-0-12-818422-6.00007-1

Piipponen, M., Li, D., & Landén, N. X. (2020). The Immune Functions of Keratinocytes in Skin Wound Healing. *International Journal of Molecular Sciences*, *21*(22), 8790. https://doi.org/10.3390/ijms21228790

Politis, C., Schoenaers, J., Jacobs, R., & Agbaje, J. O. (2016). Wound healing problems in the mouth. *Frontiers in Physiology*, *7*(NOV), 1–13. https://doi.org/10.3389/fphys.2016.00507

Puolakkainen, P. A., Bradshaw, A. D., Brekken, R. A., Reed, M. J., Kyriakides, T., Funk, S. E., Gooden, M. D., Vernon, R. B., Wight, T. N., Bornstein, P., & Sage, E. H. (2005). SPARC-thrombospondin-2-double-null mice exhibit enhanced cutaneous wound healing and increased fibrovascular invasion of subcutaneous polyvinyl alcohol sponges. *The Journal of Histochemistry and Cytochemistry : Official Journal of the Histochemistry Society*, *53*(5), 571–581. https://doi.org/10.1369/jhc.4A6425.2005

Qin, X., Yan, M., Zhang, J., Wang, X., Shen, Z., Lv, Z., Li, Z., Wei, W., & Chen, W. (2016). TGFβ3-mediated induction of Periostin facilitates head and neck cancer growth and is associated with metastasis. *Scientific Reports*, *6*, 20587. https://doi.org/10.1038/srep20587

Rambhia, K. J., & Ma, P. X. (2015). Controlled Drug Release for Tissue Engineering Graphical Abstract HHS Public Access. *J Control Release*, *219*, 119–128. https://doi.org/10.1016/j.jconrel.2015.08.049

Ravanti, L., Häkkinen, L., Larjava, H., Saarialho-Kere, U., Foschi, M., Han, J., & Kähäri, V. M. (1999). Transforming growth factor-β induces collagenase-3 expression by human gingival fibroblasts via p38 mitogen-activated protein kinase. *Journal of Biological Chemistry*, *274*(52), 37292–37300. https://doi.org/10.1074/jbc.274.52.37292

Reinboth, B., Thomas, J., Hanssen, E., & Gibson, M. A. (2006). Beta ig-h3 interacts directly with biglycan and decorin, promotes collagen VI aggregation, and

participates in ternary complexing with these macromolecules. *The Journal of Biological Chemistry*, *281*(12), 7816–7824. https://doi.org/10.1074/jbc.M511316200

Reinke, J. M., & Sorg, H. (2012). Wound repair and regeneration. *European Surgical Research. Europaische Chirurgische Forschung. Recherches Chirurgicales Europeennes*, *49*(1), 35–43. https://doi.org/10.1159/000339613

Ren, Y., Han, X., Ho, S. P., Harris, S. E., Cao, Z., Economides, A. N., Qin, C., Ke, H., Liu, M., & Feng, J. Q. (2015). Removal of SOST or blocking its product sclerostin rescues defects in the periodontitis mouse model. *The FASEB Journal*, *29*(7), 2702–2711. https://doi.org/10.1096/fj.14-265496

Rinkevich, Y., Walmsley, G. G., Hu, M. S., Maan, Z. N., Newman, A. M., Drukker, M., Januszyk, M., Krampitz, G. W., Gurtner, G. C., Lorenz, H. P., Weissman, I. L., & Longaker, M. T. (2015a). Identification and isolation of a dermal lineage with intrinsic fibrogenic potential. *Science*, *348*(6232). https://doi.org/10.1126/science.aaa2151

Rinkevich, Y., Walmsley, G. G., Hu, M. S., Maan, Z. N., Newman, A. M., Drukker, M., Januszyk, M., Krampitz, G. W., Gurtner, G. C., Lorenz, H. P., Weissman, I. L., & Longaker, M. T. (2015b). Identification and isolation of a dermal lineage with intrinsic fibrogenic potential. *Science*, *348*(6232). https://doi.org/10.1126/science.aaa2151

Rinkevich, Y., Walmsley, G. G., Hu, M. S., Maan, Z. N., Newman, A. M., Drukker, M., Januszyk, M., Krampitz, G. W., Gurtner, G. C., Lorenz, H. P., Weissman, I. L., & Longaker, M. T. (2015c). Skin fibrosis. Identification and isolation of a dermal lineage with intrinsic fibrogenic potential. *Science (New York, N.Y.)*, *348*(6232), aaa2151. https://doi.org/10.1126/science.aaa2151

Rios, H. F., Ma, D., Xie, Y., Giannobile, W. V, Bonewald, L. F., Conway, S. J., & Feng, J. Q. (2008). Periostin Is Essential for the Integrity and Function of the

Periodontal Ligament During Occlusal Loading in Mice. *Journal of Periodontology*, *79*(8), 1480–1490. https://doi.org/doi:10.1902/jop.2008.070624

Rios, H., Koushik, S. V, Wang, H., Wang, J., Zhou, H.-M., Lindsley, A., Rogers, R., Chen, Z., Maeda, M., Kruzynska-Frejtag, A., Feng, J. Q., & Conway, S. J. (2005). Periostin Null Mice Exhibit Dwarfism, Incisor Enamel Defects, and an Early-Onset Periodontal Disease-Like Phenotype. *Molecular and Cellular Biology*, *25*(24), 11131–11144. https://doi.org/10.1128/MCB.25.24.11131-11144.2005

Rodero, M. P., & Khosrotehrani, K. (2010). Skin wound healing modulation by macrophages. *International Journal of Clinical and Experimental Pathology*, *3*(7), 643–653.

Rogers, R., Markwald, R., Moreno-Rodriguez, R. A., Lindsley, A., Menick, D., Snider, P., Conway, S. J., Field, L., Firulli, A. B., Li, F., Ingram, D. A., Molkentin, J. D., Wang, J., & Hinton, R. B. (2008). Periostin Is Required for Maturation and Extracellular Matrix Stabilization of Noncardiomyocyte Lineages of the Heart. *Circulation Research*, *102*(7), 752–760. https://doi.org/10.1161/circresaha.107.159517

Rognoni, E., Pisco, A. O., Hiratsuka, T., Sipilä, K. H., Belmonte, J. M., Mobasseri, S. A., Philippeos, C., Dilão, R., & Watt, F. M. (2018). Fibroblast state switching orchestrates dermal maturation and wound healing. *Molecular Systems Biology*, *14*(8), e8174. https://doi.org/10.15252/msb.20178174

Romanos, G. E., Asnani, K. P., Hingorani, D., & Deshmukh, V. L. (2014). PERIOSTIN: role in formation and maintenance of dental tissues. *Journal of Cellular Physiology*, *229*(1), 1–5. https://doi.org/10.1002/jcp.24407

Rousselle, P., Montmasson, M., & Garnier, C. (2019). Extracellular matrix contribution to skin wound re-epithelialization. *Matrix Biology : Journal of the International Society for Matrix Biology*, *75–76*, 12–26. https://doi.org/10.1016/j.matbio.2018.01.002

Sankardas, P. A., Lavu, V., Lakakula, B. V. K. S., & Rao, S. R. (2019). Differential expression of periostin, sclerostin, receptor activator of nuclear factor-κB, and receptor activator of nuclear factor-κB ligand genes in severe chronic periodontitis. *Journal of Investigative and Clinical Dentistry*, *10*(1), e12369. https://doi.org/10.1111/jicd.12369

Sata, M., Kudo, A., Nakamura, K., Saga, Y., Fukuda, K., Saito, M., Kashima, T., Amizuka, N., Shimazaki, M., Fukayama, M., Li, M., Kitajima, S., Kii, I., & Nishiyama, T. (2008). Periostin is essential for cardiac healingafter acute myocardial infarction. *The Journal of Experimental Medicine*. https://doi.org/10.1084/jem.20071297

Schrementi, M. E., Ferreira, A. M., Zender, C., & DiPietro, L. A. (2008). Site-specific production of TGF-beta in oral mucosal and cutaneous wounds. *Wound Repair and Regeneration : Official Publication of the Wound Healing Society [and] the European Tissue Repair Society*, *16*(1), 80–86. https://doi.org/10.1111/j.1524-475X.2007.00320.x

Schwanekamp, J. A., Lorts, A., Sargent, M. A., York, A. J., Grimes, K. M., Fischesser, D. M., Gokey, J. J., Whitsett, J. A., Conway, S. J., & Molkentin, J. D. (2017). TGFBI functions similar to periostin but is uniquely dispensable during cardiac injury. *PLoS ONE*, *12*(7). https://doi.org/10.1371/journal.pone.0181945

Serini, G., Bochaton-Piallat, M.-L., Borsi, L., Geinoz, A., Ropraz, P., Gabbiani, G., & Zardi, L. (2002a). The Fibronectin Domain ED-A Is Crucial for Myofibroblastic Phenotype Induction by Transforming Growth Factor-β1. *The Journal of Cell Biology*, *142*(3), 873–881. https://doi.org/10.1083/jcb.142.3.873

Serini, G., Bochaton-Piallat, M.-L., Borsi, L., Geinoz, A., Ropraz, P., Gabbiani, G., & Zardi, L. (2002b). The Fibronectin Domain ED-A Is Crucial for Myofibroblastic Phenotype Induction by Transforming Growth Factor-β1. *The Journal of Cell Biology*, *142*(3), 873–881. https://doi.org/10.1083/jcb.142.3.873

Serita, S., Tomokiyo, A., Hasegawa, D., Hamano, S., Sugii, H., Yoshida, S., Mizumachi, H., Mitarai, H., Monnouchi, S., Wada, N., & Maeda, H. (2017). Transforming growth factor-β-induced gene product-h3 inhibits odontoblastic differentiation of dental pulp cells. *Archives of Oral Biology, 78*, 135–143. https://doi.org/10.1016/j.archoralbio.2017.02.018

Shang, L., Deng, D., Buskermolen, J. K., Janus, M. M., Krom, B. P., Roffel, S., Waaijman, T., van Loveren, C., Crielaard, W., & Gibbs, S. (2018). Multi-species oral biofilm promotes reconstructed human gingiva epithelial barrier function. *Scientific Reports*, *8*(1), 16061. https://doi.org/10.1038/s41598-018-34390-y

Shannon, D. B., McKeown, S. T. W., Lundy, F. T., & Irwin, C. R. (2006). Phenotypic differences between oral and skin fibroblasts in wound contraction and growth factor expression. *Wound Repair and Regeneration*, *14*(2), 172–178. https://doi.org/10.1111/j.1743-6109.2006.00107.x

Siriwardena, B. S. M. S., Kudo, Y., Ogawa, I., Kitagawa, M., Kitajima, S., Hatano, H., Tilakaratne, W. M., Miyauchi, M., & Takata, T. (2006). Periostin is frequently overexpressed and enhances invasion and angiogenesis in oral cancer. *British Journal of Cancer*, *95*(10), 1396–1403. https://doi.org/10.1038/sj.bjc.6603431

Song, K. M., Lee, S., & Ban, C. (2012). Aptamers and their biological applications. *Sensors*, *12*(1), 612–631. https://doi.org/10.3390/s120100612

Sorg, H., Tilkorn, D. J., Hager, S., Hauser, J., & Mirastschijski, U. (2017). Skin Wound Healing: An Update on the Current Knowledge and Concepts. *European Surgical Research. Europaische Chirurgische Forschung. Recherches Chirurgicales Europeennes*, *58*(1–2), 81–94. https://doi.org/10.1159/000454919

Sriram, G., Bigliardi, P. L., & Bigliardi-Qi, M. (2015). Fibroblast heterogeneity and its implications for engineering organotypic skin models in vitro. *European Journal of Cell Biology*, *94*(11), 483–512. https://doi.org/10.1016/j.ejcb.2015.08.001

Stephens, P., Davies, K. J., Occleston, N., Pleass, R. D., Kon, C., Daniels, J., Khaw, P. T., & Thomas, D. W. (2001). Skin and oral fibroblasts exhibit phenotypic differences in extracellular matrix reorganization and matrix metalloproteinase activity. *British Journal of Dermatology*, *144*(2), 229–237. https://doi.org/10.1046/j.1365-2133.2001.04006.x

Stephens, P., Hiscox, S., Cook, H., Jiang, W. G., Zhiquiang, W., & Thomas, D. W. (2001). Phenotypic variation in the production of bioactive hepatocyte growth factor/scatter factor by oral mucosal and skin fibroblasts. *Wound Repair and Regeneration*, *9*(1), 34–43. https://doi.org/10.1046/j.1524-475x.2001.00034.x

Su, J.-Y., Yu, C.-C., Peng, C.-Y., Liao, Y.-W., Hsieh, P.-L., Yang, L.-C., Yu, C.-H., & Chou, M.-Y. (2021). Silencing periostin inhibits myofibroblast transdifferentiation of fibrotic buccal mucosal fibroblasts. *Journal of the Formosan Medical Association*, *120*(11), 2010–2015. https://doi.org/10.1016/j.jfma.2021.04.008

Su, Y., Chen, C., Guo, L., Du, J., Li, X., & Liu, Y. (2018). Ecological Balance of Oral Microbiota Is Required to Maintain Oral Mesenchymal Stem Cell Homeostasis. *Stem Cells*, *36*(4), 551–561. https://doi.org/10.1002/stem.2762

Sundar, S., Ramani, P., Sherlin, H., & Jayaraj, G. (2018). Role of periostin in oral squamous cell carcinoma: A systematic review. *International Journal of Orofacial Biology*, *2*(2), 35. https://doi.org/10.4103/ijofb.ijofb_2_19

Suzuki, H., Amizuka, N., Kii, I., Kawano, Y., Nozawa-Inoue, K., Suzuki, A., Yoshie, H., Kudo, A., & Maeda, T. (2004). Immunohistochemical localization of periostin in tooth and its surrounding tissues in mouse mandibles during development. *The Anatomical Record. Part A, Discoveries in Molecular, Cellular, and Evolutionary Biology*, *281*(2), 1264–1275. https://doi.org/10.1002/ar.a.20080

Szpaderska, A. M., Zuckerman, J. D., & DiPietro, L. A. (2003). Differential Injury Responses in Oral Mucosal and Cutaneous Wounds. *Journal of Dental Research*, *82*(8), 621–626. https://doi.org/10.1177/154405910308200810

Tabata, C., Hongo, H., Sasaki, M., Hasegawa, T., de Freitas, P. H. L., Yamada, T., Yamamoto, T., Suzuki, R., Yamamoto, T., Oda, K., Li, M., Kudo, A., Iida, J., & Amizuka, N. (2014). Altered distribution of extracellular matrix proteins in the periodontal ligament of periostin-deficient mice. *Histology and Histopathology*, *29*(6), 731–742. https://doi.org/10.14670/HH-29.731

Takeshita, S., Kikuno, R., Tezuka, K., & Amann, E. (1993). Osteoblast-specific factor 2: Cloning of a putative bone adhesion protein with homology with the insect protein fasciclin I. *Biochemical Journal*, *294*(1), 271–278.

Tang, Y., Liu, L., Wang, P., Chen, D., Wu, Z., & Tang, C. (2017). Periostin promotes migration and osteogenic differentiation of human periodontal ligament mesenchymal stem cells via the Jun amino-terminal kinases (JNK) pathway under inflammatory conditions. *Cell Proliferation*, *50*(6), 1–11. https://doi.org/10.1111/cpr.12369

Tang, Y.-Q., Yeaman, M. R., & Selsted, M. E. (2002). Antimicrobial Peptides from Human Platelets. *Infection and Immunity*, *70*(12), 6524–6533. https://doi.org/10.1128/IAI.70.12.6524-6533.2002

Toma, A. I., Fuller, J. M., Willett, N. J., & Goudy, S. L. (2021). Oral wound healing models and emerging regenerative therapies. *Translational Research*, *236*, 17–34. https://doi.org/10.1016/j.trsl.2021.06.003

Tonnesen, M. G., Feng, X., & Clark, R. A. (2000). Angiogenesis in wound healing. *The Journal of Investigative Dermatology. Symposium Proceedings*, *5*(1), 40–46. https://doi.org/10.1046/j.1087-0024.2000.00014.x

Um, J. E., Park, J. T., Nam, B. Y., Lee, J. P., Jung, J. H., Kim, Y., Kim, S., Park, J., Wu, M., Han, S. H., Yoo, T. H., & Kang, S. W. (2017). Periostin-binding DNA aptamer treatment attenuates renal fibrosis under diabetic conditions. *Scientific Reports*, *7*(1), 1–12. https://doi.org/10.1038/s41598-017-09238-6

Van Snick, J., Jat, P. S., Field, S., Uyttenhove, C., Stroobant, V., Cheou, P., Donckers, D., Coutelier, J.-P., Simpson, P. T., Cummings, M. C., Saunus, J. M., Reid, L. E., Kutasovic, J. R., McNicol, A. M., Kim, B. R., Kim, J. H., Lakhani, S. R., & Neville, A. M. (2016). Novel highly specific anti-periostin antibodies uncover the functional importance of the fascilin 1-1 domain and highlight preferential expression of periostin in aggressive breast cancer. *International Journal of Cancer*, *138*(8), 1959–1970. https://doi.org/10.1002/ijc.29946

Velnar, T., Bailey, T., & Smrkolj, V. (2009). The wound healing process: An overview of the cellular and molecular mechanisms. *The Journal of International Medical Research*, *37*(5), 1528–1542. https://doi.org/10.1177/147323000903700531

Walker, J. T., Flynn, L. E., & Hamilton, D. W. (2021). Lineage tracing of Foxd1-expressing embryonic progenitors to assess the role of divergent embryonic lineages on adult dermal fibroblast function. *FASEB BioAdvances*, *3*(7), 541–557. https://doi.org/10.1096/fba.2020-00110

Wang, J. (2018). Neutrophils in tissue injury and repair. *Cell and Tissue Research*, *371*(3), 531–539. https://doi.org/10.1007/s00441-017-2785-7

Wells, A., Nuschke, A., & Yates, C. C. (2016). Skin tissue repair: Matrix microenvironmental influences. *Matrix Biology : Journal of the International Society for Matrix Biology*, *49*, 25–36. https://doi.org/10.1016/j.matbio.2015.08.001

Wen, W., Chau, E., Jackson-Boeters, L., Elliott, C., Daley, T. D., & Hamilton, D. W. (2010). TGF-ß1 and FAK regulate periostin expression in PDL fibroblasts.

Journal of Dental Research, *89*(12), 1439–1443. https://doi.org/10.1177/0022034510378684

Wijdeveld, M. G. M. M., Grupping, E. M., Kuijpers-Jagtman, A. M., & Maltha, J. C. (1987). Wound healing of the palatal mucoperiosteum in beagle dogs after surgery at different ages. *Journal of Cranio-Maxillofacial Surgery*, *15*, 51–57. https://doi.org/10.1016/S1010-5182(87)80018-5

Wijdeveld, M. G. M. M., Maltha, J. C., Grupping, E. M., Dejonge, J., & Kuijpersjagtman, A. M. (1991). A Histological Study of Tissue-Response to Simulated Cleft-Palate Surgery at Different Ages in Beagle Dogs. *Archives of Oral Biology*, *36*(11), 837–843.

Williams, D. W., Greenwell-Wild, T., Brenchley, L., Dutzan, N., Overmiller, A., Sawaya, A. P., Webb, S., Martin, D., Hajishengallis, G., Divaris, K., Morasso, M., Haniffa, M., & Moutsopoulos, N. M. (2021). Human oral mucosa cell atlas reveals a stromal-neutrophil axis regulating tissue immunity. *Cell*, *184*(15), 4090-4104.e15. https://doi.org/10.1016/j.cell.2021.05.013

Wong, J. W., Gallant-Behm, C., Wiebe, C., Mak, K., Hart, D. A., Larjava, H., & Häkkinen, L. (2009). Wound healing in oral mucosa results in reduced scar formation as compared with skin: Evidence from the red Duroc pig model and humans. *Wound Repair and Regeneration*, *17*(5), 717–729. https://doi.org/10.1111/j.1524-475X.2009.00531.x

Xiao, T., Yan, Z., Xiao, S., & Xia, Y. (2020). Proinflammatory cytokines regulate epidermal stem cells in wound epithelialization. *Stem Cell Research & Therapy*, *11*(1), 232. https://doi.org/10.1186/s13287-020-01755-y

Xue, M., & Jackson, C. J. (2015). Extracellular Matrix Reorganization During Wound Healing and Its Impact on Abnormal Scarring. *Advances in Wound Care*, *4*(3), 119–136. https://doi.org/10.1089/wound.2013.0485

Yamazaki, T., & Mukouyama, Y. (2018). Tissue Specific Origin, Development, and Pathological Perspectives of Pericytes. *Frontiers in Cardiovascular Medicine*, *5*, 78. https://doi.org/10.3389/fcvm.2018.00078

Yang, T., Deng, Z., Pan, Z., Qian, Y., Yao, W., & Wang, J. (2020). Prognostic value of periostin in multiple solid cancers: A systematic review with meta-analysis. *Journal of Cellular Physiology*, *235*(3), 2800–2808. https://doi.org/10.1002/jcp.29184

Yeaman, M. R. (2010). Platelets in defense against bacterial pathogens. *Cellular and Molecular Life Sciences*, *67*(4), 525–544. https://doi.org/10.1007/s00018-009-0210-4

Yu, B., Wu, K., Wang, X., Zhang, J., Wang, L., Jiang, Y., Zhu, X., Chen, W., & Yan, M. (2018). Periostin secreted by cancer-associated fibroblasts promotes cancer stemness in head and neck cancer by activating protein tyrosine kinase 7. *Cell Death and Disease*, *9*(11). https://doi.org/10.1038/s41419-018-1116-6

Yuan, X., Xu, Q., Zhang, X., Van Brunt, L. A., Ticha, P., & Helms, J. A. (2019). Wnt-Responsive Stem Cell Fates in the Oral Mucosa. *IScience*, *21*, 84–94. https://doi.org/10.1016/j.isci.2019.10.016

Zeisberg, E. M., Tarnavski, O., Zeisberg, M., Dorfman, A. L., McMullen, J. R., Gustafsson, E., Chandraker, A., Yuan, X., Pu, W. T., Roberts, A. B., Neilson, E. G., Sayegh, M. H., Izumo, S., & Kalluri, R. (2007). Endothelial-to-mesenchymal transition contributes to cardiac fibrosis. *Nature Medicine*, *13*(8), 952–961. https://doi.org/10.1038/nm1613

Zent, J., & Guo, L. W. (2018a). Signaling mechanisms of myofibroblastic activation: Outside-in and inside-out. *Cellular Physiology and Biochemistry*, *49*(3), 848–868. https://doi.org/10.1159/000493217

Zent, J., & Guo, L. W. (2018b). Signaling mechanisms of myofibroblastic activation: Outside-in and inside-out. *Cellular Physiology and Biochemistry*, *49*(3), 848–868. https://doi.org/10.1159/000493217

Zhang, Z.-R., Chen, L.-Y., Qi, H.-Y., & Sun, S.-H. (2018). Expression and clinical significance of periostin in oral lichen planus. *Experimental and Therapeutic Medicine*, *15*(6), 5141–5147. https://doi.org/10.3892/etm.2018.6029

Zhou, H.-M., Wang, J., Elliott, C., Wen, W., Hamilton, D. W., & Conway, S. J. (2010). Spatiotemporal expression of periostin during skin development and incisional wound healing: Lessons for human fibrotic scar formation. *Journal of Cell Communication and Signaling*, *4*(2), 99–107. https://doi.org/10.1007/s12079-010-0090-2

Zhu, M., Saxton, R. E., Ramos, L., Chang, D. D., Karlan, B. Y., Gasson, J. C., & Slamon, D. J. (2011). Neutralizing monoclonal antibody to periostin inhibits ovarian tumor growth and metastasis. *Molecular Cancer Therapeutics*, *10*(8), 1500–1508. https://doi.org/10.1158/1535-7163.MCT-11-0046

Chapter 2

2 Periostin and Matrix Stiffness Combine to Regulate Myofibroblast Differentiation and Fibronectin Synthesis During Palatal Healing

2.1 Introduction

Wound healing in soft connective tissues, such as skin, is defined as a coordinated series of overlapping events leading to resolution of the defect. Through the phases of hemostasis, inflammation, proliferation and remodeling, concomitant with re-epithelialization, barrier function is re-established (Karamanos et al., 2019). Much of the research related to acute healing has utilized excisional skin wounding, primarily due to ease of defect creation and the use of genetically modified mouse lines (Smith et al., 2012). However, different healing profiles have been described. In particular, wounds in the oral mucosa are known to exhibit significant differences compared with cutaneous injuries (Glim et al., n.d.; Politis et al., 2016; Wong et al., 2009). In contrast to skin, injuries to the oral mucosa, including gingival tissue, heal rapidly with minimal scar formation (Dipietro, 2003; Glim et al., n.d.; Häkkinen et al., 2000; Wong et al., 2009). Interestingly, both skin and oral mucosa are characterized by the presence of keratinized epithelium and underlying collagen dense connective tissue. However, while still part of the oral environment, the palatal mucosa is associated with excessive scarring in response to injury (Larjava et al., 2011; Wijdeveld et al., 1987, 1991). Unlike skin and gingiva however, palatal soft tissue is a rigid mucoperiosteum; mucosa and the periosteum are merged and tightly attached to the palatal bone (Nanci, 2013).

In recent years, the role of matricellular proteins in each of these phases of healing has become established (Walker et al., 2015; Wells et al., 2016). As a class of proteins, matricellular proteins (MPs) specifically modulate cell-matrix interactions and cell function (adhesion, spreading, migration, proliferation and differentiation) (Bornstein & Sage, 2002) by interacting with cell-surface receptors, including integrins. While fibrin, collagen and fibronectin provide structural support to the matrix, defined roles for MPs in

the adhesion, migration, proliferation and differentiation of macrophages, fibroblasts, and keratinocytes have been identified post-wounding (Walker et al., 2015).

Periostin is a secreted matricellular protein associated with wound healing in several connective tissues, with the cell and molecular roles of periostin mainly investigated in collagen-rich biomechanically active tissues (Hamilton, 2008). Although knockout mice are viable, periostin deletion results in disruption of several collagenous-based tissues, particularly those subject to constant mechanical loading, exhibiting severe periodontal disease, significant reduction in bone density, and structural defects in the incisors (Rios et al., 2005). Although periostin was defined as a non-structural ECM component, it has been shown to modulate cross-linking and stabilization of the extracellular matrix, including collagen fibrillogenesis (Hwang et al., 2014; Norris et al., 2007). Additionally, periostin acts as a scaffold for assembly of several extracellular matrix proteins (type I collagen, fibronectin, tenascin-C, and laminin γ2) and accessory proteins (BMP-1 and CCN3) (Amizuka et al., 2009; Elliott & Hamilton, 2011; Kudo & Kii, 2018; Maruhashi et al., 2010; Rogers et al., 2008). This demonstrates a critical role for periostin in extracellular matrix (ECM) homeostasis and the regulation of cell phenotype.

In skin, we have shown that periostin plays a pivotal role in excisional wound repair, where it facilitates myofibroblast differentiation through a β1 integrin/FAK dependent mechanism (Crawford et al., 2015; Elliott et al., 2012; Walker et al., 2015; Zhou et al., 2010). In contrast, in gingival healing periostin regulates extracellular matrix synthesis, upregulating fibronectin and collagen synthesis via integrin β1, FAK and JNK, but it is not associated with myofibroblast differentiation (S. S. Kim, Nikoloudaki, Michelsons, et al., 2019). The low number of myofibroblasts evident during gingival healing is postulated as an underlying reason for the reduced scar formation evident in healing of the gingival tissue (S. S. Kim, Nikoloudaki, Michelsons, et al., 2019). These contrasting effects on dermal and gingival fibroblasts demonstrate the tissue-specificity of matricellular protein bioactivity in relatively homologous tissues (Nikoloudaki et al., 2020). The palatal mucoperiosteum, even though part of the oral cavity, has been shown to exhibit significant scarring after surgical procedures. The investigation of distinct healing patterns among skin, gingiva and

the palatal mucoperiosteum could provide deeper understanding of how differences in molecular composition and physical properties of these tissues lead to the different healing outcomes. It would therefore be intriguing to assess the role of periostin in palatal tissues, which while still in the oral cavity, is strongly associated with scarring after injury. However, the role of periostin in palatal mucoperiosteum has yet to be investigated.

It remains critical to fully understand the underlying molecular and cellular mechanisms responsible for ECM accumulation in the palate during the wound healing process. Verstappen et al., using a rat model, found that there are significantly more myofibroblasts in the wounded mucoperiosteum than are evident in skin wounds, which they attributed to the different contractile abilities that these tissues possess and correlated their findings with the different wound healing patterns of these tissues (Verstappen et al., 2012). We hypothesized that periostin would be transiently upregulated following palatal wounding, modulating fibroblast differentiation and matrix synthesis. Using a periostin-knockout (*Postn*$^{-/-}$) mouse (Rios et al., 2005), we show that the loss of periostin results in altered wound closure kinetics. In contrast to gingiva, α-SMA myofibroblasts are present during palatal healing, and genetic deletion of periostin resulted in reduction of α-SMA and fibronectin in the newly formed granulation tissue. Furthermore, murine palatal fibroblasts isolated from *Postn*$^{-/-}$ mice showed an impaired contraction of a collagen matrix, which can be rescued by the exogenous addition of periostin. Furthermore, using silicon substrates of different elastic modulus, we show that *Acta2*/α-SMA is upregulated in stiff substrates and fibronectin is upregulated in low stiffness conditions, and that these effects were attenuated by the genetic deletion of periostin, suggesting *that the ECM stiffness is an important modulator of cell behaviour*.

2.2 Materials and Methods

2.2.1 Animals

All animal procedures were in accordance with protocols approved by the University Council on Animal Care at The University of Western Ontario. *Postn*-knockout mice (*Postn*$^{-/-}$) were generated and maintained on soft diet in order to reduce malnutrition, which was previously observed under a standard diet due to the enamel and dentin defects of the incisors and molars (Rios et al., 2005). Heterozygous mice were crossed with C57BL/6J (JAX Mice and Services, Bar Harbor, Maine) for a minimum of six generations to ensure an incipient congenic strain. Backcrossed heterozygous mice were used for breeding and all offspring were genotyped as described previously described (Rios et al., 2005).

2.2.2 Palatal wounds

For experiments, *Postn*$^{-/-}$ mice (KO) and littermate *Postn*$^{+/+}$ (WT) mice (20weeks of age) were anesthetized with an intraperitoneal injection of buprenorphine (0.05 mg/kg), followed by an injection of ketamine (90 mg/kg) and xylazine (5 mg/kg). One full-thickness excisional wound was made with a 1.5 mm disposable biopsy punch (Integra™ Miltex®, Integra York PA, Inc.) on the hard palate. The localization of the palatal punch biopsy was standardized with the anterior edge of the wound to be aligned with the first molar (Keswani et al., 2013) (shown in Appendix Figure A-1) to avoid traumatizing the palatal arteries which run on either side of the wound. The animals received 0.05 mg/kg Buprenorphine by subcutaneous injection twice daily for 48 hours post-surgery as an analgesic. Animals were maintained on a standard lab chow powdered food diet and were allowed food and water *ad libitum* for the duration of the experiment. Excised tissue was considered day 0 and was retained as normal healthy tissue. Wounds were photographed immediately after wounding and at time-points selected according to the defined phases of repair: early (day 3), inflammation and granulation tissue formation (day 3, 6), re-epithelialization (completed by day 9) (Cornelissen et al., 1999), and tissue remodeling (day 12-15). Wound area was assessed from photographs using ImageJ software. Animals were euthanized at 3, 6, 9, 12 and 15 days post-wounding by carbon dioxide inhalation.

2.2.3 Tissue Preparation

Post euthanasia, mice were decapitated, and the maxillae were fixed in 10% neutral buffered formalin (Sigma Aldrich,St. Louis, MO) for 24 hours and decalcified in 20% EDTA (ethylenediminetetraacetic acid) for 10 days at 4 °C. The maxillae were dehydrated through a graded series of ethanol, processed and embedded in paraffin, and sectioned at 5 μm thickness for various staining.

2.2.4 Histological analysis

Wounds from WT and *Postn*$^{-/-}$ mice were histologically analyzed (n=5) for the extent of re-epithelialization. Sections from the center of the wounds were stained with Masson's Trichrome (University Hospital, London, ON) and wound size as well as epithelial migration distance were calculated using ImageJ software. Epithelial migration distance was defined as the unilateral distance between the wound border and the migrating front of keratinocytes and percentage of epithelialization was determined from bilateral epithelial migration distance, normalized to wound size. Images were taken with a DM1000 light microscope (Leica, Concord, Ontario) and Leica Application Suite Software (version 3.8).

2.2.5 Immunohistochemistry & Immunofluorescence

Immunohistochemistry was performed as previously described (Elliott et al., 2012). In brief, tissue sections were deparaffinized, blocked with 10% horse serum, and immune-labeled using primary antibodies against α-smooth muscle actin (α-SMA) (ab5694, 1:200, Abcam plc, Cambridge, United Kingdom) and phosphorylated Smad2/3 (pSmad2/3) (sc11769-R, 1:100, Santa Cruz Biotechnology, Santa Cruz, CA). Sections were counterstained with haematoxylin. Negative controls excluded the primary antibody. Primary antibodies were detected using the ImmPRESS Reagent Kit Peroxidase (Vector Laboratory; Burlingame, CA) and visualized with 3,3-diaminobenzidine DAB reagent (Vector Laboratories) following the manufacturer's instructions. All sections were counterstained with haematoxylin (Sigma Aldrich).

Immunofluorescence staining carried out as above excluding haematoxylin counterstaining. Tissue sections were incubated with primary antibodies against periostin (sc49480, 1:100, Santa Cruz Biotechnology), fibronectin (ab23750, 1:150, Abcam), fibroblast-specific protein-1 was with anti-FSP1/S100A4 (1:100, Millipore, Billerica, MA), Arginase-1 (V:20, sc18354, 1:100, Santa Cruz Biotechnology), iNOS (ab15323, 1:100, Abcam) and Vimentin (ab92547, 1:200, Abcam). Primary antibodies were detected using Alexa Fluor IgG secondary antibodies (Invitrogen, Thermo Fisher Scientific). All sections were counterstained with Hoechst 33342 dye (1:1000, Invitrogen, Thermo Fisher Scientific) for nuclei. Images were taken on Carl Zeiss Imager M2m microscope (Carl Zeiss, Jena) using ZenPro 2012 software.

2.2.6 RNA isolation and real-time quantitative PCR

Palatal wounded tissues from WT and *Postn*$^{-/-}$ mice (N=7 per timepoint) were dissected using a 1.5 mm diameter punch biopsy, homogenized using BeadBug™ prefilled tubes (0.5mm zirconium beads, Z763772, Sigma-Aldrich) in 1.5 ml of TRIzol reagent (Thermo Fisher Scientific), and purified using RNeasy mini kits (Qiagen, Valencia, CA). The area that was excised for mRNA extraction is shown in Figure 2.1 C by a white box. Taqman real-time PCR was performed using qSCRIPT XLT one-step real-time quantitative PCR ToughMix (Quanta Biosciences, Gaithersburg, MD) per the manufacturer's instructions. All samples were run in triplicate and normalized to endogenous 18S rRNA (Thermo Fisher Scientific).

2.2.7 In situ hybridization (ISH)

In situ hybridization for periostin and βigh3 message using antisense and sense (control) *Postn* and *βigh3* cDNA probes (as described Lindsley et al. (Lindsley et al., 2005)) was performed on 10 μm paraffin serial sections. For both probes, serial sections were examined using at least three individual palates of each genotype.

2.2.8 Isolation of murine primary palatal fibroblasts (mPFBs)

The soft tissue covering the whole hard palate of six mice was excised and immediately transferred to sterile PBS supplemented with 10% fetal bovine serum and 7x AA (200 U penicillin, 200 mg streptomycin, 0.5 mg/ml amphotericin B) (Gibco, Carlsbad, CA). The tissue was washed 3 times in PBS, 3 times in DMEM, cut into smaller pieces (approx. $1cm^2$), and allowed to attach on tissue culture plastic for a few minutes. DMEM, 10% FBS, 1x AA was added and the explants were incubated at 37 °C, 5% CO_2 to allow fibroblasts to migrate onto the culture surface. The pieces of palatal tissue were removed, and cells were used at passage 1 and 2 for all experiments.

2.2.9 Cell treatment

mPFBs were seeded in DMEM containing 10% FBS at 8000 cells per cm^2 surface area for RTqPCR and immunocytochemistry, and at 16000 cells per cm^2 for western blot experiments in 6-well plates of different elastic modulus: 64 kPa, 8 kPa, 0.2 kPa (CytoSoft 6 well plate, Advanced BioMatrix). Tissue culture plastic plates (VWR) served as control. The plates were previously coated with 100µg/ml collagen type I (PureCol, Advanced BioMatrix, Carlsbad, CA) in DPBS as per manufacturer's instructions. After 24 hours, cells were transferred into serum-free DMEM for an additional 16 hours. Then 5 ng/mL TGF-β1 (R&D Systems, Minneapolis, MN) was added to cells and incubated for 24 to 72 hours, depending on the assay. For assessing the influence of FAK pathway inhibition, starved mPPFs were treated with PF-573,228 (10 mM), and DMSO (1:1000) served as a control for PF-573,22. All experiments were run in triplicate.

2.2.10 CyQUANT Proliferation Assay

After mPFBs from WT and periostin KO animals were seeded on collagen type I pre-coated tissue culture plastic plates as previously described (section 2.2.9) for 1, 3, 5, and 7 days, media was completely aspirated, and the plates were frozen at -80 °C. Once all time-points were captured, DNA contents were determined by performing CyQUANT® Cell

Proliferation Assay Kit (C7026, Molecular Probes). Cell numbers were extrapolated using a standard curve, as per manufacturer's instructions.

2.2.11 Western Blotting

mPFBs were cultured on plates of different elastic modulus (8 kPa, 0.2 kPa) coated with 100μg/ml collagen type I (PureCol, Advanced BioMatrix, Carlsbad, CA) in DPBS for 24 hours. Cell lysates were harvested with RIPA buffer (Sigma Aldrich) containing protease and phosphatase inhibitor cocktails. Protein concentration was determined by Pierce® BCA Protein assay kit (Pierce; Waltham, MA). 12 μg proteins of each sample were separated by sodium dodecyl sulfate polyacrylamide gel electrophoresis (SDS-PAGE) and transferred to nitrocellulose membranes. Membranes were washed with Tris-buffered saline containing 0.05% Tween-20 (TBS-T) and blocked with 5% dried milk in TBS-T or 5% bovine serum albumin (BSA) in TBS-T. Primary antibodies for fibronectin (ab1954, 1:2000, Millipore), α−SMA (A5228, 1:2000, Sigma Aldrich), pFAK Y397 (ab81298, 1:1000, Abcam), FAK (ab40794, 1:1000, Abcam), Vinculin (MAB3574, 1:1000, Millipore), β1-integrin (SAB5600100, 1:1000, Sigma-Aldrich), GAPDH (MAB374, 1:1000, Millipore) were used to incubate the membranes for 12 hours. Detection was with appropriate peroxidase-conjugated secondary antibodies (1:2500, Jackson ImmunoResearch; West Grove, PA), which were developed with Clarity Western ECL substrate (Bio-Rad; Hercules, CA). Densitometry analysis was performed using Image Lab Software (Bio-Rad).

2.2.12 Immunocytochemistry

mPFBs were cultured on plates coated with 100 μg/ml collagen type I (PureCol, Advanced BioMatrix, Carlsbad, CA) are previously described (section 2.2.9) for 24 and 72 hours. Cells were fixed with 4% paraformaldehyde, permeabilized with 0.1% Triton X-100 and blocked with 1% BSA (Thermo Fisher Scientific). Fixed and permeabilized cells were labeled with mouse anti-α-SMA (A5228, 1:100, Sigma-Aldrich), anti-fibronectin (ab23750, 1:100, Abcam), vinculin (MAB3574, Millipore), β1-integrin (AF2405, R&D Systems) which was detected with appropriate IgG conjugated to Alexa Fluor secondary

antibodies (1:100, Invitrogen, Thermo Fisher Scientific). The cells were double immunolabeled with rhodamine-conjugated phalloidin (1:100, Invitrogen) for filamentous actin. Nuclei were counterstained using Hoechst 33342 dye (1:1000, Thermo Fisher Scientific). Images were taken on Carl Zeiss Imager M2m microscope (Carl Zeiss) using ZenPro 2012 software.

2.2.13 Fixed Gel Contraction Assay

In vitro, contractility of mPFBs was evaluated by employing collagen gel matrix contraction assays as previously described (Elliott et al., 2012; S. S. Kim, Nikoloudaki, Michelsons, et al., 2019). mPFBs suspended in 0.5% FBS DMEM were mixed 1:1 with collagen mix [10% 0.2 M HEPES buffer (4-(2-hydroxyethyl)-1 piperazineethanesulfonic acid; pH = 8], 40% bovine collagen type I (Advanced BioMatrix), and 50% 2X high glucose DMEM (Gibco)) to a final density of 100,000 cells/ml. In parallel, either 5 μg/ml rhPSTN (R&D Systems) or an equivalent volume of PBS was incorporated into the collagen and cell mix. 24 well tissue culture plates were pre-coated with 1% BSA for 12 hours and washed with PBS. 1 ml of the cell and collagen mix was plated to each well and allowed to set at 37 °C. Following polymerization, 1 ml of 0.5% FBS DMEM was added to the wells. After 24 hours, the gels were detached from the plate and they were left to contract for 24 hours at 37 ºC. As contraction of the collagen matrix excluded growth medium, thereby reducing the gel weight, loss of gel weight was used to measure the extent of contraction. This accounted for contraction of gels horizontally and vertically.

2.2.14 Statistical Analysis

Statistical analysis was by one-way or two-way ANOVA, as appropriate, followed by a Bonferroni correction, using Graphpad Software version 5 (Graphpad Software, La Jolla, CA) ($P<0.05$ was considered significant). For wound healing experiments, data are expressed as a fraction of the original wound area (mean ± SD). *In vivo* gene expression data represents the mean ± standard deviation of seven $Postn^{+/+}$ and seven $Postn^{-/-}$ wounds for each time point. For quantification of phosphorylated Smad2/3 in the wounds *in vivo*, data are expressed as the percentage of positive cells/total cells per field of view ± standard

deviation. For *in vitro* study, data are expressed as the mean ± standard deviation of three individual experiments with independent primary cultures from different animals. Individual experiments included three replicates. For quantification, RT-qPCR, western blot densitometry, gel contraction statistical analysis by two-way ANOVA with Bonferroni multiple comparisons test was used.

2.3 Results

2.3.1 Periostin mRNA and protein are up-regulated after excisional palatal wounding and peak 12 days after wounding

To temporally investigate the palatal healing process, we quantified the closure of the palatal mucoperiosteum in C57Bl/6 WT mice at 3, 6, 9, 12 and 15 days post-wounding, with unwounded palatal mucoperiosteum serving as a structural baseline control (day 0) (Fig. 2.1). Analysis of *in vivo Postn* gene expression during palatal wound healing in wild-type (WT) mice by real-time quantitative polymerase chain reaction (RT-qPCR) showed that *Postn* mRNA levels were significantly increased during palatal wound repair at day 6 ($P < 0.05$), peaking at day 12 ($P < 0.01$) (Fig. 2.1 A). Using *in situ* hybridization (ISH) (Fig. 2.1 B) and immunofluorescent staining (Fig. 2.1 C) in normal unwounded palatal mucosa periostin signal was weakly detected in the basal lamina and periosteum covering the palatal bone, with intense signal at the periodontal ligament of neighbouring teeth (arrow-Figure 2.1 B, white arrowheads Figure 2.1 C). After wounding, periostin was detected throughout the ECM of the granulation tissue at days 6, 9, 12 and 15 (Fig. 2.1 B, C).

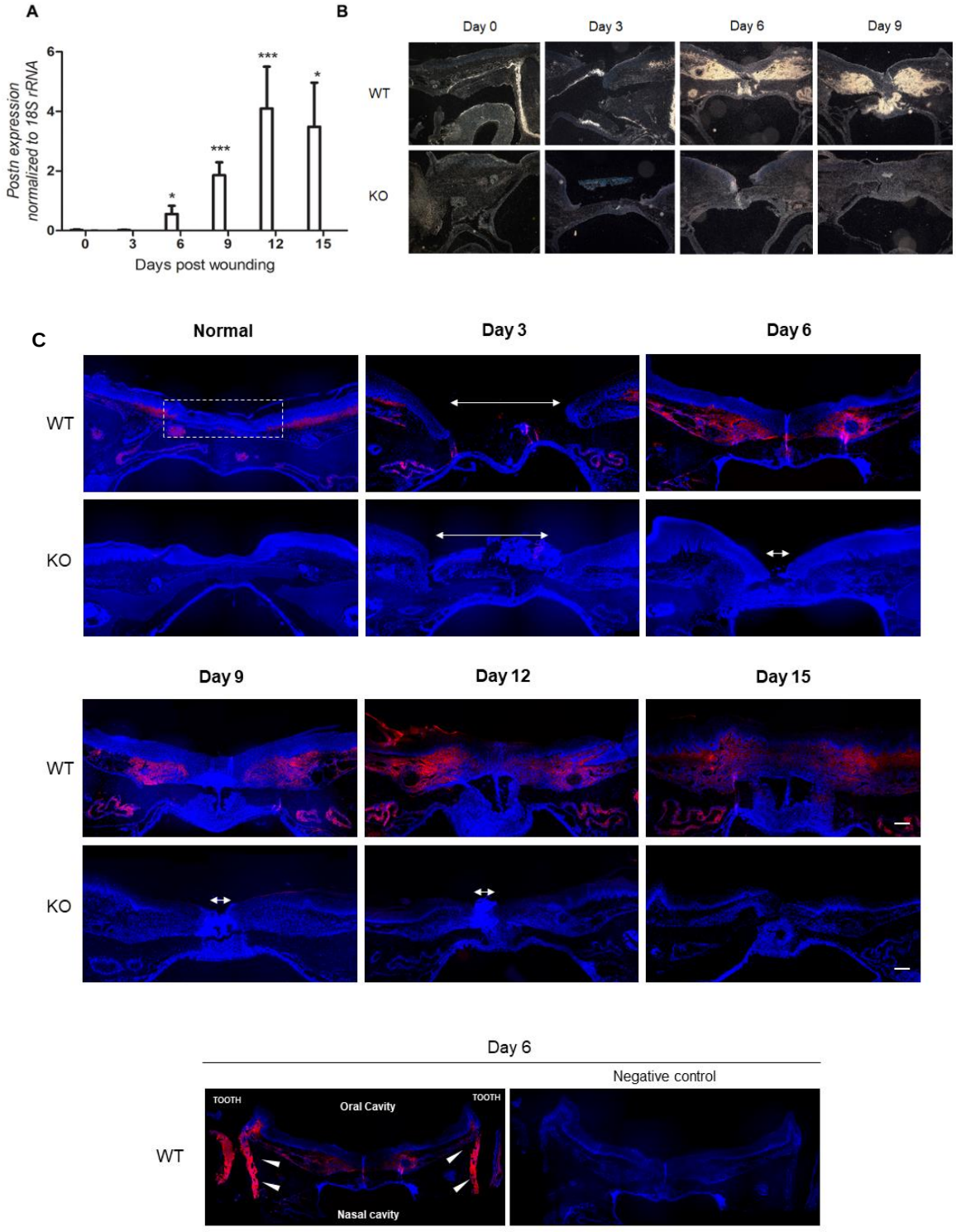
A
Postn expression normalized to 18S rRNA
Days post wounding
B
Day 0
Day 3
Day 6
Day 9
WT
KO
C
Normal
Day 3
Day 6
Day 9
Day 12
Day 15
WT
KO
Day 6
Negative control
TOOTH
Oral Cavity
TOOTH
Nasal cavity
WT

Figure 2-1 Periostin mRNA and protein are up-regulated after excisional palatal wounding

1.5mm full-thickness excisional wounds were created on the hard palate of periostin-knockout (*Postn*$^{-/-}$) and wild-type (WT) mice. **(A)** *Postn* mRNA expression was quantified in tissues from 0 to 15 days post wounding using quantitative PCR. Values are given as mean±SD. Data was analyzed using one-way ANOVA N=7 for each time-point (*$P < 0.05$; ***$P < 0.001$ comparisons to d0). All samples were run in triplicate and normalized to endogenous 18S rRNA **(B)** Periostin mRNA message detection in d0, d3, d6, d9 wounds of WT and *Postn*$^{-/-}$ mice by in situ hybridization **(C)** Immunofluorescent staining for Periostin from d0 to d15 post-wounding. White box indicates the area that was excised for mRNA extraction. White arrows indicate the length of the open wounds. White arrowheads indicate the periodontal ligament of the teeth. Scale bar: 200 μm

2.3.2 Genetic deletion of periostin results in altered wound-closure kinetics during excisional palatal healing in mice

To investigate the contribution of periostin to palatal wound repair process, full-thickness excisional wounds were created in *Postn*$^{-/-}$ (KO) and *Postn*$^{+/+}$ (WT) mice. To assess differences in the rate of wound closure between *Postn*$^{-/-}$ and WT mice, we measured wound size based on gross appearance up to 12 days after wounding. Genetic deletion of *Postn* significantly reduced wound closure rates compared to WT mice. Wounds in WT mice were macroscopically resolved by day 6, with wound size in *Postn*$^{-/-}$ animals reduced by 80% of the initial wound area (Fig. 2.2 B). Histological analysis of sections from the center of the wounds at day 6 (Fig. 2.2 C-F) confirmed that *Postn*$^{-/-}$ wounds were significantly larger than those of their WT littermates ($P < 0.05$) with decreased re-epithelialization at day 6 evident in *Postn*$^{-/-}$ mice ($P < 0.01$), although epithelial tongue length was similar in both genotypes ($P > 0.05$). Wounds in both WT and *Postn*$^{-/-}$ were closed by day 12.

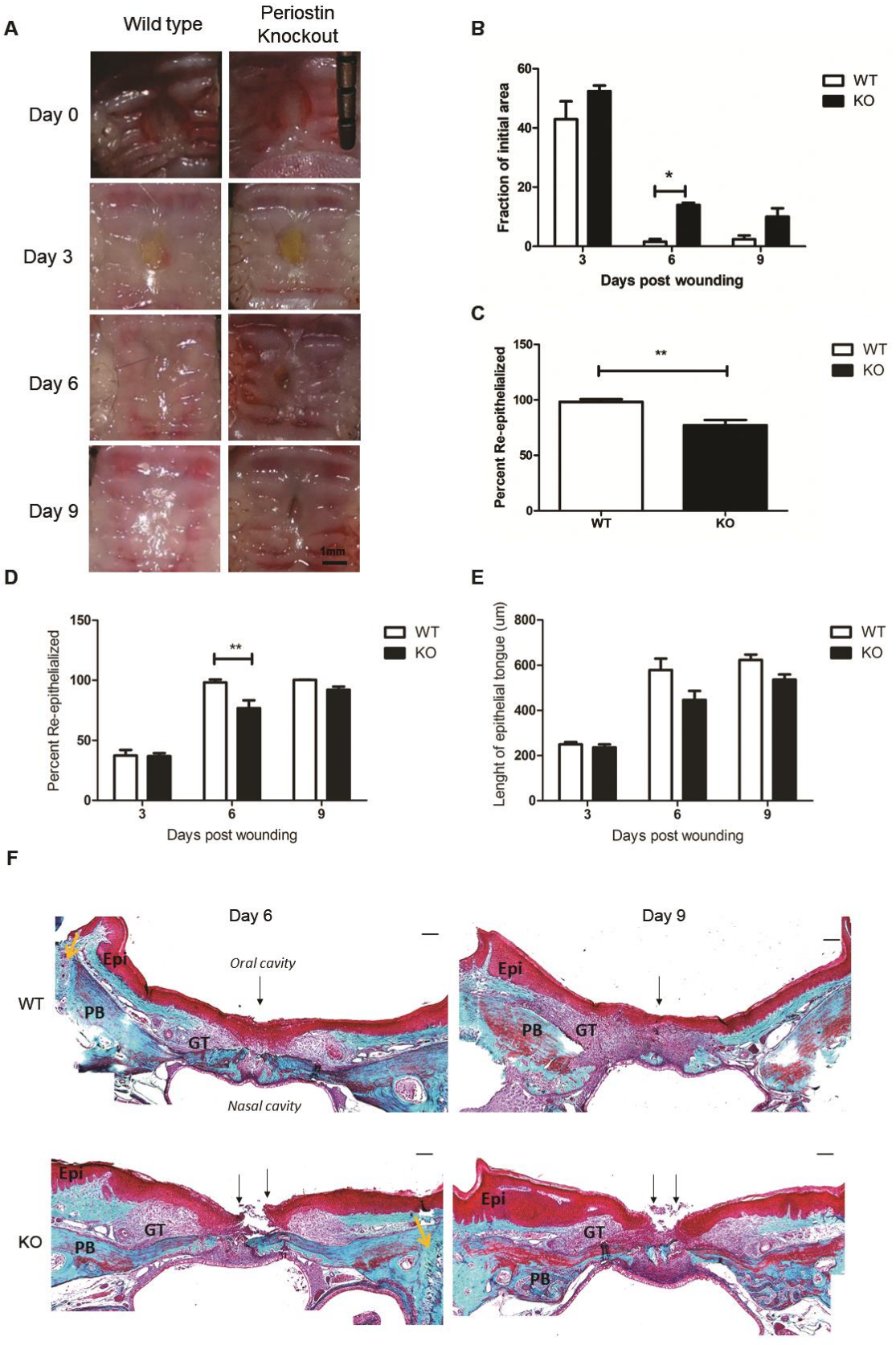
A
Wild type
Periostin Knockout
Day 0
Day 3
Day 6
Day 9
1mm
B
Fraction of initial area
60
40
20
0
*
3
6
9
Days post wounding
WT
KO
C
Percent Re-epithelialized
150
100
50
0
**
WT
KO
D
Percent Re-epithelialized
150
100
50
0
**
3
6
9
Days post wounding
WT
KO
E
Lenght of epithelial tongue (um)
800
600
400
200
0
3
6
9
Days post wounding
WT
KO
F
Day 6
Day 9
WT
KO
Epi
PB
GT
Oral cavity
Nasal cavity

Figure 2-2 Genetic deletion of periostin results in altered wound-closure kinetics during excisional palatal healing in mice

(A) Wound size was measured up to 12 days post wounding in 1.5-mm wounds from 7 *Postn*$^{-/-}$ and 7 WT animals. Representative wounds are shown at 0, 3, 6, and 9 days post wounding (top to bottom). Bar= 1 mm. Masson's trichrome-stained sections were used to analyze wound size (B), re-epithelialization (C, D) and the epithelial tongue length (E). 5 *Postn*$^{-/-}$ and 5 WT mice were quantified. Data are expressed as mean ± standard deviation. *P < 0.05; **P < 0.01. (F) **Representative images from sections stained with Masson's Trichrome Stain**. WT wounds have completely closed by day 6. However, *Postn*$^{-/-}$ wounds present delayed healing as at day 9 re-epithelialization has not been completed. Black arrows indicate edge of the wound. Yellow arrows indicate the periodontal ligament of neighbouring teeth. (**PB**= Palatal Bone, **Epi**= oral Epithelium, **GT**= Granulation Tissue) Scale bar= 125 μm

2.3.3 Absence of Postn alters transcriptional regulation of genes associated with repair and wound healing

α-SMA expression is attenuated in the granulation tissue of Postn$^{-/-}$ mice

Acta2 is expressed by mesenchymal cell types including pericytes and myofibroblasts (MF). MFs are key during wound healing, responsible for ECM synthesis, remodeling and tissue contraction (Gabbiani et al., 1971; Hinz, 2016; Tomasek et al., 2002). Assessment of α-SMA in *Postn*$^{-/-}$ and WT wounds using immunohistochemistry showed α-SMA was evident at the wound edge and within the granulation tissue of WT wounds at days 6 and 9. At day 6, increased immunoreactivity of α-SMA was detected at the wound border in WT mice, throughout the granulation tissue and in blood vessel walls (Fig. 2.3A). In day 6 *Postn*$^{-/-}$ wounds, α-SMA immunoreactivity was reduced when compared with that in WT. Quantitative PCR (RT-qPCR) on RNA isolated from WT and *Postn*$^{-/-}$ wounds at 3 ,6 ,9, 12 and 15 days post wounding demonstrated that *Acta2* mRNA levels were increased in both genotypes, but was significantly reduced in the granulation tissue of *Postn*$^{-/-}$ mice at day 6 (Fig. 2.3 B) ($P<0.05$). Double immunofluorescence staining was used to detect the spatial relationship between α-SMA and periostin signal in the wound matrix. We observed that α-SMA positive cells, indicating the presence of myofibroblasts, were in the granulation tissue and periostin matrix, indicating that periostin might have an effect to myofibroblast differentiation by direct contact (Fig. 2.3 D). To determine whether the reduction in α-SMA mRNA levels was due to impaired fibroblast recruitment into the granulation tissue, sections were labeled for fibroblast-specific protein-1 (FSP-1) (Fig. 2.4 A, B) and vimentin (Fig. 2.4 C). While no significant differences in FSP-1 immunoreactivity in *Postn*$^{-/-}$ tissue compared to WT at days 6 and 9 post-wounding, we observed decreased vimentin signal in *Postn*$^{-/-}$ wounds at day 6 when compared to WT wounds indicating impaired granulation tissue formation and reflecting the delay in wound healing kinetics (Fig. 2.4 D).

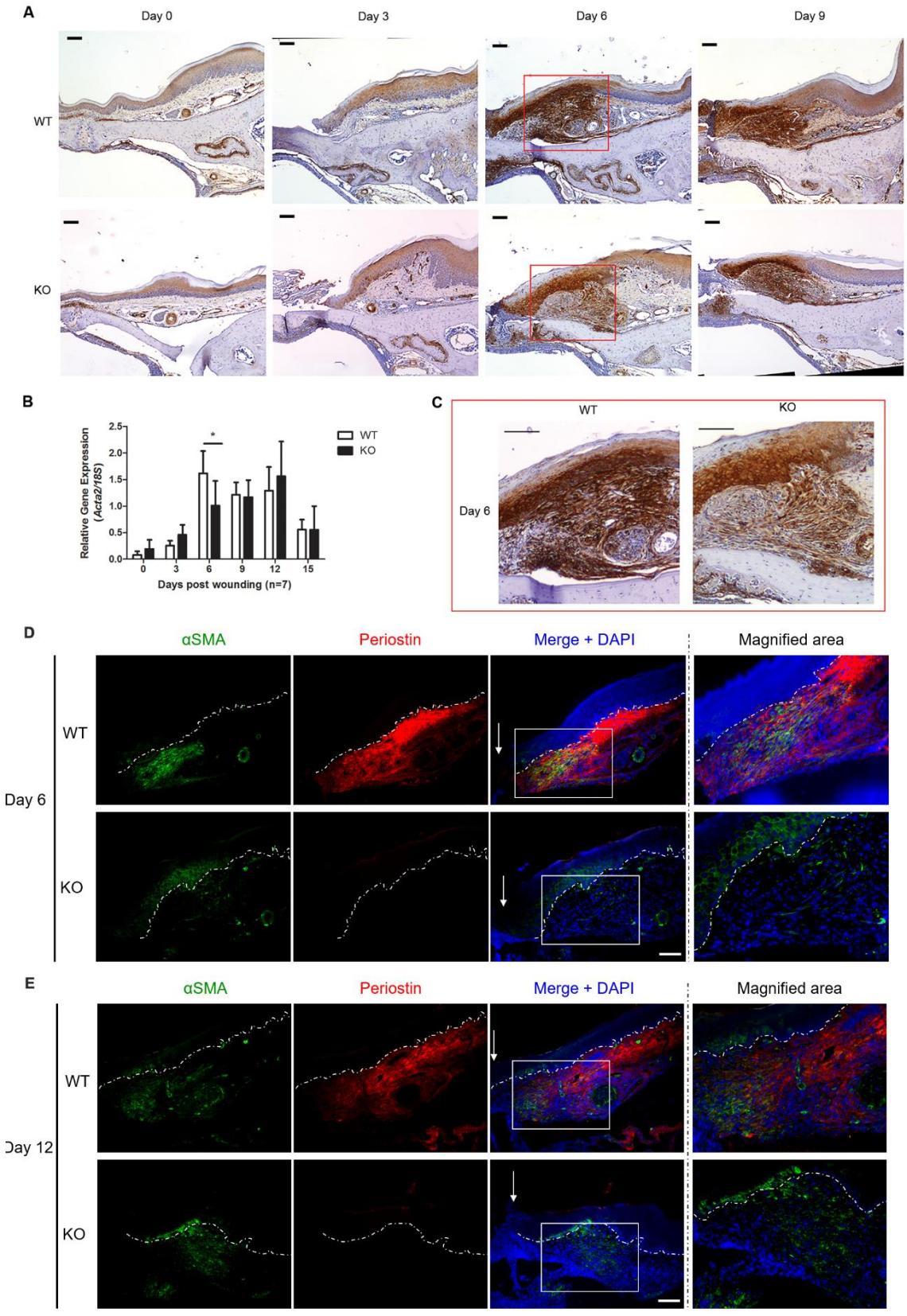
A
Day 0
Day 3
Day 6
Day 9
WT
KO
B
Relative Gene Expression (Acta2/18S)
2.5
2.0
1.5
1.0
0.5
0.0
*
WT
KO
0
3
6
9
12
15
Days post wounding (n=7)
C
WT
KO
Day 6
D
αSMA
Periostin
Merge + DAPI
Magnified area
Day 6
WT
KO
E
αSMA
Periostin
Merge + DAPI
Magnified area
Day 12
WT
KO

Figure 2-3 α-SMA expression is reduced, but not absent, in the granulation tissue of *Postn*$^{-/-}$ mice

(A) Immunohistochemical staining for α-smooth muscle actin (α-SMA). Sections of normal (day 0) tissue and day 3,6 and 9 wounds of WT and *Postn*$^{-/-}$ animals. The area highlighted in the red rectangle is magnified below in panel **(C)**. **(B)** *Acta2* expression was quantified in tissue from 3 to 15 days post wounding using RTqPCR. Values are given as mean±SD. N=7 animals per time point. *P < 0.05. **(D)** Double immunofluorescent staining to detect α-SMA (green) and periostin (red) signal at day 6 and day 12 wounds of WT and *Postn*$^{-/-}$ animals. Scale bar: 100 μm. White dashed lines indicate the border between the epithelium and the granulation tissue.

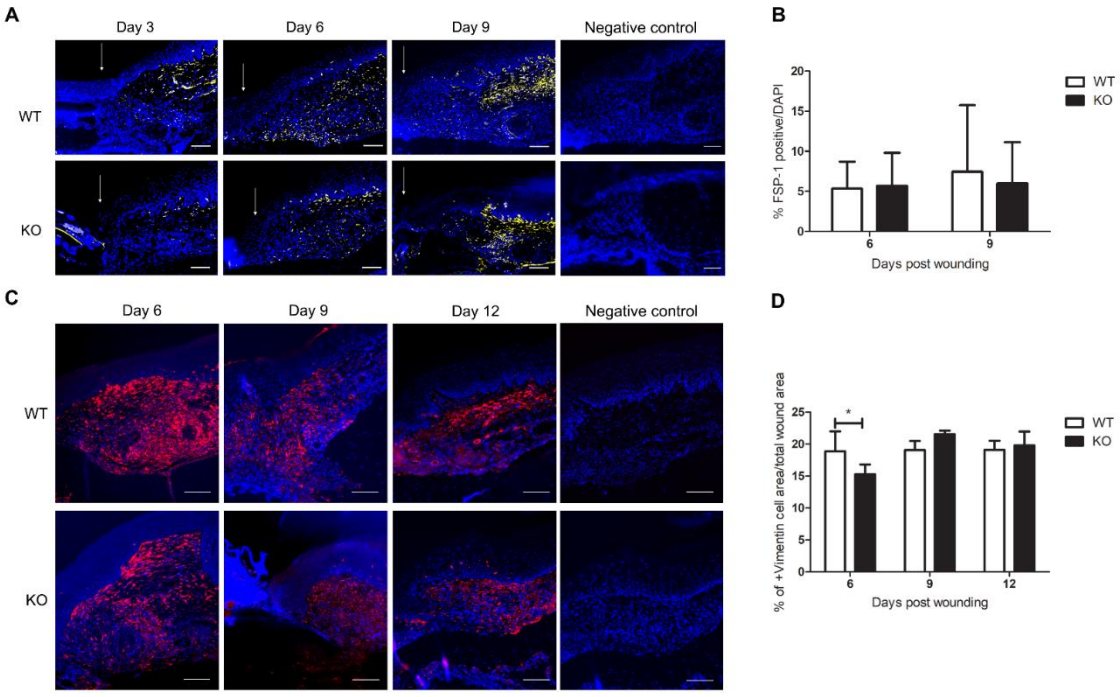

Figure 2-4 Reduction in SMA mRNA levels was not due to impaired fibroblast recruitment into the granulation tissue

(A) Immunofluorescent staining to detect fibroblasts using fibroblast-specific protein-1 antibody. Bar: 200μm. ***(B)*** Quantification presented as percentage of FSP-1-positive cells/DAPI-positive cells of wounds at days 6 and 9 post-wounding, in four WT and four *Postn*$^{-/-}$ mice. ***(C)*** Immunofluorescent staining for Vimentin. ***(D)*** Quantification presented as percentage of Vimentin positive area/wound area of wounds at days 6, 9 and 12 post-wounding, in four WT and four *Postn*$^{-/-}$ mice. Bar: 200μm. ($P < 0.05$) White arrows indicate the leading wound edge.

Genetic deletion of Postn is associated with reduced fibronectin expression and deposition during palatal healing.

Using immunofluorescence, we next assessed localization of fibronectin, a glycoprotein important in ECM organization and stability, as well as attachment sites for fibroblasts and keratinocytes, to facilitate their migration into the wound bed (Pereira et al., 2002; Zollinger & Smith, 2017). Fibronectin immunoreactivity was evident in the basal lamina and at the granulation tissue of WT wounds at day 6 and 9. However, in *Postn*$^{-/-}$ wounds the granulation tissue at the wound edge had reduced fibronectin labeling (Fig. 2.5 A). Analysis of *in vivo Fn1* mRNA levels by RT-qPCR confirmed that copy number of *Fn1* was significantly lower in *Postn*$^{-/-}$ wounds compared to WT at day 9 post-wounding ($P < 0.001$) (Fig. 2.5 C). Using double immunofluorescence staining we found that fibrillar fibronectin and periostin partially colocalize within the wound environment, further supporting the direct interaction if these biomolecules (Fig. 2.5 B)

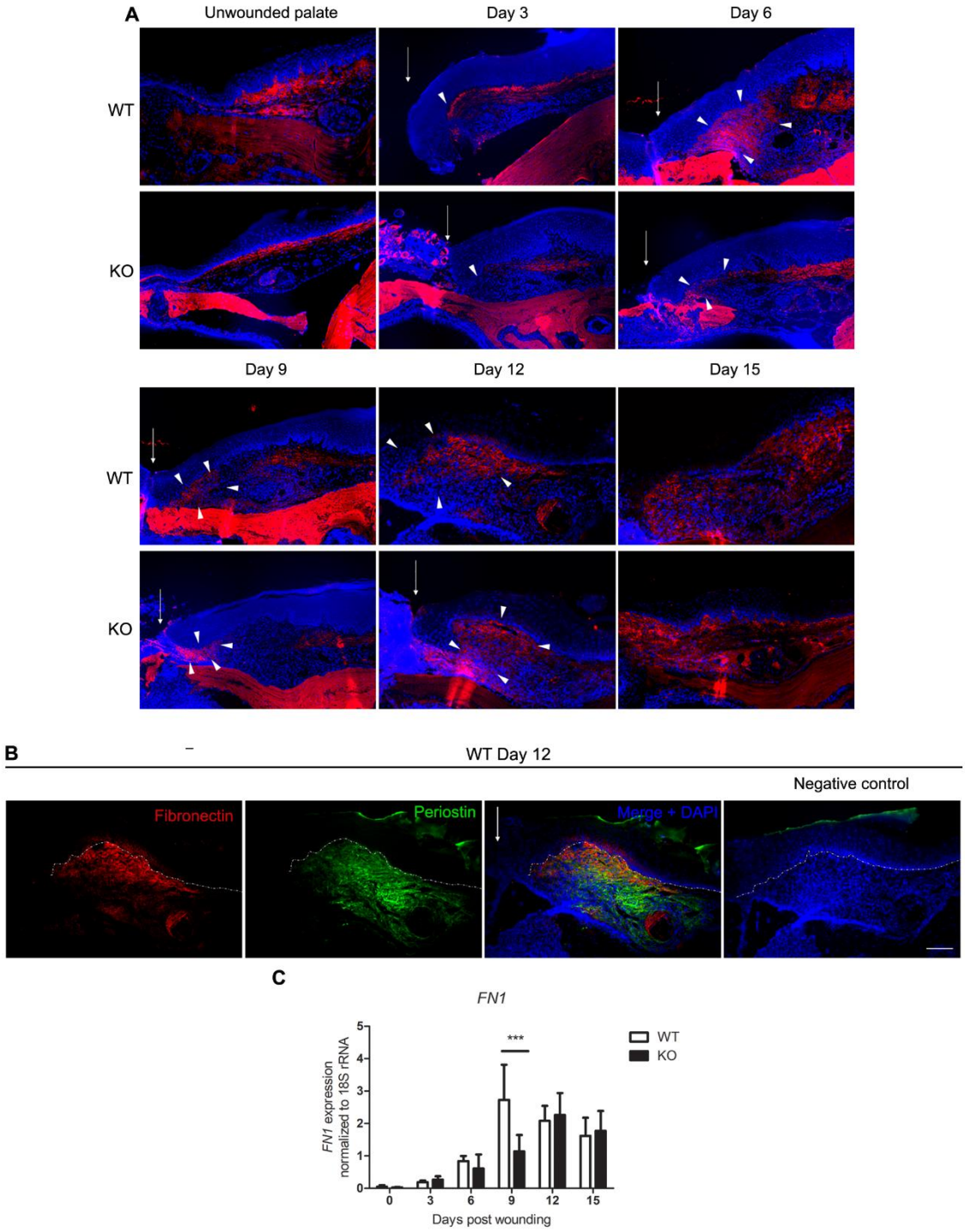
A
Unwounded palate
Day 3
Day 6
WT
KO
Day 9
Day 12
Day 15
WT
KO
B
WT Day 12
Negative control
Fibronectin
Periostin
Merge + DAPI
C
FN1
***
WT
KO
FN1 expression normalized to 18S rRNA
0
1
2
3
4
5
0
3
6
9
12
15
Days post wounding

Figure 2-5 Genetic deletion of Postn is associated with reduced fibronectin expression and deposition during palatal healing

(A) Representative images of immunoreactivity for Fibronectin of unwounded (day 0) and wounded mice palate. White arrows indicate the leading wound edge and white arrowheads indicate fibronectin labeling in the granulation tissue at the wound edge. Scale bar: 200 μm. **(B)** Double immunofluorescent staining to detect periostin (green) and fibronectin (red) localization in the granulation tissue day 12 wounds of WT animals. Scale bar: 100 μm **(C)** FN1 mRNA expression was quantified in tissues from 0 to 15 days post wounding using quantitative PCR. Values are given as mean±SD. Data was analyzed using one-way ANOVA N=7 for each time-point (***$P < 0.001$).

2.3.4 Genetic deletion of Postn affects immune cell infiltration

Inflammatory cell infiltration in the wounds was assessed by characterizing the macrophages populations in the granulation tissue of the wounds using antibodies specific for iNOS (M1 polarization), and arginase-1 (arg-1) (M2 polarization) (Jablonski et al., 2015). Overall, WT wounds appeared to have increased M1 and M2 macrophages than *Postn*$^{-/-}$ during wound healing at day 3, 6 and 9 post wounding. The presence of iNOS-positive cells was more abundant in day 6 and 9 WT wounds throughout the granulation tissue, as well as at the epithelial layers. However, *Postn*$^{-/-}$ wounds had significantly less iNOS-positive cells (WT, 30%; *Postn*$^{-/-}$, 12%; $P < 0.001$), which were located at the edge of the wound (Fig. 2.6). Similar observations were also found for Arginase-1-positive cells. These observations suggest that the reduced number of macrophages in palatal healing likely results from genetic deletion of periostin.

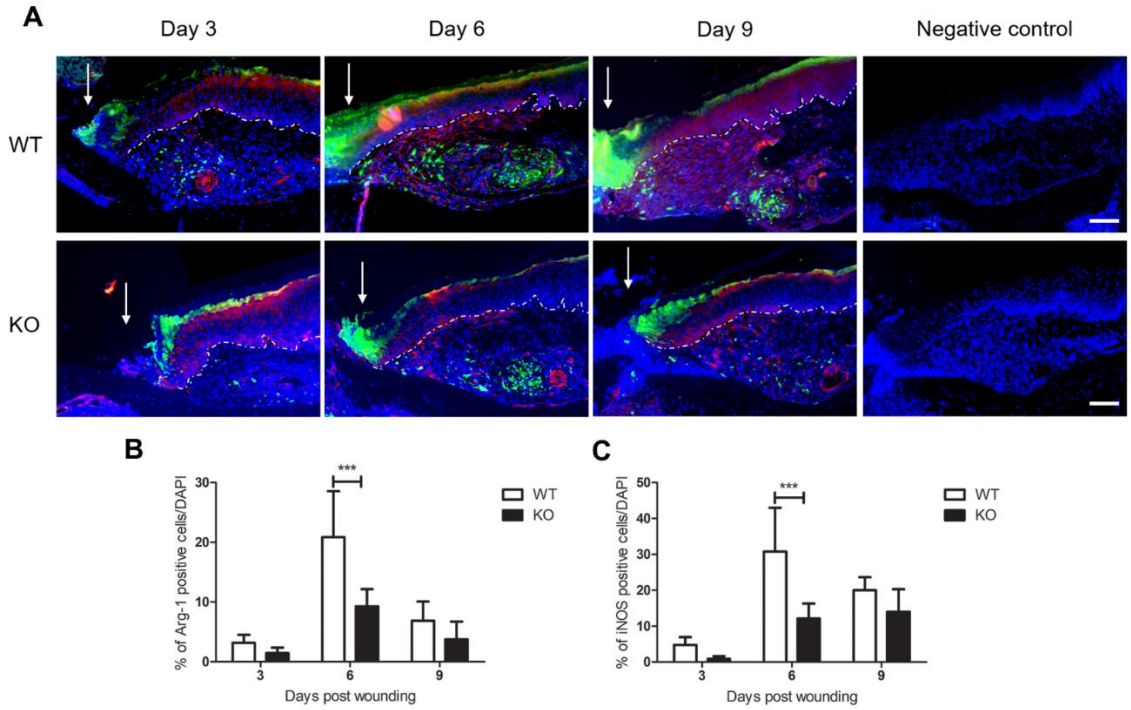

Figure 2-6 Genetic deletion of Postn affects immune cell infiltration.

(A) Double Immunofluorescent staining to detect macrophages markers Arginase-1 (M2 polarization-green) (Arg-1, V:20 sc18354) and iNOS (M1 polarization-red) (iNOS antibody ab15323). White arrows indicate the leading edge of the wound. White dashed line indicates the border between the epithelium and the granulation tissue. Scale bar: 200μm. **(B)** Quantification presented as percentage of Arginase-1-positive cells/DAPI positive cells of wounds at days 3, 6 and 9 post-wounding, in six WT and four *Postn*$^{-/-}$ mice. **(C)** Quantification presented as percentage of iNOS-positive cells/DAPI positive cells of wounds at days 3, 6 and 9 post-wounding, in six WT and four *Postn*$^{-/-}$ mice.

2.3.5 βigh3 does not have a compensatory role for the loss of periostin in Postn$^{-/-}$ animals

Also defined as a matricellular protein, transforming growth factor-β-induced gene product-h3 (TGFBI/βigh3) is considered a paralog of Postn because of their structural similarity (Kawamoto et al., 1998). *In vitro* studies showed that βigh3 promotes adhesion and migration of dermal fibroblasts and keratinocytes (Bae et al., 2002; LeBaron et al., 1995; Mosher et al., 2015). Thus, we hypothesized that βigh3 might play compensatory roles in the adhesion and migration of keratinocytes/fibroblasts at wound sites. We therefore assessed the levels of *TGFBI/βigh3* by ISH and RT-qPCR in WT and *Postn*$^{-/-}$ embryonic tissues as well as its expression in normal and wounded tissues. ISH demonstrated that *βigh3* mRNA is present in normal, uninjured palate and is upregulated during wound healing. βigh3 showed increased expression in comparison to Postn in day 3 wounds, where it is present in granulation tissue filling the wound site (Fig. 2.7). At day 6 post-wounding both *Postn* and *βigh3* are present in WT granulation tissue at the wound site, after which they are gradually reduced. RT-qPCR analysis confirmed that the mRNA level of *βigh3* in day 6 *Postn*$^{-/-}$ wounds is significantly reduced compared to WT wounds ($P < 0.05$). The different wound-response spatiotemporal expression patterns of these two matricellular proteins might be an indication that βigh3 may not compensate for the loss of Postn during palatal wound healing or that *Postn* and *βigh3* are differentially regulated via divergent upstream signaling pathways. This is supported by our observations in embryonic tissues where *Postn* mRNA message is present in the developing palatal shelves of the secondary palate and tongue at E15, while *βigh3* mRNA message is only present in the tongue (Fig. 2.7 C). Thus, βigh3 can play an independent role and exhibit non-overlapping expression and function with Postn in the development of the hard palate in mice.

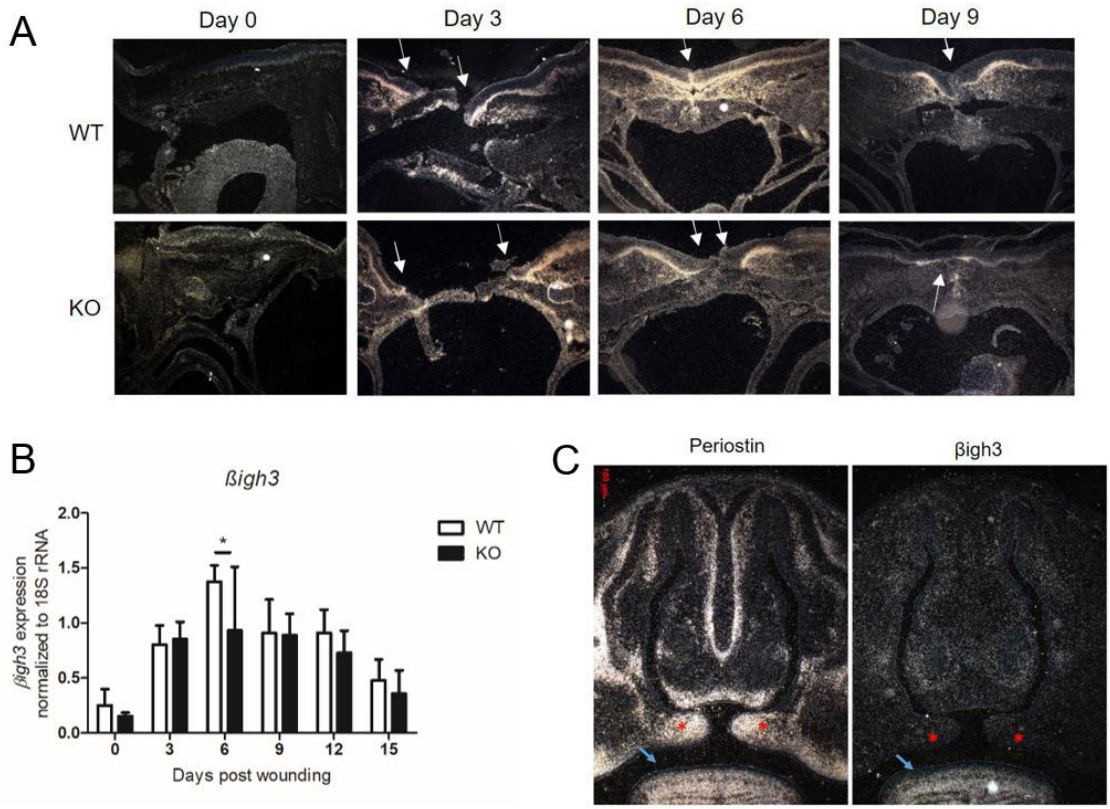

Figure 2-7 βigh3 does not have a compensatory role for the loss of periostin in *Postn*$^{-/-}$ animals.

(A) *βigh3* message detection in days 0 (normal tissue), 3, 6 and 9 WT wounds by in situ hybridization. White arrows indicate the leading wound edge. **(B)** *βigh3* expression was quantified in tissue from 3 to 15 days post wounding using RTqPCR. Values are given as mean±SD. N=7 per time point. *P < 0.05. **(C)** Postn and βigh3 message detection at E15 mice.

2.3.6 Canonical TGFβ signaling is not altered in Postn$^{-/-}$ fibroblasts

TGFβ is known to cause an increase in α-SMA expression through phosphorylation of Smad3 (Gu et al., 2007), and plays a major role in myofibroblast differentiation (Desmoulière et al., 1993). Therefore, to determine whether the reduction in α-SMA expression and immunoreactivity in *Postn*$^{-/-}$ granulation tissue was due to defective TGFβ–Smad3 signaling, we assessed the number of nuclei positive for phosphorylated Smad2 and Smad3 (pSmad2/3) within the granulation tissue of palatal wounds at day 3, 6, 9, 12 and 15 post-wounding (Figure 2.8A). The number of pSmad2/3-positive nuclei was similar in both WT and *Postn*$^{-/-}$ wounds, suggesting that canonical TGFβ signaling is active in *Postn*$^{-/-}$ wounds and unaffected by the absence of periostin (Figure 2.8B).

2.3.7 Exogenous periostin is sufficient to induce a contractile phenotype in Postn$^{-/-}$ fibroblasts

To examine the functional role of periostin in palatal healing, we utilized *in vitro* assays to investigate how genetic deletion of periostin affects the proliferation rate and myofibroblast differentiation of murine palatal fibroblasts (mPFBs). Periostin is known to modulate expression of α-SMA during skin healing (Elliott et al., 2012), but not in gingival healing (S. S. Kim, Nikoloudaki, Michelsons, et al., 2019). In our *in vivo* experiments we observed a reduced levels of α-SMA on *Postn*$^{-/-}$ wounds (0) which indicates that a defect might exist in differentiation of fibroblasts to myofibroblasts in *Postn*$^{-/-}$ wounds. When cells where cultured for 24 and 72h on tissue culture plastic (TCP), *Acta2* mRNA levels were significantly higher in WT mPFBs in comparison to *Postn*$^{-/-}$ mPFBs ($P < 0.01$, $P < 0.001$) (Figure 2.8 C). Exogenous stimulation of the cells with TGFβ (5 ng/ml) did not have a significant effect on *Acta2* mRNA levels in either cell type (Fig. 2.8 D), indicating that the cells might have already become maximally differentiated.

WT and *Postn*$^{-/-}$ mPFBs were isolated and cultured for 1,3,5 and 7 days to assess their proliferation rates. Both cell types exhibited a 4-fold increase in cell number by day 7 with no significant difference in cell number evident between the genotypes ($p > 0.05$) (Fig. 2.8 E). To assess the contractile ability of the cells we utilized *in vitro* assays to determine

their ability to contract a floating collagen gel. Quantification of contraction through measurement of gel weight showed that WT palatal fibroblasts were able to significantly contract the collagen matrix in comparison with *Postn*$^{-/-}$ palatal fibroblasts, indicating that periostin is required for contraction of a collagen matrix by palatal fibroblasts ($P < 0.01$) (Fig. 2.8 F). To further investigate this finding, 5 mg/ml recombinant human periostin (rhPSTN) was added to the collagen matrix and was found to be sufficient to induce contraction of the gels by *Postn*$^{-/-}$ palatal fibroblasts.

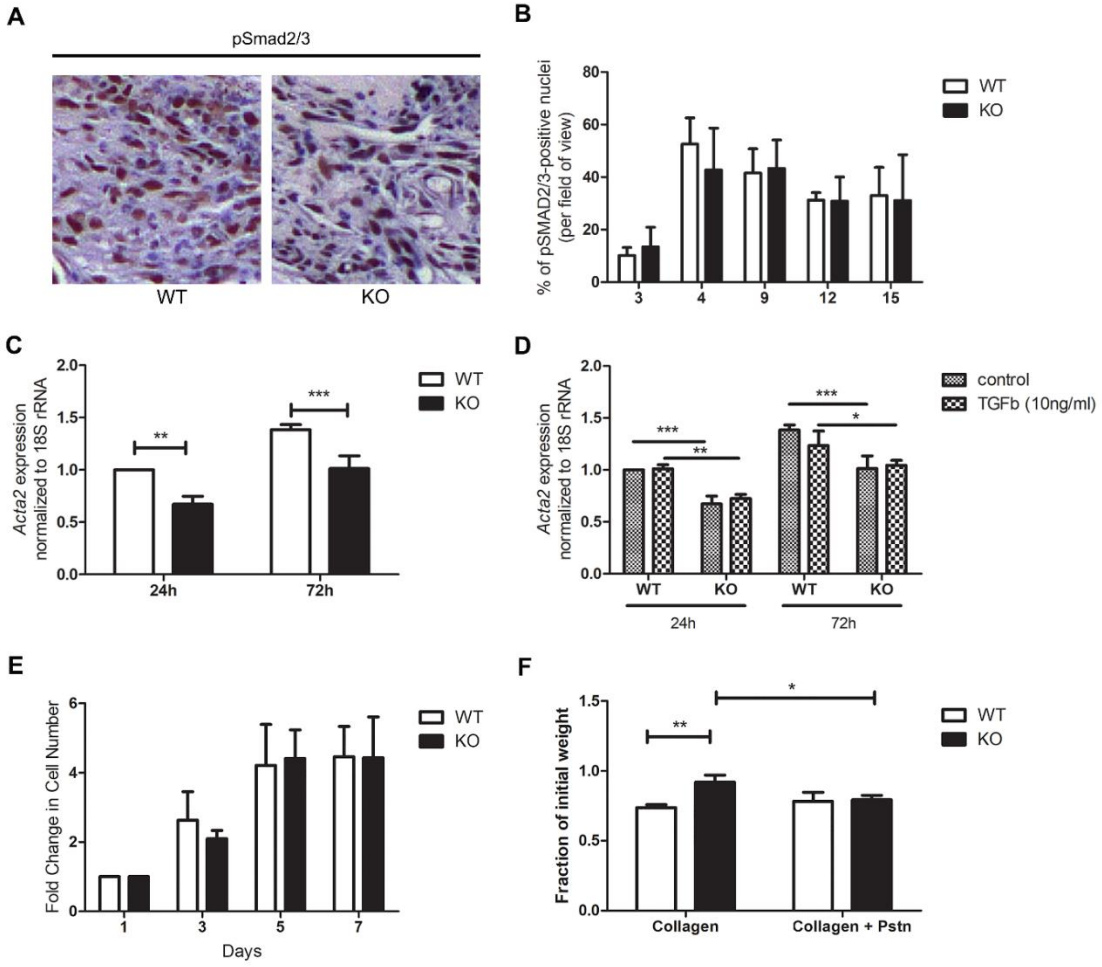
A
pSmad2/3
WT
KO
B
% of pSMAD2/3-positive nuclei (per field of view)
WT
KO
C
Acta2 expression normalized to 18S rRNA
24h
72h
D
control
TGFb (10ng/ml)
24h
72h
E
Fold Change in Cell Number
Days
F
Fraction of initial weight
Collagen
Collagen + Pstn

Figure 2-8 Canonical TGFβ signaling is not altered in *Postn*$^{-/-}$ fibroblasts & Exogenous periostin is sufficient to induce a contractile phenotype

(A) Immunohistochemical staining for phosphorylated Smad2/3 (Santa Cruz sc11769). Detection was with peroxidase-conjugated secondary antibodies- chromogen DAB. Representative images of wounds at day 6 post-wounding in WT and *Postn*$^{-/-}$ animals. **(B)** Numbers of positively stained nuclei per field of view were not significantly different between WT and *Postn*$^{-/-}$ (KO) wounds. **(C, D)** WT and *Postn-/* mPFBs (KO) were seeded on TCP, with or without TGFβ (5 ng/ml). At 24- and 72-hours Acta2 expression was quantified using RTqPCR. Data represents mean fold gene expressions ±SD relative to control 24h (without TGFβ-control) of 3 independent experiments in triplicates (N=3, n=3 per time point. *P < 0.05, **P<0.01, ***P<0.001, two-way AVONA) **(E)** WT and KO mPFBs cultured for 1, 3, 5, and 7 days were assessed for proliferation using CyQUANT assay kit to determine DNA contents. A standard curve was used to extrapolate cell number. Data represents fold cell number increase ± SD relative to day 1. Data was analyzed via two-way ANOVA ($p > 0.05$). **(F)** Gel contraction was quantified by loss of gel weight, compared with gels lacking cells. KO fibroblasts were unable to significantly contract collagen gels. WT fibroblasts were able to contract collagen gels. Exogenous addition of 5 mg/ml rhPSTN to the collagen gels rescued the contractile ability of *Postn*$^{-/-}$ fibroblasts. Data is expressed as a fraction of the initial gel weight; error bars represent SD (N=3, n=3, *P < 0.05, **P < 0.01, two-way ANOVA).

2.3.8 Periostin expression in mPFBs is regulated by matrix stiffness

To evaluate whether Periostin is differentially regulated by the stiffness of the underling substratum, mPFBs were seeded for 24- and 48 hours on substrates of different stiffness. Up to 24 hours post seeding, *Postn* expression levels were similar across different stiffness substrates (Fig. 2.9). At 48 hours, Postn mRNA levels were significantly higher in very stiff substrates (TCP) ($P < 0.01$, $P < 0.05$) (Fig.2.9 B), reducing gradually as the stiffness of the substrate decreases.

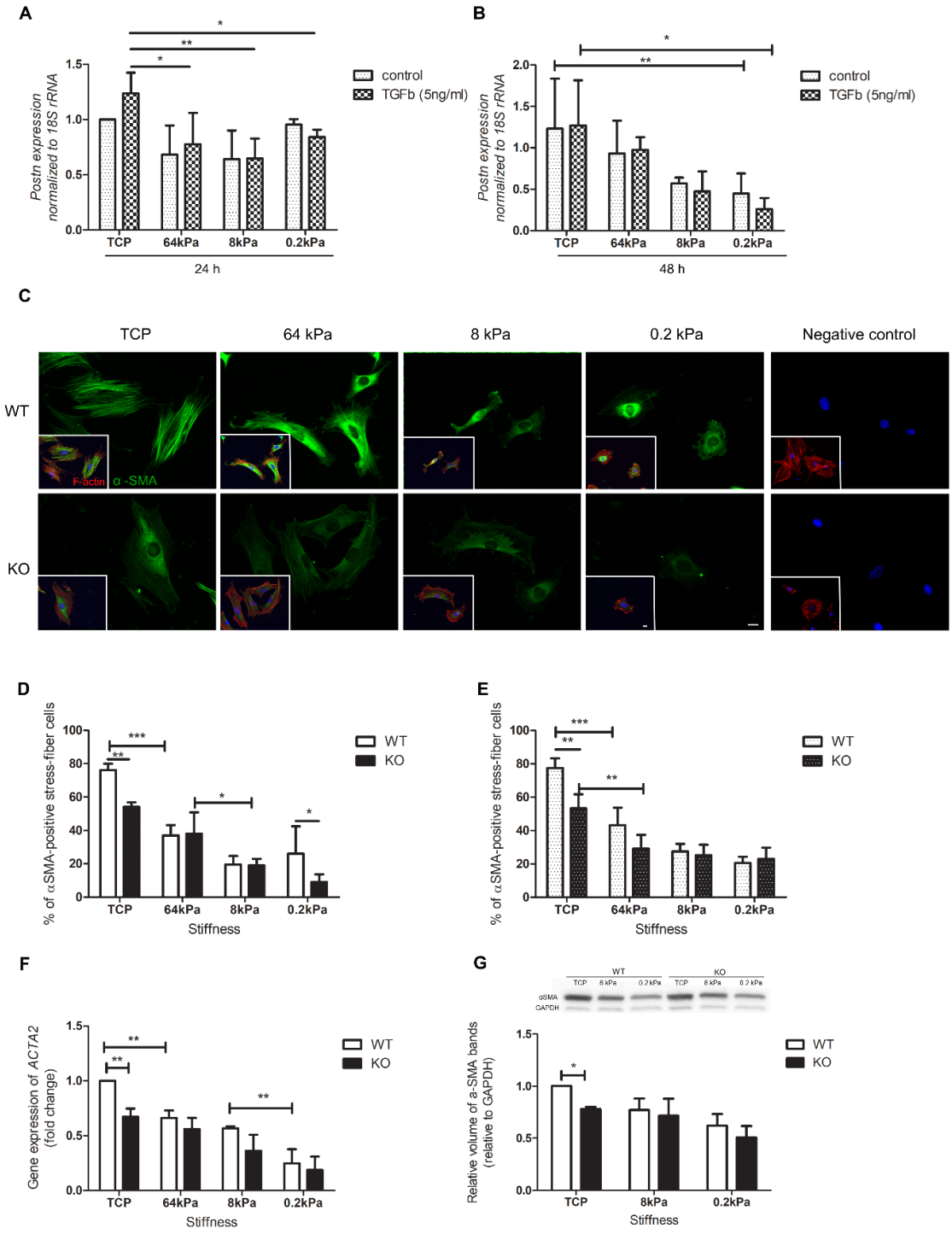
A
Postn expression normalized to 18S rRNA
control
TGFb (5ng/ml)
TCP
64kPa
8kPa
0.2kPa
24 h
B
Postn expression normalized to 18S rRNA
control
TGFb (5ng/ml)
TCP
64kPa
8kPa
0.2kPa
48 h
C
TCP
64 kPa
8 kPa
0.2 kPa
Negative control
WT
KO
F-actin
α -SMA
D
% of αSMA-positive stress-fiber cells
WT
KO
TCP
64kPa
8kPa
0.2kPa
Stiffness
E
% of αSMA-positive stress-fiber cells
WT
KO
TCP
64kPa
8kPa
0.2kPa
Stiffness
F
Gene expression of ACTA2 (fold change)
WT
KO
TCP
64kPa
8kPa
0.2kPa
Stiffness
G
WT
KO
αSMA
GAPDH
Relative volume of a-SMA bands (relative to GAPDH)
WT
KO
TCP
8kPa
0.2kPa
Stiffness

Figure 2-9 Periostin expression in mPFBs is regulated by matrix stiffness

(A, B) WT mPFBs were cultured on silicone substrates of different stiffness, with or without TGFβ, for (A) 24- and (B) 48-hours, and *Postn* mRNA levels were quantified using RTqPCR. Values are given as mean±SD from 3 independent experiments. Data was analyzed using ANOVA, (*P < 0.05; **P < 0.005). **(C)** Matrix stiffness alone is not sufficient to restore the contractile phenotype of *Postn*$^{-/-}$ cells: mPFBs were cultured on silicone substrates of different stiffness and analysed for α-SMA incorporation in stress fibers. **(D)** Quantification of α-SMA positive stress fiber-cells**. (E)** mPFBs were treated with 5ng/ml TGFβ and α-SMA positive stress fiber-cells were quantified using immunofluorescence. **(F)** *Acta2* expression was quantified RTqPCR. **(G)** Western blot was used to assess α-SMA protein level of WT and *Postn*$^{-/-}$ mPFBs. GAPDH was used as a loading control. Values are given as mean±SD from 3 independent experiments. Data was analyzed using ANOVA, (*P < 0.05; **P < 0.005). Scale bar: 20μm.

2.3.9 Matrix stiffness is not sufficient to restore the contractile phenotype of *Postn*$^{-/-}$ cells

Differentiation of fibroblasts into myofibroblasts requires TGFβ-dependent signaling, but also depends heavily on increased matrix stiffness (Hinz, 2015; Humphrey et al., 2014; Tomasek et al., 2002). To explore the contribution of microenvironment stiffness on cellular behavior, WT and *Postn*$^{-/-}$ mPFBs were seeded on silicone substrates with different Young's elastic modulus simulating different scar maturation stages, and *Acta2*/α-SMA expression was evaluated using RTqPCR, immunolabeling and western blotting. Murine palatal fibroblasts seeded on collagen-coated tissue culture plates (TCP) adopted a planar, well-spread morphology typical of fibroblasts in culture (Figure 2.9 C). These cells developed very distinct stress fibers, which often incorporated α-SMA, indicating myofibroblast differentiation. Depending on the stiffness of their environment, after 24h culture cells assume differentiated myofibroblast characteristics on tissue culture plastic (TCP-control) and ''fibrosis-rigid'' (65 kPa) substrate, formed α-SMA-negative stress fibers on ''normal tissue soft'' (8 kPa) substrates, while on very soft "granulation tissue soft" (0.2 kPa) substrates the cells were characterized by poor spreading and exhibited no contractile bundles (Fig. 2.9 C).

The percentage of fibroblasts with positive-α-SMA stress fibers increased with an increase in substrate stiffness ($P < 0.001$). The proportion of WT mPFBs with α-SMA-positive stress fibers peaked on TCP at 76%, while on substrates of low stiffness (0.2 kPa) that proportion accounted only for the 26% of the cells (Fig. 2.9 C, D). Compared with WT mPFBs, the proportion of *Postn*$^{-/-}$ cells with α-SMA-positive stress fibers was significantly lower on TCP (54%) ($P<0.01$) and 0.2 kPa (9%) ($P<0.05$) substrates. These observations were further supported by *Acta2* expression levels and α-SMA protein levels (Fig. 2.9 F, G), showing that the absence of periostin in *Postn*$^{-/-}$ cells resulted in reduction of *acta2*/α-SMA expression which was mainly manifested in very stiff conditions (TCP). When cells were treated with 5 ng/ml TGFβ, the proportion of *Postn*$^{-/-}$ cells with α-SMA-positive stress was similar to WT cells on 0.2 kPa substrates (WT, 20%; *Postn*$^{-/-}$, 23%) (Fig. 2.9 E).

2.3.10 Fibronectin secretion is regulated by Periostin and Matrix stiffness

To mimic the *in vivo* conditions and validate our observations regarding the deficit in fibronectin deposition in *Postn*$^{-/-}$ wounds, WT and *Postn*$^{-/-}$ mPFBs were seeded on silicone substrates with different Young's elastic modulus. Low stiffness substrates (0.2 kPa) resulted in upregulation of fibronectin in WT cells, when compared to control (TCP) ($p<0.05$). Similar to our *in vivo* observations, genetic deletion of periostin in *Postn*$^{-/-}$ mPFBs resulted in a trend of reduced fibronectin mRNA levels across all different substrates, a difference which was significant at low stiffness substrates (0.2 kPa) ($P<0.05$), indicating two important regulators of fibronectin synthesis during palatal healing: periostin and microenvironment stiffness (Fig. 2.10).

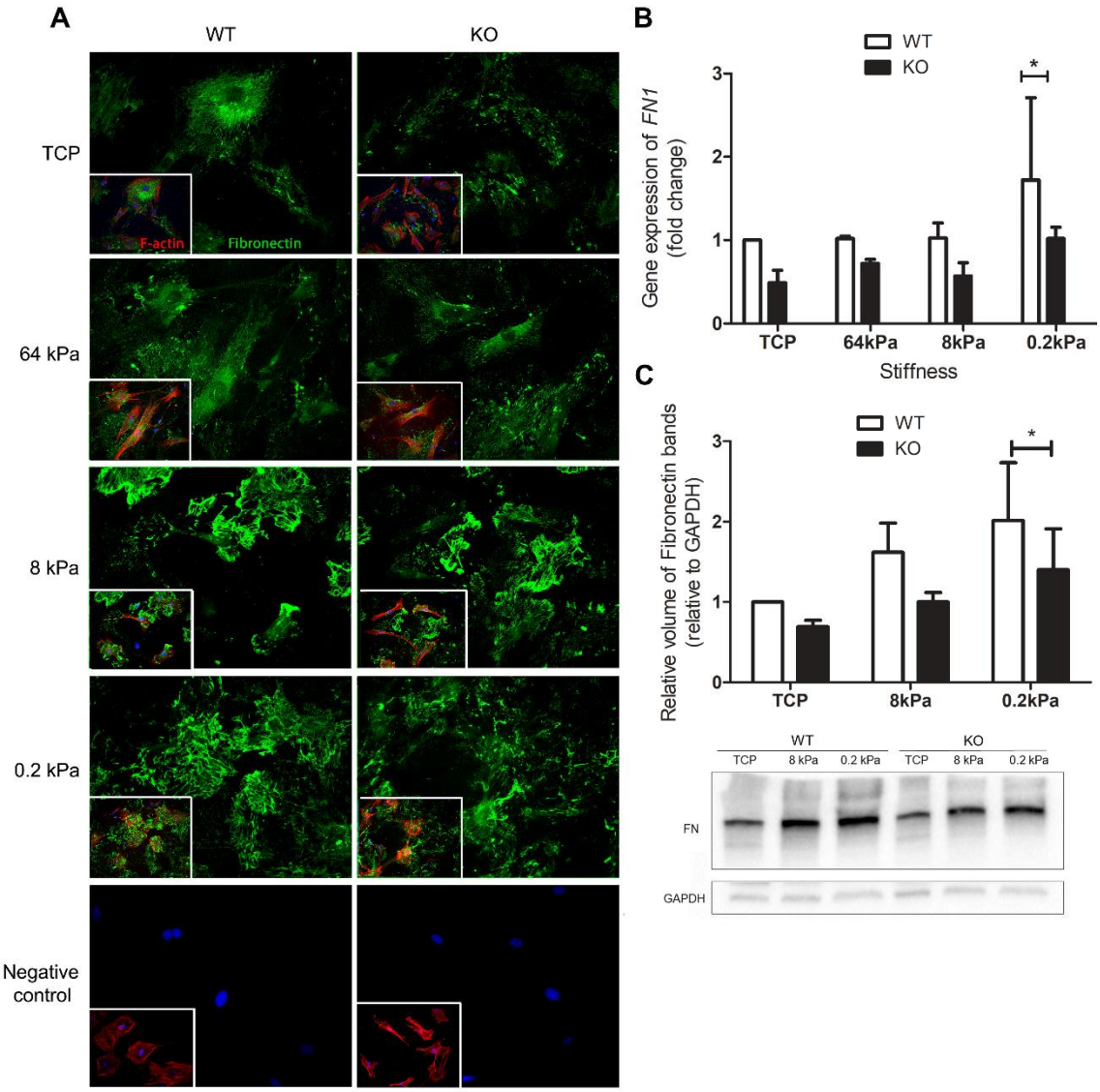

Figure 2-10 Fibronectin secretion is regulated by Periostin and Matrix stiffness.

Fibronectin secretion using immunofluorescence. **(B)** *FN1* expression was quantified using RTqPCR**. (C)** Western blot was used to assess fibronectin protein level of WT and *Postn*$^{-/-}$ mPFBs. GAPDH was used as a loading control. Values are given as mean±SD from 3 independent experiments. Data was analyzed using ANOVA, (*P < 0.05). Scale bar: 20µm.

2.3.11 Periostin modulates myofibroblast differentiation in Palatal fibroblasts via RhoA/ROCK pathway

Periostin has been shown to increase focal adhesion formation, α-SMA levels and collagen contraction in fibroblasts from hypertrophic scars, effects which were dependent on Rho-associated protein kinase (Crawford et al., 2015). To identify the signaling pathway intermediates that are activated by periostin and/or matrix stiffness and control myofibroblast differentiation and fibronectin synthesis, we utilized pharmacological inhibitors for RhoA, Y-27632, and Rac1, Z62954982. We found that both WT and *Postn*$^{-/-}$ cells on an extremely stiff environment (TCP) exhibit well spread morphology with formation of stress fibers, although in *Postn*$^{-/-}$ cells the incorporation of α-SMA in the stress fibers is reduced (53%) when compared to the WT (72%) ($P<0.01$). Rho inhibition (Y-27632) resulted in cytoskeleton remodeling characterized by a dendritic phenotype with large cytoplasmic protrusions, and complete loss of α-SMA in both cell genotypes (WT, 17%; *Postn*$^{-/-}$, 14%). Interestingly, the inhibition of RhoA on 0.2 kPa conditions did not have as prominent effect on the cytoskeletal configuration as is evident on TCP, suggesting that Rho is not active in highly elastic environments (Fig. 2.11 A). When the pharmacological inhibitor for Rac1 was used to drive ROCK activation, the development of α-SMA-positive fibers was restored in both WT (78%) and *Postn*$^{-/-}$ (70%) ($P>0.05$) cells seeded on TCP, suggesting that periostin modulates myofibroblast differentiation in stiff matrices via RhoA pathway (Fig. 2.11 A, B). On 0.2 kPa substrates, the addition of the pharmacological inhibitor to Rac1 was not sufficient to stimulate the formation of α-SMA stress fibers and myofibroblast differentiation in either cell type (WT, 2%; *Postn*$^{-/-}$,1.8%) (Fig. 2.11 A, C).

We next investigated the effect of RhoA or Rac inhibition on fibronectin synthesis. RhoA inhibition resulted in reduced fibronectin matrix assembly in both WT and *Postn*$^{-/-}$ cell types (shown in Figure A-2). In contrast, direct activation of RhoA through Rac inhibition restored fibronectin matrix assembly and protein levels similar to control levels (DMSO) in both WT and *Postn*$^{-/-}$ mPFBs, supporting that fibronectin matrix synthesis and assembly requires Rho kinases (ROCK). However, these results suggest that the mechanism through

which Periostin regulates fibronectin synthesis in mPFBs does not depend on RhoA/ROCK pathway.

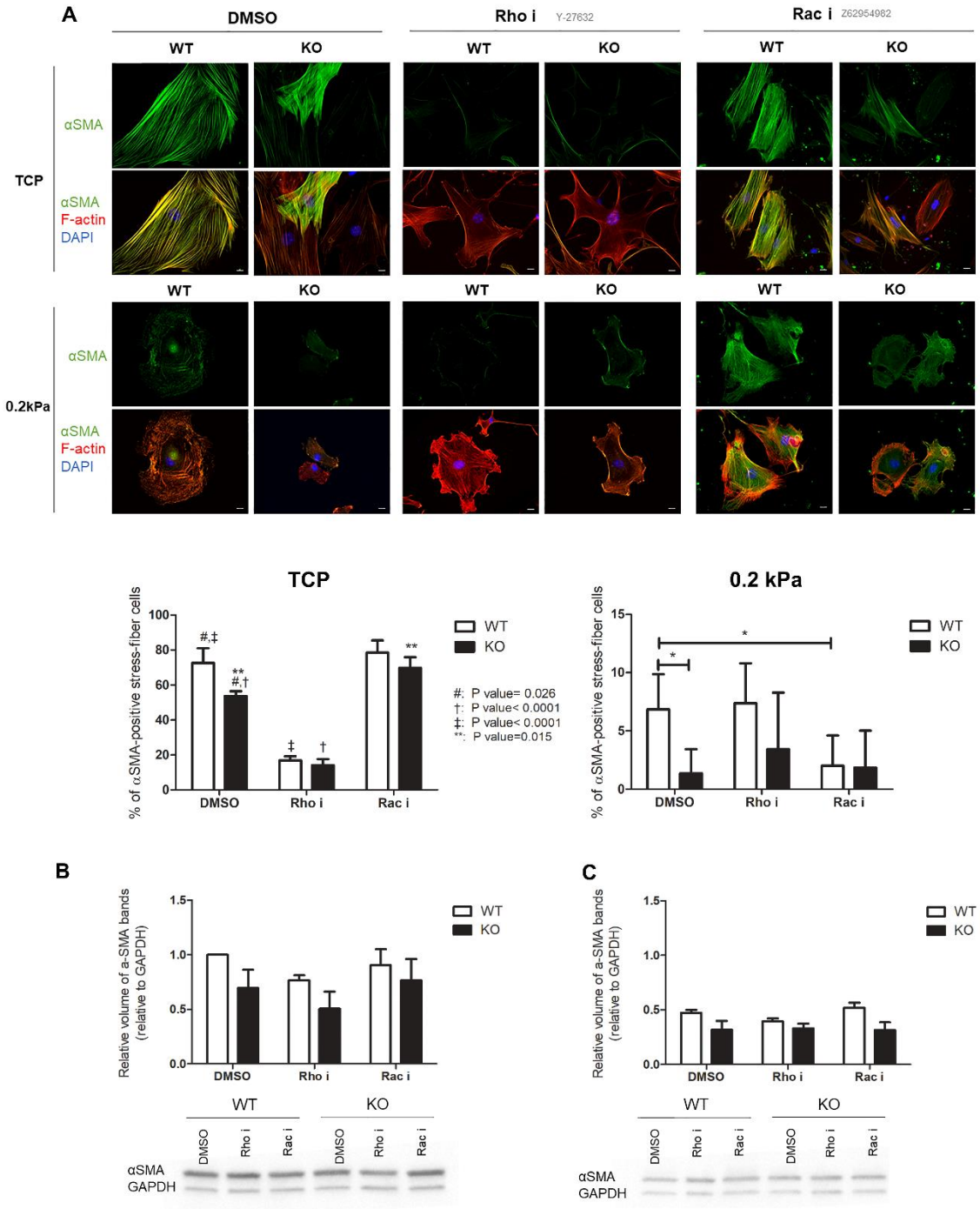
A
DMSO
Rho i Y-27632
Rac i Z62954982
WT
KO
TCP
0.2kPa
αSMA
αSMA
F-actin
DAPI
TCP
0.2 kPa
% of αSMA-positive stress-fiber cells
WT
KO
#: P value= 0.026
†: P value< 0.0001
‡: P value< 0.0001
**: P value=0.015
DMSO
Rho i
Rac i
B
C
Relative volume of a-SMA bands (relative to GAPDH)
αSMA
GAPDH

Figure 2-11 Periostin modulates myofibroblast differentiation in mPFBs via RhoA pathway

(A) mPFBs were cultured on TCP (top row) or silicon substrates with 0.2 kPa Young's modulus of elasticity (bottom row), treated with pharmacological inhibitors for RhoA, Y-27632 (10 μM), and Rac1, Z62954982 (50 μM), and analysed for α-SMA incorporation in stress fibers using immunofluorescence and western blotting. Western blot was used to assess α-SMA protein level of WT and *Postn*$^{-/-}$ mPFBs on TCP **(B)** and 0.2 kPa substrate **(C)** GAPDH was used as a loading control. Values are given as mean±SD from 3 independent experiments. Data was analyzed using ANOVA, (*P < 0.05; **P < 0.005). Scale bar: 20μm.

2.3.12 Periostin is required for the formation of focal and fibrillar adhesions in mPFBs

Organization of adhesion sites is controlled not only by the integrin-ligand interactions, but also the physical properties of the extracellular matrix which modulate local tension at the adhesion sites (Katz et al., 2000). To investigate how a change in the stiffness of the cell microenvironment (using culture substrates) affects the assembly of different types of adhesion complexes in the presence or absence of periostin, WT vs *Postn*$^{-/-}$ cells were seeded on substrates of different elastic modulus. To determine whether the absence of periostin in *Postn*$^{-/-}$ mPFBs result in defective adhesion complexes formation, we visualized focal (vinculin) and fibrillar adhesions (integrin-β1) using immunocytochemistry, and we quantified the number of adhesions/cell, the total adhesion area/cell and the average adhesion area/cell adhesion using ImageJ. The number and the size of focal adhesions as well as the total focal adhesion area increased with an increase in substrate stiffness (Fig. 2.12, 13A-C). In the absence of periostin the number of focal adhesions per cell, the size of the focal adhesions and the focal adhesion area per cell were significantly reduced across all different substrates. More specifically, on very stiff substrates (TCP) *Postn*$^{-/-}$ cells had significantly less focal adhesion sites/cell (n= 383±99) when compared to WT cells (n= 672±111) ($P<0.05$), and their average size was smaller (WT, 5±1μm^2; *Postn*$^{-/-}$, 4±0.7μm^2) resulting in a significantly smaller total adhesion area per cell in *Postn*$^{-/-}$ cells (WT, 3238±686μm^2; *Postn*$^{-/-}$, 1535±645μm^2) ($P<0.05$). On low stiffness substrates (0.2 kPa) the average size of the focal adhesions (1.9±0.1μm^2) and the number of adhesion sites per cell (n= 117±63) were significantly smaller when compared to WT cells (3.2±0.4μm^2; ($P<0.01$), n=267±81; $P<0.05$). Investigating the effect of the genetic deletion of periostin in fibrillar adhesion formation, we found that the percentage of β1-integrin-positive adhesion area/cell (Fig. 2.13 E) and the levels of β1-integrin expression (Fig. 2.13 F) were significantly reduced in *Postn*$^{-/-}$ cells when compared to WT cells. These effects were more prominent when the cells were cultured on substrates of low stiffness and could provide a potential explanation of reduced fibronectin synthesis by *Postn*$^{-/-}$ mPFBs under these conditions.

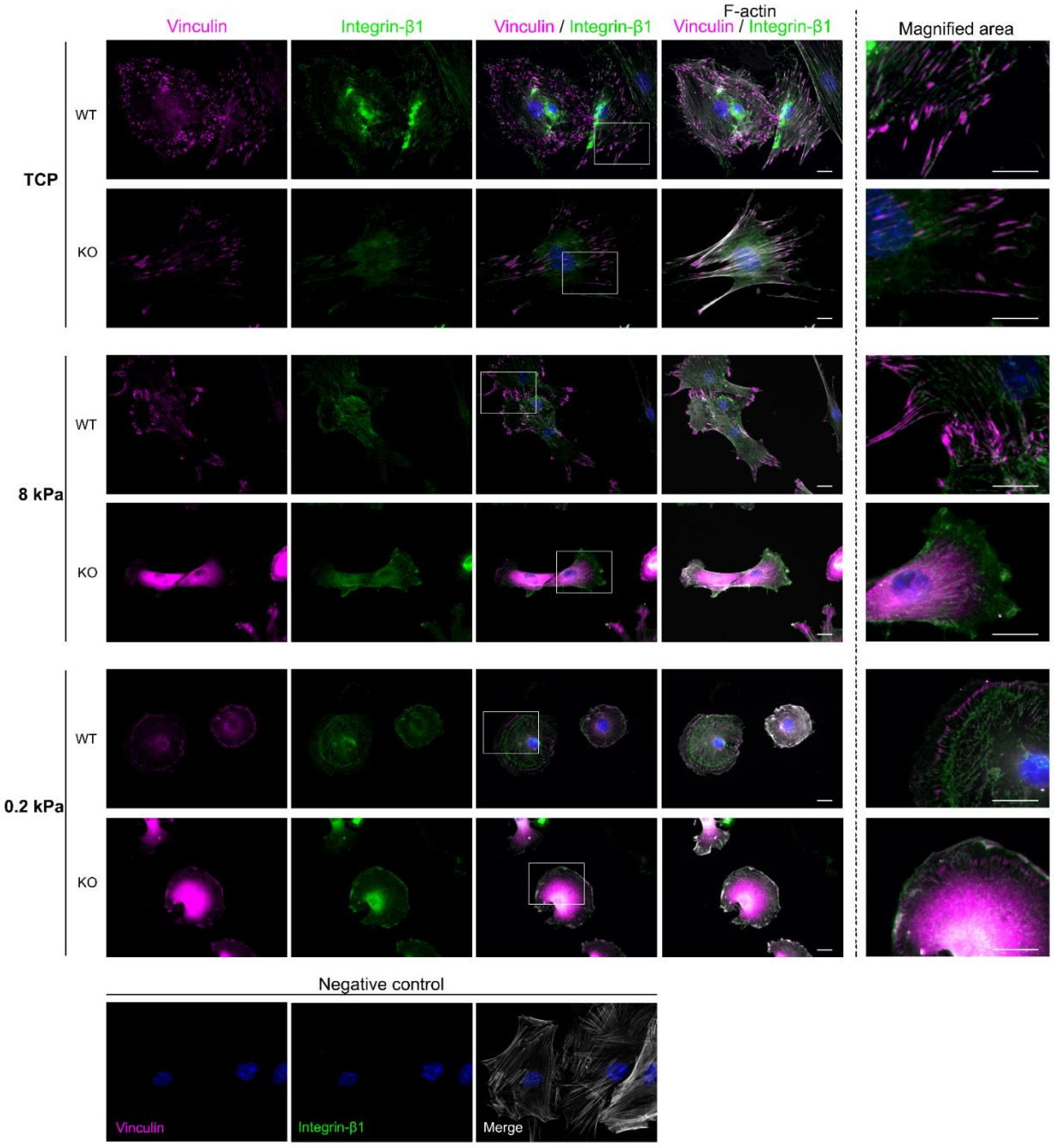
Vinculin
Integrin-β1
Vinculin / Integrin-β1
F-actin
Vinculin / Integrin-β1
Magnified area
TCP
WT
KO
8 kPa
WT
KO
0.2 kPa
WT
KO
Negative control
Vinculin
Integrin-β1
Merge

Figure 2-12 Periostin is required for the formation of focal and fibrillar adhesions in mPFBs.

mPFBs were cultured on silicone substrates of different stiffness and analysed for focal (Vinculin) and fibrillar (integrin-β1) adhesions formation using immunocytochemistry. Representative images of immunoreactivity for Vinculin (magenta) and integrin-β1 (green). Nuclei are stained with Hoechst 33342 dye (blue) F-actin with white. Scale bar: 20μm

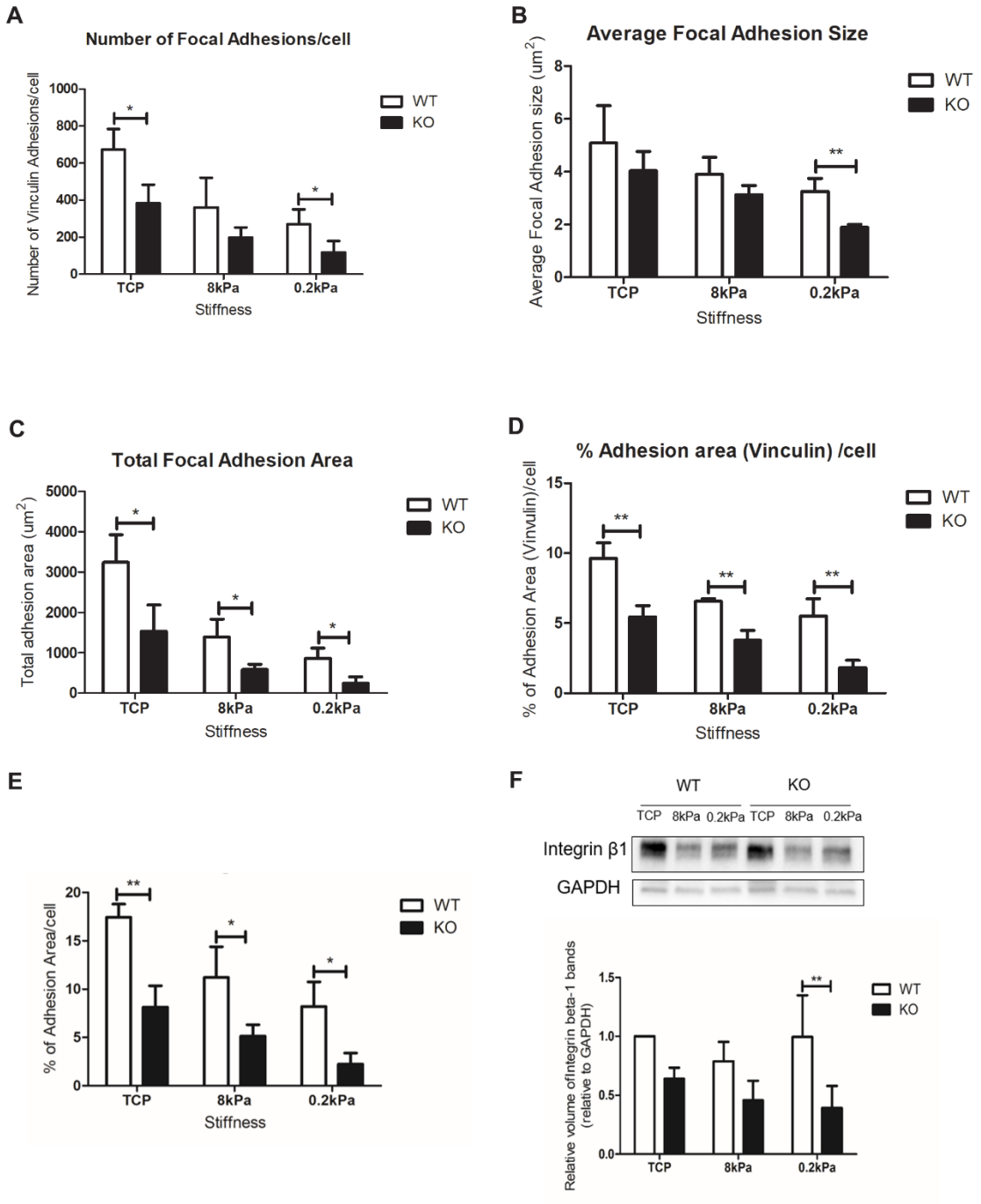
A
Number of Focal Adhesions/cell
Number of Vinculin Adhesions/cell
1000
800
600
400
200
0
*
*
WT
KO
TCP
8kPa
0.2kPa
Stiffness
B
Average Focal Adhesion Size
Average Focal Adhesion size (um2)
8
6
4
2
0
**
WT
KO
TCP
8kPa
0.2kPa
Stiffness
C
Total Focal Adhesion Area
Total adhesion area (um2)
5000
4000
3000
2000
1000
0
*
*
*
WT
KO
TCP
8kPa
0.2kPa
Stiffness
D
% Adhesion area (Vinculin) /cell
% of Adhesion Area (Vinvulin)/cell
15
10
5
0
**
**
**
WT
KO
TCP
8kPa
0.2kPa
Stiffness
E
% of Adhesion Area/cell
20
15
10
5
0
**
*
*
WT
KO
TCP
8kPa
0.2kPa
Stiffness
F
WT
KO
TCP 8kPa 0.2kPa TCP 8kPa 0.2kPa
Integrin β1
GAPDH
Relative volume ofIntegrin beta-1 bands (relative to GAPDH)
1.5
1.0
0.5
0.0
**
WT
KO
TCP
8kPa
0.2kPa

Figure 2-13 Periostin is required for the formation of focal and fibrillar adhesions in mPFBs

Immunostaining for focal (Vinculin-positive) adhesions was used to quantify: **(A)** the number of focal adhesions/cell, **(B)** the average focal adhesion size, **(C)** the total adhesion area (μm^2), and **(D)** the % of focal adhesion area/cell. **(E)** Fibrillar adhesion formation expressed as % of adhesion area/cells was quantified using immunostaining for integrin-β1, **(F)** Integrin-β1 levels were quantified using Western Blotting. Values are given as mean±SD from 3 independent experiments. Data was analyzed using ANOVA. (*$P<0.05$, **$P<0.005$)

2.4 Discussion

Periostin, a secreted ECM protein, is transiently expressed during normal cutaneous (Elliott et al., 2012) and gingival wound repair (S. S. Kim, Nikoloudaki, Michelsons, et al., 2019), but is overexpressed and persistent in abnormal scars and other benign fibroses that are characterized by fibroblast proliferation and myofibroblast differentiation (Crawford et al., 2015; Elliott & Hamilton, 2011; Zhou et al., 2010). Excessive scarring as a consequence of cleft palate reconstruction surgery results in restriction of the normal maxillary development in transversal width when the patient is in their growing phase, leading to serious functional and aesthetic problems (Larjava, 2013). The expression profile and potential roles of periostin in palatal healing have never been investigated. The distinct healing patterns among skin, gingiva and the palatal mucoperiosteum, and the contrasting tissue-specific effects of periostin's bioactivity (Nikoloudaki et al., 2020), could provide deeper understanding of how differences in molecular composition and physical properties of these tissues lead to the different healing outcomes. Applying this translatable knowledge in the fields of biotechnology, these specific biomechanical cues can be targeted and guided to enhance healing outcomes while inhibiting undesired effects, such as scarring and fibrosis (Urbanczyk et al., 2020).

In this study, we show that the loss of Postn by use of the *Postn*$^{-/-}$ mouse (Rios et al., 2005) results in altered palatal wound-closure kinetics, especially during the proliferation phase of wound healing. The alteration in wound closure corresponds with the onset at day 6, but not the peak of Postn expression at day 12 post-wounding in WT animals. Wounds in WT mice were considered closed by day 6, but wounds in *Postn*$^{-/-}$ were completely closed at day 12 post-wounding (Fig. 2.2 A-B, Fig. 2.3). Although the histological analysis of sections from the centre of the wounds at day 6 showed decreased re-epithelialization in *Postn*$^{-/-}$ mice, the epithelial tongue length (epithelial migration distance) was similar in both genotypes (Elliott et al., 2012; Gorin et al., 1996). Periostin has been shown to regulate myofibroblast differentiation, matrix synthesis and re-epithelialization in skin (Elliott et al., 2012; Norris et al., 2007; Zhou et al., 2010). Previous studies, including by our group, have shown that following excisional skin wounding in mice, periostin is upregulated at

day 3, levels peak at day 7, after which expression eventually returns to baseline (Elliott CG, Kim SS, 2012). In gingival wound healing, using gingivectomy defects in rats (S. S. Kim, Nikoloudaki, Michelsons, et al., 2019), periostin expression was increased at day 7, with protein levels increased yet further at day 14 in the ECM of the connective tissue. While the assessment of gingival healing in the *Postn*$^{-/-}$ mice would be the most direct method, it is technically challenging due to the size of the gingiva and that any defect created in the gingival tissue heals rapidly limiting timepoints for analysis. In a similar manner to skin and gingival healing, periostin upregulation in palatal mucoperiosteum coincides with the proliferative and remodeling phases of healing, but not the inflammatory phase. Interestingly, periostin protein levels are not increased at day 3 as is seen in skin healing (Jackson-Boeters et al., 2009), highlighting a difference in expression profile between the two tissue types.

We have previously shown that during skin healing myofibroblast differentiation mediates contraction of the wound edges and is modulated by periostin in mice (Elliott et al., 2012), but during gingival healing we observed a very low level of myofibroblasts, suggesting that adoption of a contractile myofibroblast phenotype is not a significant event in gingival wound healing (S. S. Kim, Nikoloudaki, Michelsons, et al., 2019), providing a potential explanation of the scarless healing of the latter. After formation of actin-myosin contractile bundles, stress fibers, it is the neo-expression and incorporation of α-SMA that significantly augments the contractile activity of activated myofibroblasts (Hinz et al., 2001). In the current study, immunohistochemistry and RT-qPCR reveal that α-SMA/*Acta2* is up-regulated in the palatal wounds during wound healing, but it was significantly reduced in the granulation tissue of *Postn*$^{-/-}$ mice at day 6 when compared with that in WT controls. These results further support that the palatal mucoperiosteum has different healing potential than the gingival tissue and could provide a potential therapeutic target for palatal scarring.

To determine whether the reduction in α-SMA expression was due to impaired fibroblast recruitment into the granulation tissue, wound sections were labeled for fibroblast-specific protein-1 and vimentin. Cell numbers showed no significant differences in FSP-1

immunoreactivity in *Postn*$^{-/-}$ wounds compared to WT, suggesting that genetic deletion of periostin does not affect fibroblast recruitment, but rather result in deficient contractility. To further investigate this finding, we sought to determine whether reduced α-SMA within *Postn*$^{-/-}$ granulation tissue was the result of a defect in differentiation of fibroblasts into myofibroblasts. Supporting this hypothesis, isolated palatal fibroblasts (mPFBs) from *Postn*$^{-/-}$ animals did not have any differences in their proliferation rate when compared to cells isolated from WT animals and showed significant reduction in their ability to contract a collagen gel. Addition of exogenous rhPSTN, however, fully rescued the phenotype of the *Postn*$^{-/-}$ fibroblasts suggesting that periostin is required for gel contraction and its presence in the extracellular matrix is sufficient to induce a contractile myofibroblast phenotype. While similar observations have been reported in murine dermal fibroblasts isolated from *Postn*$^{-/-}$ animals, highlighting the role of periostin in skin healing as a modulator of myofibroblast differentiation and contraction (Elliott et al., 2012), in gingival fibroblasts the exogenous addition of rhPSTN does not increase α-SMA protein nor induce gel contraction (S. S. Kim, Nikoloudaki, Michelsons, et al., 2019), further supporting the behavioral and phenotypic differences between gingival, palatal and dermal fibroblasts observed in vitro. Interestingly, in spite of the relative similarity of fibroblasts in connective tissues, not only is there strong evidence about the existence of different phenotypes, but also it has been proven that these phenotypes are substantially variable among different anatomical regions (Gabbiani, 1996; Giannopoulou & Cimasoni, 1996). These phenotypic differences have been proposed to be partially responsible for the different healing patterns of the tissues (DeLeon-Pennell et al., 2020a; Lepekhin et al., 2002). Recently, Mah et al. 2014 tried to shed light on the relation between the distinct phenotypes of gingival fibroblasts and skin fibroblasts and their different wound healing patterns in 3D cell cultures. They found that gingival fibroblasts proliferate faster and express higher levels of molecules involved in modulation of inflammation and ECM remodeling (MMP-1, -3, -10, TIMP-4), while skin fibroblasts displayed significantly higher expression of fibrillar (collagens and elastin) and non-fibrillar (SLRPs and matricellular proteins) ECM proteins, and molecules involved in TGF-β signaling, regulation of myofibroblast phenotype and cell contractility, such as TGF-β1,-β2, -β3, Smad, α-SMA, CXCL12, Cadherin-2, -11.

Their findings are indicative that gingival fibroblasts display a phenotype that may promote faster resolution of inflammation and ECM remodeling, which is characteristic to reduced scar formation, while skin fibroblasts have a profibrotic, scar-prone phenotype (Mah et al., 2014). On the contrary, our results provide evidence for the fibroblast heterogeneity among oral mucosa tissues, the absence of myofibroblast differentiation during both healing and scarring of the gingiva (S. S. Kim, Nikoloudaki, Darling, et al., 2019; S. S. Kim, Nikoloudaki, Michelsons, et al., 2019) suggest significant epigenetic differences compared to palatal fibroblasts.

Mechanical tension (Hinz et al., 2001; Pakshir & Hinz, 2018; Talele et al., 2015) and TGFβ secretion and activation during wound healing and ECM remodeling (Desmoulière et al., 1993; Walraven & Hinz, 2018) determine the percentage of differentiated, α-SMA-positive myofibroblasts (Desmoulière et al., 1993; Hinz, 2015; Tomasek et al., 2002). For the induction of α-SMA by TGFβ, phosphorylation of FAK is required, which is a central molecule activated in adhesive signaling (Leask, 2013). We have previously shown that in murine skin, periostin modulates α-SMA expression in a FAK and integrin-β1 engagement dependent manner (Elliott et al., 2012). To determine whether the reduction in α-SMA expression and immunoreactivity in *Postn*$^{-/-}$ granulation tissue was due to defective TGFβ–Smad3 signaling, we assessed the number of nuclei positive for phosphorylated Smad2 and Smad3 (pSmad2/3) within the granulation tissue of palatal wounds. No differences were observed in the number of pSmad2/3-positive nuclei between WT and *Postn*$^{-/-}$ wounds, suggesting that canonical TGFβ signaling is active in *Postn*$^{-/-}$ wounds. In mPFBs, pharmacological inhibition of FAK pathway did not have any effect on α-SMA/Acta2 expression (shown in Figure A-3) suggesting that periostin modulates α-SMA expression through an alternative mechanism. These observations shift our focus to investigate the role of ECM stiffness and adhesive signaling as potential modulators of periostin-induced myofibroblast differentiation.

Mechanical stress exerted by the stiffness of ECM positively feedback on the development and progression of fibrotic conditions by directly promoting myofibroblast activation and persistence through various mechanotransduction pathways (Achterberg et al., 2014;

Goffin et al., 2006; Hinz, 2015; Pakshir & Hinz, 2018; Rousselle et al., 2019). Building on our previous studies (Elliott et al., 2012; S. S. Kim, Nikoloudaki, Michelsons, et al., 2019), the differences observed in skin, gingival and palatal healing processes suggest that the ECM of these tissues may possess different level of stiffness. Changing the stiffness of the cell substrate is an efficient method to control myofibroblast activation *in vitro* (Pakshir & Hinz, 2018; Talele et al., 2015; Tomasek et al., 2002). To explore how periostin and microenvironment stiffness influence cellular behavior, cells isolated from WT and *Postn*$^{-/-}$ palates were seeded on collagen-coated silicon substrates with different Young's elastic modulus. Here we show that myofibroblast differentiation of mPFBs is stimulated by culture on stiff culture substrates (TCP, 64 kPa) but suppressed on substrates mimicking normal tissue (8 kPa) or granulation tissue (0.2 kPa) ECM stiffness, which is in agreement with other reports (Achterberg et al., 2014). Our results are consistent with studies demonstrating that mesenchymal stem cells, different fibroblasts, and hepatic stellate cells all remain relatively inactive on culture substrates mimicking the stiffness of normal tissue (Hinz, 2010; Olsen, Abby L.Uemura et al., 2011; Winer et al., 2008). *Postn*$^{-/-}$ mPFBs showed lower expression *Acta2*/α-SMA levels suggesting impaired myofibroblast differentiation capacity when compared to WT cells, which was manifested in rigid, collagen-coated tissue culture plates (TCP). We then sought to investigate whether α-SMA is incorporated in stress fibers of the cells using immunocytochemistry and we found significantly lower proportion of *Postn*$^{-/-}$ cells with α-SMA-positive stress fibers on TCP and 0.2 kPa substrates when compared to WT cells, but these differences where not observed in the intermediate stiffness conditions (64 kPa, 8 kPa). These observations indicate that in palatal fibroblasts periostin modulates myofibroblast differentiation in cases of extreme stiffness and in very compliant microenvironments. Our observations from the *in vivo* experiments in the palate show that α-SMA is still present but reduced in the granulation tissue of *Postn*$^{-/-}$ wounds, indicating that the loss of periostin is partially compensated by the stiffness of ECM environment which is sufficient to drive myofibroblast differentiation in *Postn*$^{-/-}$ wounds. During healing of excisional wound in murine skin, genetic deletion of periostin does not affect α-SMA expression in high-tension areas at the wound edge, while α-SMA is completely absent in the relatively low-tension

granulation tissue, suggesting that in skin periostin modulates myofibroblast differentiation in relatively compliant tissue (Elliott et al., 2012). On the contrary, in gingival healing the presence of periostin is not sufficient to induce α-SMA (S. S. Kim, Nikoloudaki, Michelsons, et al., 2019). Our observations in the palate highlight the distinct characteristics of the palatal soft tissue, which is an environment of increased stiffness, where, as a rigid mucoperiosteum, the mucosa and the periosteum are merged and tightly attached to the underlying palatal bone.

We next examined whether genetic deletion of periostin alters the production of fibronectin, a key ECM component. Fibronectin is a glycoprotein found in plasma and in the ECM of tissues and is expressed by multiple cell types and comes in different splice variants. It is involved in myofibroblast and TGFβ1 activation (Klingberg et al., 2018; Serini et al., 2002; Zollinger & Smith, 2017), plays a key role in cell adhesive and migratory behavior, is a regulator of collagen organization and tissue phenotype (Mao & Schwarzbauer, 2005; Singh et al., 2010; Zollinger & Smith, 2017), and is elevated in fibrosis (Koli et al., 2005). Extracellularly, periostin directly binds to fibronectin through the EMI domain (Kii et al., 2009; Norris et al., 2007). Intracellularly, it has been observed a proximal localization between periostin and fibronectin in the endoplasmic reticulum of fibroblastic cells indicating that the two proteins interact before fibronectin's secretion (Kii et al., 2016), and evidence suggests that periostin enhances secretion of fibronectin from the endoplasmic reticulum to the extracellular environment (Kii et al., 2016; Kudo & Kii, 2018). Our *in vivo* data from RT-qPCR and immunolabeling assays showed that fibronectin is increased during palatal healing, but *Postn*$^{-/-}$ wounds had significantly less fibronectin than WT wounds. This observation further supports our previous finding, where human gingival fibroblasts cultured in the presence rhPSTN had increased fibronectin production, an effect which was attenuated by pharmacological inhibition of FAK and JNK signaling (S. S. Kim, Nikoloudaki, Michelsons, et al., 2019). In mPFBs, pharmacological inhibition of FAK pathway did not have any effect on fibronectin expression (shown in Figure A-3 A, B).

To explore whether the microenvironment stiffness influences fibronectin expression, we cultured mPFBs isolated from WT *and Postn*$^{-/-}$ animals on silicon substrates of different stiffness. On very stiff substrates the cells acquired a contractile phenotype with upregulation of α-SMA and down-regulation of fibronectin. Fibronectin synthesis was up-regulated in conditions of low stiffness (0.2 kPa), but genetic deletion of periostin in *Postn*$^{-/-}$ cells resulted in significantly reduced fibronectin expression compared to WT cells. Taken together, our findings provide further evidence of the role of periostin as a modulator of fibronectin synthesis. A potential mechanism of fibronectin synthesis modulation by periostin is via integrin β1. Cells mediate fibronectin matrix assembly through integrin binding to the RGD binding domain (Singh et al., 2010). The primary receptor for fibronectin matrix assembly is α5β1. Receptor binding stimulates fibronectin self-association and organizes the actin cytoskeleton to promote cell contractility. Fibronectin conformational changes expose additional binding sites that participate in fibril formation and in conversion of fibrils into a stabilized, insoluble form. Once assembled, the fibronectin matrix impacts tissue organization by contributing to the assembly of other ECM protein (Singh et al., 2010; Zollinger & Smith, 2017). Our *in vitro* results show that β1-integrin expression is significantly reduced *in Postn*$^{-/-}$ cells compared to WT cells when cultured on low stiffness substrates, providing an additional explanation of reduced fibronectin synthesis by *Postn*$^{-/-}$ mPFBs under these conditions.

Cells are subjected to mechanical stresses and receive and respond to stimuli from the ECM through integrins. The coupling of internal and external forces through integrins allows the cells to structurally modify the ECM through cytoskeletal forces that pull on integrins and to respond to external forces by remodeling their cytoskeleton (Moore et al., 2010; Schwarz & Gardel, 2012). β1 integrins are the primary plasma membrane receptors transmitting tensional forces from the actin cytoskeleton to the extracellular matrix (Danen et al., 2002; Guilluy et al., 2011). Myosin-II-mediated contractility is required for cells to actively sense changes in the rigidity of the extracellular matrix (Engler et al., 2006; Pelham & Wang, 1998). The action of myosin II along actin stress fibers maintains the basal tension on the cell-matrix adhesions. This basal tension enables mechanosensitive focal adhesion proteins to sense the increase in resistance, which results when the basal actomyosin tension pulls

on a more rigid extracellular matrix. The increased tension at focal adhesions can cause calcium influx through stretch-activated calcium channels, trigger the integrin-dependent activation of FAK and Src, and change the conformation of certain mechanosensing proteins, such as p130Cas, talin and vinculin, to initiate intracellular signaling and mechanotransduction (Moore et al., 2010). In this study we found that focal adhesion formation and size are increased with an increase in the stiffness of the cell microenvironment, and that the genetic deletion of periostin resulted in a significant defect in focal adhesion formation in *Postn*$^{-/-}$ cells. This finding provides a possible explanation of the reduced contractility and fibronectin synthesis in the absence of periostin. Collectively, we found that in the absence of periostin, the formation of both focal and fibrillar adhesions is defective demonstrating the direct functional role of periostin in adhesion properties of the cells.

Rho signaling also plays key roles in mechanotransduction: The RhoA–ROCK–myosin-II signaling axis is capable of sensing changes in the structure of the extracellular matrix and responding to it by increasing actomyosin contractility (Maekawa et al., 1999). Activation of RhoA (ROCK) promotes stress fibers maintenance, increases ECM tension, integrin clustering and the formation of large focal adhesion complexes (Maekawa et al., 1999). Further, a recent study shows that β1 and β3 integrins binding and interaction regulate in a reciprocal, antagonizing manner each other's activities in the regulation of intercellular adhesion and collective cell migration by Rho GTPase activities (van der Bijl et al., 2020). Also, it has been shown these kinases (ROCK I & II) play a significant role in fibronectin matrix assembly and are implicated in microfilament bundle assembly and smooth muscle contractility (Yoneda et al., 2005, 2006). An important feature of this mechanical signaling network is the crosstalk between Rac1 and RhoA signaling that potentially regulates the mechanosensing of matrix rigidity, as well as the contribution of extrinsic soluble factors, such as growth factors or cytokines, which can modulate RhoA activity to increase or decrease actomyosin contractility independently of matrix rigidity (Ridley & Hall, 1992). The actin-binding motor protein myosin II maintains a low level of tension on actin fibers that are coupled to the extracellular matrix through cell–matrix adhesions. This basal tension enables myosin II to respond to changes in matrix rigidity or elastic behavior by

increasing the tension on cell–matrix adhesions to activate the GEFs (guanide-exchange factors). These GEFs activate RhoA, which in turn activates ROCK to phosphorylate myosin actin chain (MLC) phosphatase, resulting in an increase of MLC phosphorylation, thereby further increasing myosin II activity and actomyosin-based contractility (Nakano et al., 2013). This mechanical feedback loop can increase integrin clustering as well as adhesion maturation and might increase intracellular pressure and plasma membrane tension to prevent lamellipodia formation and bleb-based motility. In these experiments, we examined the hypothesis that Rho is activated when cells are in a very stiff substrate, while Rac is activated in environment of low stiffness (0.2 kPa). To test our hypothesis, we used the RhoA pharmacological inhibitor Y-27632, and we examined whether its effect results in Rac1-activation effects on the cells, such as loss of stress fibers and formation of lamellipodia, using immunocytochemistry for α-SMA and fibronectin. We then used the pharmacological inhibitor Z62954982, to test whether Rac1 inhibition forces cells to activate Rho and consequently drives the cells to form stress fibers and become contractile even at environments of low stiffness (0.2 kPa), as it has been shown that RhoA and Rac1 suppress one another's activity (Higashida et al., 2002). RhoA activity prevents Rac1-stimulated formation of lamellipodia. On the other hand, RhoA-induced contractility is suppressed while Rac1 activity suppresses actomyosin contractility and drives the formation of lamellipodia via enhanced actin-mediated protrusions(Huveneers & Danen, 2009). Here, we have shown that myofibroblast differentiation in *Postn*$^{-/-}$ cells was rescued with the addition of Rac inhibitor, suggesting that periostin modulates myofibroblast differentiation in stiff matrices via RhoA/ROCK pathway.

In this study, we also showed that periostin likely influences the immune response, as shown by the reduced inflammatory cells infiltration in *Postn*$^{-/-}$ wounds. Quantification of macrophage subpopulations during palatal healing shows a significant reduction in both iNOS and arginase-I macrophage populations in *Postn*$^{-/-}$ animals when compared to wild type at day 6 post wounding. During wound healing, macrophages play various roles in addition to clearing debris by phagocytosis. They secrete enzymes important for collagen production (Hesse et al., 2014) and crosslinking (Lupher & Gallatin, 2006), and ECM turn over and resolution (Sprangers & Everts, 2017). Macrophages also stimulate fibroblast-to-

myofibroblast activation (Pakshir & Hinz, 2018), a crucial function in tissue repair and fibrosis. On the other hand, myofibroblasts indirectly establish mechanical communication with macrophages by creating stiff ECM as an important environmental cue. Recently, Pakshir & Hinz proposed that contracting (myo)fibroblasts directly transmit mechanical signals through fibrillar ECM that have the potential to attract migratory macrophages (Pakshir & Hinz, 2018). Thus, it is plausible that the reduced recruitment of macrophages in *Postn*$^{-/-}$ is a consequence of reduced myofibroblast differentiation. There is considerable evidence in the literature to support the hypothesis that there is a reduction in macrophage recruitment as a result of periostin deletion. Using a model of arteriosclerosis, it has been shown that wild type macrophages showed enhanced migration in the presence of recombinant periostin protein, an effect not evident in *Postn*$^{-/-}$ macrophages. Moreover, they concluded that *Postn*$^{-/-}$ macrophages show an impaired ability to migrate toward TGF-β (Schwanekamp et al., 2016), which could account for reduced macrophage numbers during wound healing. In addition, it has been demonstrated that periostin itself can act as a chemoattractant for macrophages in a model of glioblastoma (Squadrito & De Palma, 2015). Furthermore, in a renal ischemia-reperfusion injury model, it has been shown that periostin-overexpressing mice exhibit diminished expression of proinflammatory molecules and accumulate more F4/80+ macrophages when compared to periostin knockout mice. Interestingly, both coculturing macrophages with hypoxia-treated primary tubules that overexpress periostin, or alternatively treating macrophages with recombinant periostin, directly induced macrophage proliferation and expression of proregenerative molecules (Kormann et al., 2020). Periostin has also been strongly implicated in the recruitment of tumor associated macrophages in both intrahepatic cholangiocarcinoma (Zeng et al., 2018) and ovarian cancer (Tang et al., 2018). In summary, the reduced number of macrophages in palatal healing likely results from genetic deletion of periostin. Whether this occurs as a result of chemoattraction or as a result of macrophages expressing periostin is yet to be elucidated in wound healing systems. This will be an area of further investigation for our lab in the future.

Periostin and TGF-β-induced protein (βigh3) are considered paralogs because of their structural similarity.Here we showed that levels of βigh3 are upregulated during palatal

healing, but its expression is reduced in day-6 *Postn*$^{-/-}$ wounds. The alteration in wound closure kinetics in *Postn*$^{-/-}$ animals corresponds with the onset- but not the peak- of Postn expression in WT animals, as well as with the peak of βigh3 expression, indicating that βigh3 may not compensate for the loss of Postn during palatal wound healing. This is further supported by our observations in embryonic tissues where periostin and βigh3 did not exhibit overlapping expression, suggesting that they have independent roles in the development of the hard palate in mice. Recently, Schwanekamp et al. also showed that βigh3 has a distinct function during cardiac healing. After myocardial infarction, deletion of βigh3 does not alter cardiac disease, unlike loss of Postn in *Postn*$^{-/-}$ mice, and its loss is fully compensated by the more prominently expressed periostin (Schwanekamp et al., 2017).

In conclusion, in this study we demonstrated that periostin is upregulated during palatal healing in mice, where it is associated with fibronectin production, myofibroblast differentiation and infiltration of macrophages to the wound site. In vitro, *Postn*$^{-/-}$ fibroblasts show reduced contractile ability and fibronectin synthesis, effects which were also modulated by the stiffness of the microenvironment via integrin-β1/RhoA pathway (Figure 13), providing further evidence that periostin and the stiffness of the ECM act as modulators of matrix synthesis and myofibroblast differentiation during palatal healing. These findings could provide new insights for the development of novel approaches and biomaterials with specific biochemical and biomechanical properties targeted to accelerate and enhance the healing process (Urbanczyk et al., 2020), while suppressing fibrosis, after dental and maxillofacial surgical procedures.

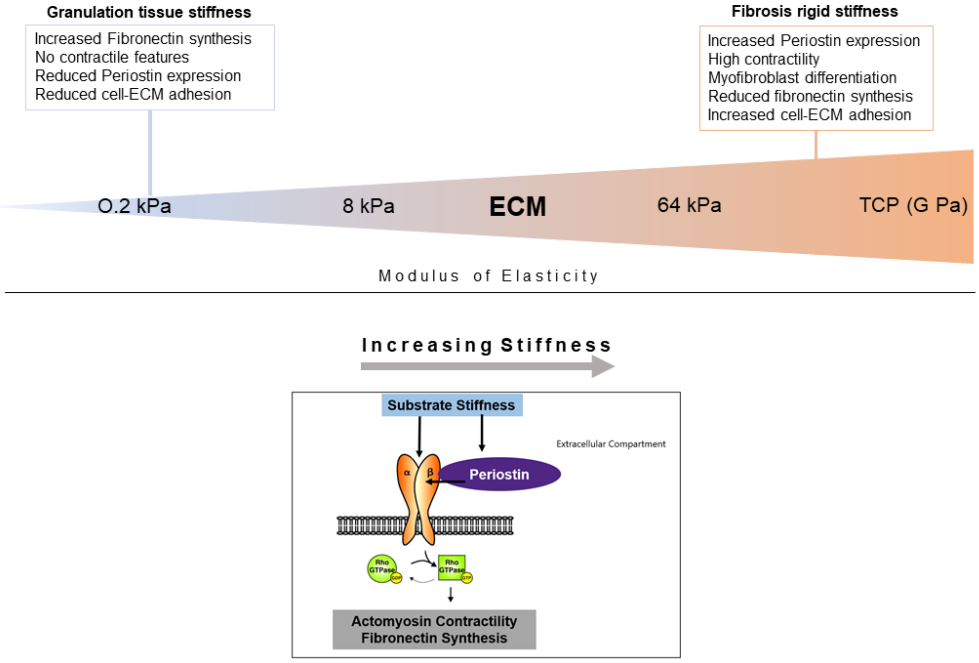

Figure 2-14 Proposed Mechanism

The biomechanical properties of a tissue in terms of stiffness (modulus of elasticity) vary across the different phases of wound healing. During the early phases of wound healing, the loose newly formed granulation tissue exhibits low stiffness, while, as the healing process progresses, the stiffness of the tissue increases with the deposit and remodeling of the ECM. Here, we demonstrate how the cellular behavior is modulated by the matrix stiffness, the molecular events that govern this process, as well as the role of periostin in palatal wound healing.

2.5 References

Achterberg, V. F., Buscemi, L., Diekmann, H., Smith-Clerc, J., Schwengler, H., Meister, J. J., Wenck, H., Gallinat, S., & Hinz, B. (2014). The nano-scale mechanical properties of the extracellular matrix regulate dermal fibroblast function. *Journal of Investigative Dermatology*, *134*(7), 1862–1872. https://doi.org/10.1038/jid.2014.90

Amizuka, N., Nishiyama, T., Saito, M., Li, M., Matsumoto, K., Kudo, A., & Kii, I. (2009). Incorporation of Tenascin-C into the Extracellular Matrix by Periostin Underlies an Extracellular Meshwork Architecture. *Journal of Biological Chemistry*, *285*(3), 2028–2039. https://doi.org/10.1074/jbc.m109.051961

Bae, J.-S., Lee, S.-H., Kim, J.-E., Choi, J.-Y., Park, R.-W., Yong Park, J., Park, H.-S., Sohn, Y.-S., Lee, D.-S., Bae Lee, E., & Kim, I.-S. (2002). Betaig-h3 supports keratinocyte adhesion, migration, and proliferation through alpha3beta1 integrin. *Biochemical and Biophysical Research Communications*, *294*(5), 940–948. https://doi.org/10.1016/S0006-291X(02)00576-4

Bornstein, P., & Sage, E. H. (2002). Matricellular proteins: Extracellular modulators of cell function. *Current Opinion in Cell Biology*, *14*(5), 608–616. https://doi.org/10.1016/S0955-0674(02)00361-7

Cornelissen, a M., Maltha, J. C., Von den Hoff, H. W., & Kuijpers-Jagtman, a M. (1999). Palatal mucoperiosteal wound healing in the rat. *European Journal of Oral Sciences*, *107*(5), 344–351.

Crawford, J., Nygard, K., Gan, B. S., & O'Gorman, D. B. (2015). Periostin induces fibroblast proliferation and myofibroblast persistence in hypertrophic scarring. *Experimental Dermatology*, *24*(2), 120–126. https://doi.org/10.1111/exd.12601

Danen, E. H. J., Sonneveld, P., Brakebusch, C., Fässler, R., & Sonnenberg, A. (2002). The fibronectin-binding integrins α5β1 and αvβ3 differentially modulate RhoA-

GTP loading, organization of cell matrix adhesions, and fibronectin fibrillogenesis. *Journal of Cell Biology*, *159*(6), 1071–1086. https://doi.org/10.1083/jcb.200205014

DeLeon-Pennell, K. Y., Barker, T. H., & Lindsey, M. L. (2020a). Fibroblasts: The arbiters of extracellular matrix remodeling. *Matrix Biology*. https://doi.org/10.1016/j.matbio.2020.05.006

DeLeon-Pennell, K. Y., Barker, T. H., & Lindsey, M. L. (2020b). Fibroblasts: The arbiters of extracellular matrix remodeling. *Matrix Biology*. https://doi.org/10.1016/j.matbio.2020.05.006

Desmoulière, a, Geinoz, A., Gabbiani, F., & Gabbiani, G. (1993). Transforming growth factor-beta 1 induces alpha-smooth muscle actin expression in granulation tissue myofibroblasts and in quiescent and growing cultured fibroblasts. *The Journal of Cell Biology*, *122*(1), 103–111. https://doi.org/10.1083/jcb.122.1.103

Dipietro, L. a. (2003). *In Oral Mucosal and Cutaneous Wounds*. 621–626. https://doi.org/10.1177/154405910308200810

Elliott, C. G., & Hamilton, D. W. (2011). Deconstructing fibrosis research: Do pro-fibrotic signals point the way for chronic dermal wound regeneration? *Journal of Cell Communication and Signaling*, *5*(4), 301–315. https://doi.org/10.1007/s12079-011-0131-5

Elliott, C. G., Wang, J., Guo, X., Xu, S. -w., Eastwood, M., Guan, J., Leask, A., Conway, S. J., & Hamilton, D. W. (2012). Periostin modulates myofibroblast differentiation during full-thickness cutaneous wound repair. *Journal of Cell Science*, *125*(1), 121–132. https://doi.org/10.1242/jcs.087841

Elliott CG, Kim SS, H. DW. (2012). Functional significance of periostin in excisional skin repair. Is the devil in the detail? .Pdf. *Cell Adhesion and Migration*, *6*(4), 319–326. https://doi.org/10.4161/cam.20879

Engler, A. J., Sen, S., Sweeney, H. L., & Discher, D. E. (2006). Matrix elasticity directs stem cell lineage specification. *Cell*, *126*(4), 677–689. https://doi.org/10.1016/j.cell.2006.06.044

Gabbiani, G. (1996). The cellular derivation and the life span of the myofibroblast. *Pathology, Research and Practice*, *192*(7), 708–711. https://doi.org/10.1016/S0344-0338(96)80092-6

Gabbiani, G., Ryan, G. B., & Majne, G. (1971). Presence of modified fibroblasts in granulation tissue and their possible role in wound contraction. *Experientia*, *27*(5), 549–550.

Giannopoulou, C., & Cimasoni, G. (1996). Functional Characteristics of Gingival and Periodontal Ligament Fibroblasts. *Journal of Dental Research* , *75*(3), 895–902. https://doi.org/10.1177/00220345960750030601

Glim, J. E., Van Egmond, M., Niessen, F. B., Everts, V., Beelen, R. H. J., Judith, M., & Glim, E. (n.d.). *Detrimental dermal wound healing: What can we learn from the oral mucosa?* https://doi.org/10.1111/wrr.12072

Goffin, J. M., Pittet, P., Csucs, G., Lussi, J. W., Meister, J. J., & Hinz, B. (2006). Focal adhesion size controls tension-dependent recruitment of α-smooth muscle actin to stress fibers. *Journal of Cell Biology*, *172*(2), 259–268. https://doi.org/10.1083/jcb.200506179

Gorin, D. R., Cordts, P. R., LaMorte, W. W., & Menzoian, J. O. (1996). The influence of wound geometry on the measurement of wound healing rates in clinical trials. *Journal of Vascular Surgery*, *23*(3), 524–528. https://doi.org/10.1016/S0741-5214(96)80021-8

Gu, L., Zhu, Y. J., Yang, X., Guo, Z. J., Xu, W. B., & Tian, X. L. (2007). Effect of TGF-β/Smad signaling pathway on lung myofibroblast differentiation. *Acta*

Pharmacologica Sinica, *28*(3), 382–391. https://doi.org/10.1111/j.1745-7254.2007.00468.x

Guilluy, C., Swaminathan, V., Garcia-Mata, R., O'Brien, E. T., Superfine, R., & Burridge, K. (2011). The Rho GEFs LARG and GEF-H1 regulate the mechanical response to force on integrins. *Nature Cell Biology*. https://doi.org/10.1038/ncb2254

Häkkinen, L., Uitto, V. J., & Larjava, H. (2000). Cell biology of gingival wound healing. *Periodontology 2000*, *24*, 127–152. https://doi.org/10.1034/j.1600-0757.2000.2240107.x

Hamilton, D. W. (2008). Functional role of periostin in development and wound repair: Implications for connective tissue disease. *Journal of Cell Communication and Signaling*, *2*(1–2), 9–17. https://doi.org/10.1007/s12079-008-0023-5

Hashimoto, K., Noshiro, M., Ohno, S., Kawamoto, T., Satakeda, H., Akagawa, Y., Nakashima, K., Okimura, A., Ishida, H., Okamoto, T., Pan, H., Shen, M., Yan, W., & Kato, Y. (1997). Characterization of a cartilage-derived 66-kDa protein (RCD-CAP/βig-h3) that binds to collagen. *Biochimica et Biophysica Acta - Molecular Cell Research*. https://doi.org/10.1016/S0167-4889(96)00147-4

Hesse, M., Cheever, A. W., Modolell, M., Fuentes, J. M., Pearce, E. J., Wynn, T. A., La Flamme, A. C., & Schito, M. (2014). Differential Regulation of Nitric Oxide Synthase-2 and Arginase-1 by Type 1/Type 2 Cytokines In Vivo: Granulomatous Pathology Is Shaped by the Pattern of L-Arginine Metabolism. *The Journal of Immunology*, *167*(11), 6533–6544. https://doi.org/10.4049/jimmunol.167.11.6533

Higashida, C., Hirai, H., Kimura, K., Okamoto, M., Birge, R., Narumiya, S., Furuyashiki, T., Ishizaki, T., Nakamoto, T., Tsuji, T., & Arakawa, Y. (2002). ROCK and mDia1 antagonize in Rho-dependent Rac activation in Swiss 3T3 fibroblasts. *JOURNAL OF CELL BIOLOGY*. https://doi.org/10.1083/jcb.200112107

Hinz, B. (2010). The myofibroblast: Paradigm for a mechanically active cell. *Journal of Biomechanics*, *43*(1), 146–155. https://doi.org/10.1016/j.jbiomech.2009.09.020

Hinz, B. (2015). The extracellular matrix and transforming growth factor-β1: Tale of a strained relationship. *Matrix Biology*, *47*, 54–65. https://doi.org/10.1016/j.matbio.2015.05.006

Hinz, B. (2016). Myofibroblasts. *Experimental Eye Research*, *142*, 56–70. https://doi.org/10.1016/j.exer.2015.07.009

Hinz, B., Celetta, G., Tomasek, J. J., Gabbiani, G., & Chaponnier, C. (2001). *Alpha-Smooth Muscle Actin Expression Upregulates Fibroblast Contractile Activity*. *12*(September), 2730–2741.

Holmberg, C., Quante, M., Steele, I., Kumar, J. D., Balabanova, S., Duval, C., Czepan, M., Rakonczay, Z., Tiszlavicz, L., Nemeth, I., Lazar, G., Simonka, Z., Jenkins, R., Hegyi, P., Wang, T. C., Dockray, G. J., & Varro, A. (2012). Release of TGFβig-h3 by gastric myofibroblasts slows tumor growth and is decreased with cancer progression. *Carcinogenesis*. https://doi.org/10.1093/carcin/bgs180

Humphrey, J. D., Dufresne, E. R., & Schwartz, M. A. (2014). Mechanotransduction and extracellular matrix homeostasis. *Nature Reviews Molecular Cell Biology*, *15*(12), 802–812. https://doi.org/10.1038/nrm3896

Huveneers, S., & Danen, E. H. J. (2009). Adhesion signaling—Crosstalk between integrins, Src and Rho. *Journal of Cell Science*, *122*(8), 1059–1069. https://doi.org/10.1242/jcs.039446

Hwang, E. Y., Jeong, M. S., Park, E. K., Kim, J. H., & Jang, S. B. (2014). Structural characterization and interaction of periostin and bone morphogenetic protein for regulation of collagen cross-linking. *Biochemical and Biophysical Research Communications*, *449*(4), 425–431. https://doi.org/10.1016/j.bbrc.2014.05.055

Jablonski, K. A., Amici, S. A., Webb, L. M., Ruiz-Rosado, J. D. D., Popovich, P. G., Partida-Sanchez, S., & Guerau-De-arellano, M. (2015). Novel markers to delineate murine M1 and M2 macrophages. *PLoS ONE*, *10*(12), 5–11. https://doi.org/10.1371/journal.pone.0145342

Jackson-Boeters, L., Wen, W., & Hamilton, D. W. (2009). Periostin localizes to cells in normal skin, but is associated with the extracellular matrix during wound repair. *Journal of Cell Communication and Signaling*, *3*(2), 125–133. https://doi.org/10.1007/s12079-009-0057-3

Karamanos, N. K., Theocharis, A. D., Neill, T., & Iozzo, R. V. (2019). Matrix modeling and remodeling: A biological interplay regulating tissue homeostasis and diseases. *Matrix Biology : Journal of the International Society for Matrix Biology*, *75–76*, 1–11. https://doi.org/10.1016/j.matbio.2018.08.007

Katz, B. Z., Zamir, E., Bershadsky, A., Kam, Z., Yamada, K. M., & Geiger, B. (2000). Physical state of the extracellular matrix regulates the structure and molecular composition of cell-matrix adhesions. *Molecular Biology of the Cell*, *11*(3), 1047–1060. https://doi.org/citeulike-article-id:6656192

Kawamoto, T., Noshiro, M., Shen, M., Nakamasu, K., Hashimoto, K., Kawashima-Ohya, Y., Gotoh, O., & Kato, Y. (1998). Structural and phylogenetic analyses of RGD-CAP/beta ig-h3, a fasciclin-like adhesion protein expressed in chick chondrocytes. *Biochimica et Biophysica Acta*, *1395*(3), 288–292. http://dx.doi.org/10.1016/S0167-4781(97)00172-3

Keswani, S. G., Balaji, S., Le, L. D., Leung, A., Parvadia, J. K., Frischer, J., Yamano, S., Taichman, N., & Crombleholme, T. M. (2013). Role of salivary vascular endothelial growth factor (VEGF) in palatal mucosal wound healing. *Wound Repair and Regeneration : Official Publication of the Wound Healing Society [and] the European Tissue Repair Society*, *21*(4), 554–562. https://doi.org/10.1111/wrr.12065

Kii, I., Amizuka, N., Nishiyama, T., Saito, M., Li, M., Matsumoto, K., & Kudo, A. (2009). Incorporation of Tenascin-C into the Extracellular Matrix by Periostin Underlies an Extracellular Meshwork Architecture. *Journal of Biological Chemistry*, *285*(3), 2028–2039. https://doi.org/10.1074/jbc.m109.051961

Kii, I., Nishiyama, T., & Kudo, A. (2016). Periostin promotes secretion of fibronectin from the endoplasmic reticulum. *Biochemical and Biophysical Research Communications*, *470*(4), 888–893. https://doi.org/10.1016/j.bbrc.2016.01.139

Kim, B. Y., Olzmann, J. A., Choi, S. Il, Ahn, S. Y., Kim, T. I., Cho, H. S., Suh, H., & Kim, E. K. (2009). Corneal dystrophy-associated R124H mutation disrupts TGFBI interaction with periostin and causes mislocalization to the lysosome. *Journal of Biological Chemistry*. https://doi.org/10.1074/jbc.M109.013607

Kim, S. S., Nikoloudaki, G., Darling, M., Rieder, M. J., & Hamilton, D. W. (2019). Phenytoin activates smad3 phosphorylation and periostin expression in drug-induced gingival enlargement. *Histology and Histopathology*. https://doi.org/10.14670/HH-18-015

Kim, S. S., Nikoloudaki, G. E., Michelsons, S., Creber, K., & Hamilton, D. W. (2019). Fibronectin synthesis, but not α-smooth muscle expression, is regulated by periostin in gingival healing through FAK/JNK signaling. *Scientific Reports*, *9*(1), 2708. https://doi.org/10.1038/s41598-018-35805-6

Klingberg, F., Wells, R. G., Walraven, M., Olsen, A. L., Koehler, A., Hinz, B., Chau, G., Chow, M. L., Lodyga, M., Im, M., White, E. S., & Boo, S. (2018). The fibronectin ED-A domain enhances recruitment of latent TGF-β-binding protein-1 to the fibroblast matrix. *Journal of Cell Science*, *131*(5), jcs201293. https://doi.org/10.1242/jcs.201293

Koli, K., Hyytiäinen, M., Ryynänen, M. J., & Keski-Oja, J. (2005). Sequential deposition of latent TGF-β binding proteins (LTBPs) during formation of the extracellular

matrix in human lung fibroblasts. *Experimental Cell Research*, *310*(2), 370–382. https://doi.org/10.1016/J.YEXCR.2005.08.008

Kormann, R., Kavvadas, P., Placier, S., Vandermeersch, S., Dorison, A., Dussaule, J.-C., Chadjichristos, C. E., Prakoura, N., & Chatziantoniou, C. (2020). Periostin Promotes Cell Proliferation and Macrophage Polarization to Drive Repair after AKI. *Journal of the American Society of Nephrology : JASN*, *31*(1), 85–100. https://doi.org/10.1681/ASN.2019020113

Kudo, A., & Kii, I. (2018). Periostin function in communication with extracellular matrices. *Journal of Cell Communication and Signaling*, *12*(1), 301–308. https://doi.org/10.1007/s12079-017-0422-6

Larjava, H. (2013). Oral Wound Healing: Cell Biology and Clinical Management. In *Oral Wound Healing: Cell Biology and Clinical Management*. https://doi.org/10.1002/9781118704509

Larjava, H., Wiebe, C., Gallant-Behm, C., Hart, D. a., Heino, J., & Häkkinen, L. (2011). Exploring scarless healing of oral soft tissues. *Journal of the Canadian Dental Association*, *77*(C), 1–5.

Leask, A. (2013). Focal Adhesion Kinase: A Key Mediator of Transforming Growth Factor Beta Signaling in Fibroblasts. *Advances in Wound Care*. https://doi.org/10.1089/wound.2012.0363

LeBaron, R. G., Bezverkov, K. I., Zimber, M. P., Pavelec, R., Skonier, J., & Purchio, A. F. (1995). Beta IG-H3, a novel secretory protein inducible by transforming growth factor-beta, is present in normal skin and promotes the adhesion and spreading of dermal fibroblasts in vitro. *The Journal of Investigative Dermatology*, *104*(5), 844–849. https://doi.org/0022202X9500061O [pii]

Lepekhin, E., Gron, B., Berezin, V., Bock, E., & Dabelsteen, E. (2002). Differences in motility pattern between human buccal fibroblasts and periodontal and skin

fibroblasts. *European Journal of Oral Sciences*, *110*(1), 13–20. https://doi.org/10.1034/j.1600-0722.2002.00139.x

Lindsley, A., Li, W., Wang, J., Maeda, N., Rogers, R., & Conway, S. J. (2005). Comparison of the four mouse fasciclin-containing genes expression patterns during valvuloseptal morphogenesis. *Gene Expression Patterns*. https://doi.org/10.1016/j.modgep.2005.03.005

Lupher, M. L., & Gallatin, W. M. (2006). Regulation of Fibrosis by the Immune System. In *Advances in Immunology*. https://doi.org/10.1016/S0065-2776(05)89006-6

Maekawa, M., Ishizaki, T., Boku, S., Watanabe, N., Fujita, A., Iwamatsu, A., Obinata, T., Ohashi, K., Mizuno, K., & Narumiya, S. (1999). Signaling from Rho to the actin cytoskeleton through protein kinases ROCK and LIM-kinase. *Science*, *285*(5429), 895–898. https://doi.org/10.1126/science.285.5429.895

Mah, W., Jiang, G., Olver, D., Cheung, G., Kim, B., Larjava, H., & Häkkinen, L. (2014). Human gingival fibroblasts display a non-fibrotic phenotype distinct from skin fibroblasts in three-dimensional cultures. *PloS One*, *9*(3), e90715. https://doi.org/10.1371/journal.pone.0090715

Mao, Y., & Schwarzbauer, J. E. (2005). Fibronectin fibrillogenesis, a cell-mediated matrix assembly process. In *Matrix Biology*. https://doi.org/10.1016/j.matbio.2005.06.008

Maruhashi, T., Kii, I., Saito, M., & Kudo, A. (2010). Interaction between periostin and BMP-1 promotes proteolytic activation of lysyl oxidase. *Journal of Biological Chemistry*, *285*(17), 13294–13303. https://doi.org/10.1074/jbc.M109.088864

Moore, S. W., Roca-Cusachs, P., & Sheetz, M. P. (2010). Stretchy proteins on stretchy substrates: The important elements of integrin-mediated rigidity sensing. *Developmental Cell*, *19*(2), 194–206. https://doi.org/10.1016/j.devcel.2010.07.018

Mosher, D. F., Johansson, M. W., Gillis, M. E., & Annis, D. S. (2015). Periostin and TGF- β -induced Protein: Two Peas in a Pod ? *Critical Reviews in Biochemistry and Molecular Biology*, *50*(5), 427–439. https://doi.org/10.3109/10409238.2015.1069791.Periostin

Nakano, K., Takaishi, K., Kodama, A., Mammoto, A., Shiozaki, H., Monden, M., & Takai, Y. (2013). Distinct Actions and Cooperative Roles of ROCK and mDia in Rho Small G Protein-induced Reorganization of the Actin Cytoskeleton in Madin-Darby Canine Kidney Cells. *Molecular Biology of the Cell*, *10*(8), 2481–2491. https://doi.org/10.1091/mbc.10.8.2481

Nanci, A. (2013). Ten Cate's Oral Histology. In *Elsevier: Vol. 8th ed* (p. 166). Elsevier.

Nikoloudaki, G., Creber, K., & Hamilton, D. W. (2020). Wound Healing and Fibrosis: A Contrasting Role for Periostin in Skin and the Oral Mucosa. *American Journal of Physiology-Cell Physiology*. https://doi.org/10.1152/ajpcell.00035.2020

Norris, R. A., Damon, B., Kern, C. B., Wen, X., Forgacs, G., Hoffman, S., Trusk, T., Molkentin, J. D., Goodwin, R. L., Conway, S. J., Norris, R. A., Kasyanov, V., Potts, J. D., Mjaatvedt, C. H., Oka, T., Moreno-Rodriguez, R., Markwald, R. R., Sugi, Y., Davis, J., … Mironov, V. (2007). Periostin regulates collagen fibrillogenesis and the biomechanical properties of connective tissues. *Journal of Cellular Biochemistry*, *101*(3), 695–711. https://doi.org/10.1002/jcb.21224

Olsen, Abby L.Uemura, M., Janmey, P. A., Chan, E. P., Wells, R. G., Sackey, B., Georges, P. C., Bloomer, S. A., & Gaça, M. D. A. (2011). Hepatic stellate cells require a stiff environment for myofibroblastic differentiation. *American Journal of Physiology-Gastrointestinal and Liver Physiology*, *301*(1), G110–G118. https://doi.org/10.1152/ajpgi.00412.2010

Pakshir, P., & Hinz, B. (2018). The big five in fibrosis: Macrophages, myofibroblasts, matrix, mechanics, and miscommunication. *Matrix Biology*, *68–69*, 81–93. https://doi.org/10.1016/j.matbio.2018.01.019

Pelham, R. J., & Wang, Y. L. (1998). Cell locomotion and focal adhesions are regulated by the mechanical properties of the substrate. *Biological Bulletin*, *194*(3), 348–350. https://doi.org/10.2307/1543109

Pereira, M., Rybarczyk, B. J., Odrljin, T. M., Hocking, D. C., Sottile, J., & Simpson-Haidaris, P. J. (2002). The incorporation of fibrinogen into extracellular matrix is dependent on active assembly of a fibronectin matrix. *Journal of Cell Science*, *115*(Pt 3), 609–617.

Politis, C., Schoenaers, J., Jacobs, R., & Agbaje, J. O. (2016). Wound healing problems in the mouth. *Frontiers in Physiology*, *7*(NOV), 1–13. https://doi.org/10.3389/fphys.2016.00507

Ridley, A. J., & Hall, A. (1992). The small GTP-binding protein rho regulates the assembly of focal adhesions and actin stress fibers in response to growth factors. *Cell*, *70*(3), 389–399. https://doi.org/10.1016/0092-8674(92)90163-7

Rios, H., Koushik, S. V, Wang, H., Wang, J., Zhou, H.-M., Lindsley, A., Rogers, R., Chen, Z., Maeda, M., Kruzynska-Frejtag, A., Feng, J. Q., & Conway, S. J. (2005). Periostin Null Mice Exhibit Dwarfism, Incisor Enamel Defects, and an Early-Onset Periodontal Disease-Like Phenotype. *Molecular and Cellular Biology*, *25*(24), 11131–11144. https://doi.org/10.1128/MCB.25.24.11131-11144.2005

Rogers, R., Markwald, R., Moreno-Rodriguez, R. A., Lindsley, A., Menick, D., Snider, P., Conway, S. J., Field, L., Firulli, A. B., Li, F., Ingram, D. A., Molkentin, J. D., Wang, J., & Hinton, R. B. (2008). Periostin Is Required for Maturation and Extracellular Matrix Stabilization of Noncardiomyocyte Lineages of the Heart. *Circulation Research*, *102*(7), 752–760. https://doi.org/10.1161/circresaha.107.159517

Rousselle, P., Montmasson, M., & Garnier, C. (2019). Extracellular matrix contribution to skin wound re-epithelialization. *Matrix Biology : Journal of the International*

Society for Matrix Biology, 75–76, 12–26. https://doi.org/10.1016/j.matbio.2018.01.002

Schwanekamp, J. A., Lorts, A., Sargent, M. A., York, A. J., Grimes, K. M., Fischesser, D. M., Gokey, J. J., Whitsett, J. A., Conway, S. J., & Molkentin, J. D. (2017). TGFBI functions similar to periostin but is uniquely dispensable during cardiac injury. *PLoS ONE*, *12*(7). https://doi.org/10.1371/journal.pone.0181945

Schwanekamp, J. A., Lorts, A., Vagnozzi, R. J., Vanhoutte, D., & Molkentin, J. D. (2016). Deletion of Periostin Protects Against Atherosclerosis in Mice by Altering Inflammation and Extracellular Matrix Remodeling. *Arteriosclerosis, Thrombosis, and Vascular Biology*, *36*(1), 60–68. https://doi.org/10.1161/ATVBAHA.115.306397

Schwarz, U. S., & Gardel, M. L. (2012). United we stand – integrating the actin cytoskeleton and cell–matrix adhesions in cellular mechanotransduction. *Journal of Cell Science*, *125*(13), 3051–3060. https://doi.org/10.1242/jcs.093716

Serini, G., Bochaton-Piallat, M.-L., Borsi, L., Geinoz, A., Ropraz, P., Gabbiani, G., & Zardi, L. (2002). The Fibronectin Domain ED-A Is Crucial for Myofibroblastic Phenotype Induction by Transforming Growth Factor-β1. *The Journal of Cell Biology*, *142*(3), 873–881. https://doi.org/10.1083/jcb.142.3.873

Singh, P., Carraher, C., & Schwarzbauer, J. E. (2010). Assembly of Fibronectin Extracellular Matrix. *Annual Review of Cell and Developmental Biology*. https://doi.org/10.1146/annurev-cellbio-100109-104020

Skonier, J., Neubauer, M., Madisen, L., Bennett, K., Plowman, G., & Purchio, A. (1992). CDNA cloning and sequence analysis of beta ig-h3, a novel gene induced in a human adenocarcinoma cell line after treatment with transforming growth factor-beta. *DNA Cell Biol*.

Smith, A. J., Scheven, B. A., Takahashi, Y., Ferracane, J. L., Shelton, R. M., & Cooper, P. R. (2012). Dentine as a bioactive extracellular matrix. *Archives of Oral Biology*, *57*(2), 109–121. https://doi.org/10.1016/J.ARCHORALBIO.2011.07.008

Sprangers, S., & Everts, V. (2017). Molecular pathways of cell-mediated degradation of fibrillar collagen. *Matrix Biology*. https://doi.org/10.1016/j.matbio.2017.11.008

Squadrito, M. L., & De Palma, M. (2015). A niche role for periostin and macrophages in glioblastoma. *Nature Cell Biology*, *17*(2), 107–109. https://doi.org/10.1038/ncb3095

Talele, N. P., Fradette, J., Davies, J. E., Kapus, A., & Hinz, B. (2015). Expression of α-Smooth Muscle Actin Determines the Fate of Mesenchymal Stromal Cells. *Stem Cell Reports*, *4*(6), 1016–1030. https://doi.org/10.1016/j.stemcr.2015.05.004

Tang, M., Liu, B., Bu, X., & Zhao, P. (2018). Cross-talk between ovarian cancer cells and macrophages through periostin promotes macrophage recruitment. *Cancer Science*, *109*(5), 1309–1318. https://doi.org/10.1111/cas.13567

Tomasek, J. J., Gabbiani, G., Hinz, B., Chaponnier, C., & Brown, R. a. (2002). Myofibroblasts and mechano-regulation of connective tissue remodelling. *Nature Reviews. Molecular Cell Biology*, *3*(5), 349–363. https://doi.org/10.1038/nrm809

Urbanczyk, M., Layland, S. L., & Schenke-Layland, K. (2020). The role of extracellular matrix in biomechanics and its impact on bioengineering of cells and 3D tissues. *Matrix Biology*, *85–86*, 1–14. https://doi.org/10.1016/j.matbio.2019.11.005

van der Bijl, I., Nawaz, K., Kazlauskaite, U., van Stalborch, A.-M., Tol, S., Jimenez Orgaz, A., van den Bout, I., Reinhard, N. R., Sonnenberg, A., & Margadant, C. (2020). Reciprocal integrin/integrin antagonism through kindlin-2 and Rho GTPases regulates cell cohesion and collective migration. *Matrix Biology : Journal of the International Society for Matrix Biology*. https://doi.org/10.1016/j.matbio.2020.05.005

Verstappen, J., Van Rheden, R. E. M., Katsaros, C., Torensma, R., & Von Den Hoff, J. W. (2012). Preferential recruitment of bone marrow-derived cells to rat palatal wounds but not to skin wounds. *Archives of Oral Biology*, *57*(1), 102–108. https://doi.org/10.1016/j.archoralbio.2011.08.005

Walker, J. T., Kim, S. S., Michelsons, S., Creber, K., Elliott, C. G., Leask, A., & Hamilton, D. W. (2015). *Cell – matrix interactions governing skin repair: Matricellular proteins as diverse modulators of cell function*. 73–88.

Walraven, M., & Hinz, B. (2018). Therapeutic approaches to control tissue repair and fibrosis: Extracellular matrix as a game changer. *Matrix Biology*, *71–72*, 205–224. https://doi.org/10.1016/j.matbio.2018.02.020

Wells, A., Nuschke, A., & Yates, C. C. (2016). Skin tissue repair: Matrix microenvironmental influences. *Matrix Biology : Journal of the International Society for Matrix Biology*, *49*, 25–36. https://doi.org/10.1016/j.matbio.2015.08.001

Wijdeveld, M. G. M. M., Grupping, E. M., Kuijpers-Jagtman, A. M., & Maltha, J. C. (1987). Wound healing of the palatal mucoperiosteum in beagle dogs after surgery at different ages. *Journal of Cranio-Maxillofacial Surgery*, *15*, 51–57. https://doi.org/10.1016/S1010-5182(87)80018-5

Wijdeveld, M. G. M. M., Maltha, J. C., Grupping, E. M., Dejonge, J., & Kuijpersjagtman, A. M. (1991). A Histological Study of Tissue-Response to Simulated Cleft-Palate Surgery at Different Ages in Beagle Dogs. *Archives of Oral Biology*, *36*(11), 837–843.

Winer, J. P., Janmey, P. A., McCormick, M. E., & Funaki, M. (2008). Bone Marrow-Derived Human Mesenchymal Stem Cells Become Quiescent on Soft Substrates but Remain Responsive to Chemical or Mechanical Stimuli. *Tissue Engineering Part A*. https://doi.org/10.1089/ten.tea.2007.0388

Wong, J. W., Gallant-Behm, C., Wiebe, C., Mak, K., Hart, D. A., Larjava, H., & Häkkinen, L. (2009). Wound healing in oral mucosa results in reduced scar formation as compared with skin: Evidence from the red Duroc pig model and humans. *Wound Repair and Regeneration*, *17*(5), 717–729. https://doi.org/10.1111/j.1524-475X.2009.00531.x

Yoneda, A., Multhaupt, H. A. B., & Couchman, J. R. (2005). The Rho kinases I and II regulate different aspects of myosin II activity. *Journal of Cell Biology*. https://doi.org/10.1083/jcb.200412043

Yoneda, A., Ushakov, D., Multhaupt, H. A. B., & Couchman, J. R. (2006). Fibronectin Matrix Assembly Requires Distinct Contributions from Rho Kinases I and -II. *Molecular Biology of the Cell*. https://doi.org/10.1091/mbc.e06-08-0684

Zeng, J., Liu, Z., Sun, S., Xie, J., Cao, L., Lv, P., Nie, S., Zhang, B., Xie, B., Peng, S., & Jiang, B. (2018). Tumor-associated macrophages recruited by periostin in intrahepatic cholangiocarcinoma stem cells. *Oncology Letters*, *15*(6), 8681–8686. https://doi.org/10.3892/ol.2018.8372

Zhou, H.-M., Wang, J., Elliott, C., Wen, W., Hamilton, D. W., & Conway, S. J. (2010). Spatiotemporal expression of periostin during skin development and incisional wound healing: Lessons for human fibrotic scar formation. *Journal of Cell Communication and Signaling*, *4*(2), 99–107. https://doi.org/10.1007/s12079-010-0090-2

Zollinger, A. J., & Smith, M. L. (2017). Fibronectin, the extracellular glue. *Matrix Biology*, *60–61*, 27–37. https://doi.org/10.1016/j.matbio.2016.07.011

Chapter 3

3 Role of periostin in the maintenance and mineralization of the periodontal ligament

3.1 Introduction

The periodontium is the name given to the teeth-supporting tissues, consisting specifically of the alveolar bone, gingiva, periodontal ligament (PDL) and cementum. In particular, the PDL is a principal tissue as it transmits forces between the tooth and adjacent tissues. Dispersion of stress is achieved through the PDL collagen fiber network, that inserts into both the cementum and the alveolar bone through Sharpey's fibers (Liang et al., 2020; Nanci, 2017). The PDL is highly cellular and well vascularized, containing fibroblasts that remodel and maintain the PDL, as well as populations of pericytes, cementoblasts, osteoblasts and multipotent mesenchymal stem cells (T. R. Gould, 1983; T. R. L. Gould et al., 1980; Komaki, 2019; Lekic & McCulloch, 1996; McCulloch, 1985; Seo et al., 2004). The PDL is central to maintenance of tooth health and the homeostasis of periodontal tissues by facilitating transmission of mechanical loading between the tooth and the bone. (Beertsen et al., 1997).

The extracellular matrix of the periodontal ligament is composed of a loose plexus of crimped collagen fibrils embedded in a highly hydrated interfibrillar matrix. Only close to their cemental insertion points do these fibrils gather into thick, parallel fascicles (Sharpey's fibres). As the collagen fibrils cross the mineralization front, they become infiltrated by the mineral phase and continue directly with the cementum matrix. Sharpey's fibres, "extrinsic" and "intrinsic" fibres all appear to be the same fibres, which bend and branch repeatedly during their course within the thickness of the cementum (Raspanti et al., 2000). Collagen fibrils are continuous between the PDL and cementum, yet there is an extremely sharp interface between mineralized and unmineralized tissues. Collagen fibrils in the PDL have a mostly parallel arrangement, especially where they insert into the cementum at approximately right angles to the root surface. The PDL fibrils form closely packed bundles. As the PDL fibrils insert into cementum, they merge together and exhibit

an increase in diameter of up to 40% (Quan & Sone, 2015). The processes that regulate mineralization of the cementum-PDL junction is attributed to the unique extracellular matrix composition of the constituent tissues of the periodontium: dentin, cementum, periodontal ligament, and bone.

The non-collagenous protein (NCP) compositions of these tissues differ significantly which likely controls where mineralization occurs. For instance, in dentin the most abundant NCPs are dentin sialophosphoprotein (DSPP), dentin matrix protein-1 (DMP- 1), bone sialoprotein (BSP), and osteopontin (OPN). BSP and OPN are also found in fibrillar cementum, along with osteocalcin and osteonectin (Nanci, 2017). In the PDL, the main non-collagenous components are hyaluronan and proteoglycans aggregates, the latter representing decorin, biglycan (chondroitin sulfate PGs) (Häkkinen et al., 1993; Lausch & Sone, 2015; Wojtas et al., 2020). Despite better characterization of the components of the PDL ECM, the molecular mechanism that regulate the spatial mineralization of tissues in the periodontium is still unclear. Significantly, several matricellular proteins are now known to be prominently expressed in the PDL, including periostin, matrix gla protein and SPARC (Nikoloudaki, 2021). Despite being heavily expressed in healthy PDL, the exact biological function of periostin in tissue homeostasis has not been determined.

Periostin was initially named and classified based on its apparent restricted expression and localization to the PDL and periosteum of adult mice (Horiuchi et al., 1999). Immunoelectron microscopic observation of the mature PDL verified the location of periostin to be between the cytoplasmic processes of periodontal fibroblasts and cementoblasts with adjacent collagen fibrils. In adult humans, our laboratory demonstrated that periostin is highly also expressed in the PDL and periosteum of alveolar bone (Wen et al., 2010), closely mirroring the distribution evident in mice.

Further research focusing on the investigation of periostin in maintenance of PDL integrity assessed using transgenic mice where periostin is genetically deleted showed that knockout (*Postn*$^{-/-}$) mice exhibit defective collagen fibrillogenesis, evident through reductions in fibril diameter and defective crosslinking (Norris et al., 2007; Sata et al., 2008). This manifest in loss of architecture and functional disruption of several collagenous-based

tissues, including the PDL (H. Rios et al., 2005). Micro-computed topography imaging analysis on *Postn*$^{-/-}$ mice skulls revealed the early onset of severe periodontal disease, significant reduction in bone density, and structural defects in the incisors resulting in enhanced tooth wear (Hamilton, 2008). Removal of masticatory forces reduced periodontal and enamel defects, showing periostin can alter PDL structural or mechanical properties allowing dispersion of applied loading stresses (H. F. Rios et al., 2008).

While periostin has been shown to organize the ECM at the tooth interface of the alveolar bone and PDL (Kruzynska-Frejtag et al., 2004), possibly through its regulation of collagen fibrillogenesis (Norris et al., 2007), evidence suggest that it can also act directly on cell populations within the PDL (Tkatchenko et al., 2009). Previous studies have reported that periostin promotes cell mobility, adhesion and survival in periodontal ligament cells by binding to integrin αvβ3 and αvβ5 via the Integrin/FAK/AKT signalling pathway (Matsuzawa et al., 2015). Recently, it was also shown that periostin promotes migration, proliferation, and differentiation of human periodontal ligament mesenchymal stem cells *in vitro* (Z. Wu et al., 2018), and promotes osteogenic differentiation of human periodontal ligament mesenchymal stem cells via the Jun amino-terminal kinases (JNK) pathway under inflammatory conditions *in vitro* in these cells (Tang et al., 2017).

Despite our extensive knowledge of periostin expression in the periodontium, comparatively little is known about its role in the maintenance of periodontal structures or on cellular phenotype, particularly of PDL resident cell populations. The aim of this chapter was to investigate the potential role of periostin in the maintenance and mineralization of the periodontal ligament cells *in vitro* via functional and gene-expression analyses.

3.2 Materials and Methods

3.2.1 Animals

All animal procedures were in accordance with protocols approved by the University Council on Animal Care at The University of Western Ontario. *Postn*-knockout mice (*Postn*$^{-/-}$) were generated and maintained on soft diet in order to reduce malnutrition, which was previously observed under a standard diet due to the enamel and dentin defects of the incisors and molars (H. Rios et al., 2005). Heterozygous mice were crossed with C57BL/6J (JAX Mice and Services, Bar Harbor, Maine) for a minimum of six generations to ensure an incipient congenic strain. Backcrossed heterozygous mice were used for breeding and all offspring were genotyped as described previously described (H. Rios et al., 2005).

3.2.2 Ex vivo remineralization assay (Performed by Laboratory of Eli Sone, University of Toronto)

Formalin fixed and EDTA-decalcified hemimandibles from adult periostin WT and *Postn*$^{-/-}$ mice were trimmed and processed for 210 nm thick sections and exposed the dentin-cementum-PDL junction at the apical portion of the tooth root. The ultrathin tissue sections were remineralized as previously reported (Lausch et al., 2013). Briefly, mineralizing solution was prepared immediately before remineralization by combining equal volume of four previously prepared solutions (stored at 4 °C). One milligram of polyaspartic acid (pAsp, Alamanda Polymers, AL, USA; MW = 14 kDa) was dissolved in 2 mL of 50 mM Tris buffer by vortex mixing. Two milliliters of pAsp solution, NaCl (0.5M), $NaHPO_4$ (36 mM), and $CaCl_2$ (6.8 mM) solutions (all buffered by 50 mM Tris buffer and adjusted to pH 7.4) were combined in this order, vortexed and filtered through a 0.2 μm syringe filter, and warmed to 37 °C. The resulting solution was 133 mM Na+, 3.5 mM K+, 1.7 mM Ca^{2+}, 123 mM Cl−, 9.1 mM Pi (inorganic phosphate), and 125 μg/mL pAsp at pH 7.4. Grids were floated on 1 mL of mineralizing solution in open 1.5 mL microcentrifuge tubes, at 37 °C and 100% relative humidity. After remineralization, grids were removed after 3−8 h, washed in three changes of ultrapure water, wicked dry, and stored in a grid box.

3.2.3 Electron Microscopy (Performed by Laboratory of Eli Sone, University of Toronto)

Electron microscopy was conducted using a Tecnai 20 TEM (FEI, Hillsboro, OR) with an AMT 1600 side mount camera and LaB6 filament operating at 200 kV. The ultrathin tissue sections were remineralized in supersaturated calcium phosphate solution (50 mM Tris-HCl, 125 mM NaCl, 9 mM $Na2HPO_4$, 1.7 mM $CaCl_2$, pH=7.4 at 37°C) stabilized with 125 µg/mL of polyaspartic acid (MW=14 kDa, Alamanda Polymers). Grids with sections were floated on 1 mL of mineralization solution at 37°C and 100% humidity. After remineralization grids were washed with milliQ water and analyzed with TEM.

3.2.4 Isolation of Human Periodontal Ligament Cells

Human periodontal ligament (hPDL) cells were isolated from samples of healthy periodontal ligament obtained from 4 patients from 15 to 38 years of age who underwent routine extractions at the Oral Surgery Clinic at Schulich Dentistry, Western University. (Patient ID: F15= Female,15 y.o.; F38= Female, 38 y.o.; M24- Male, 24 y.o.; M31= Male, 31 y.o.) The use of this tissue was under informed patient consent and in accordance with the guidelines of the University's Research Ethics Board for Health Sciences Research involving Human Subjects (HSREB 4988; Appendix B). hPDL cells were isolated using an explant technique as described previously by Somerman and colleagues (Somerman et al. 1988). Briefly, tissue was removed from the middle third of the root surface, rinsed several times with Dulbecco's Modified Eagle Medium (DMEM; Gibco, Grand Island, NY, USA) supplemented with 4.5 g/mL D-glucose (high glucose) and cultured for several weeks until outgrown cells reached confluence. Cell cultures were maintained in DMEM supplemented with 10% fetal bovine serum (FBS; Gibco, Grand Island, NY, USA) and 1% AA (Antibiotic-Antimycotic; 100 U/mL penicillin, 100 µg/mL streptomycin, and 0.25 mg/mL amphotericin B; Gibco, Grand Island, NY, USA). Cultures were maintained in a 5% CO_2 atmosphere with 100% relative humidity at 37°C. For passaging and use in experiments, cells were detached using a 0.05% trypsin and 0.2g/L EDTA·4Na solution. hPDL cells were used between passages 1 and 5 for experiments.

3.2.5 Cell Treatment

hPDL cells were seeded in DMEM containing 10% FBS at a density of 200,000-cells per well of a 6-well plate for RNA isolation, and at 50,000-cells per well of a 24-well plate for the Alizarin Red S assay. The plates were previously coated with either 10 μg/ml collagen type I (PureCol, Advanced BioMatrix, Carlsbad, CA) in PBS or 10 μg/ml Collagen + 10 μg/ml periostin (rhPSTN) (3548-F2, R&D Biosystems) in PBS. After cells reached confluency, they were transferred into serum-free DMEM for an additional 16 hours. To induce osteogenic differentiation, cells were cultured in DMEM with 10% FBS, 1% AA, containing 14.58 mM Beta Glycerophosphate (Sigma-Aldrich, St. Louis, MO, USA) and 0.284 mM L-ascorbic acid (Sigma-Aldrich, St. 36 Louis, MO, USA). Control samples were cultured in DMEM with 10% FBS and 1% AA. To investigate the influence of periostin on the mineralization capacity of hPDL, cells were seeded on plates coated with or without 10 μg/ml rhPSTN and in media supplemented with 100 ng/ml rhPSTN, and media was changed every 2-3 days for 2 and 4 weeks.

3.2.6 Alizarin Red S Staining

Calcium deposition was visualized with Alizarin Red S staining and elution. Cells were fixed with 4% paraformaldehyde (PFA) in PBS for 5 minutes, rinsed with PBS 3 times, followed by thorough washing with deionized water and were dried prior to staining. A 1% (w/v) solution of Alizarin Red S (Fisher Scientific, Waltham, MA, USA) was applied to each sample for 30 minutes followed by several rinses with deionized water to remove excess dye. Matrix calcification was quantified by extracting the dye. A solution of 0.5N HCl in 5 % Sodium Dodecyl Sulfate (SDS; Sigma-Aldrich, St. Louis, MO, USA) was applied to dried samples for 10 minutes and absorbance was measured at 415 nm with a Safire microplate reader (Tecan Group Ltd, Maennedorf, Switzerland).

3.2.7 Quantitative Reverse Transcription Polymerase Chain Reaction Analysis (RT-qPCR)

Total RNA was extracted using Trizol® reagent (Ambion, Life Technologies, Carlsbad, CA, USA) and purified using RNeasy mini kits (Qiagen, Valencia, CA). Taqman real-time

PCR was performed using qSCRIPT XLT one-step real-time quantitative PCR ToughMix (Quanta Biosciences, Gaithersburg, MD) per the manufacturer's instructions. All samples were run in triplicate and normalized to endogenous 18S rRNA (Thermo Fisher Scientific). Taqman® (Applied Biosystems, Life Technologies, Carlsbad, CA, USA) primers and probes were used for alkaline phosphatase (ALPL, Hs01029144_m1), and cementum protein 1 (CEMP1, Hs04185363_s1) All samples were run in triplicate and normalized to endogenous 18S rRNA (Thermo Fisher Scientific).

3.2.8 RNA sequencing

RNA quality analysis was performed using electrophoresis (Appendix A-4). Raw reads were trimmed with the TrimGalore wrapper script around the sequence-grooming tool cutadapt version 0.4.1 (Martin, 2011). The trimmed reads were aligned to the GRCh38 human reference genome from ensembl (version 104) using STAR version 2.7.9a (Dobin et al., 2013). The count matrix for each gene was computed using featureCounts from the Rsubread package (Liao et al., 2019). Gene expression values were normalized using the variance-stabilizing transformation (Anders & Huber, 2010) to then conduct principal component analysis. We performed differential gene expression analyses adjusted for patientID and stratified on medium using DESeq2 R/Bioconductor package (Love et al., 2014). We used the independent hypothesis weighting R/Bioconductor package to weight P-values (Ignatiadis et al., 2016) and adjust for multiple testing using the Benjamini-Hochberg procedure (Benjamini & Hochberg, 1995). We selected genes significantly associated with rhPSTN treatment for each medium (FDR < 0.1) and conducted pathway enrichment analyses using the topGO R package (Alexa et al., 2006). The heatmaps depict the z-score of normalized gene expression across samples from each patient. We ordered samples according to the average of gene ranks. We first partition genes into 2 groups around meloids (M1 and M2) using correlation as the distance metric. In a univariate fashion, each M1 gene is used to rank n samples from the lowest to the highest expression. Expression values of each gene are then replaced by (1,...,n) ranks. M2 transcripts are ordered from the highest to lowest expression and ranks are assigned similarly.

3.2.9 Statistical analysis

All data were analyzed using GraphPad Prism software with Student's t test (unpaired, two-tailed) or one-way ANOVA for experiments with one variable or two-way repeated-measures ANOVA with post hoc test for experiments with two variables. All results are depicted as mean ± SD unless indicated otherwise. P values of less than 0.05 were considered to indicate significance.

3.3 Results

3.3.1 Loss of periostin does not affect the re-mineralization of the periodontal ligament *ex vivo*

Ex vivo mineralization using WT and *Postn*$^{-/-}$ KO dental tissues showed that the remineralization potential of the tissues was not affected by the absence or presence of periostin. After 16h of remineralization, dentin and parts of the PDL were remineralized- to different degrees- in both WT and *Postn*$^{-/-}$ samples, suggesting that the presence of periostin in the PDL does not prevent mineralization (Fig, 3.1). *(Data from our collaborator Dr. Eli Sone, University of Toronto)*

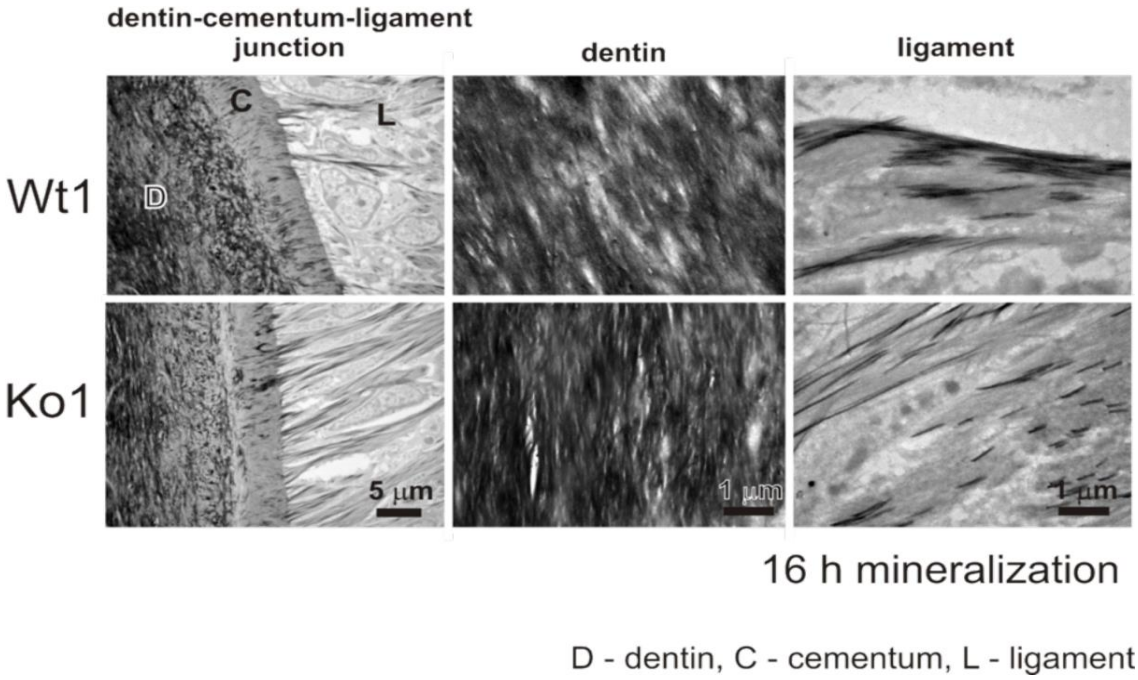

Figure 3-1 *Ex Vivo* Remineralization Assay

After 16h of remineralization, dentin and parts of the PDL were remineralized- to different degrees- in both WT and *Postn*$^{-/-}$*samples,* suggesting that the presence of periostin in the PDL does not prevent mineralization. *(Data from our collaborator Dr. Eli Sone, University of Toronto)*

3.3.2 Periostin promotes the osteogenic mineralization of hPDL cells *in vitro*

Initial assessment of the osteogenic potential of hPDL cells was examined with Alizarin Red S staining to visualize and quantify calcium deposition in response to culture with osteogenic media. In all patients, culturing in control (DMEM without Beta Glycerophosphate and L-ascorbic acid) media did not significantly influence the amount of matrix-bound calcium, while culture in osteogenic media induced deposition of a mineralized matrix, as shown in Figure 3.2. In all patients, calcium content at 4 weeks was significantly higher than the control conditions ($p<0.001$). The exogenous addition of periostin resulted in significantly more calcium content at 4 weeks when compared to osteogenic media alone ($P <0.001$), suggesting that the exogenous addition of periostin promotes the functional mineralization ability of hPDL cells under osteogenic conditions.

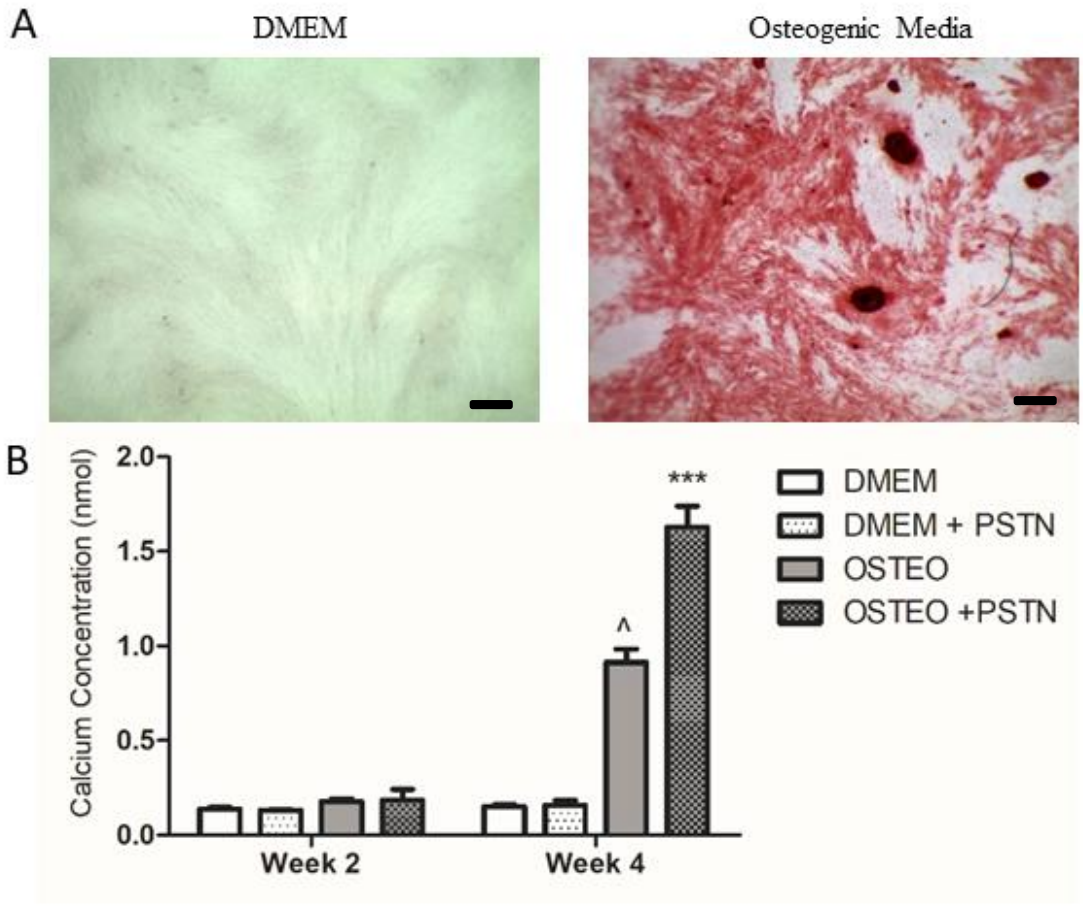

Figure 3-2 Alizarin Red S staining of calcium in hPDL cells during osteogenic differentiation.

Alizarin Red S staining was used to visualize calcium (stained red) deposited by cells at 2 and 4 weeks post-seeding. Dye was subsequently eluted to quantify calcium content. Data presented as mean ± SD of 3 internal replicates, of 3 patients, from 3 independent experiments. Two-way ANOVA with Tukey post-test for multiple comparisons was completed and multiplicity adjusted p-values are reported. (^ $P<0.001$, *** $P<0.001$)

3.3.3 Exploratory analysis of gene expression profiles

To identify transcriptional changes in human PDL cells after exposure to exogenous periostin or/and osteogenic culture conditions, RNA sequencing analysis was performed on hPDL cells isolated from four patients (F15, F38, M24, M31-as mentioned in 3.2.4) cultured in four different experimental conditions: with/without osteogenic media, with/without exogenous periostin. Initial unsupervised (PCA plot) and supervised (differential expression) analysis revealed strong patient-specific effects (Fig. 3.4) (Full table of results in Appendix Table 1).

We therefore conducted similar analyses stratified by patient AND condition which also showed still very strong patient-specific effect. Due to the relative "closeness" of profiles from patients F38 and M31 in Figure 3.4 and due to the similarity in age for these two patients, we reran the analyses restricted to these profiles (Fig. 3.5). One sample in osteogenic medium was an outlier on the PCA plot and was therefore excluded from the downstream analyses:

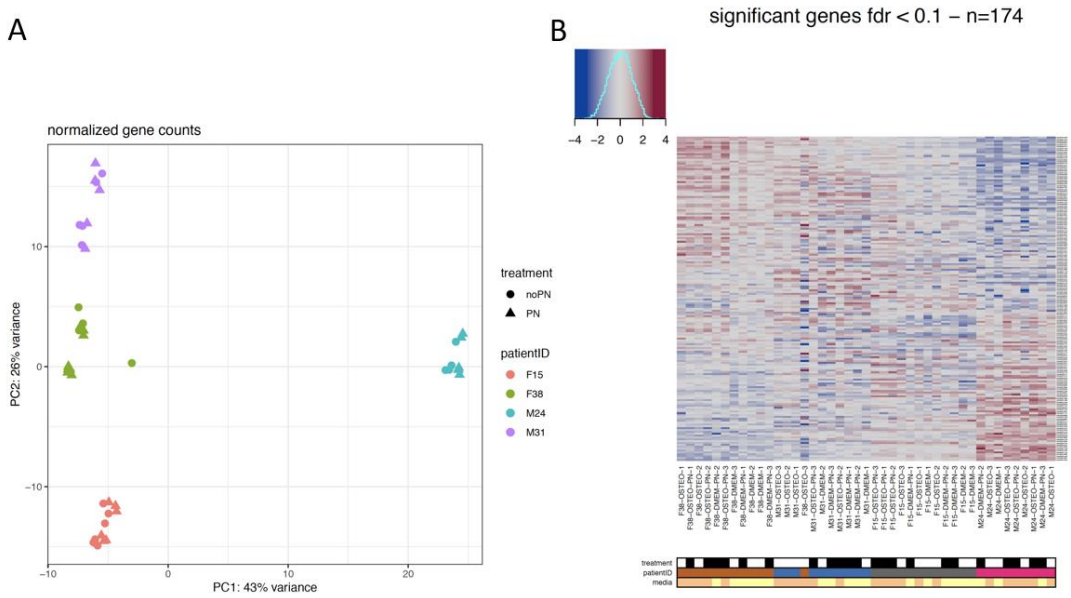
A
normalized gene counts
PC2: 26% variance
PC1: 43% variance
treatment
noPN
PN
patientID
F15
F38
M24
M31
B
significant genes fdr < 0.1 – n=174
treatment
patientID
media

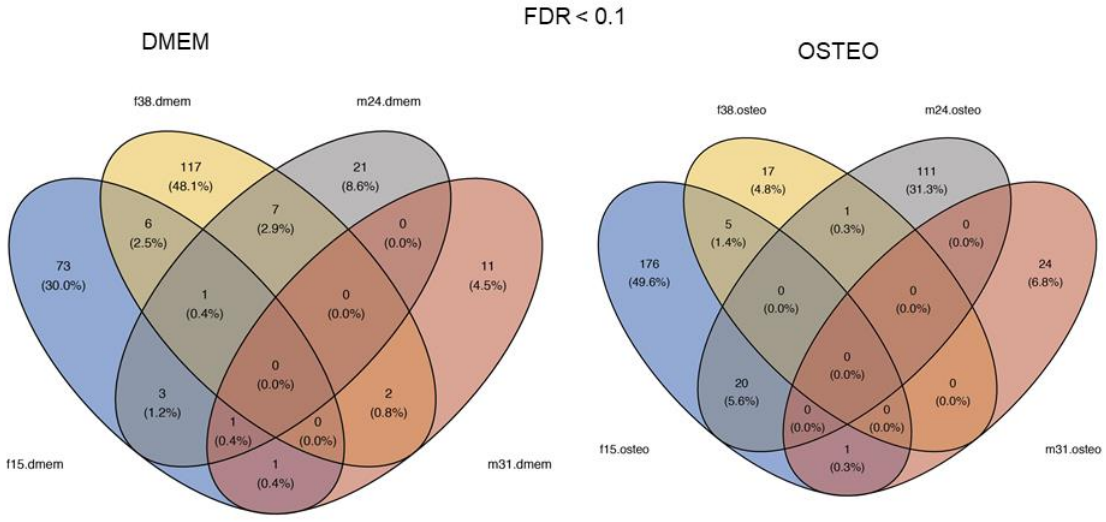
FDR < 0.1
DMEM
f38.dmem
m24.dmem
f15.dmem
m31.dmem
117 (48.1%)
21 (8.6%)
73 (30.0%)
11 (4.5%)
6 (2.5%)
7 (2.9%)
0 (0.0%)
1 (0.4%)
0 (0.0%)
0 (0.0%)
3 (1.2%)
2 (0.8%)
1 (0.4%)
0 (0.0%)
1 (0.4%)
OSTEO
f38.osteo
m24.osteo
f15.osteo
m31.osteo
17 (4.8%)
111 (31.3%)
176 (49.6%)
24 (6.8%)
5 (1.4%)
1 (0.3%)
0 (0.0%)
0 (0.0%)
0 (0.0%)
0 (0.0%)
20 (5.6%)
0 (0.0%)
0 (0.0%)
0 (0.0%)
1 (0.3%)

Figure 3-3 RNA sequencing analysis on hPDL cells in different in vitro conditions

(A) Principal component analysis on PCA plot Genes associated with periostin treatment, adjusted for patientID, **(B)** Heatmap Genes associated with rhPSTN treatment adjusted for patientID and media **(C)** Venn diagram (Full table of results in Appendix table 1 and 2)

Unsupervised analysis show a relatively good separation of the samples according to rhPSTN treatment in each medium (Fig 3.5 A,B). After adjustment on patientID, we identified 125 and 93 genes altered upon addition of exogenous periostin in hPDL cells in unsupplemented media and in osteogenic conditions, respectively (FDR < 0.1, Fig. 3.5 C-F). We observe very little overlap between the genes differentially expressed by periostin in osteogenic and unsupplemented medium (Fig. 3.4 C). This result indicates that the effect of periostin on hPDL cells is strongly dependent on the culture medium. Figure 3.5 C, F depicts the expression of the medium-specific periostin-altered genes in hPDL cells from F38 and M31 patients, respectively.

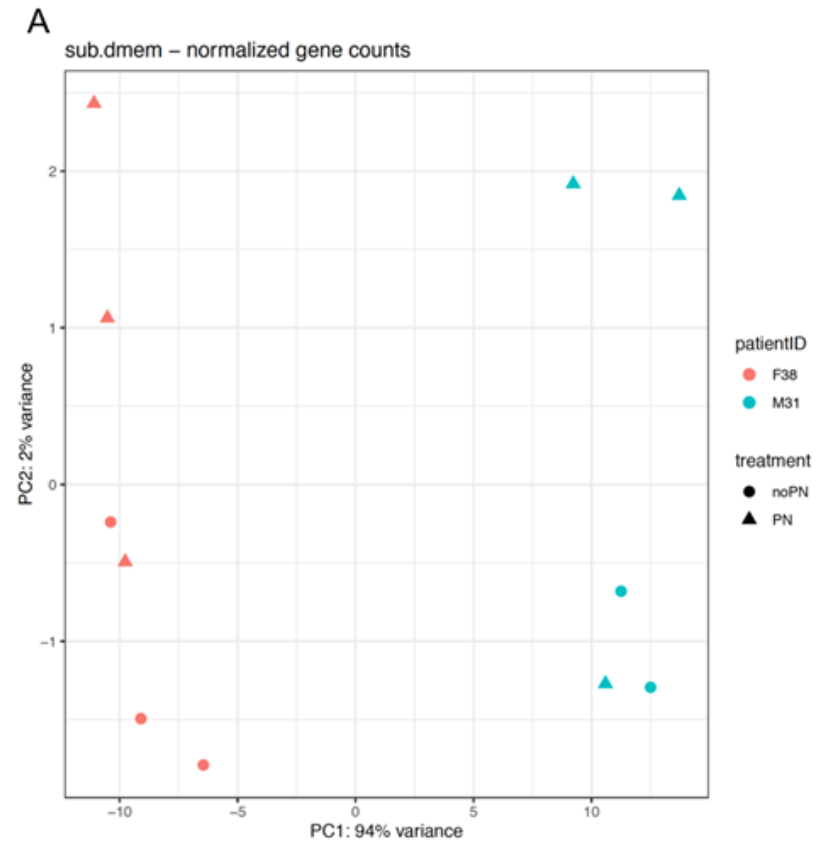
A
sub.dmem – normalized gene counts
PC2: 2% variance
PC1: 94% variance
patientID
F38
M31
treatment
noPN
PN

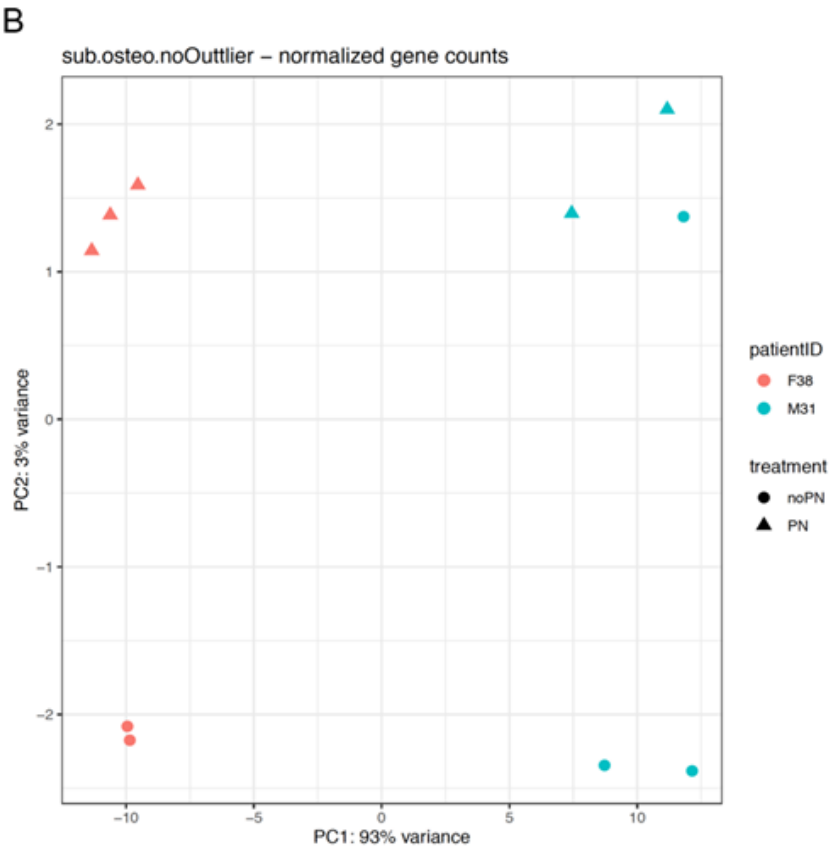
B
sub.osteo.noOuttlier – normalized gene counts
PC2: 3% variance
PC1: 93% variance
patientID
F38
M31
treatment
noPN
PN

C

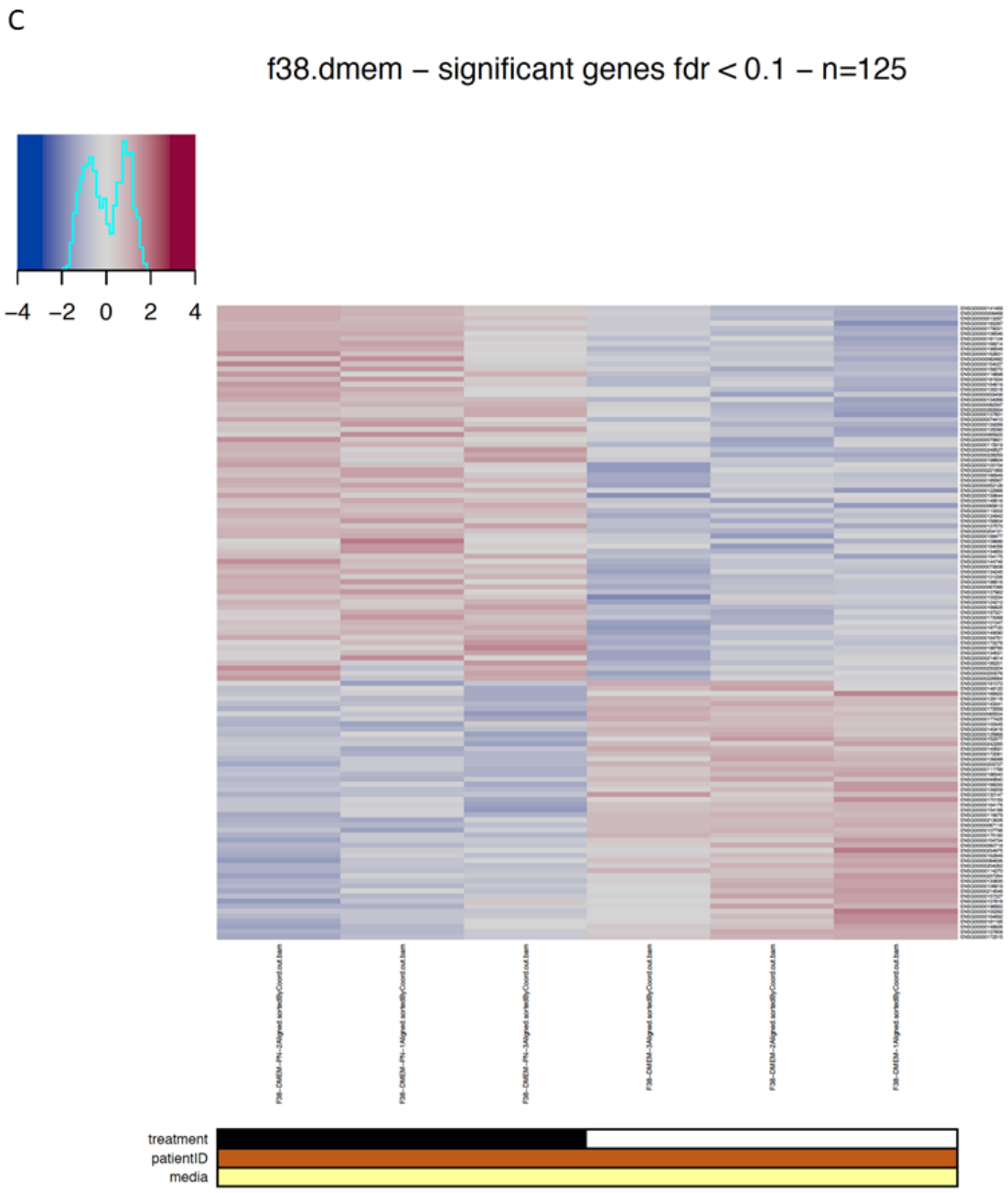
f38.dmem – significant genes fdr < 0.1 – n=125
−4 −2 0 2 4
treatment
patientID
media

D

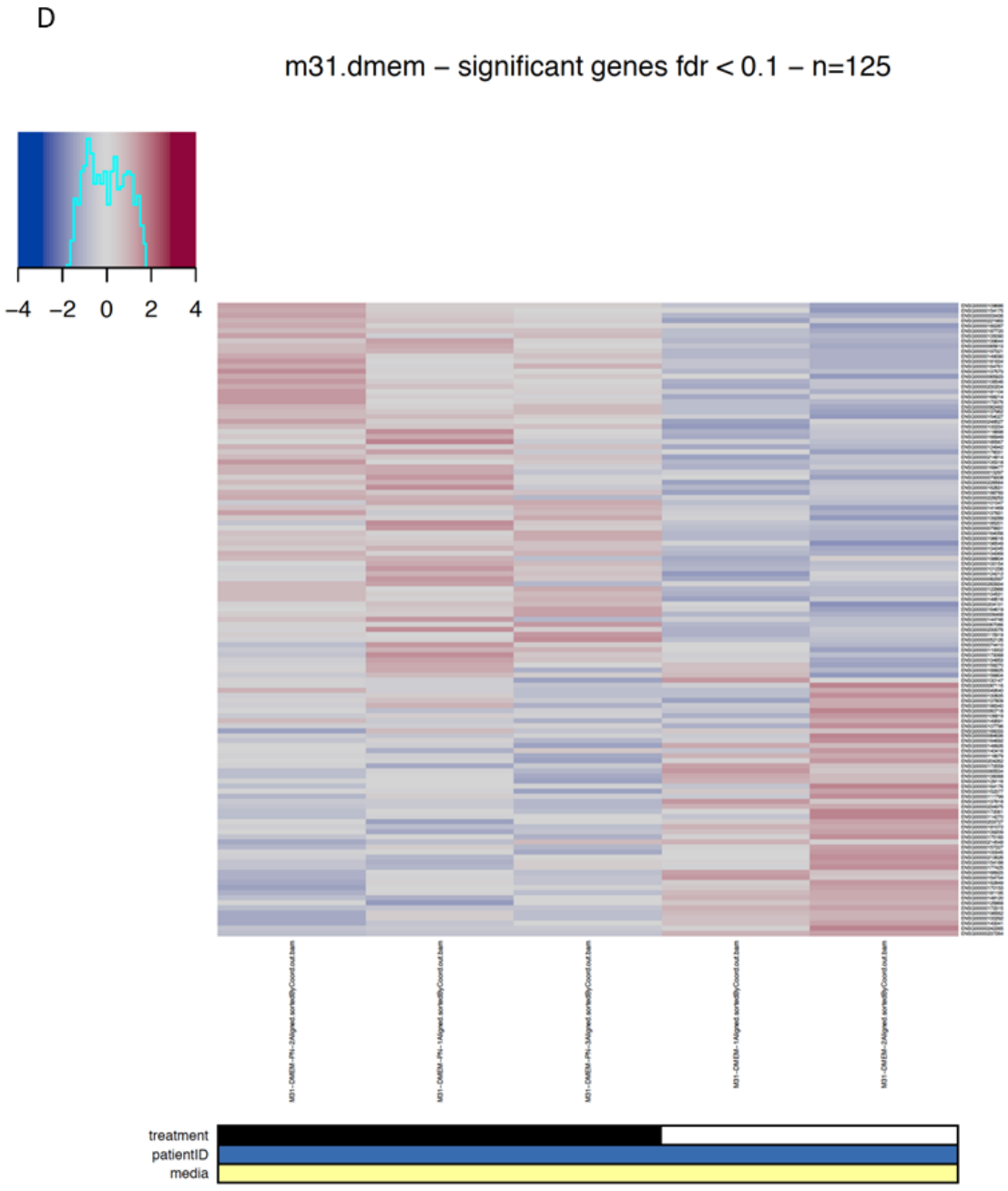
m31.dmem – significant genes fdr < 0.1 – n=125
−4 −2 0 2 4
treatment
patientID
media

E

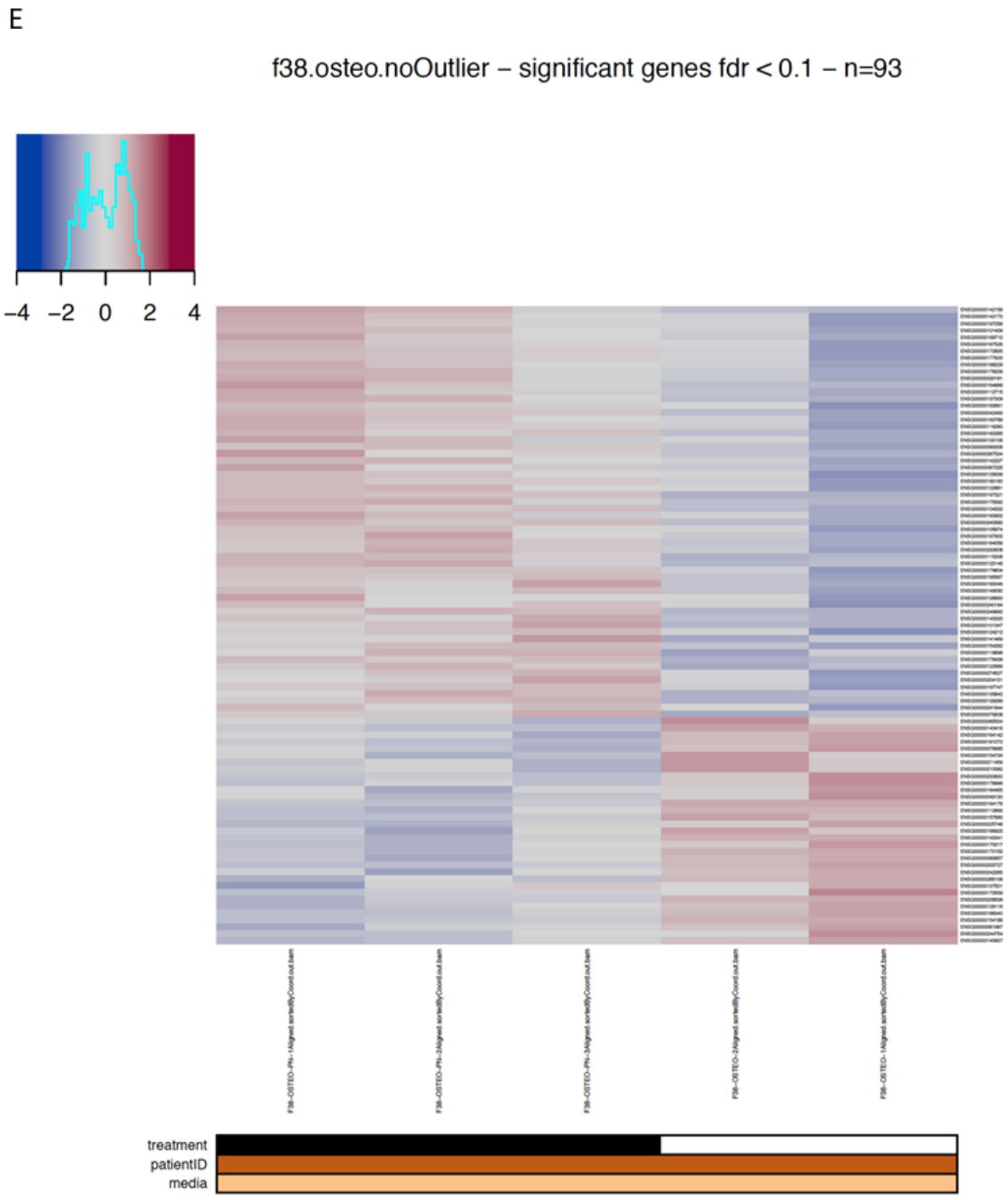
f38.osteo.noOutlier – significant genes fdr < 0.1 – n=93
−4 −2 0 2 4
treatment
patientID
media

F

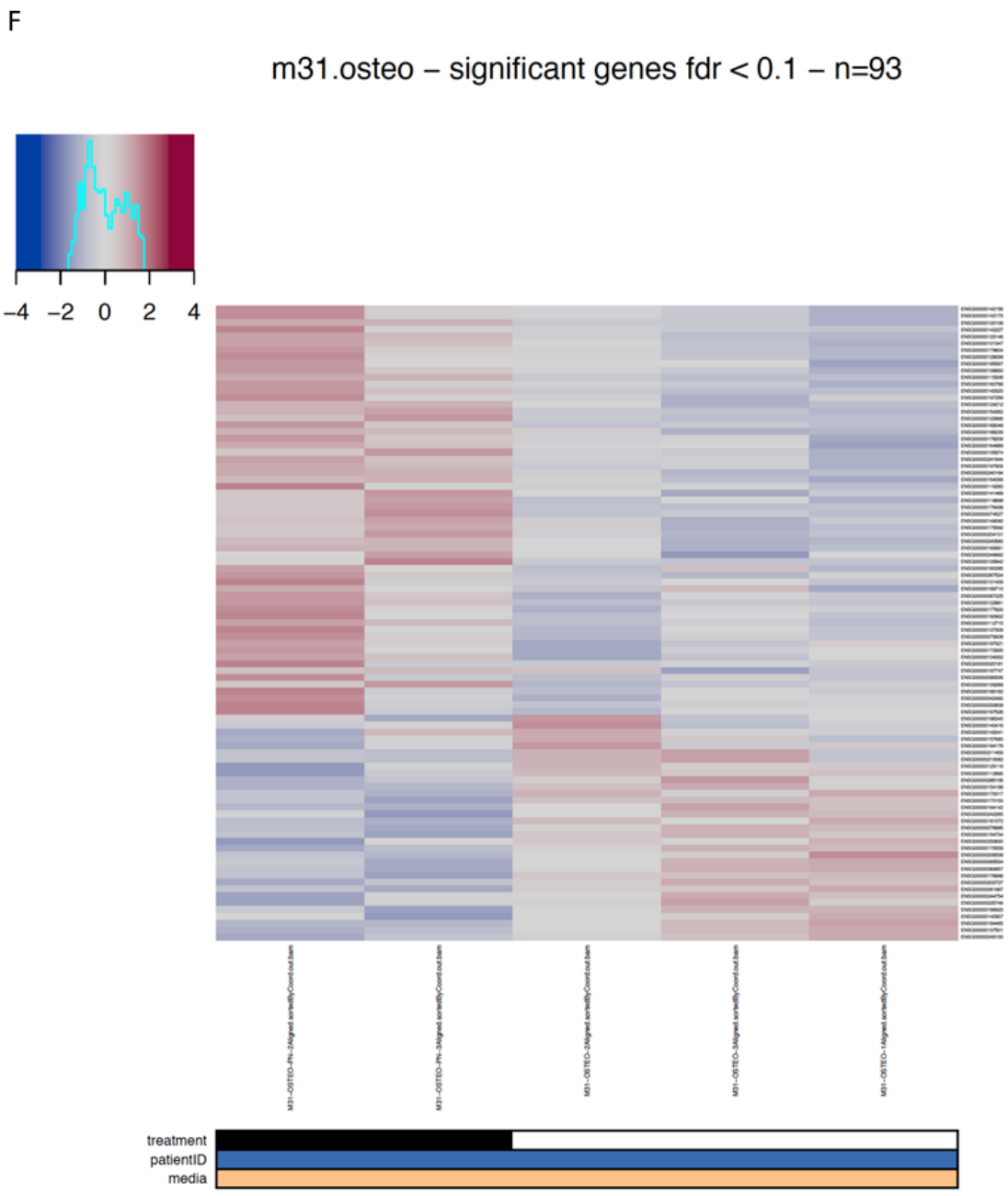
m31.osteo – significant genes fdr < 0.1 – n=93
−4 −2 0 2 4
treatment
patientID
media

Figure 3-4 Gene expression analysis on a selective subset of patients (F38, M31)

(A,B): PCA plots **(C,D)** Heat maps of Genes associated with rhPSTN treatment in DMEM (F38 & M31) **(E, F) :** Heat maps of Genes associated with rhPSTN treatment in Osteogenic media (F38 & M31). (Full table of results in Appendix tables 1 and 2).

To gain mechanistic insight into gene lists generated from our experimental conditions, pathway enrichment analysis of differentially expressed genes was used to identify biological pathways that are enriched in the gene lists more than would be expected by chance. In cells cultured in DMEM, results from the pathway enrichment analysis revealed that differentially expressed genes (DEG) by the exogenous addition of periostin were mainly enriched in “collagen fibril organization, “extracellular matrix organization”, “endodermal cells differentiation” and “actin filament severing” (Fig. 3.6 A). In hPDL cells cultured in osteogenic conditions, pathway enrichment analysis of DEG by the exogenous addition of periostin revealed involvement of “peptidyl-tyrosine autophosphorylation”, “regulation of bone remodeling”, regulation of receptor internalization”, regulation of focal adhesion assembly”, regulation of osteoblast differentiation” (Fig. 3.6 B).

A

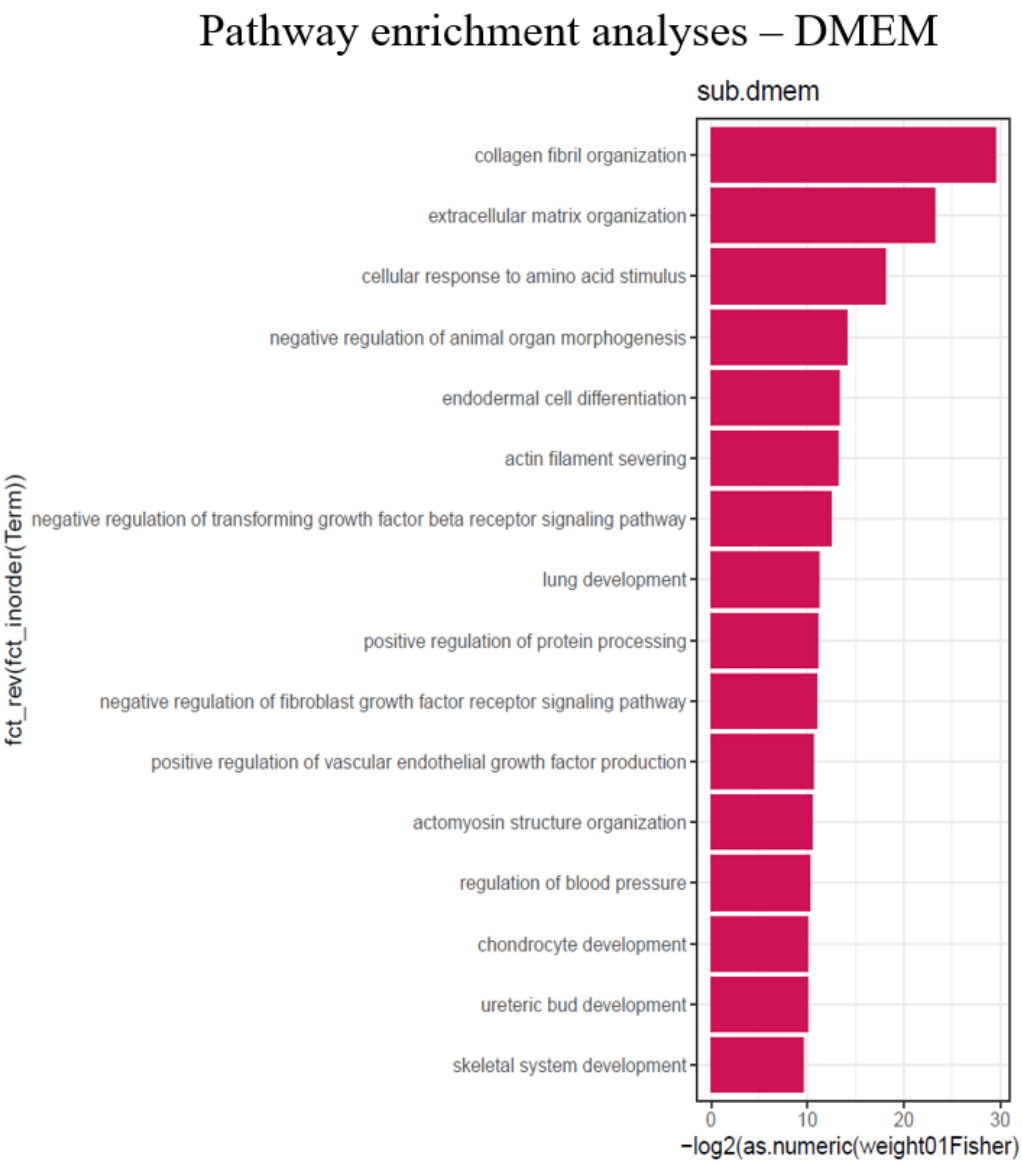
Pathway enrichment analyses – DMEM
sub.dmem
collagen fibril organization
extracellular matrix organization
cellular response to amino acid stimulus
negative regulation of animal organ morphogenesis
endodermal cell differentiation
actin filament severing
negative regulation of transforming growth factor beta receptor signaling pathway
lung development
positive regulation of protein processing
negative regulation of fibroblast growth factor receptor signaling pathway
positive regulation of vascular endothelial growth factor production
actomyosin structure organization
regulation of blood pressure
chondrocyte development
ureteric bud development
skeletal system development
fct_rev(fct_inorder(Term))
0
10
20
30
−log2(as.numeric(weight01Fisher)

B

Pathway enrichment analyses - Osteogenic condition

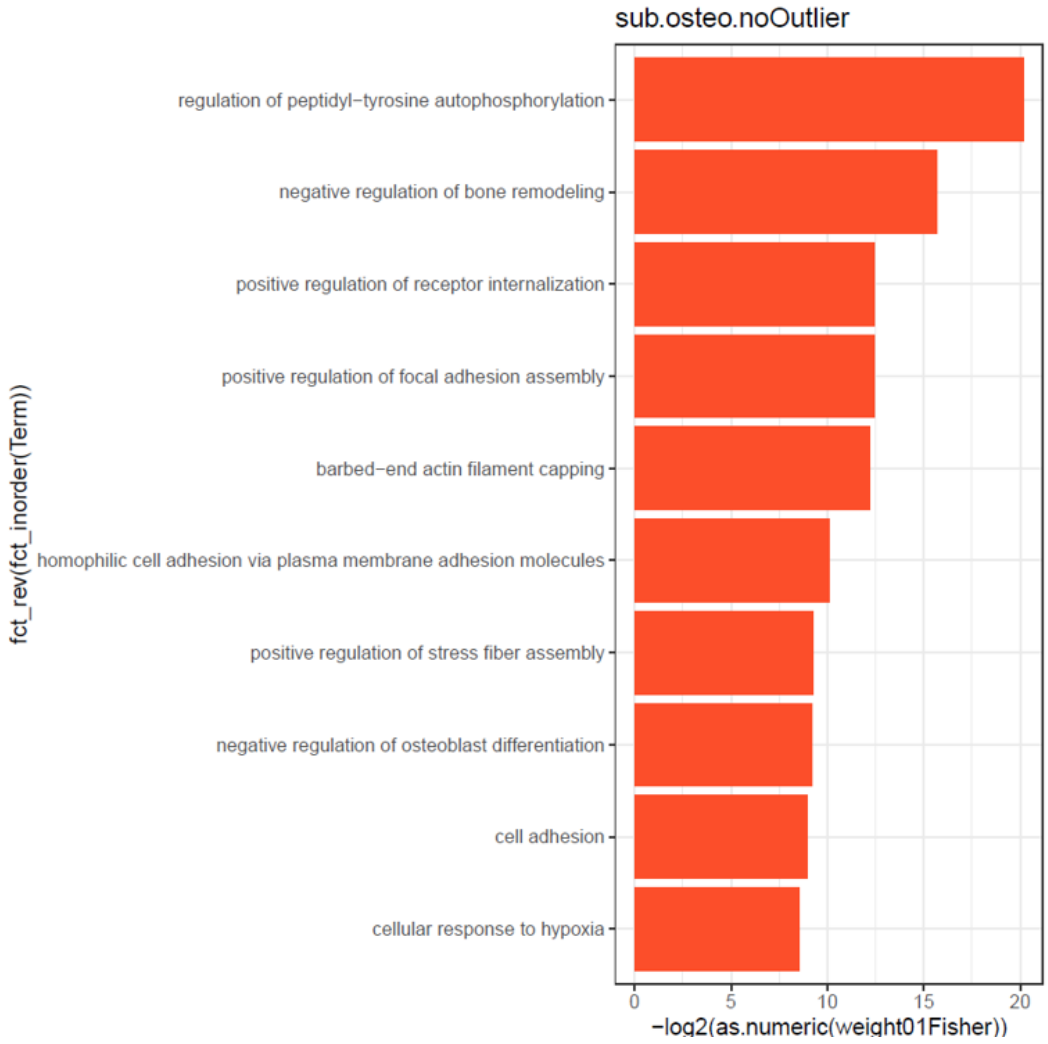

Figure 3-5 Pathway Enrichment Analysis

(A) Pathway enrichment analyses of differentially expressed genes (DEG) by exogenous periostin treatment in DMEM (DEG_{DMEM}=125) Top significant pathways from gene ontology analysis. For the barplot, the top40 enrichment was selected where the gene list had at least 5 genes annotated to a term and the enrichment had a weight01 fisher p-value < 0.01. Top100 GO enrichment results can be found in Appendix Table 1 **(B)** Pathway enrichment analyses of differentially expressed genes by exogenous periostin treatment in osteogenic conditions (DEG_{OSTEO} = 93). Top100 GO enrichment results can be found in Appendix Table 2

3.3.4 Patient's age effect on hPDL transcriptional profile

Increased age is an important factor that appears to adversely affect biological properties, including differentiation capacity, of hPDL cells (Li et al., 2020; R.-X. Wu et al., 2015; Zhang et al., 2012). In our study, we selectively analyzed the dataset from the youngest donor (F15) separately (Fig. 3.7 A-D). Pathway enrichment analysis of DEG in DMEM (Fig. 3.7 E) or OSTEO (Fig. 3.7 F) conditions by the addition of periostin revealed enrichment in different pathways than the dataset from older patients: In DMEM, DEG from the addition of periostin (DEG_{DMEM}=85) appeared enriched in "regulation of telomerase activity"," regulation of smooth muscle cells, "osteoblast differentiation" and "aging". In osteogenic conditions, DEG by the addition of exogenous periostin (DEG_{OSTEO}=202) were enriched in "nuclear-transcribed mRNA catabolic", "nonsense-mediated decay", "viral transcription", regulation of RNA splicing", regulation of telomerase activity", and "oncostatin-M-mediated signaling pathway".

A

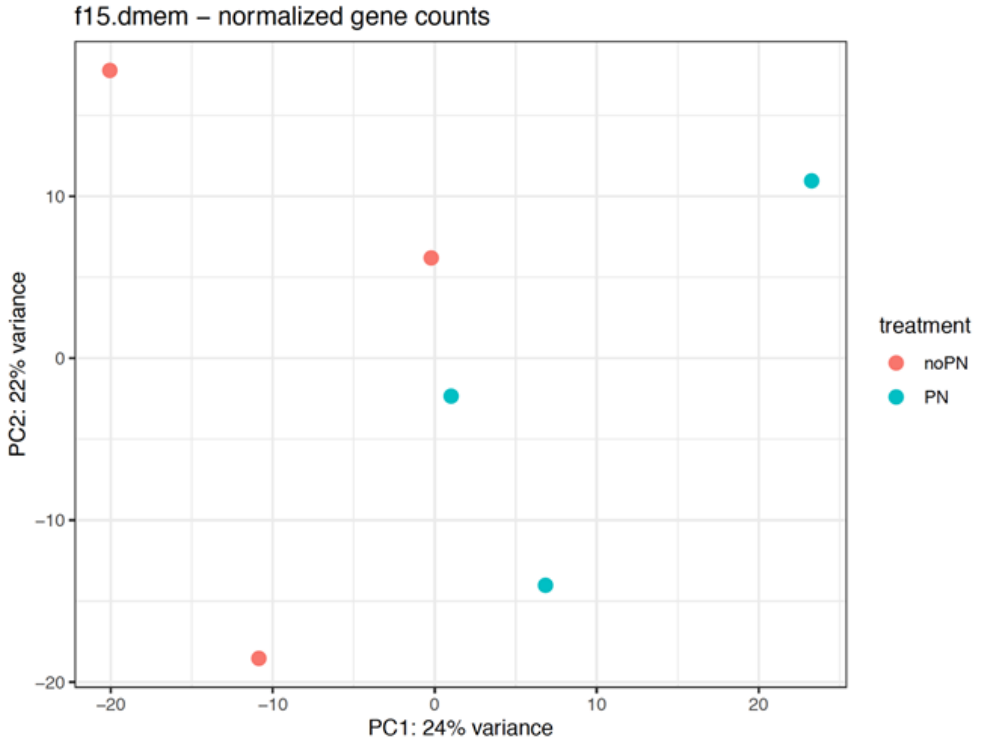
f15.dmem – normalized gene counts
PC2: 22% variance
PC1: 24% variance
10
0
−10
−20
−20
−10
0
10
20
treatment
noPN
PN

B

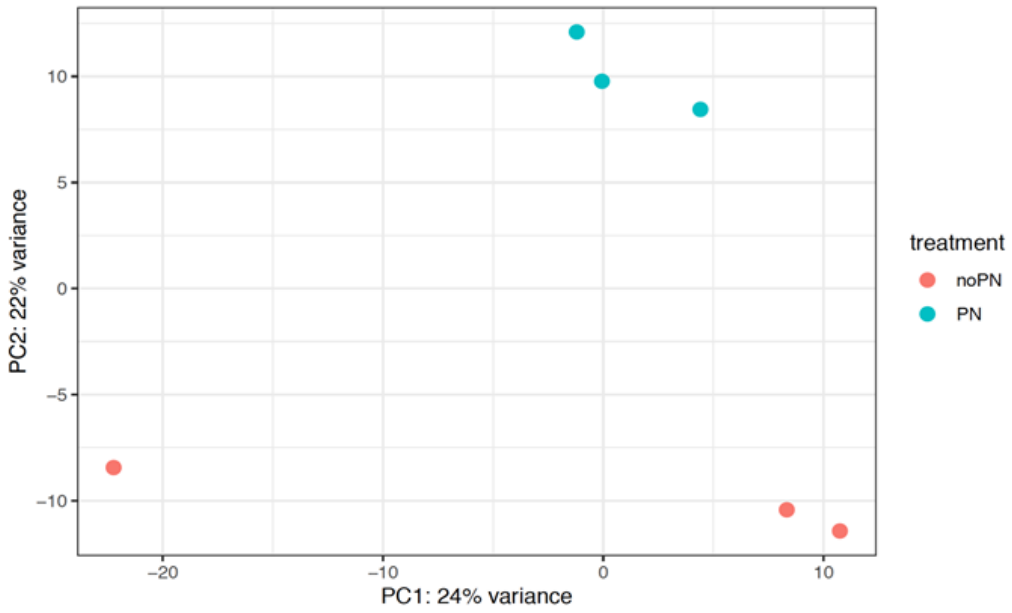
PC2: 22% variance
PC1: 24% variance
10
5
0
−5
−10
−20
−10
0
10
treatment
noPN
PN

C

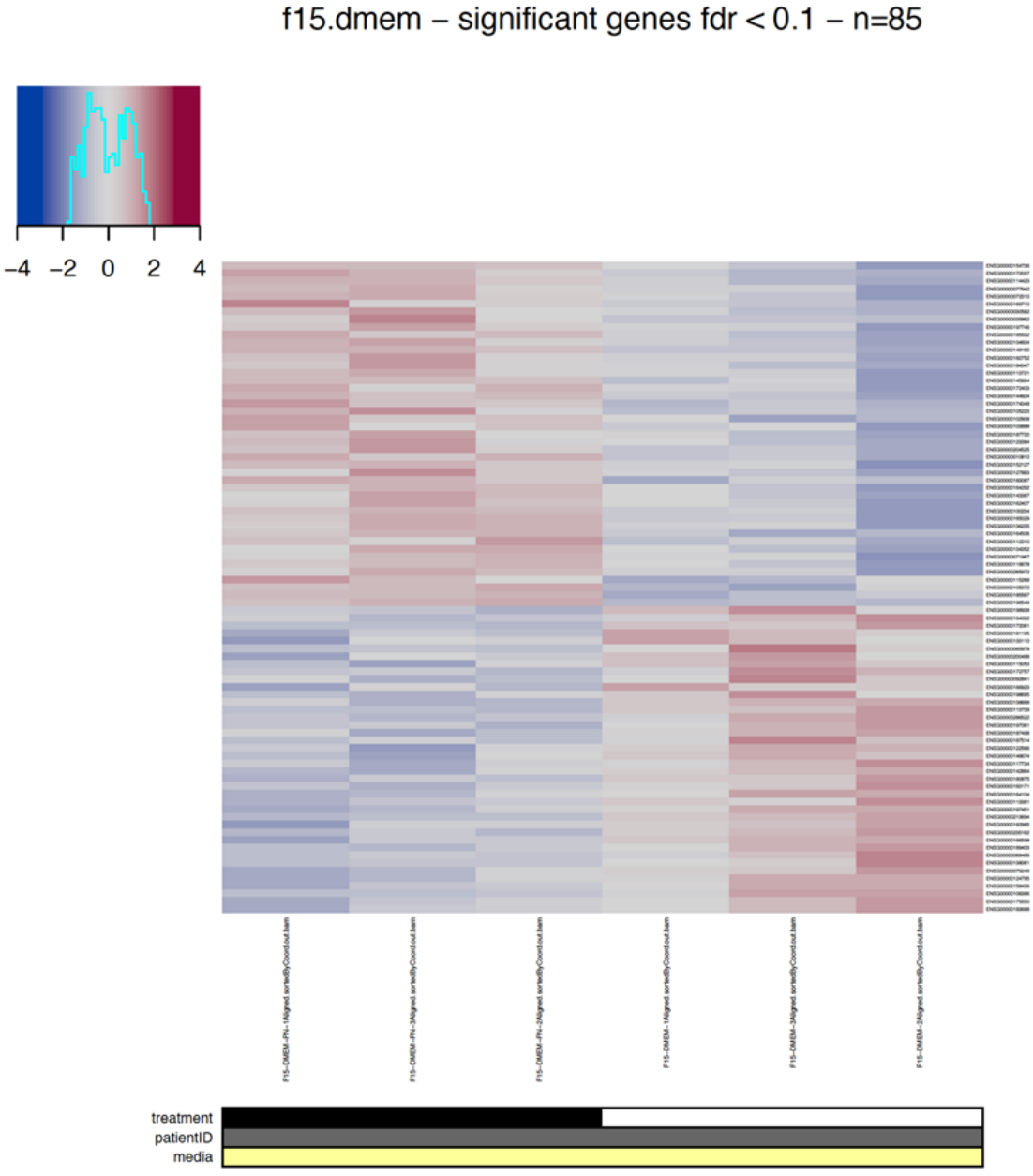
f15.dmem – significant genes fdr < 0.1 – n=85
−4 −2 0 2 4
F15-DMEM-Ph-1Aligned.sortedByCoord.out.bam
F15-DMEM-Ph-3Aligned.sortedByCoord.out.bam
F15-DMEM-Ph-2Aligned.sortedByCoord.out.bam
F15-DMEM-1Aligned.sortedByCoord.out.bam
F15-DMEM-3Aligned.sortedByCoord.out.bam
F15-DMEM-2Aligned.sortedByCoord.out.bam
treatment
patientID
media

D

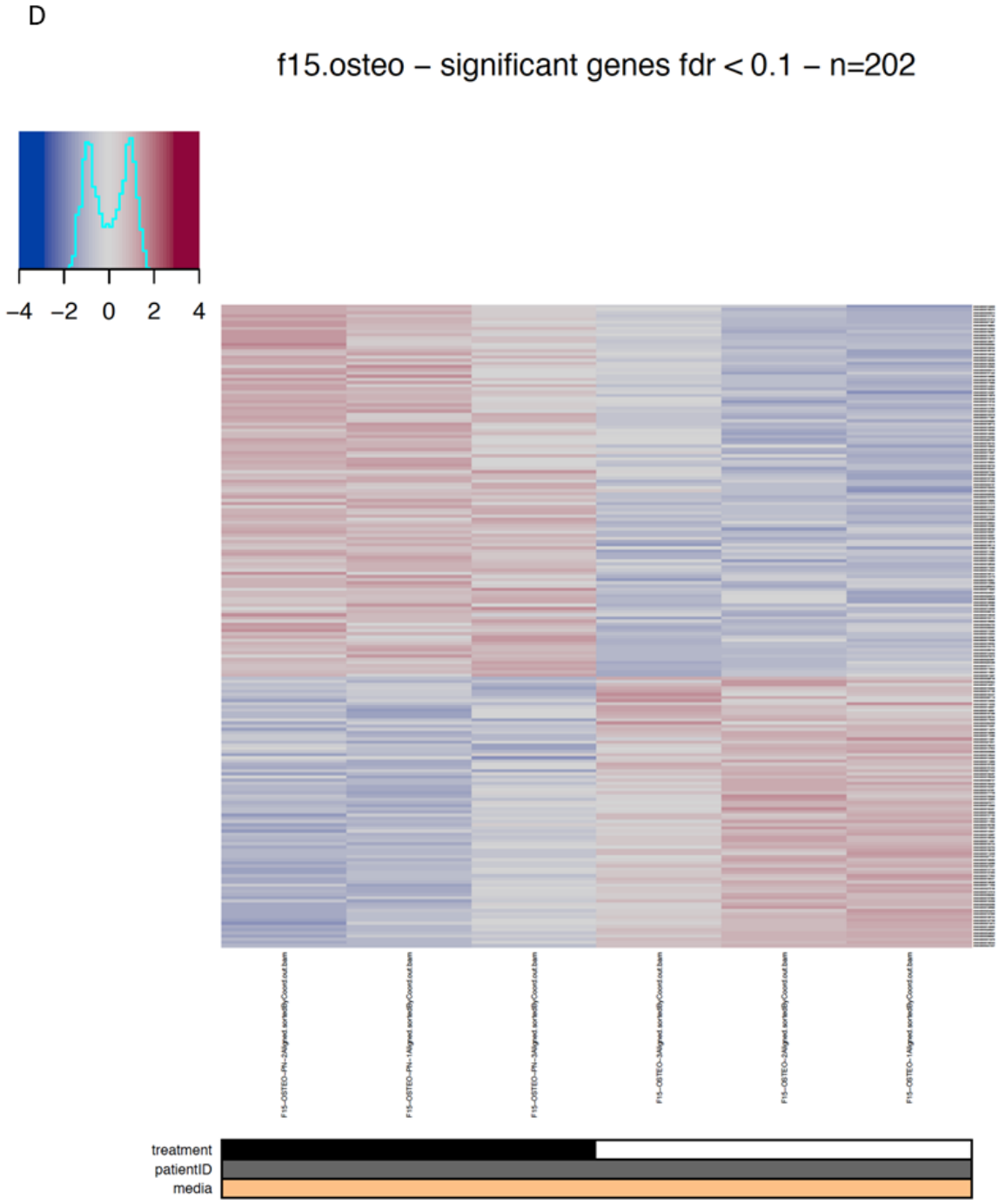
f15.osteo – significant genes fdr < 0.1 – n=202
−4 −2 0 2 4
F15−OSTEO−FN−3Aligned.sortedByCoord.out.bam
F15−OSTEO−FN−1Aligned.sortedByCoord.out.bam
F15−OSTEO−FN−2Aligned.sortedByCoord.out.bam
F15−OSTEO−3Aligned.sortedByCoord.out.bam
F15−OSTEO−2Aligned.sortedByCoord.out.bam
F15−OSTEO−1Aligned.sortedByCoord.out.bam
treatment
patientID
media

E

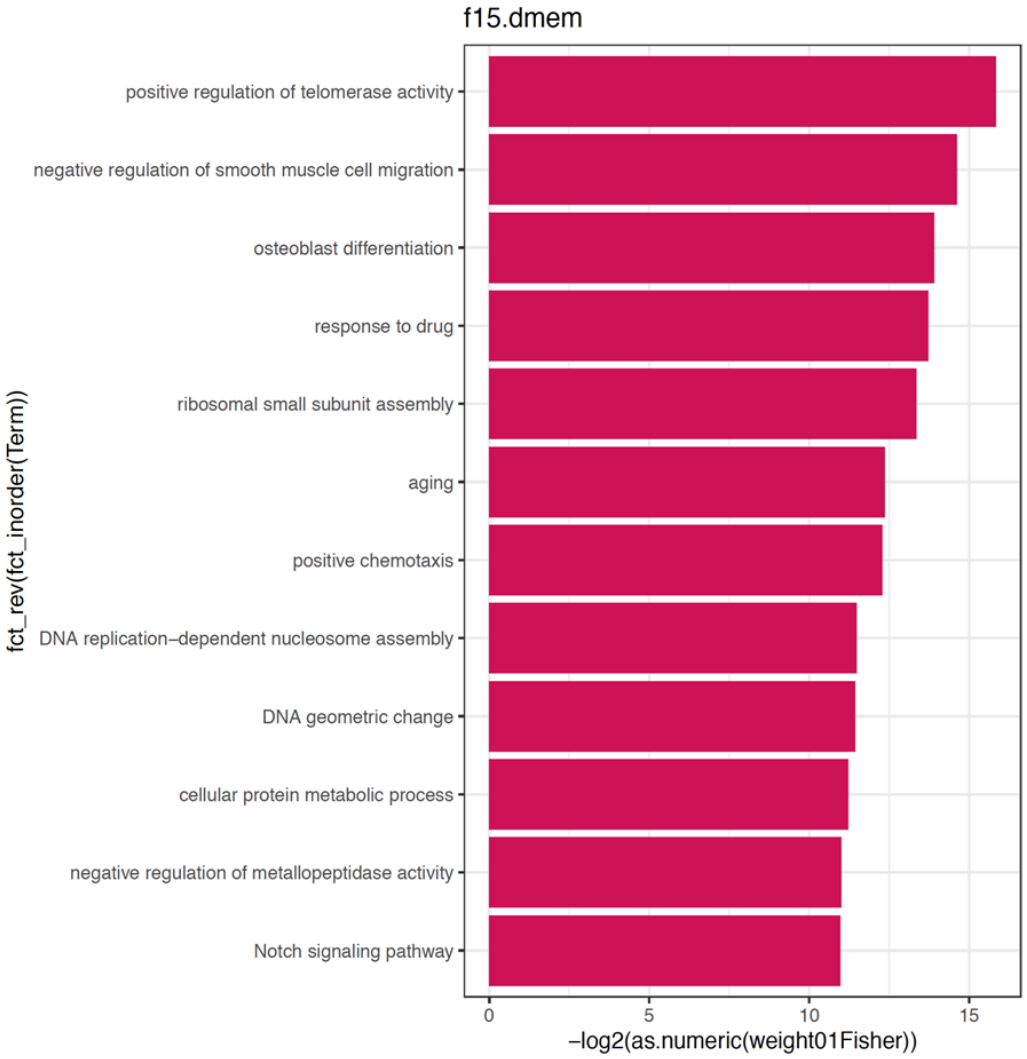
f15.dmem
positive regulation of telomerase activity
negative regulation of smooth muscle cell migration
osteoblast differentiation
response to drug
ribosomal small subunit assembly
aging
positive chemotaxis
DNA replication−dependent nucleosome assembly
DNA geometric change
cellular protein metabolic process
negative regulation of metallopeptidase activity
Notch signaling pathway
fct_rev(fct_inorder(Term))
0
5
10
15
−log2(as.numeric(weight01Fisher))

F

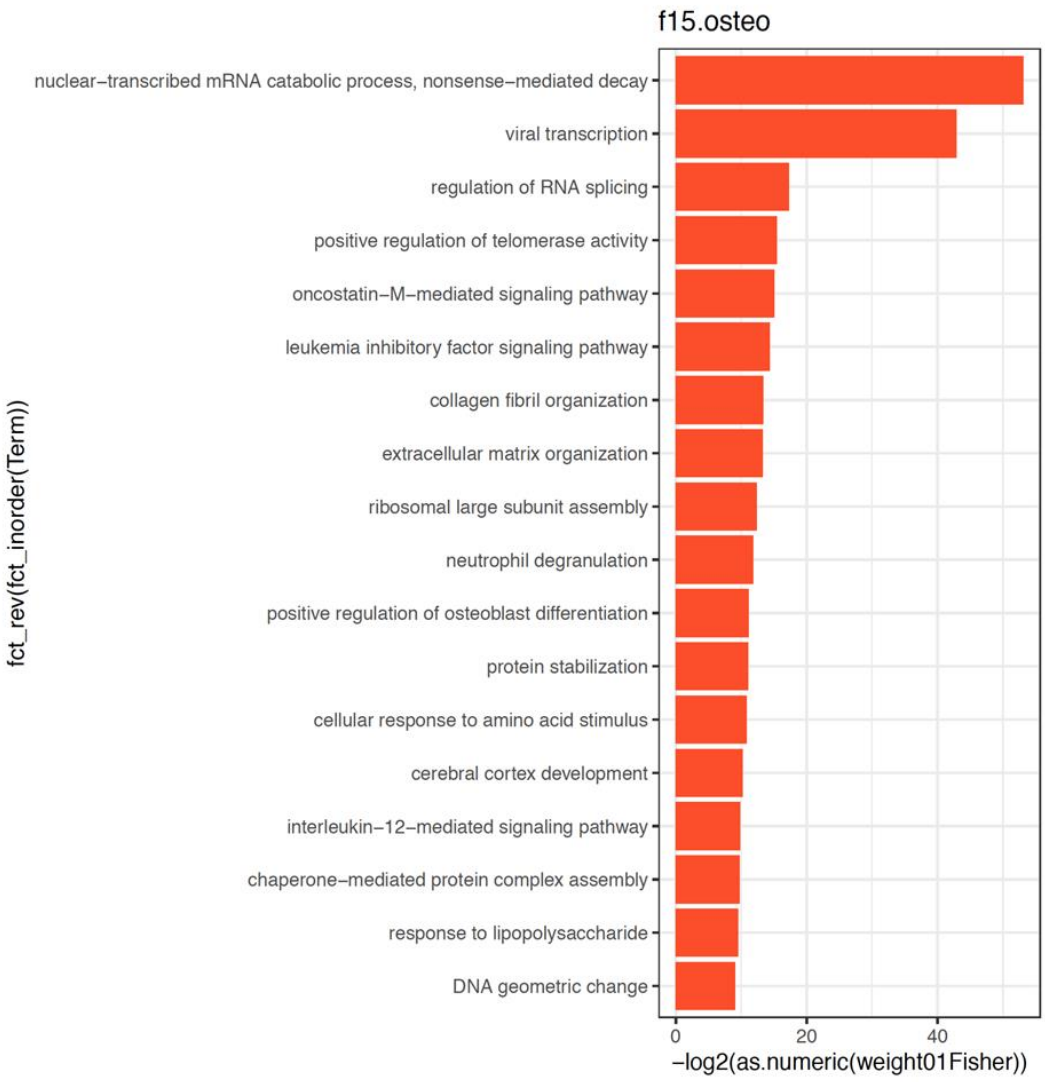
f15.osteo
nuclear−transcribed mRNA catabolic process, nonsense−mediated decay
viral transcription
regulation of RNA splicing
positive regulation of telomerase activity
oncostatin−M−mediated signaling pathway
leukemia inhibitory factor signaling pathway
collagen fibril organization
extracellular matrix organization
ribosomal large subunit assembly
neutrophil degranulation
positive regulation of osteoblast differentiation
protein stabilization
cellular response to amino acid stimulus
cerebral cortex development
interleukin−12−mediated signaling pathway
chaperone−mediated protein complex assembly
response to lipopolysaccharide
DNA geometric change
fct_rev(fct_inorder(Term))
0
20
40
−log2(as.numeric(weight01Fisher))

Figure 3-6 Gene expression analysis on young patient (F15)

(A, B) PCA plots. **(C)** Heat map of Genes associated with rhPSTN treatment in DMEM. **(D)** Heat map of Genes associated with rhPSTN treatment in Osteogenic media. (Full table of results in Appendix Table 3). **(E)** Pathway enrichment analyses of differentially expressed genes in patient F15 (DEG) by exogenous periostin treatment in DMEM (DEG_{DMEM}=85). **(F)** Pathway enrichment analyses of differentially expressed genes in F15 by exogenous periostin treatment in OSTEO (DEG_{OSTEO}=202. Top significant pathways from gene ontology analysis. For the barplot, the top40 enrichment was selected where the gene list had at least 5 genes annotated to a term and the enrichment had a weight01 fisher p-value < 0.01. Top100 GO enrichment results can be found in Appendix Table 4

3.4 Discussion

Previous studies have highlighted the role of periostin on the adhesion, survival migration, proliferation, and differentiation of human periodontal ligament mesenchymal stem cells *in vitro* (Matsuzawa et al., 2015; Z. Wu et al., 2018). Interestingly, periostin has been shown to promote osteogenic differentiation of human periodontal ligament mesenchymal stem cells under inflammatory conditions (Tang et al., 2017). In this chapter we explored the potential role of periostin in the maintenance and mineralization of the periodontal ligament cells *in vitro* via functional and gene-expression analyses.

Using an *ex-vivo* tissue-based model of collagen remineralization, we assessed whether periodontal tissues from WT and *Postn*$^{-/-}$ animals have the capacity to remineralize. It has been shown that this *ex vivo* model can reproduce the finely controlled biomineralization evident in the periodontium, in fixed sections of mouse mandible, with similar fidelity (Lausch et al., 2013). This assay results in the preferential mineralization of bone, dentin, and acellular extrinsic fiber cementum, leaving the ligament relatively unmineralized. This selective mineralization shows that extracellular matrix factors are capable of controlling the rate of mineralization in tissue void of cellular and enzymatic activity (Lausch et al., 2013; Lausch & Sone, 2015; Nudelman et al., 2013). Utilizations of this *ex vivo* model allows the investigation of the particular matrix factors responsible for the biological control of mineral deposition. Here, using this *ex vivo* mineralization model in collaboration with Dr Eli Sone at The University of Toronto we showed the fixed, demineralized extracellular matrix (ECM) of mouse dental and periodontal tissues retains sufficient molecular memory to direct selective remineralization from metastable calcium and phosphate-containing solutions. The natively mineralized tissues (dentin, cementum and bone) remineralize preferentially over the periodontal ligament, with high level of spatial control, similar to what is observed *in vivo*. In mandibles dissected from *Postn*$^{-/-}$ mice, we observed similar levels of re-mineralization within the natively mineralized tissues and the collagen fibers of the PDL when compared to the WT animals, suggesting that the presence or absence of matrix-bound periostin does not influence mineralization in the periodontal tissues.

We next investigated whether the exogenous addition of periostin affect the human PDL cell mineralization in vitro. It is well established that PDL cells will mineralize when cultured in osteogenic media, although evidence suggests that this decreases with increasing age (Li et al., 2020; Morissette Martin et al., 2017). Alizarin Red S staining for calcium confirmed that isolated hPDL cells readily produced a mineralized matrix in response to osteogenic culture conditions. The addition of exogenous periostin resulted in significantly more calcium when compared to osteogenic media alone, suggesting that extracellular periostin enhances hPDL osteogenic gene expression and mineralization osteogenic conditions, which is in agreement with previous reports (Z. Wu et al., 2018). Wu et al. demonstrated that 2 weeks after osteogenic induction, mineralization was markedly enhanced in hPDL cells treated with 100 ng/mL rhPSTN compared with the untreated group, as determined by Alizarin Red staining and quantitative calcium measurements. Further, using RTqPCR and Western blotting they showed that exogenous addition of 100 ng/ml rhPSTN in hPDL cells from young individuals (aged 16–20) results in increased the expression of osteogenic gene (OCN, OPN, OSX, RUNX2) levels compared with untreated hPDLSCs. When PSTN was silenced, mineralization was significantly inhibited in the POSTN-knockdown hPDL cells compared with the control group (Z. Wu et al., 2018).

Based on our results we confirmed that exogenous periostin increases mineralization of PDL cell cultures *in vitro*, we next investigated transcriptional changes in human PDL cells after exposure to exogenous periostin and/or osteogenic culture conditions using RNA sequencing analysis. My goal in these experiments was two fold; how does periostin influence PDL fibroblast phenotype and how does the addition of osteogenic media alter this response at the transcriptional level? Recently, a number of studies have utilized RNA sequencing to investigate gene expression changes in PDL cells following mechanical stimulus (Kim et al., 2020), or following occlusion establishment (Denes et al., 2019, 2020), as well as differences in gene expression profiles between highly osteoblastic/cementoblastic and fibroblastic periodontal ligament cell clones (Saito et al., 2020), and PDL stem cells and dental pulp stem cells (Lee et al., 2022). In this study, cells lines from 4 different patients were used, and initial analysis regardless of stratifiction

strategy showed a very strong patient-specific effect. Due to high variability between patient responses to treatment condition and minimal overlap of common genes differentially expressed among the 4 patients, we proceeded to analyse and compile the data from only 2 patients (F28 and M31) that appeared to have similar expression profile trends.

Using this strategy, results from the pathway enrichment analysis in cells cultured in DMEM revealed that differentially expressed genes (DEG) by the exogenous addition of periostin were mainly enriched in “collagen fibril organization, “extracellular matrix organization”, “endodermal cells differentiation” and “actin filament severing” (Fig. 3.5 A). This observation could suggest that in non-osteogenic conditions periostin contributes to ECM remodelling and maintenace of the PDL structure. Our results are consistent with the reported functions of periostin in the literature that it can be involved in ECM assembly and cross-linking, influencing mechanical properties of the tissues in which it is expressed. Specifically, it is known that periostin can act as a scaffold for assembly of extracellular matrix proteins (type I collagen, fibronectin, tenascin-C, and laminin γ2) and accessory proteins (BMP-1 and CCN3), (Elliott & Hamilton, 2011; Kii & Ito, 2017a, p. 201; Maruhashi et al., 2010), although the binding site for collagens has not been identified (Kii & Ito, 2017b; Norris et al., 2007).

Periostin induced transcriptional changes in PDL cells including genes associated with fibrillar collagen expression (COL11A1, COL5A2, COL1A2, and COL5A1) (Bella & Hulmes, 2017) and ADAM Metallopeptidase with Thrombospondin Type 1 Motif 2 (ADAMTS2) - an enzyme that processes several types of procollagen molecules- genes that were differentially expressed when periostin was added exogenously to the cells. The latter reduces the solubility of the collagen molecules and induces their almost spontaneous assembly into elongated and cylindrical collagen fibrils (Bekhouche & Colige, 2015), further highlighting periostin’s likely role is collagen fibril organization. Periostin addition also resulted in changed of TNXB gene expression levels coding for Tenascin-X, which is a large extracellular matrix protein that its deficiency in humans is associated with Ehlers–Danlos syndrome (Schalkwijk et al., 2001), a generalized connective tissue disorder

resulting from altered metabolism of the fibrillar collagens (Mao et al., 2002). These genes are known to influence collagen fibril and extracellular matrix organization, and is consistent with previous studies describing a role for periostin in collagen crosslinking and stabilization of the ECM (Kudo, 2011; Maruhashi et al., 2010; Norris et al., 2007).

The multi-domain structure of periostin allows proteins with which it binds to assemble into a large interacting complex. Extracellularly, fibronectin directly binds to the EMI domain of periostin (Kii et al., 2009; Norris et al., 2007), and tenascin-C binds to the fas 1 domain (Kii et al., 2009). For collagen cross-linking in fibrillogenesis, the interaction of periostin with fibronectin and tenascin-C is dependent on the association of periostin with BMP-1 followed by activation of lysyl oxidase (LOX) for the formation of covalent cross-links in collagen and elastic fibers (Maruhashi et al., 2010). Furthermore, BMP-1 processes the precursors of laminin 5 (γ2) and collagen type VII, both of which are involved in securing the epidermis to the underlying dermis. In addition to activation of LOX, BMP-1 functions in processing the C-propeptides of procollagens types I–III to yield the major fibrous components of vertebrate ECM, and that of NH2- terminal globular domains and C-propeptides of types of V and XI procollagen chains, to yield monomers that control the diameters of collagne type I and II fibrils by its incorporation (Ge & Greenspan, 2006). GREM1, a BMP antagonist from the DAN family, was also identified in the pool of the differentially expressed genes in response to rhPSTN treatment. GREM1 binds to BMPs and prevents them from interacting with BMP receptors, thus playing a key role in regulating the TGF-β/BMP signaling pathway (provided by NCBI Reference Sequences; https://www.ncbi.nlm.nih.gov/gene/26585). This change in GREM1 expression further supports periostin in ECM maintenance and homeostasis, as inhibition or induction of GREM-1 has been shown to change the osteogenic differentiation of PDLSCs under inflammatory conditions (Xu et al., 2020). Similar results have been reported by Ghuman, showing that GREM-1 can also limit coronal alveolar bone regenerative potential during oral and periodontal surgery by inhibiting BMP-induced bone formation (Ghuman et al., 2019).

TNF Receptor Superfamily Member 11b gene (TNFRSF11B)- an osteoblast-secreted decoy receptor that functions as a negative regulator of bone resorption encoding the protein Osteoprotegerin (OPG)- was also identified to be differentially expressed in rhPSTN treated hPDL cells. This protein specifically binds to its ligand, OPG-Ligand, both of which are key extracellular regulators of osteoclast development (Boyce & Xing, 2008). PDL fibroblasts have the capacity to select and attract osteoclast precursors and subsequently to retract and enable migration of osteoclast precursors to the bone surface. There, fusion of precursors takes place, giving rise to osteoclasts. The RANKL-RANK-(OPG) axis is considered crucial in this process. PDL fibroblasts produce primarily OPG, an osteoclastogenesis-inhibitory molecule (Sokos et al., 2015). In totality, this information demonstrates a critical role for periostin in extracellular matrix organization, homeostasis and the regulation of cell phenotype.

On the contrary, when hPDL cells were cultured in osteogenic conditions, pathway enrichment analysis of DEG by the exogenous addition of periostin revealed involvement of "peptidyl-tyrosine autophosphorylation", "regulation of bone remodeling", regulation of receptor internalization", regulation of focal adhesion assembly", regulation of osteoblast differentiation" , among others (Fig. 3.5 B), suggesting a potential contribution of periostin in the bone remodeling process. In this study, the gene coding for secreted frizzled-related protein 1 (sFRP1) was identified to be differentially expressed upon treatment with osteogenic media supplemented with rhPSTN. sFRP1 is an antagonist of Wnt signaling, that controls osteoblast and osteocyte apoptosis (Bodine et al., 2005). Our data are in line with previous observations: in MC3T3-E11 osteoblastic cells, overexpression of periostin increases cell proliferation and differentiation (Horiuchi et al., 1999), while injection of an adenovirus overexpressing periostin, increased bone formation rate and bone mass in rats (Zhu et al., 2009). Our results also revealed DEGs involved in "regulation of focal adhesion assembly", which is consistent with effects of periostin on attachment related to mineralization (Cobo et al., 2016). Evidence suggests that Postn deletion results in a defective attachment of osteoblasts to the bone matrix, which affects their differentiation into mature osteoblasts as shown by a severe reduction of the

expression of type I collagen, osteocalcin, osteopontin and alkaline phosphatase, as well as a decreased mineralization process in vitro (Bonnet et al., 2012, 2016; Litvin et al., 2004).

In combination, our results suggest that periostin's presence in the ECM of PDL might not be directly linked to the mineralization or inhibition, but rather provide a continuous signal to support ECM organization and homeostasis to maintain a healthy and PDL interface with surrounding bone remodeling.

Increased age is an important factor that appears to adversely affect biological properties, including differentiation capacity, of hPDL cells (Li et al., 2020; R.-X. Wu et al., 2015; Zhang et al., 2012). With increasing age, the proliferation and osteogenic/adipogenic differentiation ability of hPDL cells decrease (Zhang et al., 2012). In our study, we selectively analysed the dataset from the youngest donor (F15) separately and we found unique gene expression patterns, both in unsupplemented and osteogenic media conditions. It is of great interest that we identified 202 differentially expressed genes (DEG_{OSTEO}) in osteogenic conditions in the young patient, when compared to 98 DEGs in adult patients, providing further evidence of the increased differentiation capacity of hPDL cells isolated from young individuals. It is well established that the PDL- contains among other cells populations (fibroblasts, pericytes, cementoblasts, osteoblasts)- multipotent mesenchymal stem cells (Komaki, 2019; Lekic & McCulloch, 1996; Seo et al., 2004). When hPDL cells are isolated in vitro, approximately 30% of the isolated cells possess crucial stem cell properties, such as self-renewal and multipotency, and express the mesenchymal stem cell markers CD105, CD166, and STRO-1 on their cell surface, although there were some variations (Nagatomo et al., 2006). Thus, our data further support that aging is associated with reduced differentiation potential of hPDL cells and our results could provide an important theoretical basis for later cell therapy and tissue regeneration applications.

In conclusion, our current study provides preliminary insights into the effects of periostin on the mineralization potential of PDL cells under different culture conditions. Our findings suggest that periostin has condition-specific actions: in non-osteogenic conditions it contributes to ECM maintenance in the PDL cells, while in osteogenic conditions periostin further promotes the mineralization capacity of PDL cells and contributes to gene

expression changes associated with bone remodeling. Further studies are required to be performed in future to demonstrate the interactions found in the sequencing results. A better understating of the molecular and cellular effects of periostin on PDL cells could be helpful for periodontal regeneration and stem cell-targeted therapy.

3.5 References

Alexa, A., Rahnenführer, J., & Lengauer, T. (2006). Improved scoring of functional groups from gene expression data by decorrelating GO graph structure. *Bioinformatics (Oxford, England)*, *22*(13), 1600–1607. https://doi.org/10.1093/bioinformatics/btl140

Anders, S., & Huber, W. (2010). Differential expression analysis for sequence count data. *Genome Biology*, *11*(10), R106. https://doi.org/10.1186/gb-2010-11-10-r106

Beertsen, W., McCulloch, C. A., & Sodek, J. (1997). The periodontal ligament: A unique, multifunctional connective tissue. *Periodontology 2000*, *13*, 20–40. https://doi.org/10.1111/j.1600-0757.1997.tb00094.x

Bekhouche, M., & Colige, A. (2015). The procollagen N-proteinases ADAMTS2, 3 and 14 in pathophysiology. *Matrix Biology*, *44–46*, 46–53. https://doi.org/10.1016/j.matbio.2015.04.001

Bella, J., & Hulmes, D. J. S. (2017). Fibrillar Collagens. *Sub-Cellular Biochemistry*, *82*, 457–490. https://doi.org/10.1007/978-3-319-49674-0_14

Benjamini, Y., & Hochberg, Y. (1995). Controlling the False Discovery Rate: A Practical and Powerful Approach to Multiple Testing. *Journal of the Royal Statistical Society. Series B (Methodological)*, *57*(1), 289–300. JSTOR.

Bodine, P. V. N., Billiard, J., Moran, R. A., Ponce-de-Leon, H., McLarney, S., Mangine, A., Scrimo, M. J., Bhat, R. A., Stauffer, B., Green, J., Stein, G. S., Lian, J. B., & Komm, B. S. (2005). The Wnt antagonist secreted frizzled-related protein-1 controls osteoblast and osteocyte apoptosis. *Journal of Cellular Biochemistry*, *96*(6), 1212–1230. https://doi.org/10.1002/jcb.20599

Bonnet, N., Conway, S. J., & Ferrari, S. L. (2012). Regulation of beta catenin signaling and parathyroid hormone anabolic effects in bone by the matricellular protein

periostin. *Proceedings of the National Academy of Sciences*, *109*(37), 15048–15053. https://doi.org/10.1073/pnas.1203085109

Bonnet, N., Garnero, P., & Ferrari, S. (2016). Periostin action in bone. *Molecular and Cellular Endocrinology*, *432*, 75–82. https://doi.org/10.1016/j.mce.2015.12.014

Boyce, B. F., & Xing, L. (2008). Functions of RANKL/RANK/OPG in bone modeling and remodeling. *Archives of Biochemistry and Biophysics*, *473*(2), 139–146. https://doi.org/10.1016/j.abb.2008.03.018

Cobo, T., Viloria, C. G., Solares, L., Fontanil, T., González-Chamorro, E., De Carlos, F., Cobo, J., Cal, S., & Obaya, A. J. (2016). Role of Periostin in Adhesion and Migration of Bone Remodeling Cells. *PLOS ONE*, *11*(1), e0147837. https://doi.org/10.1371/journal.pone.0147837

Denes, B. J., Ait-Lounis, A., Wehrle-Haller, B., & Kiliaridis, S. (2020). Core Matrisome Protein Signature During Periodontal Ligament Maturation From Pre-occlusal Eruption to Occlusal Function. *Frontiers in Physiology*, *11*. https://www.frontiersin.org/article/10.3389/fphys.2020.00174

Denes, B. J., Bolton, C., Illsley, C. S., Kok, W. L., Walker, J. V., Poetsch, A., Tredwin, C., Kiliaridis, S., & Hu, B. (2019). Notch Coordinates Periodontal Ligament Maturation through Regulating Lamin A. *Journal of Dental Research*, *98*(12), 1357–1366. https://doi.org/10.1177/0022034519871448

Dobin, A., Davis, C. A., Schlesinger, F., Drenkow, J., Zaleski, C., Jha, S., Batut, P., Chaisson, M., & Gingeras, T. R. (2013). STAR: Ultrafast universal RNA-seq aligner. *Bioinformatics*, *29*(1), 15–21. https://doi.org/10.1093/bioinformatics/bts635

Elliott, C. G., & Hamilton, D. W. (2011). Deconstructing fibrosis research: Do pro-fibrotic signals point the way for chronic dermal wound regeneration? *Journal of*

Cell Communication and Signaling, *5*(4), 301–315. https://doi.org/10.1007/s12079-011-0131-5

Ge, G., & Greenspan, D. S. (2006). Developmental roles of the BMP1/TLD metalloproteinases. *Birth Defects Research. Part C, Embryo Today: Reviews*, *78*(1), 47–68. https://doi.org/10.1002/bdrc.20060

Ghuman, M. S., Al-Masri, M., Xavier, G., Cobourne, M. T., McKay, I. J., & Hughes, F. J. (2019). Gingival fibroblasts prevent BMP-mediated osteoblastic differentiation. *Journal of Periodontal Research*, *54*(3), 300–309. https://doi.org/10.1111/jre.12631

Gould, T. R. (1983). Ultrastructural characteristics of progenitor cell populations in the periodontal ligament. *Journal of Dental Research*, *62*(8), 873–876. https://doi.org/10.1177/00220345830620080401

Gould, T. R. L., Melcher, A. H., & Brunette, D. M. (1980). Migration and division of progenitor cell populations in periodontal ligament after wounding. *Journal of Periodontal Research*, *15*(1), 20–42. https://doi.org/10.1111/j.1600-0765.1980.tb00258.x

Häkkinen, L., Oksala, O., Salo, T., Rahemtulla, F., & Larjava, H. (1993). Immunohistochemical localization of proteoglycans in human periodontium. *The Journal of Histochemistry and Cytochemistry: Official Journal of the Histochemistry Society*, *41*(11), 1689–1699. https://doi.org/10.1177/41.11.8409375

Hamilton, D. W. (2008). Functional role of periostin in development and wound repair: Implications for connective tissue disease. *Journal of Cell Communication and Signaling*, *2*(1–2), 9–17. https://doi.org/10.1007/s12079-008-0023-5

Horiuchi, K., Amizuka, N., Takeshita, S., Takamatsu, H., Katsuura, M., Ozawa, H., Toyama, Y., Bonewald, L. F., & Kudo, A. (1999). Identification and

characterization of a novel protein, periostin, with restricted expression to periosteum and periodontal ligament and increased expression by transforming growth factor beta. *Journal of Bone and Mineral Research : The Official Journal of the American Society for Bone and Mineral Research*, *14*(7), 1239–1249. https://doi.org/10.1359/jbmr.1999.14.7.1239

Ignatiadis, N., Klaus, B., Zaugg, J. B., & Huber, W. (2016). Data-driven hypothesis weighting increases detection power in genome-scale multiple testing. *Nature Methods*, *13*(7), 577–580. https://doi.org/10.1038/nmeth.3885

Kii, I., Amizuka, N., Nishiyama, T., Saito, M., Li, M., Matsumoto, K., & Kudo, A. (2009). Incorporation of Tenascin-C into the Extracellular Matrix by Periostin Underlies an Extracellular Meshwork Architecture. *Journal of Biological Chemistry*, *285*(3), 2028–2039. https://doi.org/10.1074/jbc.m109.051961

Kii, I., & Ito, H. (2017a). Periostin and its interacting proteins in the construction of extracellular architectures. *Cellular and Molecular Life Sciences*, *74*(23), 4269–4277. https://doi.org/10.1007/s00018-017-2644-4

Kii, I., & Ito, H. (2017b). Periostin and its interacting proteins in the construction of extracellular architectures. *Cellular and Molecular Life Sciences*, *74*(23), 4269–4277. https://doi.org/10.1007/s00018-017-2644-4

Kim, K., Kang, H. E., Yook, J. I., Yu, H.-S., Kim, E., Cha, J.-Y., & Choi, Y. J. (2020). Transcriptional Expression in Human Periodontal Ligament Cells Subjected to Orthodontic Force: An RNA-Sequencing Study. *Journal of Clinical Medicine*, *9*(2), E358. https://doi.org/10.3390/jcm9020358

Komaki, M. (2019). Pericytes in the Periodontal Ligament. *Advances in Experimental Medicine and Biology*, *1122*, 169–186. https://doi.org/10.1007/978-3-030-11093-2_10

Kruzynska-Frejtag, A., Wang, J., Maeda, M., Rogers, R., Krug, E., Hoffman, S., Markwald, R. R., & Conway, S. J. (2004). Periostin Is Expressed Within the Developing Teeth at the Sites of Epithelial-Mesenchymal Interaction. *Developmental Dynamics*, *229*(4), 857–868. https://doi.org/10.1002/dvdy.10453

Kudo, A. (2011). Periostin in fibrillogenesis for tissue regeneration: Periostin actions inside and outside the cell. *Cellular and Molecular Life Sciences*, *68*(19), 3201–3207. https://doi.org/10.1007/s00018-011-0784-5

Lausch, A. J., Quan, B., Miklas, J., & Sone, E. (2013). *Extracellular Matrix Control of Collagen Mineralization In Vitro*. https://doi.org/10.1002/adfm.201203760

Lausch, A. J., & Sone, E. D. (2015). A Top-down Approach to Elucidate the Role of Matrix-Bound Phosphoproteins in Control of Collagen Biomineralization. *Biomacromolecules*, *16*(7), 1938–1947. https://doi.org/10.1021/acs.biomac.5b00287

Lee, S., Chen, D., Park, M., Kim, S., Choi, Y. J., Moon, S. J., Shin, D. M., Lee, J. H., & Kim, E. (2022). Single-Cell RNA Sequencing Analysis of Human Dental Pulp Stem Cell and Human Periodontal Ligament Stem Cell. *Journal of Endodontics*, *48*(2), 240–248. https://doi.org/10.1016/j.joen.2021.11.005

Lekic, P., & McCulloch, C. A. (1996). Periodontal ligament cell population: The central role of fibroblasts in creating a unique tissue. *The Anatomical Record*, *245*(2), 327–341. https://doi.org/10.1002/(SICI)1097-0185(199606)245:2<327::AID-AR15>3.0.CO;2-R

Li, X., Zhang, B., Wang, H., Zhao, X., Zhang, Z., Ding, G., & Wei, F. (2020). The effect of aging on the biological and immunological characteristics of periodontal ligament stem cells. *Stem Cell Research & Therapy*, *11*(1), 326. https://doi.org/10.1186/s13287-020-01846-w

Liang, Y., Hu, Z., Chang, B., & Liu, X. (2020). Quantitative characterizations of the Sharpey's fibers of rat molars. *Journal of Periodontal Research*, *55*(2), 307–314. https://doi.org/10.1111/jre.12716

Liao, Y., Smyth, G. K., & Shi, W. (2019). The R package Rsubread is easier, faster, cheaper and better for alignment and quantification of RNA sequencing reads. *Nucleic Acids Research*, *47*(8), e47. https://doi.org/10.1093/nar/gkz114

Litvin, J., Selim, A.-H., Montgomery, M. O., Lehmann, K., Rico, M. C., Devlin, H., Bednarik, D. P., & Safadi, F. F. (2004). Expression and function of periostin-isoforms in bone. *Journal of Cellular Biochemistry*, *92*(5), 1044–1061. https://doi.org/10.1002/jcb.20115

Love, M. I., Huber, W., & Anders, S. (2014). Moderated estimation of fold change and dispersion for RNA-seq data with DESeq2. *Genome Biology*, *15*(12), 550. https://doi.org/10.1186/s13059-014-0550-8

Mao, J. R., Taylor, G., Dean, W. B., Wagner, D. R., Afzal, V., Lotz, J. C., Rubin, E. M., & Bristow, J. (2002). Tenascin-X deficiency mimics Ehlers-Danlos syndrome in mice through alteration of collagen deposition. *Nature Genetics*, *30*(4), 421–425. https://doi.org/10.1038/ng850

Martin, M. (2011). Cutadapt removes adapter sequences from high-throughput sequencing reads. *EMBnet.Journal*, *17*(1), 10–12.

Maruhashi, T., Kii, I., Saito, M., & Kudo, A. (2010). Interaction between periostin and BMP-1 promotes proteolytic activation of lysyl oxidase. *Journal of Biological Chemistry*, *285*(17), 13294–13303. https://doi.org/10.1074/jbc.M109.088864

Matsuzawa, M., Arai, C., Nomura, Y., Murata, T., Yamakoshi, Y., Oida, S., Hanada, N., & Nakamura, Y. (2015). Periostin of human periodontal ligament fibroblasts promotes migration of human mesenchymal stem cell through the αvβ3

integrin/FAK/PI3K/Akt pathway. *Journal of Periodontal Research*, *50*(6), 855–863. https://doi.org/10.1111/jre.12277

McCulloch, C. A. (1985). Progenitor cell populations in the periodontal ligament of mice. *The Anatomical Record*, *211*(3), 258–262. https://doi.org/10.1002/ar.1092110305

Morissette Martin, P., Creber, K., & Hamilton, D. W. (2017). 6—Measuring gene expression changes on biomaterial surfaces. In R. J. Narayan (Ed.), *Monitoring and Evaluation of Biomaterials and their Performance In Vivo* (pp. 111–131). Woodhead Publishing. https://doi.org/10.1016/B978-0-08-100603-0.00006-7

Nagatomo, K., Komaki, M., Sekiya, I., Sakaguchi, Y., Noguchi, K., Oda, S., Muneta, T., & Ishikawa, I. (2006). Stem cell properties of human periodontal ligament cells. *Journal of Periodontal Research*, *41*(4), 303–310. https://doi.org/10.1111/j.1600-0765.2006.00870.x

Nanci, A. (2017). *Ten Cate's Oral Histology - E-Book: Development, Structure, and Function*. Elsevier Health Sciences.

Nikoloudaki, G. (2021). Functions of Matricellular Proteins in Dental Tissues and Their Emerging Roles in Orofacial Tissue Development, Maintenance, and Disease. *International Journal of Molecular Sciences*, *22*(12). https://doi.org/10.3390/ijms22126626

Norris, R. A., Damon, B., Kern, C. B., Wen, X., Forgacs, G., Hoffman, S., Trusk, T., Molkentin, J. D., Goodwin, R. L., Conway, S. J., Norris, R. A., Kasyanov, V., Potts, J. D., Mjaatvedt, C. H., Oka, T., Moreno-Rodriguez, R., Markwald, R. R., Sugi, Y., Davis, J., … Mironov, V. (2007). Periostin regulates collagen fibrillogenesis and the biomechanical properties of connective tissues. *Journal of Cellular Biochemistry*, *101*(3), 695–711. https://doi.org/10.1002/jcb.21224

Nudelman, F., Lausch, A. J., Sommerdijk, N. A. J. M., & Sone, E. D. (2013). In vitro models of collagen biomineralization. *Journal of Structural Biology*, *183*(2), 258–269. https://doi.org/10.1016/j.jsb.2013.04.003

Quan, B. D., & Sone, E. D. (2015). Structural changes in collagen fibrils across a mineralized interface revealed by cryo-TEM. *Bone*, *77*, 42–49. https://doi.org/10.1016/j.bone.2015.04.020

Raspanti, M., Cesari, C., De Pasquale, V., Ottani, V., Strocchi, R., Zucchelli, G., & Ruggeri, A. (2000). A histological and electron-microscopic study of the architecture and ultrastructure of human periodontal tissues. *Archives of Oral Biology*, *45*(3), 185–192. https://doi.org/10.1016/S0003-9969(99)00145-4

Rios, H. F., Ma, D., Xie, Y., Giannobile, W. V, Bonewald, L. F., Conway, S. J., & Feng, J. Q. (2008). Periostin Is Essential for the Integrity and Function of the Periodontal Ligament During Occlusal Loading in Mice. *Journal of Periodontology*, *79*(8), 1480–1490. https://doi.org/doi:10.1902/jop.2008.070624

Rios, H., Koushik, S. V, Wang, H., Wang, J., Zhou, H.-M., Lindsley, A., Rogers, R., Chen, Z., Maeda, M., Kruzynska-Frejtag, A., Feng, J. Q., & Conway, S. J. (2005). Periostin Null Mice Exhibit Dwarfism, Incisor Enamel Defects, and an Early-Onset Periodontal Disease-Like Phenotype. *Molecular and Cellular Biology*, *25*(24), 11131–11144. https://doi.org/10.1128/MCB.25.24.11131-11144.2005

Saito, M. T., Mofatto, L. S., Albiero, M. L., Casati, M. Z., Sallum, E. A., Nociti Junior, F. H., & SilvÉrio, K. G. (2020). Transcriptome profile of highly osteoblastic/cementoblastic periodontal ligament cell clones. *Journal of Applied Oral Science: Revista FOB*, *28*, e20200242. https://doi.org/10.1590/1678-7757-2020-0242

Sata, M., Kudo, A., Nakamura, K., Saga, Y., Fukuda, K., Saito, M., Kashima, T., Amizuka, N., Shimazaki, M., Fukayama, M., Li, M., Kitajima, S., Kii, I., & Nishiyama, T. (2008). Periostin is essential for cardiac healingafter acute

myocardial infarction. *The Journal of Experimental Medicine*. https://doi.org/10.1084/jem.20071297

Schalkwijk, J., Zweers, M. C., Steijlen, P. M., Dean, W. B., Taylor, G., van Vlijmen, I. M., van Haren, B., Miller, W. L., & Bristow, J. (2001). A recessive form of the Ehlers-Danlos syndrome caused by tenascin-X deficiency. *The New England Journal of Medicine*, *345*(16), 1167–1175. https://doi.org/10.1056/NEJMoa002939

Seo, B.-M., Miura, M., Gronthos, S., Bartold, P. M., Batouli, S., Brahim, J., Young, M., Robey, P. G., Wang, C.-Y., & Shi, S. (2004). Investigation of multipotent postnatal stem cells from human periodontal ligament. *Lancet (London, England)*, *364*(9429), 149–155. https://doi.org/10.1016/S0140-6736(04)16627-0

Sokos, D., Everts, V., & de Vries, T. J. (2015). Role of periodontal ligament fibroblasts in osteoclastogenesis: A review. *Journal of Periodontal Research*, *50*(2), 152–159. https://doi.org/10.1111/jre.12197

Tang, Y., Liu, L., Wang, P., Chen, D., Wu, Z., & Tang, C. (2017). Periostin promotes migration and osteogenic differentiation of human periodontal ligament mesenchymal stem cells via the Jun amino-terminal kinases (JNK) pathway under inflammatory conditions. *Cell Proliferation*, *50*(6), 1–11. https://doi.org/10.1111/cpr.12369

Tkatchenko, T. V, Moreno-Rodriguez, R. A., Conway, S. J., Molkentin, J. D., Markwald, R. R., & Tkatchenko, A. V. (2009). Lack of periostin leads to suppression of Notch1 signaling and calcific aortic valve disease. *Physiological Genomics*, *39*(3), 160–168. https://doi.org/10.1152/physiolgenomics.00078.2009

Wen, W., Chau, E., Jackson-Boeters, L., Elliott, C., Daley, T. D., & Hamilton, D. W. (2010). TGF-β1 and FAK regulate periostin expression in PDL fibroblasts. *Journal of Dental Research*, *89*(12), 1439–1443. https://doi.org/10.1177/0022034510378684

Wojtas, M., Lausch, A. J., & Sone, E. D. (2020). Glycosaminoglycans accelerate biomimetic collagen mineralization in a tissue-based in vitro model. *Proceedings of the National Academy of Sciences*, *117*(23), 12636–12642. https://doi.org/10.1073/pnas.1914899117

Wu, R.-X., Bi, C.-S., Yu, Y., Zhang, L.-L., & Chen, F.-M. (2015). Age-related decline in the matrix contents and functional properties of human periodontal ligament stem cell sheets. *Acta Biomaterialia*, *22*, 70–82. https://doi.org/10.1016/j.actbio.2015.04.024

Wu, Z., Dai, W., Wang, P., Zhang, X., Tang, Y., Liu, L., Wang, Q., Li, M., & Tang, C. (2018). Periostin promotes migration, proliferation, and differentiation of human periodontal ligament mesenchymal stem cells. *Connective Tissue Research*, *59*(2), 108–119. https://doi.org/10.1080/03008207.2017.1306060

Xu, X.-Y., Tian, B.-M., Xia, Y., Xia, Y.-L., Li, X., Zhou, H., Tan, Y.-Z., & Chen, F.-M. (2020). Exosomes derived from P2X7 receptor gene-modified cells rescue inflammation-compromised periodontal ligament stem cells from dysfunction. *STEM CELLS Translational Medicine*, *9*(11), 1414–1430. https://doi.org/10.1002/sctm.19-0418

Zhang, J., An, Y., Gao, L.-N., Zhang, Y.-J., Jin, Y., & Chen, F.-M. (2012). The effect of aging on the pluripotential capacity and regenerative potential of human periodontal ligament stem cells. *Biomaterials*, *33*(29), 6974–6986. https://doi.org/10.1016/j.biomaterials.2012.06.032

Zhu, S., Barbe, M. F., Liu, C., Hadjiargyrou, M., Popoff, S. N., Rani, S., Safadi, F. F., & Litvin, J. (2009). Periostin-like-factor in osteogenesis. *Journal of Cellular Physiology*, *218*(3), 584–592. https://doi.org/10.1002/jcp.21633

Chapter 4

4 Myofibroblast Origin in Palatal Repair: Assessing the Contribution and the Fate of Foxd1 and NG2 Populations and Their Progeny During Palatal Development and Repair

4.1 Introduction

During wound healing, extracellular matrix is deposited, and the wound is contracted through the actions of myofibroblasts (Hinz, 2010). The embryonic origin of resident fibroblasts in connective tissues such as skin and gingiva during development and in postnatal tissues from mesodermal origins is well-established. However, the origin of mesenchymal populations and their contractile counterpart, the myofibroblast, that are recruited during tissue repair and fibrosis continues to be a subject of intense research and debate (Gomes et al., 2021; LeBleu et al., 2013). Tissue resident fibroblasts were originally hypothesized to be a relatively homogeneous cell population in connective tissues, responsible for producing and remodeling the extracellular matrix. However, recent advances in technologies, including lineage tracing, have allowed researchers to identify and investigate subpopulations of fibroblasts, which arise from different lineages of embryonic precursor cells (Driskell & Watt, 2015; Goss et al., 2021; LeBleu & Neilson, 2020). As myofibroblasts are the main source of extracellular matrix (ECM) production during tissue injury (Gabbiani et al., 1971, p. 20; Hinz, 2015; Tomasek et al., 2002; Zent & Guo, 2018), investigation into the cellular origin from whichpopulations originate after injury is important for development of new strategies to improve wound healing outcomes while reducing scar formation (Driskell & Watt, 2015).

Potential sources of myofibroblasts progenitors include epithelial cells and endothelial cells, derived through a process termed epithelial-mesenchymal (Kalluri & Weinberg, 2009) or endothelial-mesenchymal transition (Zeisberg et al., 2007); circulating bone marrow–derived fibrocytes, tissue-resident fibroblasts, and other mesenchymal cells related to blood vessels, including pericytes, adventitial cells, and mesenchymal stem cells

(MSCs) (Crisan et al., 2008; Di Carlo & Peduto, 2018; Hinz, 2010; Zent & Guo, 2018). Pericytes are peri-endothelial cells found encircling the endothelial cells of the microvasculature (Greenhalgh et al., 2013). The contribution of pericytes in fibrosis of different organs remains controversial (Guimarães-Camboa et al., 2017; Kramann et al., 2013; Lemos & Duffield, 2018). Different markers have been used to detect pericytes, such as Rgs5, Pdgfrβ, nestin Tbx18, CD146 and NG2 (Neuron-glial antigen 2, which encodes chondroitin sulfate proteoglycan expressed in oligodendrocytes progenitor, myeloid, and perivascular cells) (Cathery et al., 2018; Yamazaki & Mukouyama, 2018). From these, NG2 is widely used not only because it is highly expressed by pericytes, but also because it consistently labels cells with pericyte features on multiple types of vasculature in different organs, such as skin, embryonic brain microvasculature, embryonic heart micro- and macro-vasculature, and retinal microvasculature (Ozerdem et al., 2001; Ozerdem & Stallcup, 2004). Overall, these studies show that various types of cells can contribute to cells participating in the wound healing process, with perivascular cells.

Lineage tracing experiments have identified cell populations associated with the perivascular space which are activated upon tissue injury and exhibit profibrotic phenotypes, characterized by expression of α-SMA and production of fibrillar collagen and other ECM proteins (Dulauroy, Di Carlo, et al., 2012). Genetic fate mapping has shown that resident pericytes in the liver (hepatic stellate cells) (Mederacke et al., 2013), the kidney (Chen et al., 2011; Humphreys et al., 2010a) and the lungs (Hung et al., 2013) account for the major sources of myofibroblasts post-injury and contribute significantly to tissue repair.

Previous research has shown that cell progeny derived from Foxd1 embryonic progenitors to be myofibroblast precursors following tissue damage. More specifically, as a lineage tracing marker, resident Foxd1 lineage-derived populations in the kidney and lung contributed to the myofibroblast populations in induced renal fibrosis following unilateral ureteral obstruction and ischemia reperfusion injury, as well as bleomycin induced lung fibrosis, respectively (Humphreys et al., 2010a; Hung et al., 2013). Foxd1 is a transcription factor expressed primarily during development, in paraxial mesoderm-derived populations

(Guillaume et al., 2009). Using a Foxd1-Cre knock-in mouse crossed with a Rosa26-loxp-stop-loxp(lsl)-*lacZ* reporter mouse, Humphreys *et al.* (2010) were able to provide evidence for a mesenchymal source of myofibroblasts during kidney fibrosis (Humphreys et al., 2010b). This group used this same model to demonstrate that Foxd1-progenitor– derived pericytes expand after bleomycin lung injury, and activate expression of collagen-I(a)1 and the myofibroblast marker α-SMA in fibrotic foci, showing that 68% of α-SMA-expressing cells in fibrotic lungs are pericyte-derived (Hung et al., 2013). A recent study from our laboratory using a murine cutaneous wounding model showed that Foxd1-lineage progeny cells expand upon injury and contribute to the stromal population and α-SMA-positive myofibroblasts, but did not contribute to perivascular and endothelial cells (Walker et al., 2021). In summary, these studies do show that Foxd1 lineage derived populations can contribute to myofibroblast precursors following tissue injury, but the cell of origin varies depending on the tissue.

Although lineage tracing is a powerful method, it is highly dependent on the gene used to track cell populations. Previous studies investigating the potential contribution of pericytes in mice to bleomycin-induced lung fibrosis utilized NG2 as the genetic marker for this cell type, but did not find any significant contribution of $NG2^{+}$ pericytes to myofibroblast populations and the resulting fibrosis even though the pericyte population itself did expand significantly (Rock et al., 2011). LeBleu et al. (2013) demonstrated in a murine renal fibrosis model that cells positive for the pericyte markers PDGFRβ and NG2 did not contribute to ECM production post-injury. Additionally, preventing the expansion of these pericyte populations did not affect fibrotic tissue formation (LeBleu et al., 2013).

In summary, the totality of the studies to date suggests that multiple subpopulations of pericytes may exist within different tissues and differentially contribute to myofibroblast formation and fibrosis. To date, evidence of perivascular cell recruitment and differentiation into myofibroblasts appears to be organ specific (Di Carlo & Peduto, 2018; Gomes et al., 2021; LeBleu & Neilson, 2020; Lemos & Duffield, 2018), and, currently, whether this process occurs within the palatal mucoperiosteum has yet to be tested. Since myofibroblasts contribute to palatal wound healing and are considered largely responsible

for fibrotic tissue formation, it is pertinent to analyze their origin and recruitment in palatal wound healing.

In the present study, using a Cre/Lox lineage tracing system in mice, two distinct lineages that label perivascular cells, Foxd1- and NG2- lineages of stromal cells were investigated during palatal development, homeostasis, and excisional wound healing. It was hypothesized that embryonic progenitors that express Foxd1 and their progeny would contribute to myofibroblast progenitors within the palatal mucoperiosteum in adult tissues, and that binary expression of Foxd1 or NG2 could be used to stratify palatal fibroblasts and cells within the wounded tissue to identify unexplored embryonic lineages of myofibroblast progenitors present within the adult palatal tissues upon wounding.

4.2 Materials and Methods

4.2.1 Animals

All animal procedures were in accordance with protocols approved by the University Council on Animal Care at The University of Western Ontario. Animal use protocol # 2015-101). *Foxd1GC* (Foxd1tm1(GFP/Cre)Amc/J), *Foxd1GCE* (B6;129S4-Foxd1tm2(GFP/Cre/ERT2)Amc/J), *Ai14* (B6.Cg-Gt(ROSA)26Sortm14(CAG-tdTomato)Hze/J), *mTmG* (B6.129(Cg)-Gt(ROSA)26Sortm4(ACTB-tdTomato,-EGFP)Luo/J), *NG2-cre-GFP* (B6;FVB-Ifi208Tg(Cspg4-cre)1Akik/J) and *NG2-CreER-GFP* (B6.Cg-Tg(Cspg4-cre/Esr1*)BAkik/J) mice were purchased from The Jackson Laboratory (Farmington, CT). Schematics and brief descriptions of each of the Cre/Lox models used in this study are provided in Figure 4.1 and 4.2Mice were genotyped as per The Jackson Laboratory's instructions. Mice that were heterozygous for the alleles of interest were used for all experiments.

4.2.2 Murine embryonic tissues

Foxd1-Cre-GFP mice were bred with *ROSA26-mTmG/þ* mice to produce offspring that express a Cre-GFP fusion protein under control of the Foxd1 promoter. The reporter used was *mT/mG* (membrane-Tomato before Cre/membrane-GFP after Cre) expressed from the Rosa26 locus. In bigenic mice, cells that expressed Foxd1 at some point in development are green and cells that never expressed Foxd1 are red. Embryonic tissues were harvested at E17.5 and sectioned in the frontal plane to include the developing palatal tissues from the anterior (hard palate) to the most posterior (soft palate) part of the palate. For timed pregnancy, females were monitored for vaginal plugs and the day following was considered embryonic day 0.5 (E0.5). Embryos were isolated from pregnant females at E12.5, E14.5, and E17.5. For all time-points, at least 3 embryos were analyzed from at least 2 independent litters.

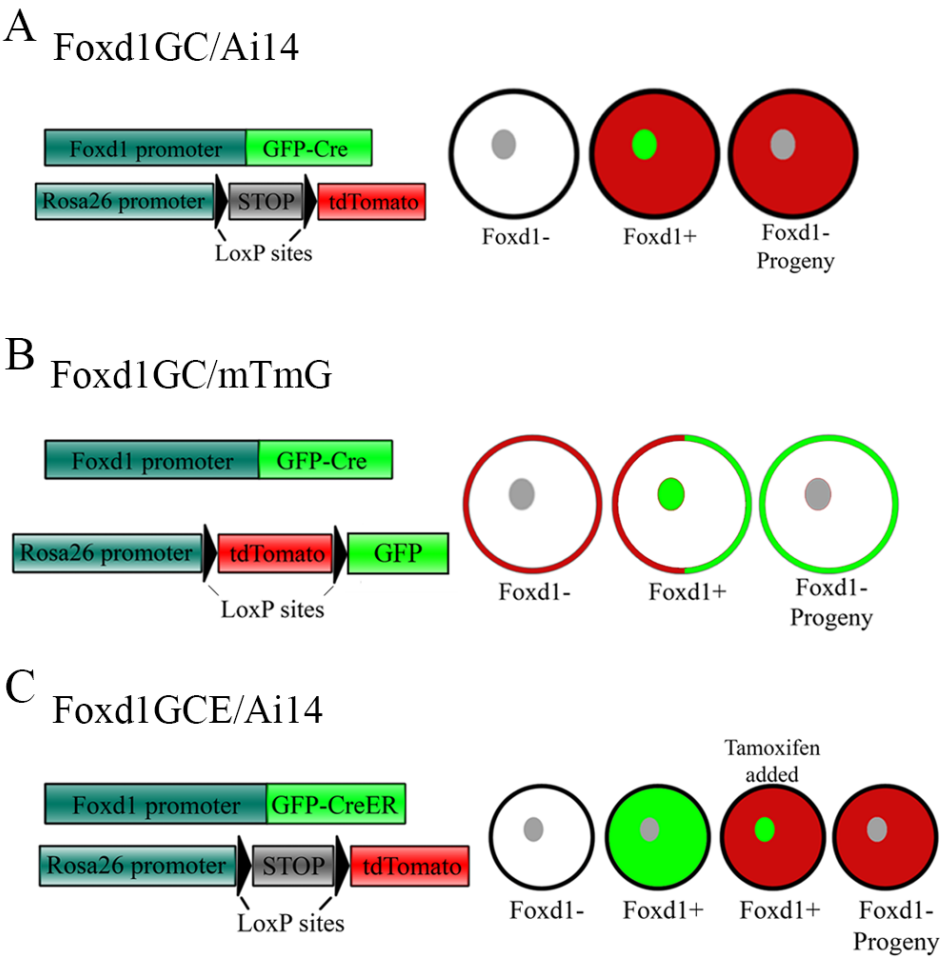

Figure 4-1 Schematics of Cre/Lox strategies used to track *Foxd1* lineage-positive populations.

(A) A cross between *Foxd1*GC and *Ai14* mice yields tdTomato positive populations in cells derived from *Foxd1*-expressing progenitors. **(B)** A cross between *Foxd1*GC and *mTmG* results in membrane-targeted tdTomato expression in all *Foxd1* lineage-negative populations and membrane-bound eGFP in all *Foxd1* lineage-positive populations. (**C)** A cross between *Foxd1GCE* and *Ai14* mice is similar to the cross in (A), however the modified human estrogen receptor (ER) fragment attached to the Cre-recombinase impedes translocation into the nucleus preventing recombination in the absence of the synthetic ER ligand, tamoxifen (Metzger and Chambon 2001).

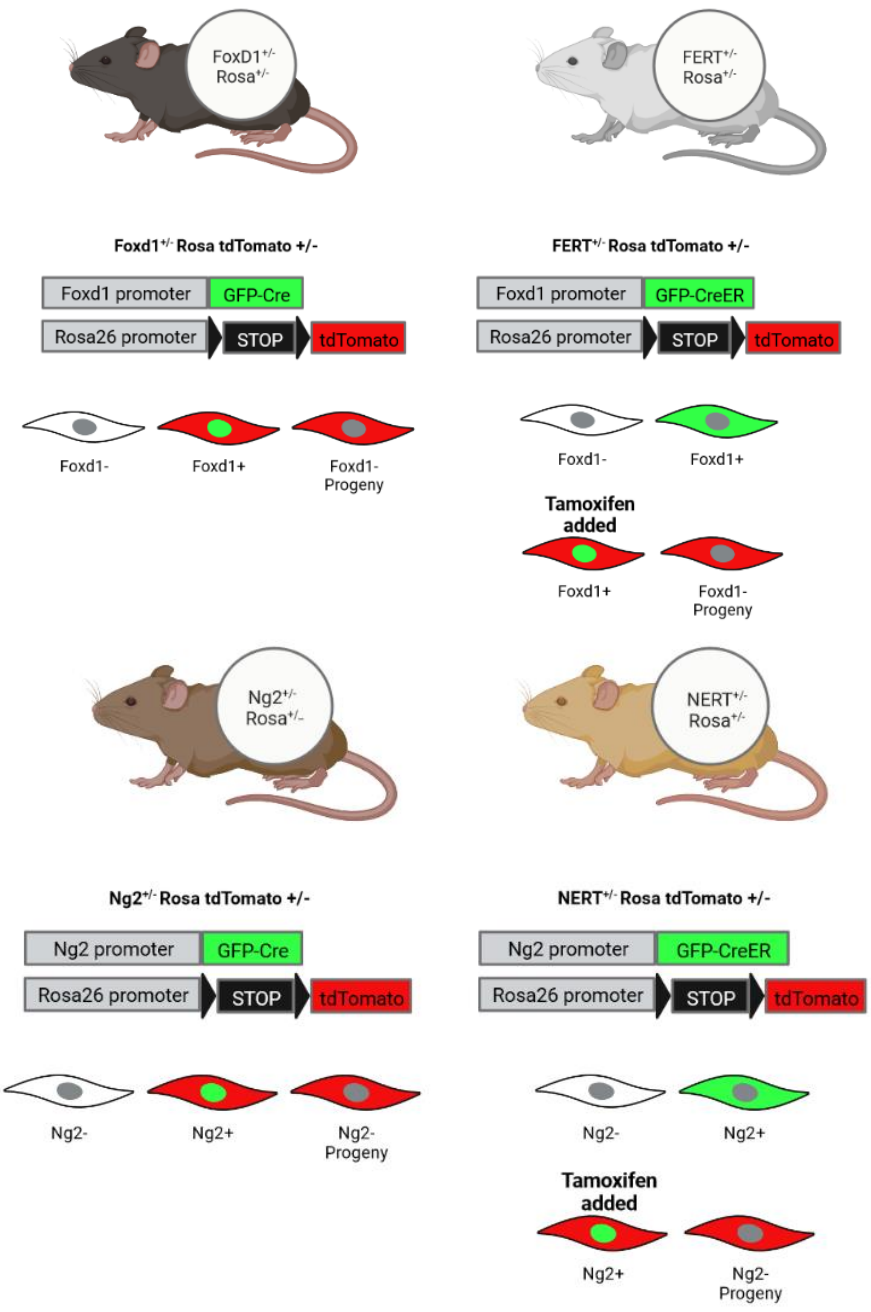

Figure 4-2 Schematics of Cre/Lox strategies used to track *Foxd1- and Ng2* lineage-positive populations

4.2.3 Palatal wounds

For experiments, mice heterozygous for the alleles *Foxd1GC/ Ai14*, *Foxd1GCE/ Ai14*, *NG2-cre-GFP/ Ai14* and *NG2-CreER-GFP/ Ai14* (20 weeks of age) were anesthetized with an intraperitoneal injection of buprenorphine (0.05 mg/kg), followed by an injection of ketamine (90 mg/kg) and xylazine (5 mg/kg). One full-thickness excisional wound was made with a 1.5 mm disposable biopsy punch (Integra™ Miltex®, Integra York PA, Inc.) on the hard palate. The localization of the palatal punch biopsy was standardized with the anterior edge of the wound to be aligned with the first molar (Keswani et al., 2013) (Fig. 4.2) to avoid traumatizing the palatal arteries which run on either side of the wound. The animals received 0.05 mg/kg Buprenorphine by subcutaneous injection twice daily for 48 hours post-surgery as an analgesic. Animals were maintained on a standard lab chow powdered food diet and were allowed food and water *ad libitum* for the duration of the experiment. Excised tissue was considered day 0 and was retained as normal healthy tissue. Animals were euthanized at 6 and 10 days post-wounding by carbon dioxide inhalation.

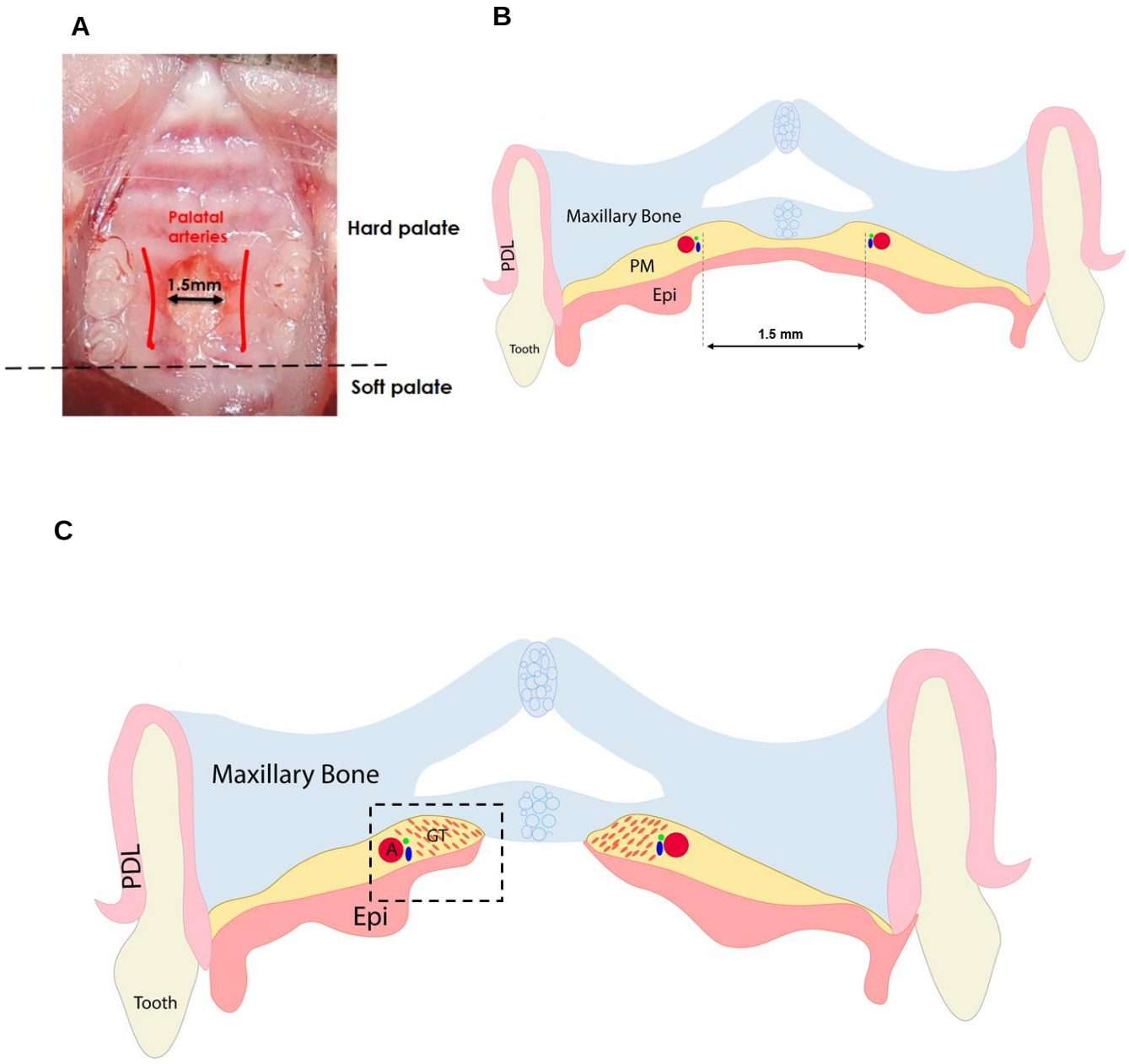
A
Palatal arteries
1.5mm
Hard palate
Soft palate
B
Maxillary Bone
PDL
PM
Epi
Tooth
1.5 mm
C
Maxillary Bone
PDL
GT
A
Epi
Tooth

Figure 4-3 Experimental wound model

One full-thickness excisional wound was made with a 1.5 mm disposable biopsy punch (Integra™ Miltex®, Integra York PA, Inc.) on the hard palate. The localization of the palatal punch biopsy was standardized with the anterior edge of the wound to be aligned with the first molar to avoid traumatizing the palatal arteries which run on either side of the wound. **B. Coronal view of the palatal tissues**: Black arrow indicate the diameter of the wound. **C. Coronal view of palatal wounded tissues.** The area of interest is highlighted in black dashed box (**PM**: palatal mucoperiosteum, **Epi**: oral Epithelium, **PDL**: periodontal ligament, **GT**: granulation tissue, **A**: major palatine artery)

4.2.4 Tamoxifen Injections

To temporally control Cre-mediated recombination, mice carrying a tamoxifen-inducible Cre variant, *CreERT2,* were crossed to *Ai14* reporter mice (Figure 2.1C) (Metzger & Chambon, 2001) Using this strategy, injection of tamoxifen was used to determine the temporal expression of Foxd1 or NG2 [chondroitin sulfate proteoglycan 4 *(Cspg)*] in adult palatal tissues. For all studies, a solution of 10 mg/mL tamoxifen in 90% corn oil (Sigma) and 10% ethanol was administered. Tamoxifen injection in postnatal mice was performed on mice heterozygous for both *Foxd1GCE* and *Ai14* alleles, or *NG2-CreER-GFP* and *Ai14* alleles. Directly following wounding, mice were subjected to a tamoxifen regimen of 1 mg each day for 3 consecutive days. At 6 and 10 days post wounding, the animals were euthanized, and tissues were collected for histological analyses. Postnatal tamoxifen injection and wounding was performed on 3 animals per timepoint. Tissues from these animals were compared to unwounded palatal tissues, and granulation tissue at 6 and 10 days post wounding from constitutively active *Foxd1GC/Ai14* mice. Tissues from these animals were also compared to unwounded and wounded tissues in *Foxd1GCE/Ai14*, or *NG2-CreER-GFP/Ai14* that did not receive tamoxifen as a negative control (mice were injected with equal amount of sterile saline).

4.2.5 Tissue Preparation

Isolated embryos, palatal and maxillary tissues were fixed in 10% neutral buffered formalin (Sigma Aldrich, St. Louis, MO) for 24 hours at 4ºC and decalcified in 20% EDTA (ethylenediminetetraacetic acid) for 10 days at 4 °C. These tissue samples were then dehydrated in a sucrose gradient prior to embedding in frozen section compound (Leica). Samples were frozen on dry ice and were stored at -20ºC. Cryosections were cut to 8 μm thickness for subsequent histological analysis.

4.2.6 Immunohistochemistry & Immunofluorescence

Unstained sections to investigate only endogenous fluorescent proteins, were washed in phosphate buffered saline (PBS) and counterstained with Hoechst 33342 dye (1:1000, Invitrogen, Thermo Fisher Scientific) for nuclei visualization. For antibody labelling, slides

were first washed with 1% sodium dodecyl sulfate (SDS) for 5 minutes, rinsed three times in PBS, and incubated for 30 minutes in 10% horse serum in PBS for blocking. Tissue sections were then incubated with primary antibodies as shown in Table 1. Primary antibodies were detected using Alexa Fluor IgG secondary antibodies (Invitrogen, Thermo Fisher Scientific). All sections were counterstained with Hoechst 33342 dye (1:1000, Invitrogen, Thermo Fisher Scientific) for nuclei visualization. Images were taken on Carl Zeiss Imager M2m microscope (Carl Zeiss, Jena) using ZenPro 2012 software. Tissue sections incubated without primary antibodies served as negative controls.

4.2.7 Quantitative Histological Analysis

For all measurements, only the wounded tissue was quantified, and not the epithelium or the signal from the palatal bone. Quantification of fluorescence staining was performed using macros in ImageJ software to measure the number of tdTomato-positive cells as a ratio to the total number of cells (Hoechst positive nuclei), as well as the percentage of tdTomato-positive cells per field of view (3 different histology sections/ wound, N=3 animals). For specific cell markers colocalization of the signal of interest with tdTomato-positive cells was manually quantified and presented as ratio of marker-tdTomato-positive cells/total number of tdTomato-positive cells. GraphPad Prism software version 6 (GraphPad, La Jolla, CA) was used to produce graphs. Statistical analyses were performed using 1-way ANOVA or 2-way ANOVA, followed by a Tukey post hoc test as needed. p-values <0.05 were considered to be statistically significant.

Table 1 Antibodies used for histological assessment

	Tissue investigated	Antibody ID	Dilution
α-SMA	Adult	Ab5694 (Abcam)	1:100
GFP	Embryonic/Adult	Ab6673 (Abcam)	1:200
PDGFRα	Adult	AF1062 (R&D systems)	1:100
PDGFRβ	Adult	AF1042 (R&D systems)	1:50
CD31	Embryonic/Adult	Ab28364 (Abcam)	1:200
Vimentin	Adult	Ab92547 (Abcam)	1:500
CD146	Embryonic/Adult	Ab75769 (Abcam)	1:500
S100β	Adult	Ab52642 (Abcam)	1:500
p75NTR	Embryonic/Adult	Ab52987 (Abcam)	1:50
CD105	Embryonic/Adult	MAB1320 (R&D systems)	1:100
SOX10	Embryonic	Ab155279 (Abcam)	1:500

4.3 Results

4.3.1 Foxd1-lineage-positive (FLP) cells are present at the developing secondary palate during embryogenesis

Using a lineage tracing strategy to track Foxd1 derived populations (schematic shown in Figure 4.1A), we investigated the contribution of this lineage to cell populations during early maxillofacial development. Foxd1-lineage-positive (FLP) cells were present within the head, especially at the anterior area/hard palate (median palatine process and nasal process) (Fig. 4.3 B). Within the developing orofacial tissues, FLP cells contributed to various mesenchymal and ectomesenchymal tissues. FLP cells were associated with the mesenchyme within meninges, nasal process of the secondary palate (Fig. 4.3 i, iv), whisker follicles, nasal cartilage (Fig.4.3 iii), the dental mesenchyme, the dental papilla and dental follicle of developing teeth (Fig. 4.3 ii, 4.3 vii), the eye retina and fiber bundles in the extraocular muscles (Fig. 4.3 vi), and the tongue (Fig. 4.3 v). These FLP cells, however, were selective in the cartilages they contribute to, as they were absent from Meckel's cartilage in the mandible (Fig. 4.3 ii). FLP cells were sparsely distributed in lateral maxillary processes, that fuse together with the nasal process to form the secondary palate. FLP cells were not observed in the tissues of the soft palate.

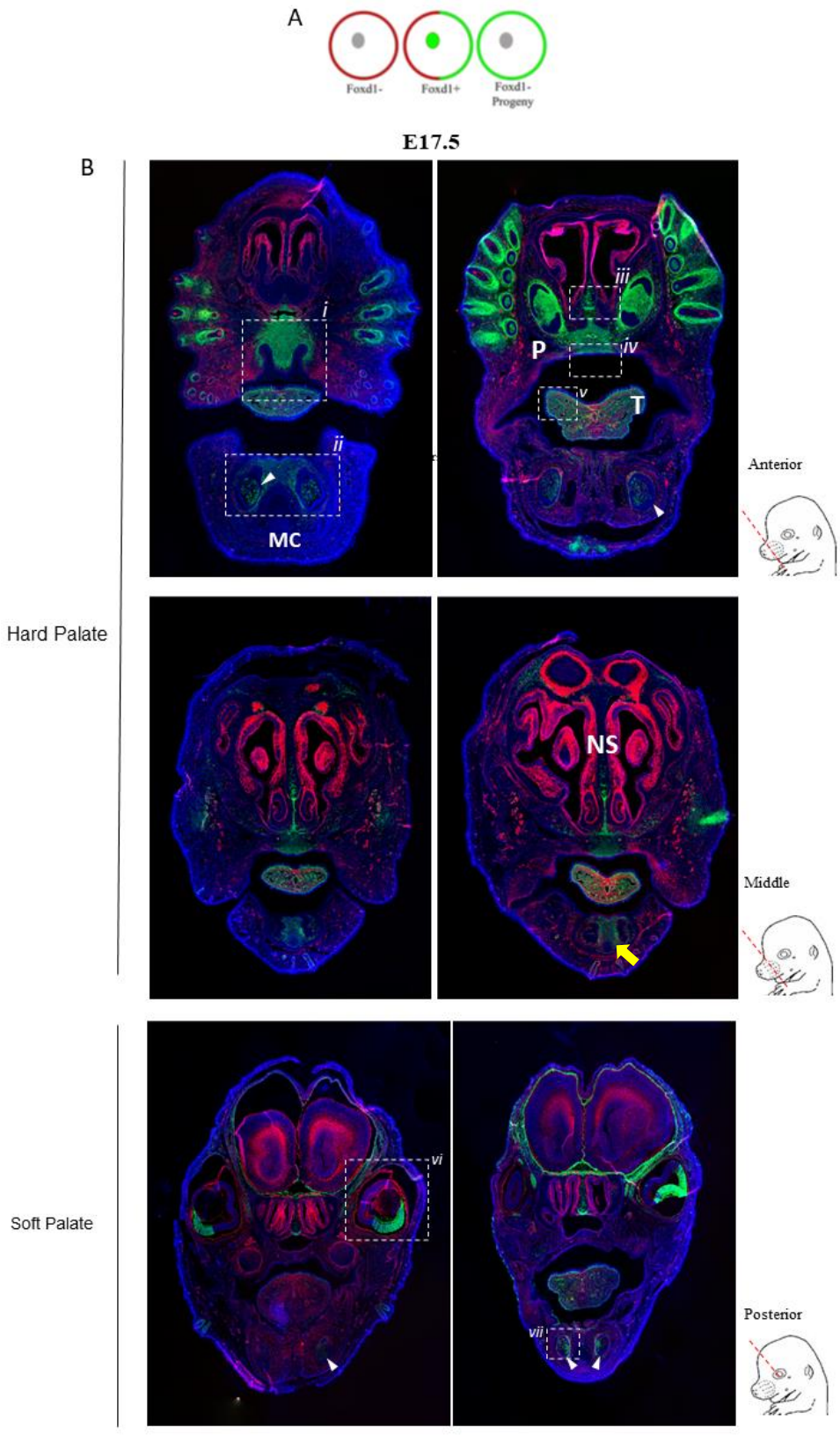
A
Foxd1-
Foxd1+
Foxd1-
Progeny
E17.5
B
i
ii
MC
iii
P
iv
v
T
Anterior
Hard Palate
NS
Middle
vi
vii
Soft Palate
Posterior

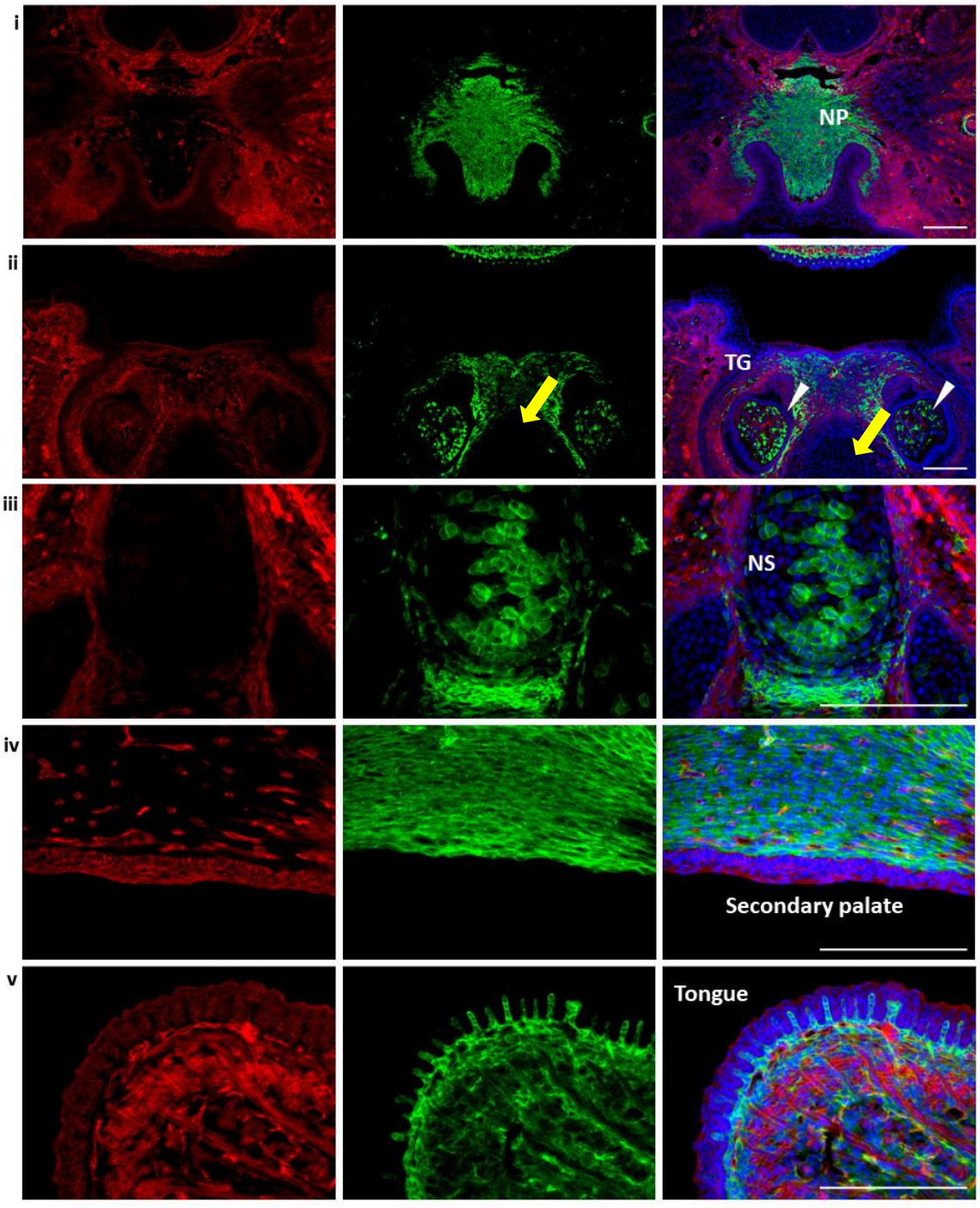
i
NP
ii
TG
iii
NS
iv
Secondary palate
v
Tongue

vi

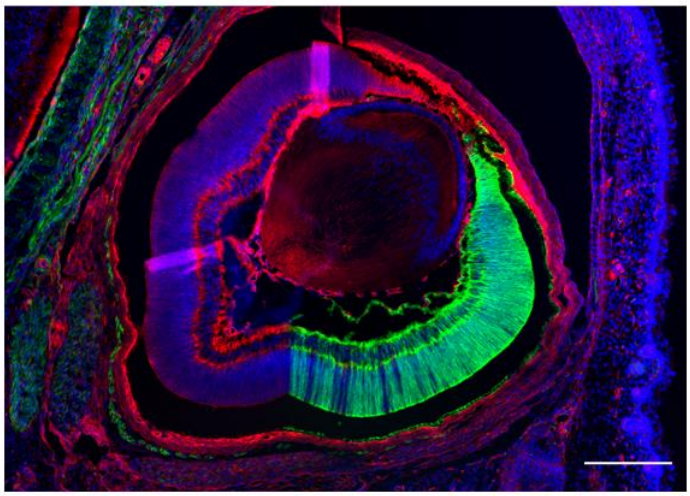

vii

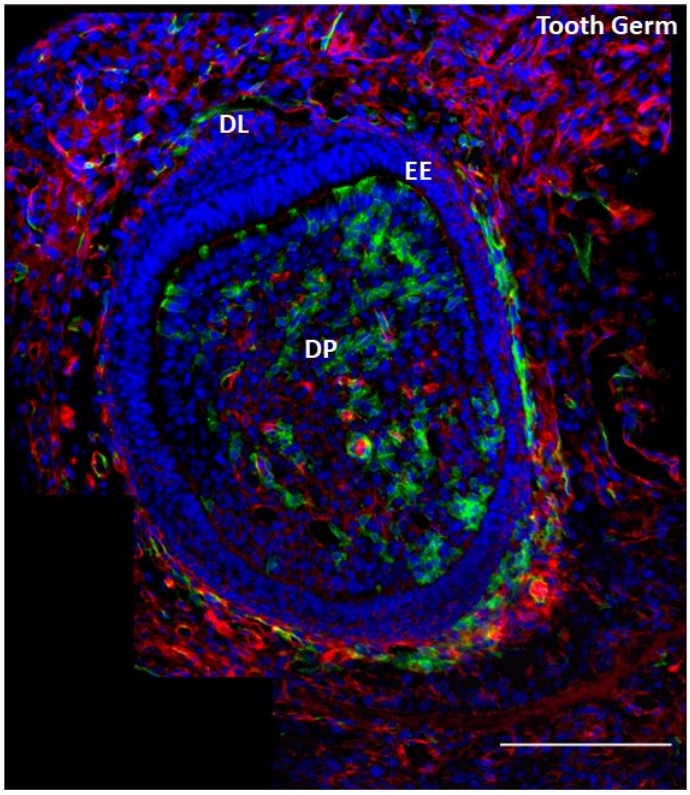

Figure 4-4 Foxd1-positive progenitor cells in the developing embryos contributed to FLP cells within the developing orofacial tissues

(A) *Foxd1GC* mice were crossed with an *mTmG* reporter to investigate FLP (Green) and FLN (Red) contributions to orofacial tissues during embryonic development. **(B)** Embryonic tissues were harvested at E17.5 and sectioned in the frontal plane to include the developing palatal tissues from the anterior (hard palate) to the most posterior (soft palate) part of the palate. FLP cells are present within the head, especially at the anterior part/hard palate, but are not present in the area of the soft palate. Representative images from at least 3 embryos are shown. White arrowheads indicate the developing tooth germs. Yellow arrows indicate the Meckel's cartilage. The areas highlighted in the white rectangle are magnified in the panels *i-vi* below. **NP**= nasal process, **MC**= Meckel's Cartilage, **P**= Palate, **NS**= Nasal Septum, **B**= Brain, **T**=Tongue, **TG**= Tooth Germ, **DL**= Dental Lamina, **EE**=Enamel epithelium, **DP**=Dental Papilla. Scale bar: 200 μm

4.3.2 Foxd1-lineage-positive (FLP) cells contribute to vascular cell populations within the developing secondary palate

To determine the type of cells that are FLP during the various stages of the palatal embryonic development, tissues from embryos heterozygote for both Foxd1GC and Ai14 alleles were labelled for different cell markers associated with vasculature structures and neural crest cells. High magnification images were taken of tissues labelled for CD105 (Fig. 4.4), CD31 (Fig. 4.5) and CD146 (Fig. 4.6) markers for vascular cell lineages. From E12.5 to E17.5 tdTomato positive cells (FLP) show considerable overlap with all tested vascular markers, although Foxd1-lineage-negative (FLN) cells were also noted to label for these markers. Nevertheless, these observations demonstrate that Foxd1-lineage progeny cells are a major contributor to pericytes and endothelial cells for the neovascularization of the developing palatal tissues.

At early stages of murine embryogenesis (E12.5-E14.5) tdTomato-positive cells appear to be negative for SOX10 and p75NTR neural crest markers, indicating that Foxd1-lineage positive cells are not of neural-crest origin (Fig.4.7, 4.8**)**

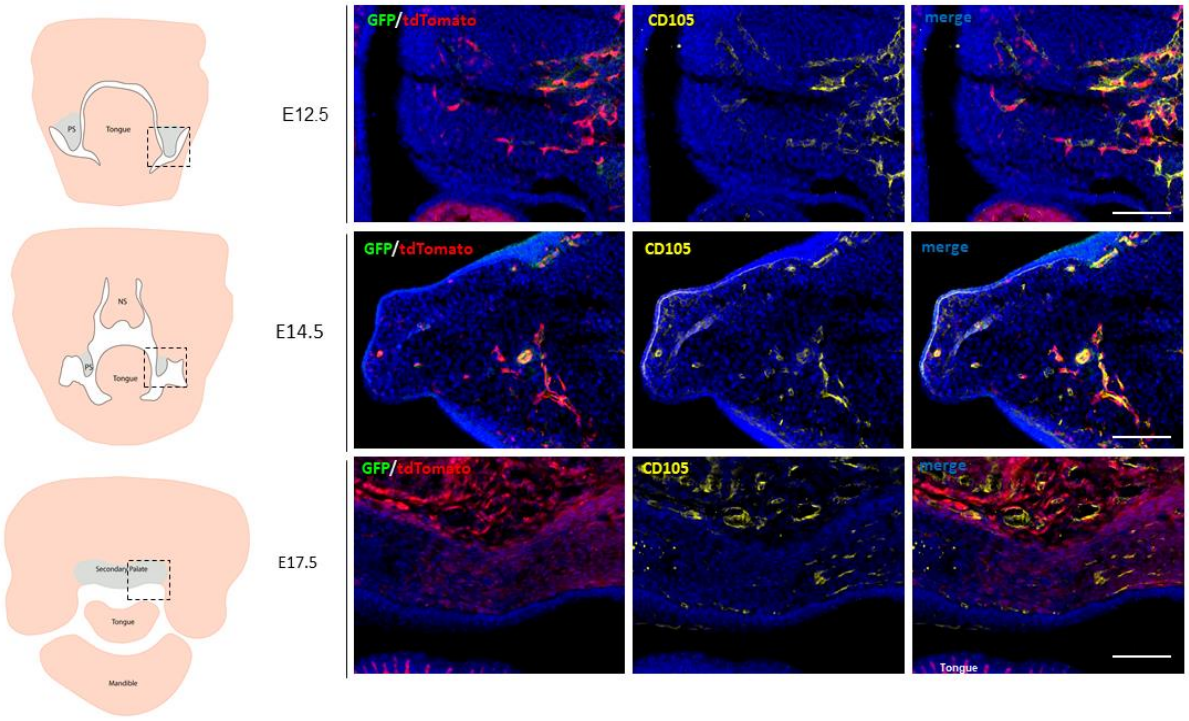

Figure 4-5 Foxd1-positive progenitor cells in the developing embryos contributed to vascular endothelial cells within the secondary palate.

Tissues were stained for CD105 to detect vascular endothelial cells within the palatal tissues from E12.5 to E17.5. Scale bar: 200μm. *On the left*- Schematic representation of murine orofacial tissues at E12.5-E17.5, highlighting with blue the areas that contribute to secondary palate development (palatal processes/shelves). The area in black dashed box indicates the area of interest. (PS: Palatal shelve, NS: Nasal Septum)

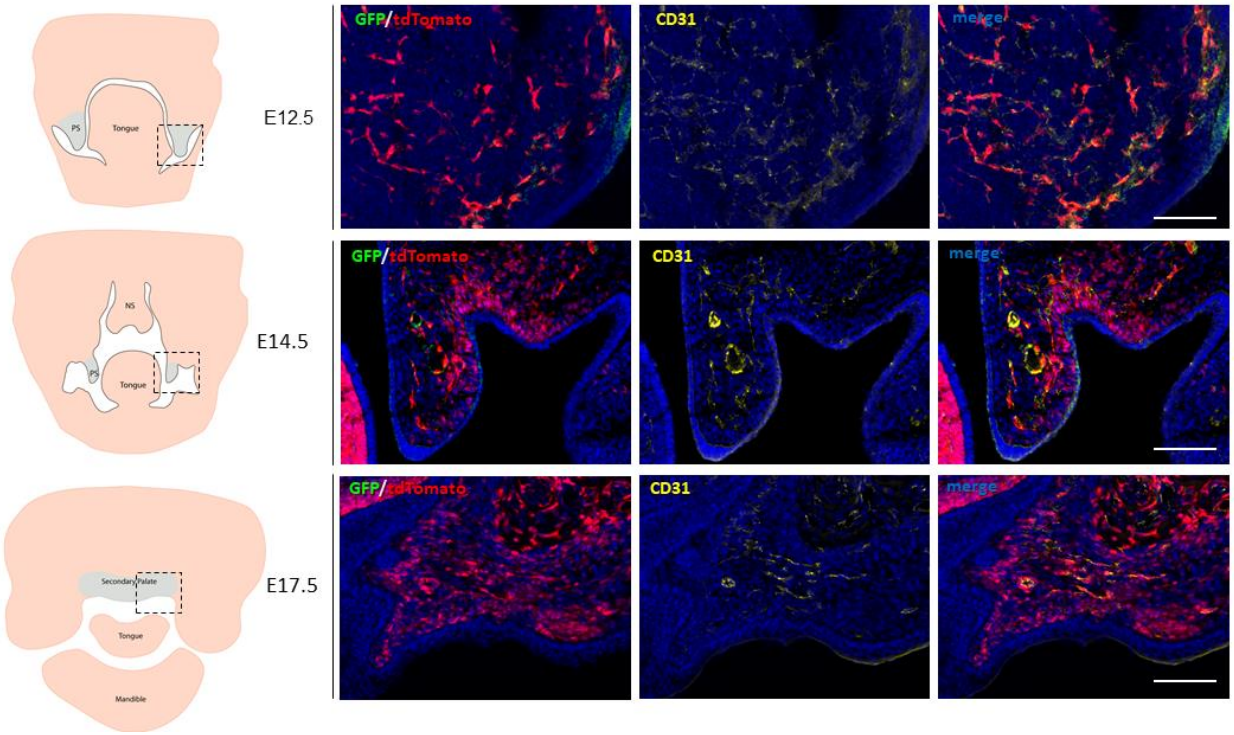

Figure 4-6 Foxd1-positive progenitor cells in the developing embryos contributed to vasculature cells within the secondary palate.

Tissues were stained for CD31 to detect vascular endothelial cells within the palatal tissues from E12.5 to E17.5. Scale bar: 200μm.

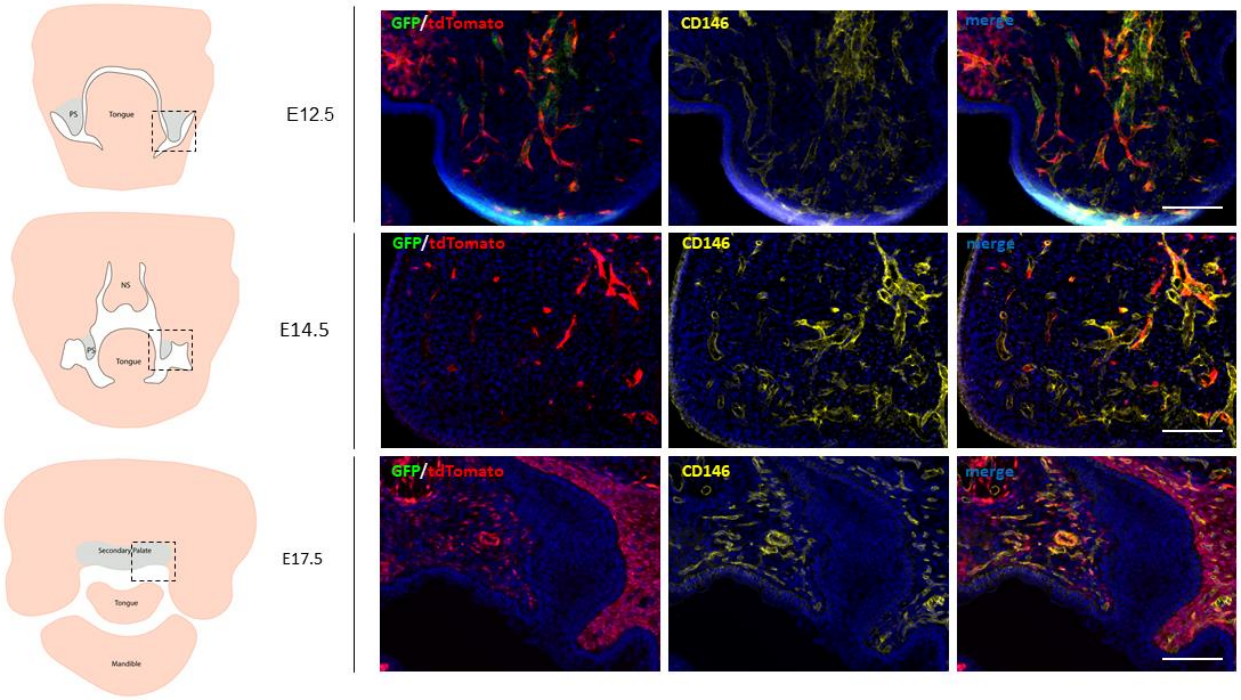

Figure 4-7 During development, FLP cells (red) contribute to vascular cells.

Tissues were stained for CD146 to detect pericytes and endothelial cells within the palatal tissues from E12.5 to E17.5. Scale bar: 200μm.

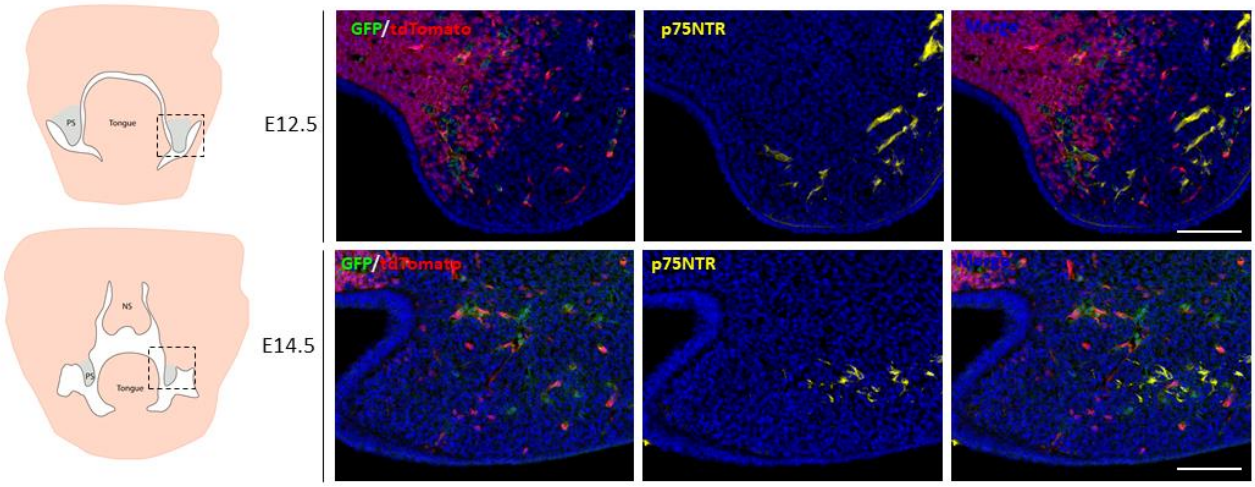

Figure 4-8 During development, FLP cells (red) are not associated with markers of neural crest-derived cell populations.

Tissues were stained for p75NTR to detect post-migratory neural crest cells within the palatal tissues from E12.5 to E14.5. Scale bar: 200μm.

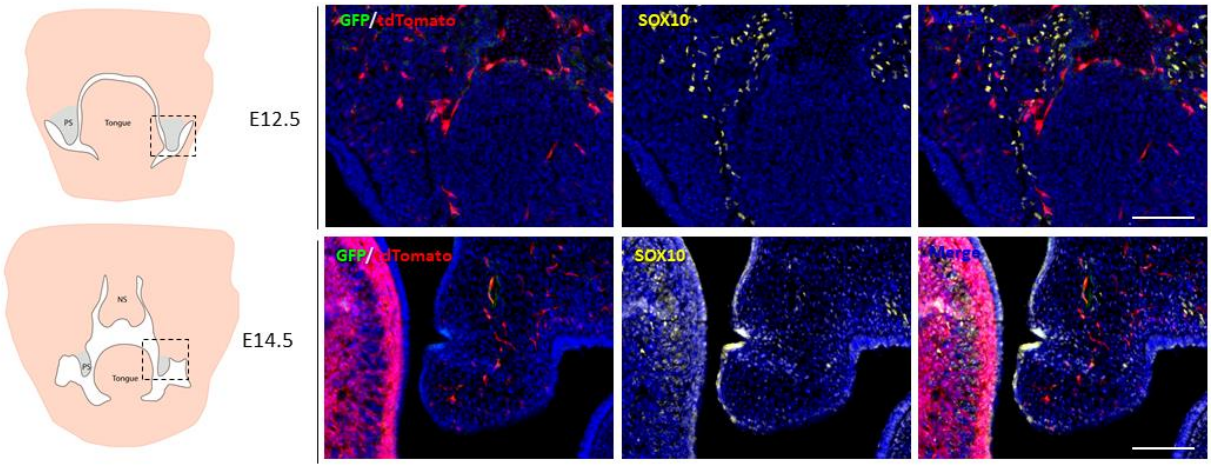

Figure 4-9 During development, FLP cells (red) are not associated with markers of pre-migratory neural crest cell populations.

Tissues were stained for SOX10 to detect neural crest-derived cells within the developing palatal tissues from E12.5 to E14.5. Scale bar: 200μm.

4.3.3 Foxd1-expressing cells are rare in postnatal tissue during homeostasis and following wounding

We employed two different mouse strains to identify perivascular cell localization and lineage tracing within wounded tissue. Both *B6;129S4-Foxd1tm1(GFP/cre)Amc/J,* and the inducible *B6;129S4-Foxd1tm2(GFP/cre/ERT2)Amc/J* strains were bred with *B6.CgGt(ROSA)26Sortm14 (CAG-tdTomato)Hze/J.* Non-inducible mice containing both the Foxd1 driven, Cre-GFP fusion protein, and the Rosa26 driven, tdTomato preceded by a loxp flanked stop codon, express GFP in any cells actively expressing Foxd1, and tdTomato in any cell derived from a Foxd1 positive precursor cell (Foxd1-lineage-positive cells; FLP cells). The inducible strain adds the ability to temporally control when the Cre recombinase is functional through the injection of tamoxifen. Wound repair was assessed following excisional wounding in the palatal mucoperiosteum of these mice and histological analysis was performed to investigate the contribution of Foxd1 positive cells and their progeny in wound healing.

To determine whether Foxd1 is expressed in normal adult palatal mucoperiosteum, palatal tissues were harvested from heterozygote Foxd1GC/Ai14 mice. Recombination in Foxd1-Cre-GFP is constitutively active in cells expressing the Foxd1 promoter, inducing expression of tdTomato driven by the ubiquitously expressed Rosa26 promoter. Foxd1 expression was not observed within the healthy/unwounded palatal samples taken, as indicated by the absence of GFP/Foxd1 signal (Fig. 4.9 B). In the unwounded palatal mucoperiosteum, tdTomato signal was seen in certain cells that were mainly associated with blood vessels and the perineurium of nerves, suggesting that these cells are derived from Foxd1 positive precursors during development [Foxd1-lineage-positive cells (FLP cells)] (Fig. 4.9 B). To determine more specifically which populations these FLP cells were contributing to within the palatal tissues, adult mouse palate was labeled with several markers including the smooth muscle and myofibroblast marker α-SMA (Fig. 4.9 C), the endothelial/pericyte marker CD146 (Fig. 4.9 D), and S100β to identify Schwann cells (Fig.4.9 E). Immunolabelling with α-SMA, CD146 and S100β showed that FLP cells are in close association with blood vessels, where they give rise to some smooth muscle cells

of peripheral veni, pericytes and some endothelial cells. FLP cells also constitute cells of the perineurium of nerves as well as some cell population within the endoneurium (endoneural fibroblasts/pericytes).

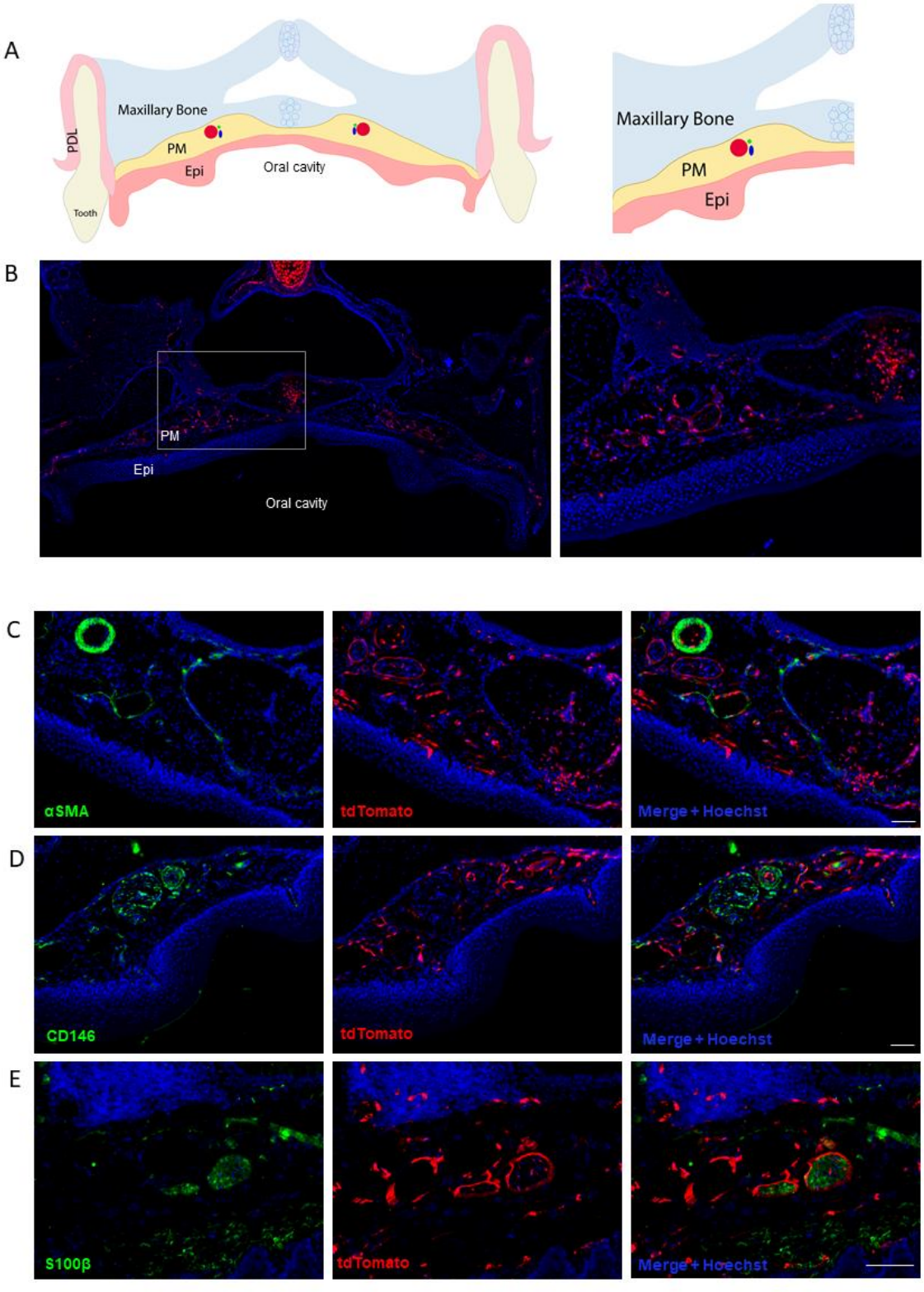
A
Maxillary Bone
PDL
PM
Epi
Oral cavity
Tooth
Maxillary Bone
PM
Epi
B
PM
Epi
Oral cavity
C
αSMA
tdTomato
Merge + Hoechst
D
CD146
tdTomato
Merge + Hoechst
E
S100β
tdTomato
Merge + Hoechst

Figure 4-10 *Foxd1*-positive progenitors give rise to perivascular and perineural populations within the adult palatal mucoperiosteum

To characterize the differentiated populations represented by the Foxd1 lineage, the constitutively active Foxd1GC line crossed to the Ai14 reporter was assessed. **A.** Schematic diagram: Coronal view of the palatal tissues. PM: palatal mucoperiosteum, Epi: oral Epithelium, PDL: periodontal ligament. **B.** Within the unwounded palatal mucoperiosteum Foxd1 positive (green) cells were absent. Derivatives of this population (red -FLP) are sparse in in the unwounded palatal mucoperiosteum and mainly associated with blood vessels and the perineurium of nerves. The area highlighted in the white rectangle is magnified on the right. Adult mouse palatal tissues were labeled for the smooth muscle and myofibroblast marker α-SMA (**C**), the endothelial marker CD146 (**D**), and S100β-marker for Schwann cells (**E**). Scale Bar: 100μm.

4.3.4 Foxd1-expressing cells are absent in postnatal palatal mucoperiosteum following injury

To determine whether Foxd1 expressing cells participate in palatal wound healing, full-thickness excisional wounds were created in the palates of constitutively active *Foxd1*GC/*Ai14* mice. Tissues were harvested at days 6 and 10 post-wounding and the tissues were subjected to histological analysis (N=3 animals/time-point). Upon wounding, GFP-positive cells were absent from the granulation tissue. Our observations were further confirmed by the absence of signal of anti-GFP (Fig. 4.10 A). tdTomato-positive cells (FLP cells) begin to appear at 6 days post wounding within the granulation tissues and increase in density over time to 10 days post wounding (Fig. 4.10 B, C).

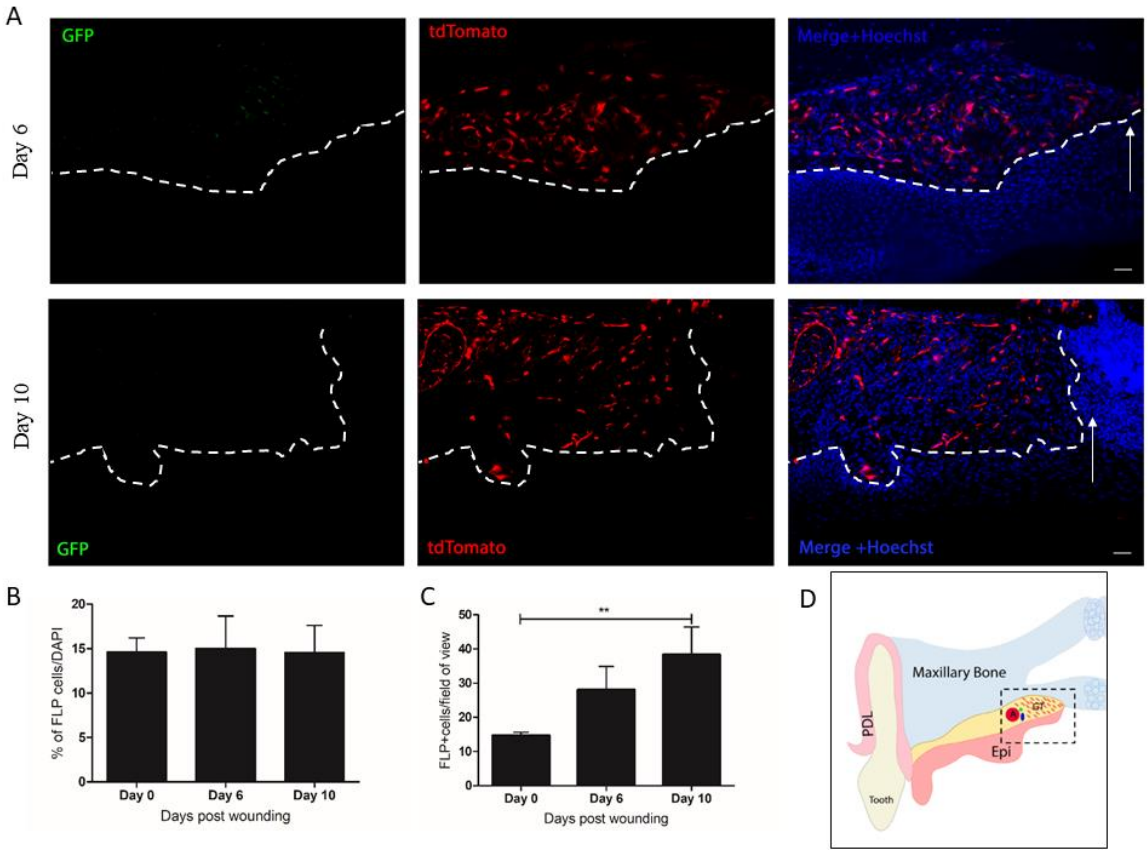

Figure 4-11 Foxd1-expressing cells are absent in postnatal palatal mucoperiosteum following injury

(A) Anti-GFP antibody was used to detect GFP signal in the wounded tissues. Absence of signal verified that GFP (Foxd1) is not expressed in adult tissues upon injury. White arrows indicate the leading edge of the wound. White dashed line indicates the border between the epithelium and the granulation tissue. Scale bar: 100μm. (**B)** Quantification analysis of the tdTomato-positive cells present within the wounded tissues revealed that FLP cells appear at 6 days post wounding within the granulation tissues and increase in density over time to 10 days post wounding. Quantification presented as percentage of FLP cells/total cells (tdTomato/DAPI). **(C)** Quantification presented as percentage of FLP cells/field of view. (**D)** Schematic representation: Coronal view of palatal wounded tissues. The area of interest is highlighted in black dashed box (**Epi**: oral Epithelium, **PDL**: periodontal ligament, **GT**: granulation tissue, **A**: major palatine artery)

4.3.5 Foxd1-lineage-positive cells contribute to diverse populations in adult palatal mucoperiosteum upon injury

To determine more specifically which populations these cells were contributing to, adult mouse wounded palatal tissues from *Foxd1*GC/*Ai14* mice were labeled with smooth muscle and myofibroblast marker α-SMA, several markers expressed in fibroblasts (vimentin, PDGFRα, PDGFRβ), the endothelial marker CD31, the pericyte marker CD146, as well as neural crest-derived cell markers p75NR and S100β (Schwann cells). The FLP cells within the wound tissue were present in the granulation tissue but did not show any overlap with vimentin (Fig. 4.11), PDGFRα, PDGFRβ (Fig. 4.12) and p75NTR markers (Fig. 4.13). Quantification of the α-SMA-positive FLP cells showed that only minimal fraction of FLP cells contribute to the myofibroblast population (unwounded <3%; day 6 <3%; day 10 <4%, N=3 animals/timepoint) (Fig. 4.14).

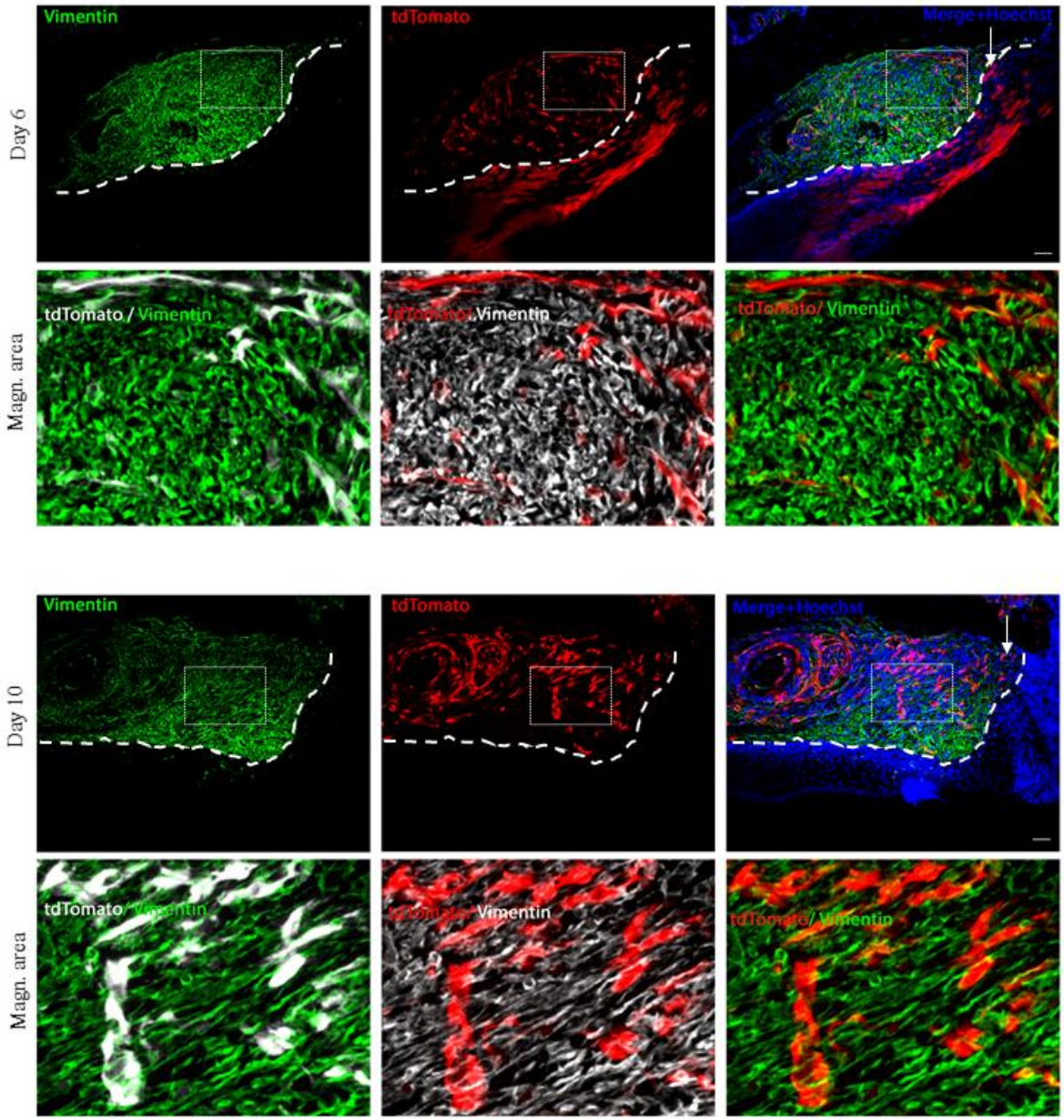
Vimentin
tdTomato
Merge+Hoechst
Day 6
tdTomato / Vimentin
tdTomato/ Vimentin
Magn. area
Vimentin
tdTomato
Merge+Hoechst
Day 10
tdTomato/ Vimentin
Magn. area

Figure 4-12 FLP cells within day-6 and -10 granulation tissue are not associated with Vimentin

FLP cells (tdTomato positive) do not overlap with staining for Vimentin (green) within the granulation tissue. Nuclei are stained with Hoechst dye (blue). Representative images are shown from a sample of 3 mice. White arrows indicate the leading edge of the wound. White dashed lines indicate the border between the epithelium and the granulation tissue. Scale bar: 100μm

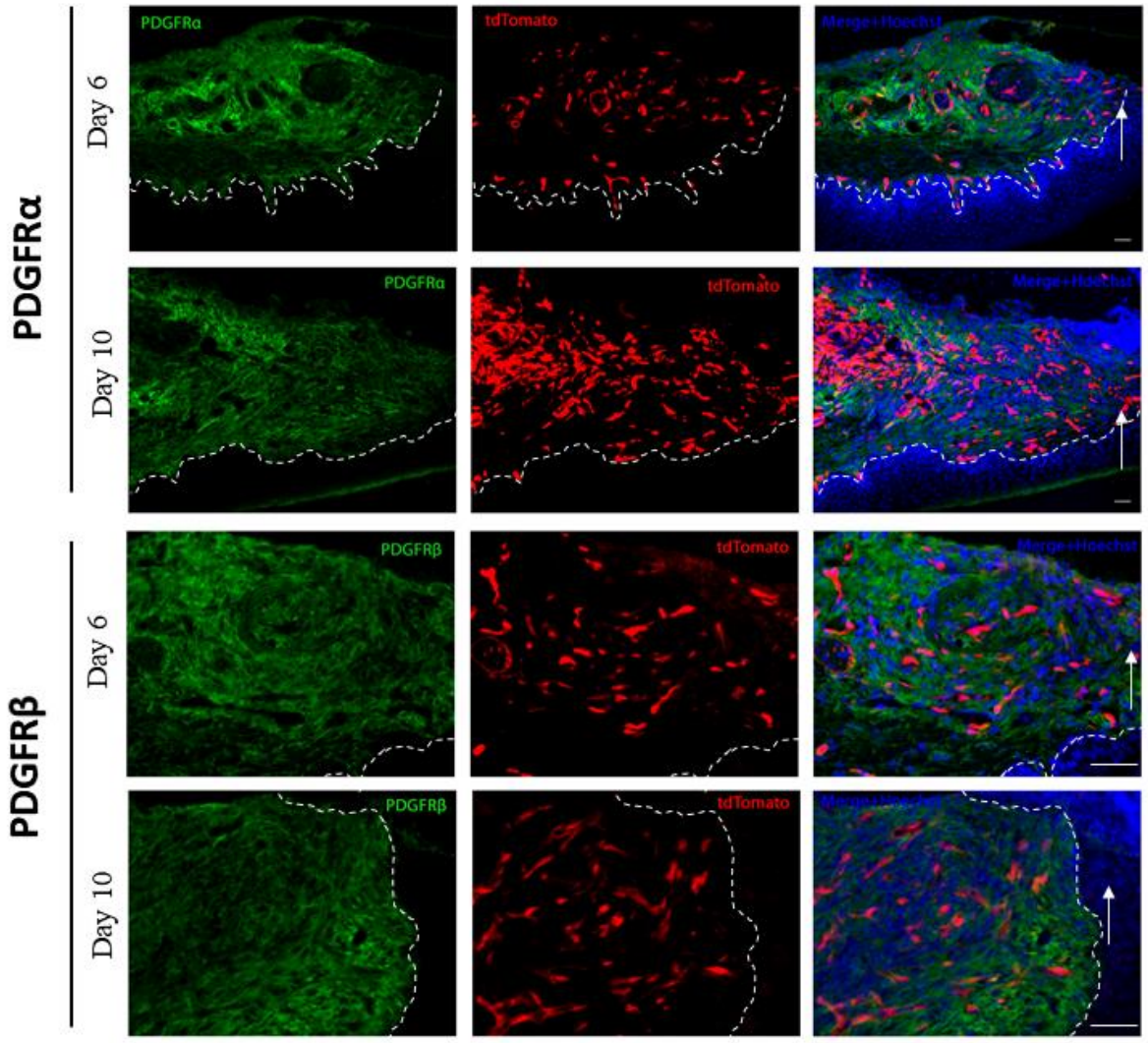

Figure 4-13 FLP cells within day-6 and -10 granulation tissue are not labelled with fibroblast markers

FLP cells (tdTomato positive) do not overlap with staining for fibroblast markers PDGFRα and PDGFRβ (green) within the granulation tissue. Nuclei are stained with Hoechst dye (blue). Representative images are shown from a sample of 3 mice per timepoint. Arrows indicate leading wound edge. White dashed lines indicate the border between the epithelium and the granulation tissue. Scare bar: 100μm.

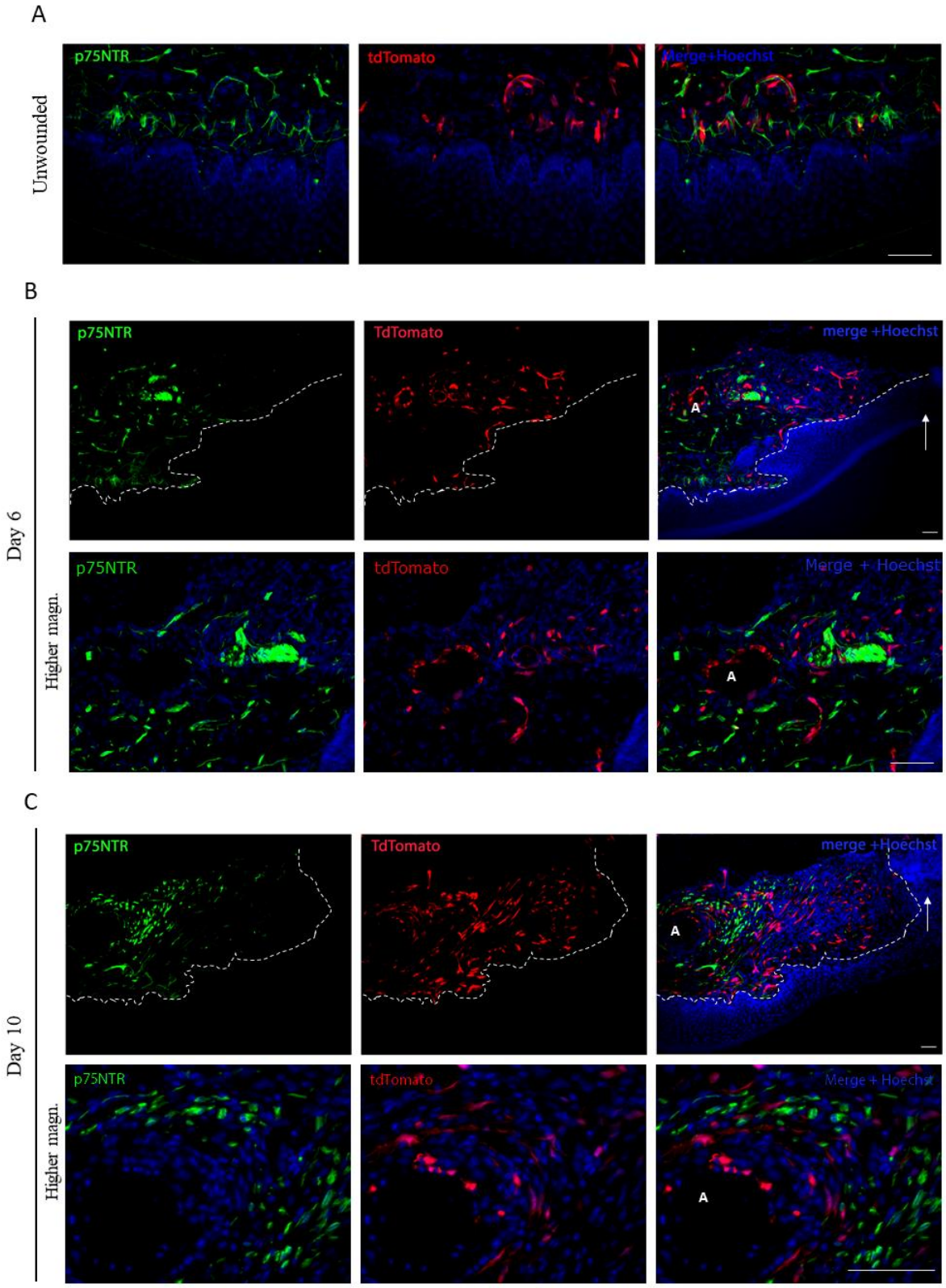
A
Unwounded
p75NTR
tdTomato
Merge+Hoechst
B
Day 6
p75NTR
TdTomato
merge +Hoechst
A
Higher magn.
p75NTR
tdTomato
Merge + Hoechst
A
C
Day 10
p75NTR
TdTomato
merge +Hoechst
A
Higher magn.
p75NTR
tdTomato
Merge + Hoechst
A

Figure 4-14 FLP cells are not associated with p75NTR-positive cell populations.

Immunofluorescent staining for neural-crest derived cells p75NTR (green) at normal, unwounded palatal tissues (**A**), days 6- (**B**) and 10- (**C**) post wounding, did not reveal any overlap between tdTomato and p75NTR suggesting that FLP cells are not neural-crest derived. Representative images are shown from a sample of 3 mice per timepoint. Arrows indicate leading wound edge. White dashed lines indicate the border between the epithelium and the granulation tissue. Scare bar: 100μm

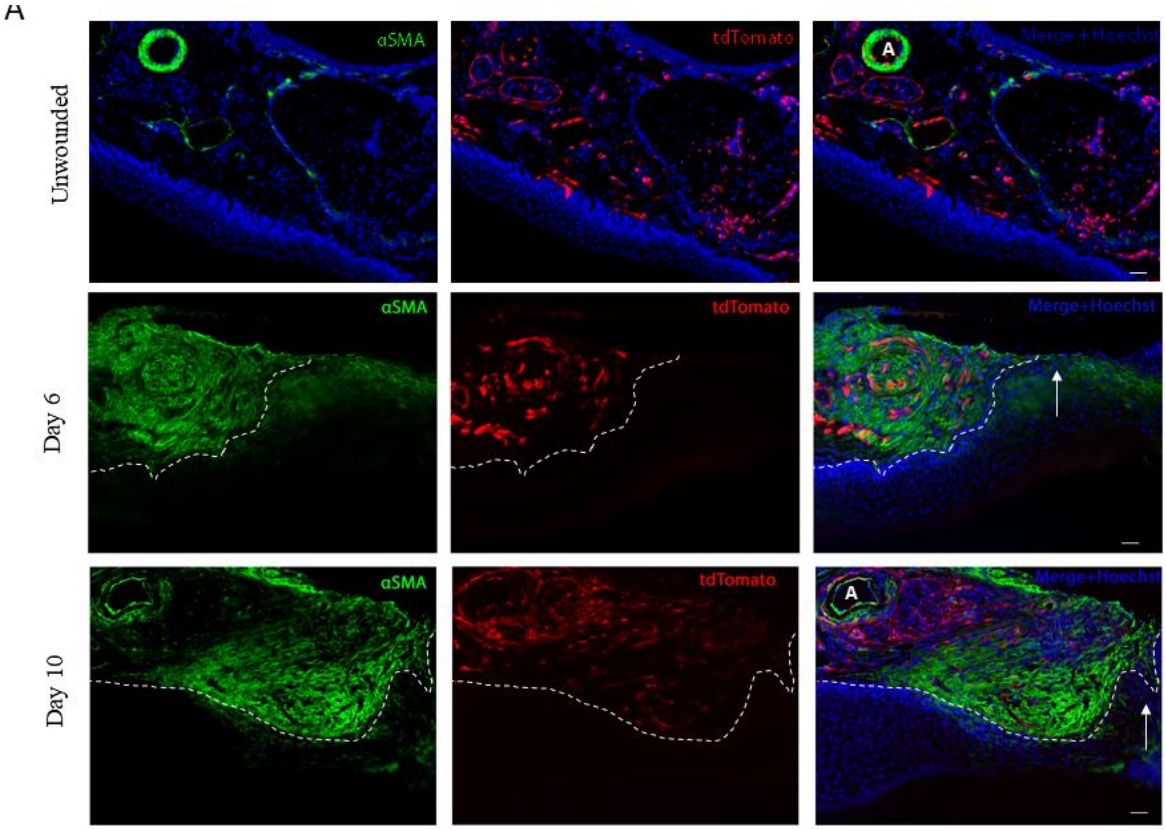
A
Unwounded
Day 6
Day 10
αSMA
tdTomato
Merge+Hoechst
A

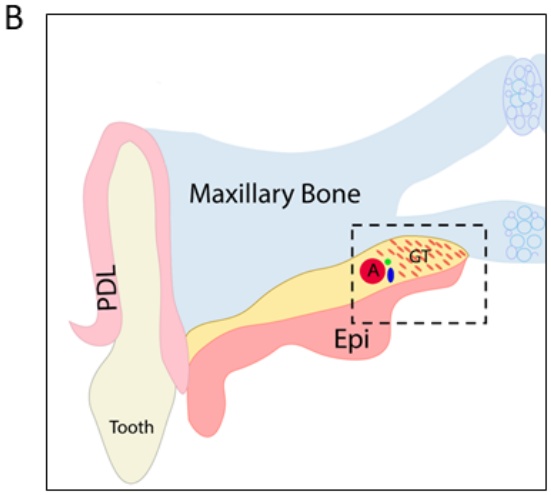
B
Maxillary Bone
PDL
GT
A
Epi
Tooth

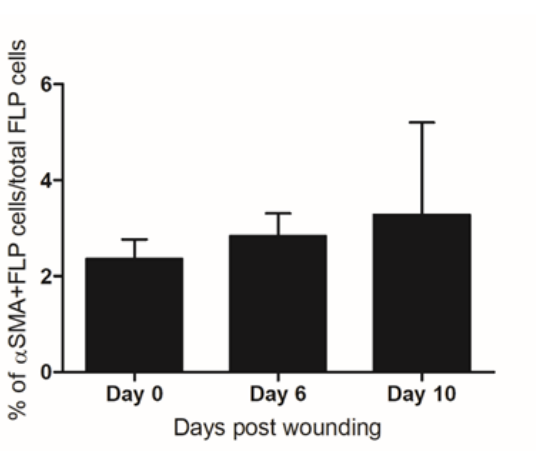
C
% of αSMA+FLP cells/total FLP cells
6
4
2
0
Day 0
Day 6
Day 10
Days post wounding

Figure 4-15 FLP cells are not a significant contributor to the myofibroblast population during wound repair.

(A) In normal, unwounded palatal tissues derivatives of this population (red) are sparse and mainly associated with blood vessels, as shown by the co-localization of the signal with α-SMA. Foxd1-lineage-positive cells begin to appear at 6 days post wounding at the wound edge and increase in density over time to 10 days post wounding. These cells do not contribute to the myofibroblast population as shown by the absence of overlap between tdTomato and α-SMA. White arrows indicate the leading edge of the wound. White dashed lines indicate the border between the epithelium and the granulation tissue. Scale bar: 100μm. (**B)** Schematic representation: Coronal view of palatal wounded tissues. The area of interest is highlighted in black dashed box (Epi: oral Epithelium, PDL: periodontal ligament, GT: granulation tissue, A: major palatine artery). (**C)** Quantification presented as percentage of α-SMA-positive FLP cells/total FLP cells showed that only minimal fraction of FLP cells contribute to the myofibroblast population (unwounded < 3%; day 6 < 3%; day 10 < 4%, N=3 animals/timepoint)

To determine whether FLP cells contribute to emerging populations of neural cells that enter the granulation tissue as it matures, we used the Schwann marker S100β. The histological analysis revealed that S100β+ cells are absent within the granulation tissue (Fig. 4.15A, B). Quantification analysis of S100β+FLP cells distal to the wound, in close proximity to the neurovascular bundle of the palate, showed that S100+FLP cells constitute only a minor part of the FLP population in normal tissue and at early stages of wound healing-day 6 (<3%, N=3 animals/timepoint), while their density increased by day 10 (9%, N=3 animals/timepoint).

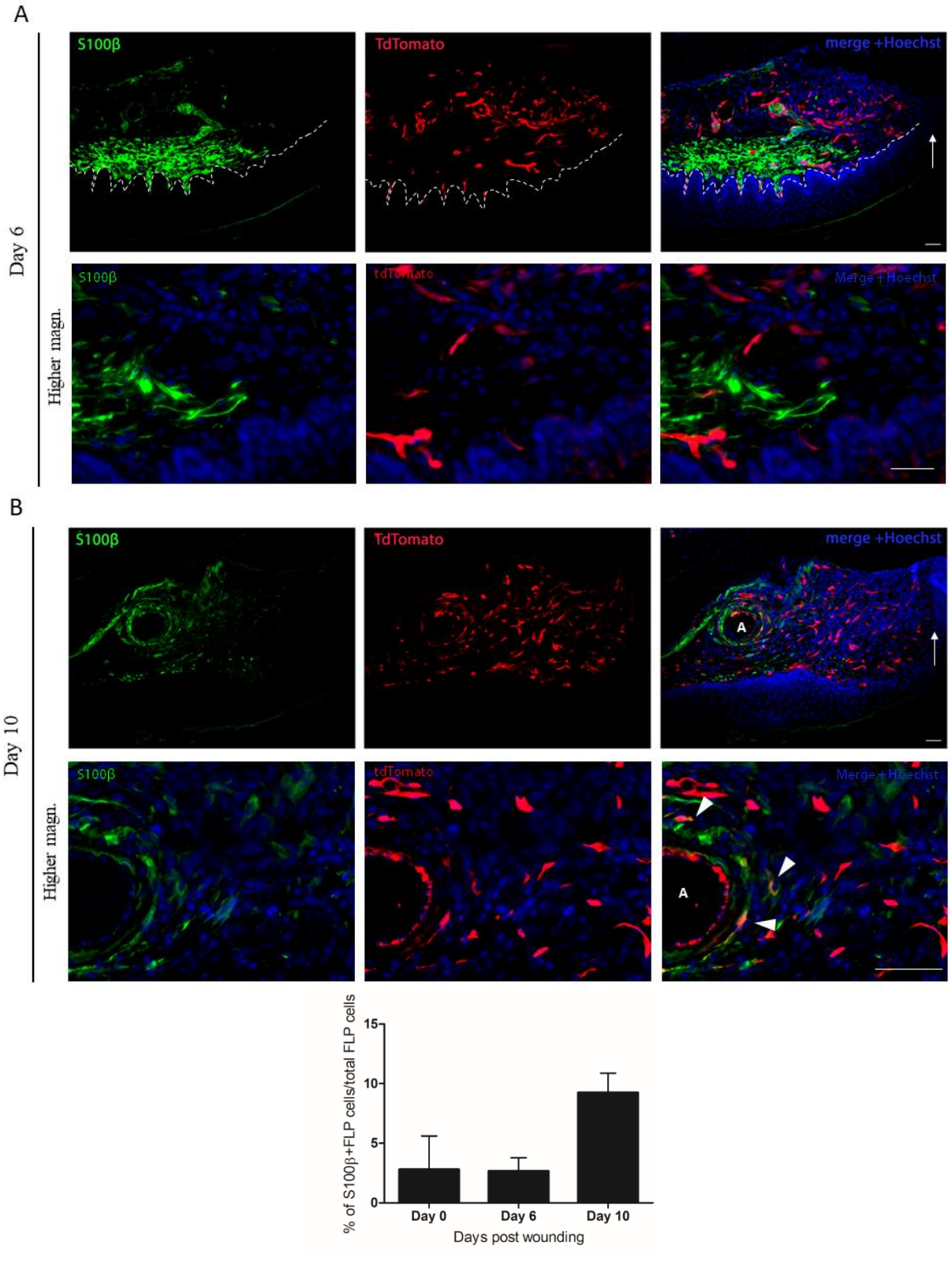
A
S100β
TdTomato
merge +Hoechst
Day 6
Higher magn.
S100β
tdTomato
Merge +Hoechst
B
S100β
TdTomato
merge +Hoechst
A
Day 10
Higher magn.
S100β
tdTomato
Merge +Hoechst
A
% of S100β+FLP cells/total FLP cells
15
10
5
0
Day 0
Day 6
Day 10
Days post wounding

Figure 4-16 S-100 β immunofluorescent staining

S100 β -positive cells emerge from the distal side of the wound and are absent from the granulation tissue and FLP cells only minimally contribute to S100β+ populations distal to the wound. Immunofluorescent staining for S100β (green) at days 6 **(A)** and 10 post wounding **(B).** White arrows indicate the leading edge of the wound. White dashed lines indicate the border between the epithelium and the granulation tissue. White arrowheads indicate FLP cells positive for S100β marker, as indicated by the colocalization of the signal. Scale bar: 100μm. Quantification presented as percentage of S100-positive FLP cells/total FLP cells. N=3 animals/timepoint.

4.3.6 Foxd1 lineage progeny contribute to vascular cell populations during wound repair

To determine which populations these cells were contributing to, adult mouse wounded palatal tissues were labeled with markers for vascular cells (endothelial cells, pericytes). In unwounded tissues less than 3% of FLP cells were positive for CD31 marker. Interestingly, post-wounding a significant overlap between tdTomato (FLP cells) and CD31 was observed, suggesting that FLP cells significantly contribute to the increasing endothelial population post-wounding (>40% of FLP cells were found to be CD31 positive) (Fig. 4.16). However, it was evident that the FLP population only give rise to a subset of these populations, with FLN cells also contributing.

Similar observations were made when the pericyte -CD146 and Endoglin-CD105 markers were utilized (Fig. 4.17-4.18).

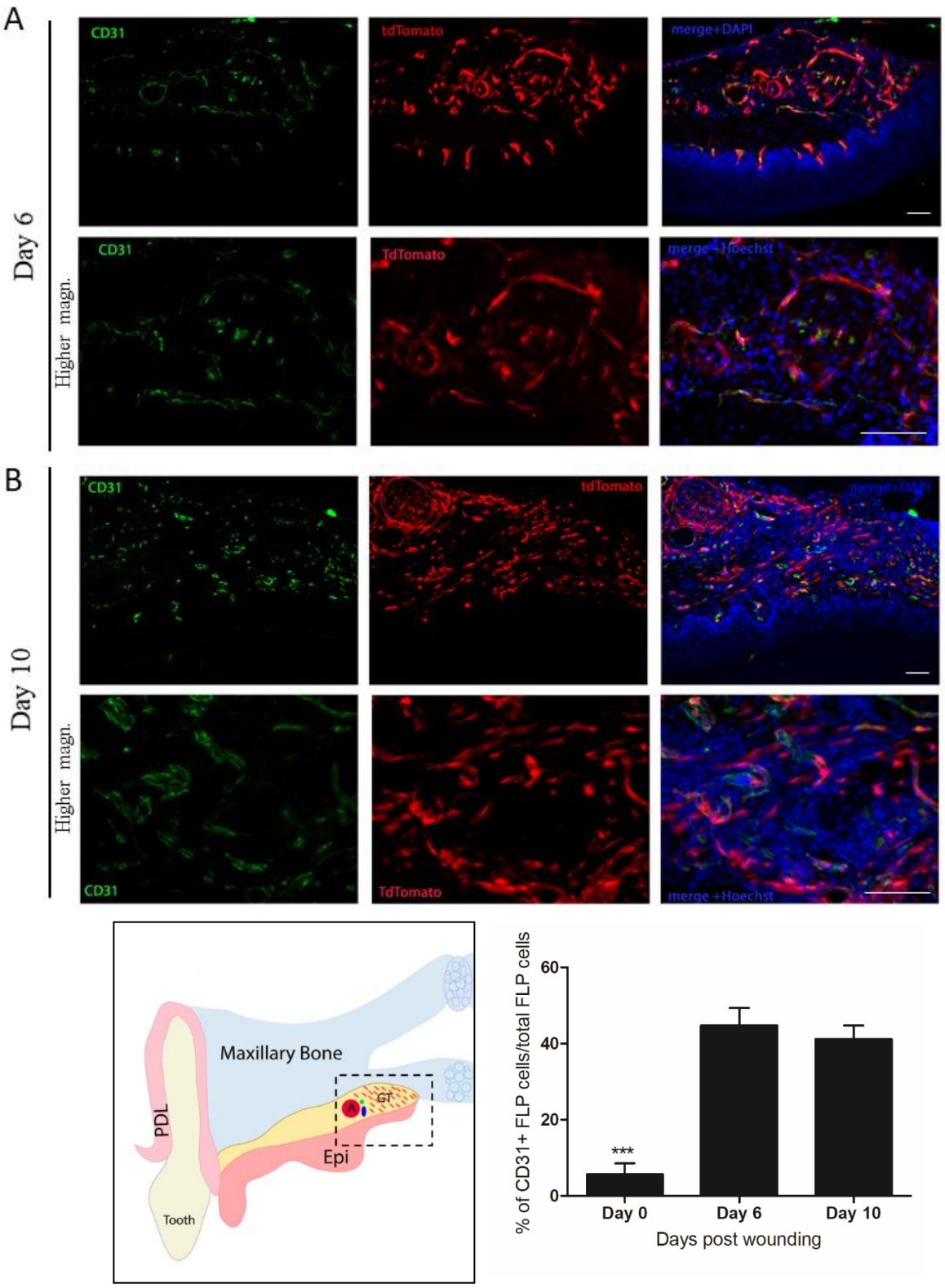
A
Day 6
CD31
tdTomato
merge+DAPI
Higher magn.
CD31
TdTomato
merge +Hoechst
B
Day 10
CD31
tdTomato
Higher magn.
CD31
TdTomato
merge +Hoechst
Maxillary Bone
PDL
GT
A
Epi
Tooth
% of CD31+ FLP cells/total FLP cells
60
40
20
0
***
Day 0
Day 6
Day 10
Days post wounding

Figure 4-17 FLP cells within day-6 and -10 granulation tissue contribute to CD31+ populations within the wounded tissues

Immunofluorescent staining for CD31 (green) at days 6 **(A)** and 10 **(B)** post-wounding. Scale bar: 100 μm. Quantification presented as percentage of CD31-positive FLP cells/total FLP cells. Data were analyzed using 1-way ANOVA and Tukey post hoc test. N=3 (*** $P < 0.001$)

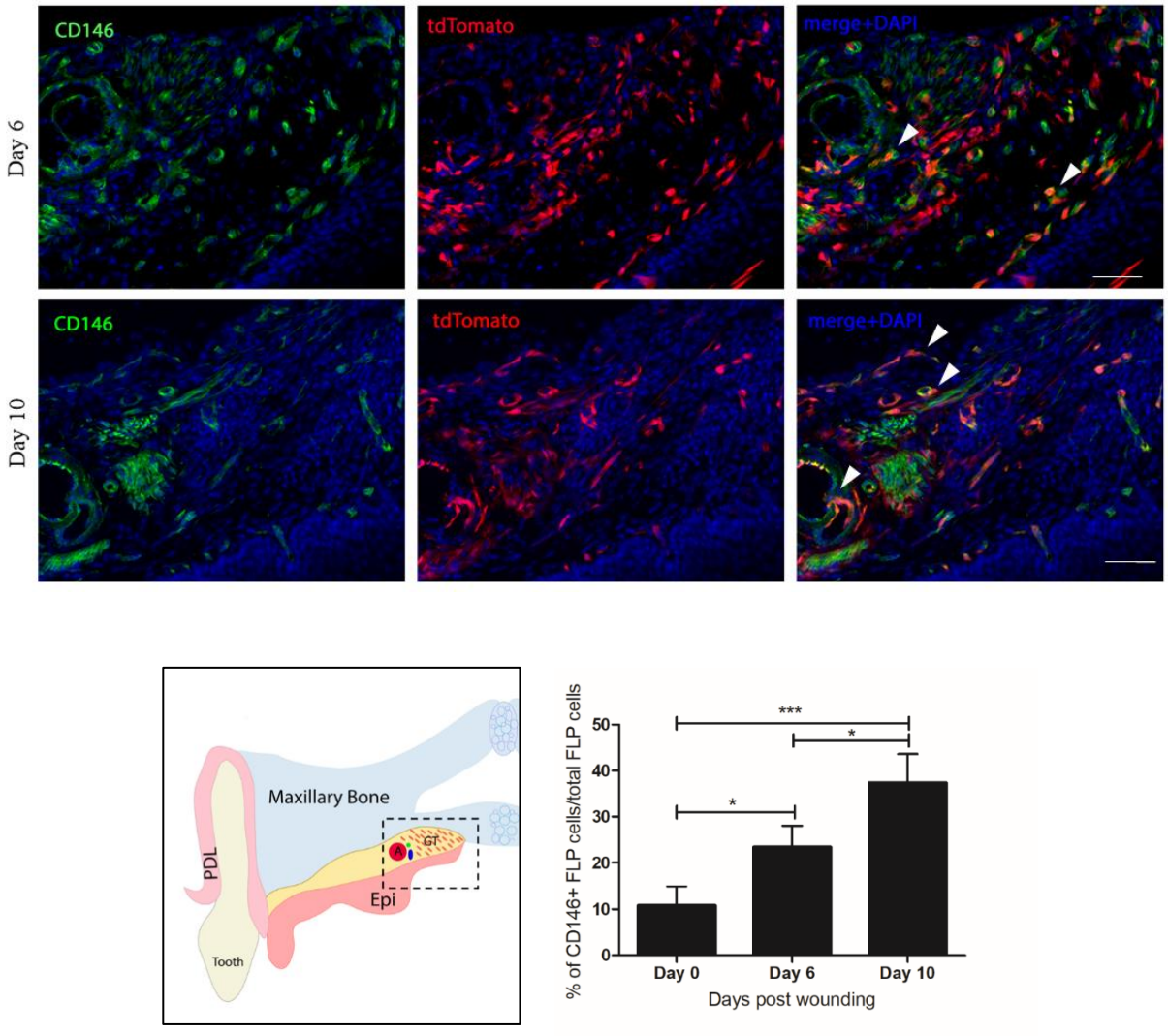

Figure 4-18 FLP cells within day-6 and -10 granulation tissue contribute to CD146+ populations within the wounded tissues

Immunofluorescent staining for CD146 (green) at days 6 and 10 post-wounding. White arrowheads indicate representative cells with dual labeling between FLP cells and CD146-positive cells Scale bar: 100 μm. Quantification presented as percentage of CD146-positive FLP cells/total FLP cells. Data were analyzed using 1-way ANOVA and Tukey post hoc test. N=3 (* $P < 0.05$, *** $P < 0.001$)

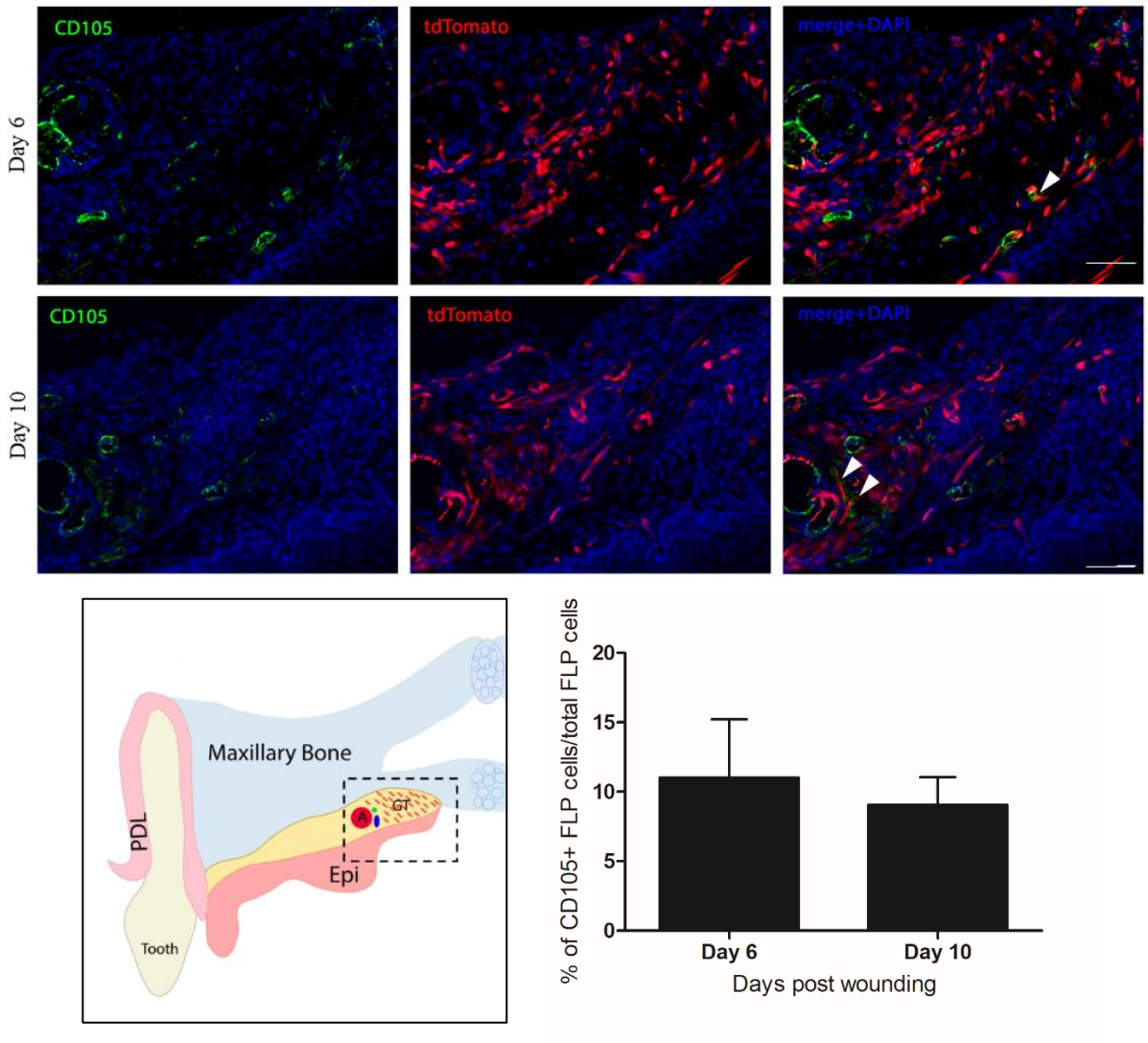

Figure 4-19 FLP cells within day-6 and -10 granulation tissue contribute to CD105+ populations within the wounded tissues

Immunofluorescent staining for CD105 (green) at days 6 and 10 post-wounding. White arrowheads indicate representative cells with dual labeling between FLP cells and CD105-positive cells. Scale bar: 100 μm. Quantification presented as percentage of CD105-positive FLP cells/total FLP cells. N=3

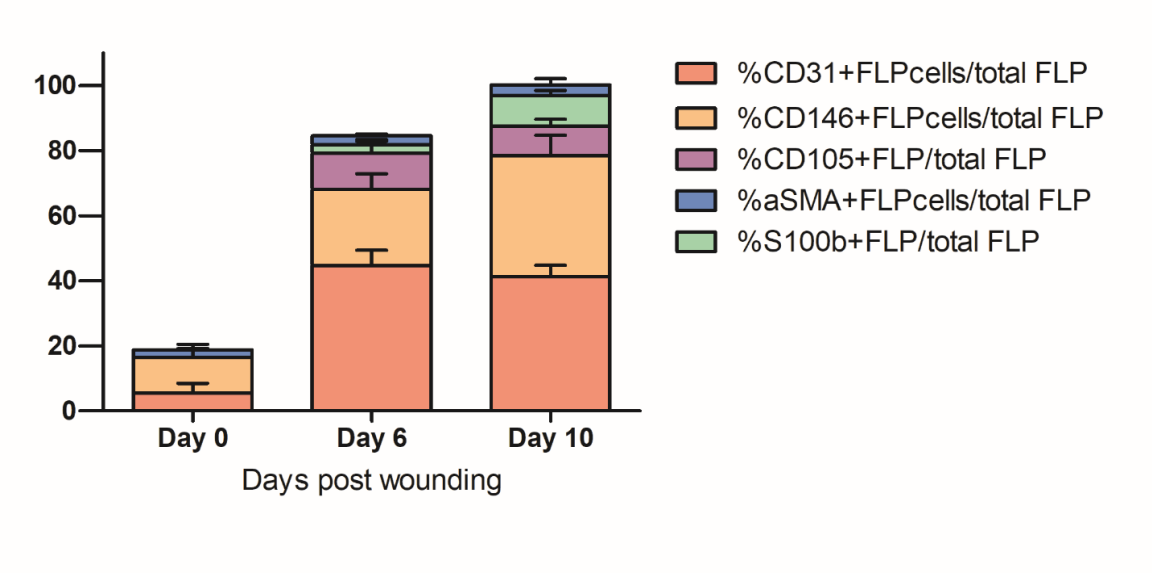

Figure 4-20 Overall contribution of FLP cells

Quantification presented as percentage of selected-marker-positive FLP cells/total FLP cells at normal and wounded palatal tissues at days 6 and 10 post-wounding.

4.3.7 Foxd1-linage-positive cells can adopt a fibrotic phenotype in culture

To determine whether these populations could be further investigated in a controlled culture environment, explant cultures from adult palatal mucoperiosteum from *Foxd1*GC/*Ai14* mice were established and the effect of culturing on substrates of different elastic modulus was investigated. First, we tested whether tdTomato+ cells can be detected and expanded in culture. Quantification analysis of tdTomato+ (FLP) and tdTomato- (FLN) cells after expansion in explant cultures for 2 weeks did not reveal any differences in expansion potential,as both FLP and FLN cells were present in similar numbers in culture (FLP 46.41%, FLN 53.59%, N=3). It is interesting that even though in adult, unwounded tissues these cells compose a small percentage of cells, in culture they are able to expand.

To explore the contribution of microenvironment stiffness on cellular behavior, cells were seeded on silicone substrate with high Young's elastic modulus (0.2 kPa) and tissue culture plastic (low elastic modulus, high stiffness; TCP), and α-SMA expression and localization on the stress fibers was evaluated using immunolabeling. Both FLP and FNL populations assumed a fibroblastic phenotype in culture, with incorporation of α-SMA in the stress fibers. After 24h, FLP and FNL cells assumed differentiated myofibroblast characteristics with α-SMA-positive stress fibers when cultured on a high stiffness tissue culture plastic (TCP), while on low stiffness (0.2 kPa) substrates the cells were characterized by poor spreading and exhibited no contractile bundles (Fig. 4.20).

These observations indicate that FLP cell populations do not maintain their characteristics when in culture but rather they can differentiate into myofibroblasts in an environment of increased stiffness.

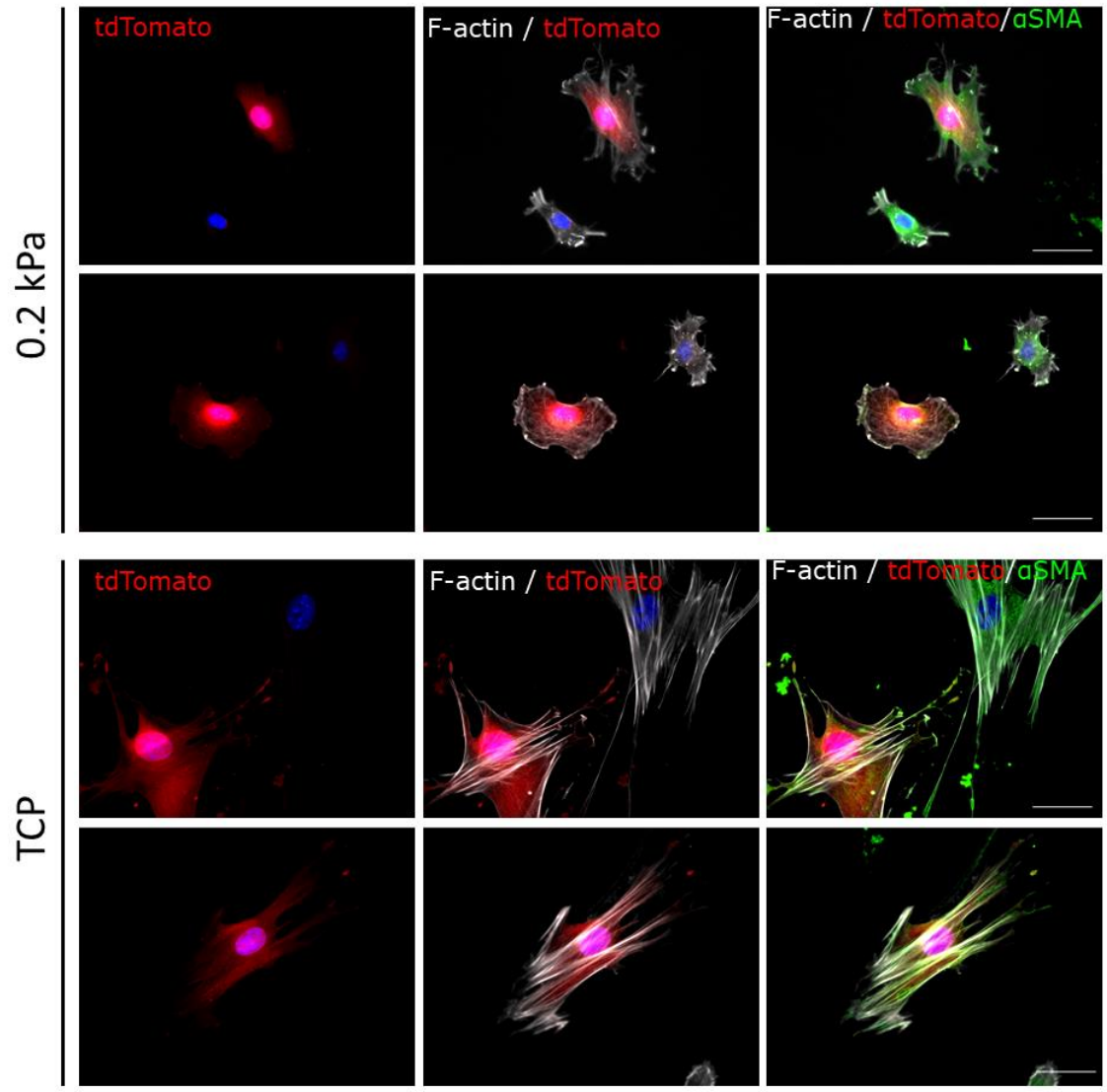

Figure 4-21 FLP and FLN cells in vitro assumed a fibroblastic phenotype

Cells were cultured on silicon substrates with 0.2 kPa Young's modulus of elasticity top rows) or TCP (bottom rows) and stained for α-SMA protein (green). Nuclei were labelled with Hoechst (blue), F-actin in white Scale bar is 20 μm.

4.3.8 FLP populations in adult palate and granulation tissue were not derived from de novo Foxd1 expression in postnatal tissue.

To determine if postnatal expression of Foxd1 was contributing to the FLP populations observed in these tissues, recombination in a tamoxifen inducible Cre model was investigated by crossing the *Foxd1GCE* line with the *Ai14* reporter. Tamoxifen was delivered to postnatal mice after wounding and tissues were harvested for histological assessment of recombination at days 6 and 10 post-wounding. Histological images revealed the absence of recombination, as indicated by the lack of cells expressing tdTomato (N=2) (Fig. 4.21).

Combined with the expression patterns observed during embryogenesis, these data suggest that the FLP cells present within the palatal mucoperiosteum were primarily derived from embryonic precursors that expressed *Foxd1*, and that *de novo* expression of *Foxd1* in postnatal palate during homeostasis and wound healing was absent.

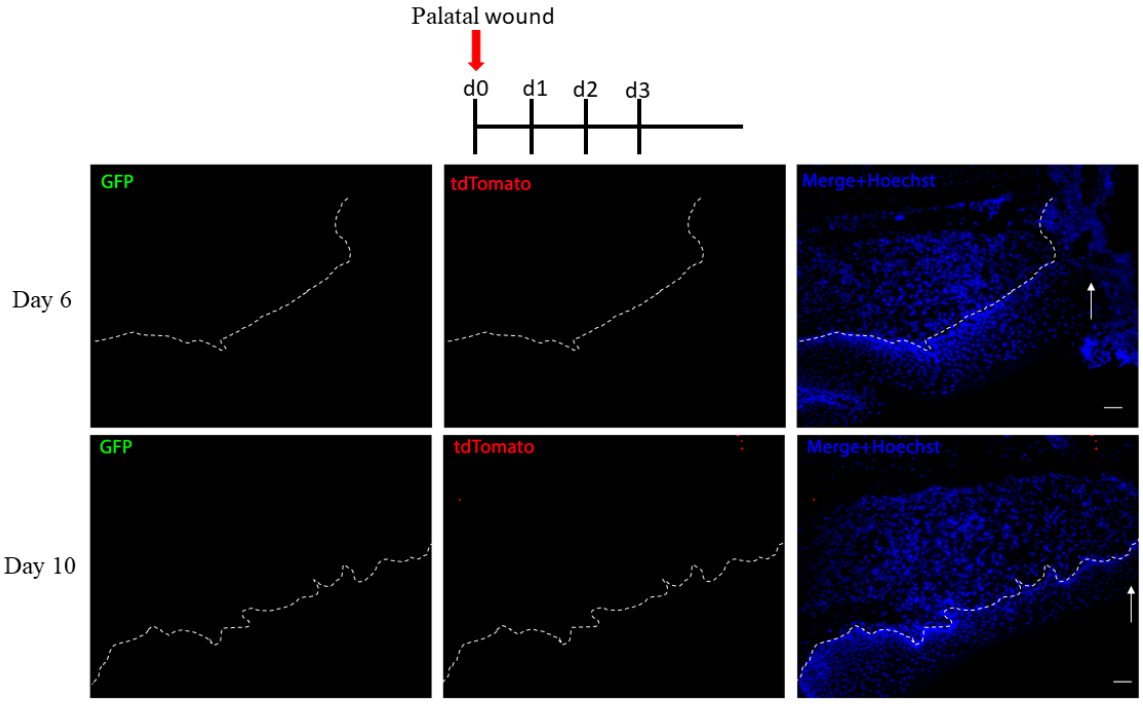

Figure 4-22 FLP populations in granulation tissue were not derived from de novo *Foxd1* expression in postnatal tissue

In a tamoxifen inducible model utilizing the Foxd1GCE/Ai14 cross, tamoxifen injection into postnatal tissue did not yield any tdTomato positive cells (N=2) Scale bar= 100 μm

4.3.9 NG2-lineage-positive cells contribute to mesenchymal cells and myofibroblast populations within the wounded palatal mucoperiosteum

In the palate, the two greater palatine arteries contribute to the blood supply of the hard palate. Observations from our current data suggest that Foxd1-positive-lineage cells have higher density near the greater palatine arteries, at the proximity of the wound. Thus, we hypothesize that these arteries could be a potential source for these cells. To investigate whether arterial endothelial cells contribute to wound healing in the palate, *NG2-cre-GFP* and the inducible *NG2-CreERT2-GFP* mouse strains was used. Cspg4 – or NG2, is a cell surface chondroitin sulfate proteoglycan identified as a marker for vascular pericytes (Bergers & Song, 2005; Cooke et al., 2012; Ozerdem et al., 2001; You et al., 2014)

In normal unwounded palatal tissues, NG2-positive (GFP-positive) cells are absent and NG2-lineage-positive cells (in red) appear throughout the connective tissue. Upon wounding, GFP-positive cells are absent from granulation tissue at day 6 post-wounding, while NG2-lineage-positive cells appear throughout the palatal connective tissue, vascular structures within the maxillary bone and the granulation tissue (Fig. 4.22).

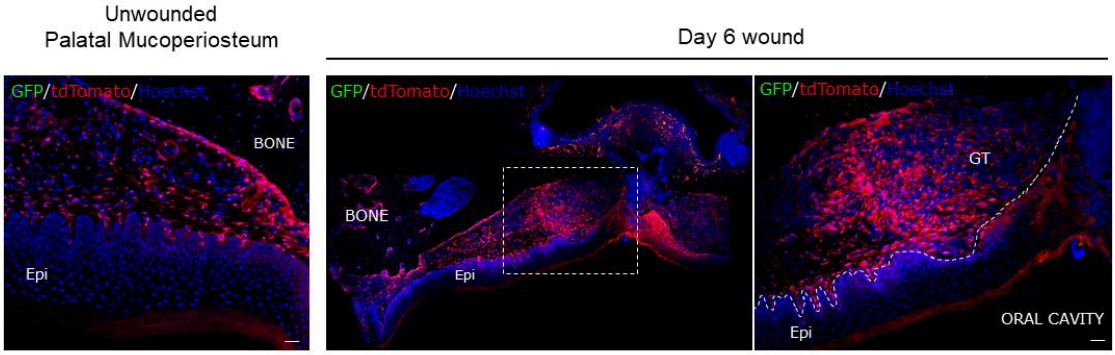

Figure 4-23 NG2-lineage-positive cells gave rise to most of the cell populations within the connective tissues of the adult palatal mucoperiosteum.

Unwounded and wounded tissues 6 days post-wounding palatal tissues were isolated from mice expressing NG2-cre-GFP and Ai14 alleles. Merged images show tdTomato (NG2-lineage-positive) cells in red and nuclei are labelled with Hoechst in blue. The area highlighted in the white rectangle is magnified on the right. **Epi**= oral Epithelium, **GT**= Granulation Tissue. Scale bar= 100 μm. (N=2)

To determine more specifically which populations these cells were contributing to within the dermis, palatal wounded tissues were labeled with mesenchymal cell marker vimentin, and the smooth muscle and myofibroblast marker α-SMA. Both markers partially overlapped with tdTomato expression, however tdTomato negative populations were also noted to label for these markers (Fig. 4.23). Schwann cells are glial cells that produce the myelin sheath around nerve axons of the peripheral nervous system and are essential in maintaining normal nerve function (Jessen & Mirsky, 2005). Schwann cell reprogramming and differentiation are required for neuronal regeneration and re-myelination to occur following injury to peripheral nerves (Gonçalves et al., 2019). Minimal overlap between tdTomato and p75NTR and S100β markers was observed, suggesting that NG2-lineage-positive cells were not a major contributor to the neural cell (Schwann cells) populations and the re-innervation of the damaged tissue (Fig. 4.24). Similar pattern was observed between tdTomato and Sox10 signal overlap (Fig. 4.25). As constitutive NG2-Cre mice reveal extensive labeling when crossed with Ai14, it was deemed not useful for imaging and further analysis.

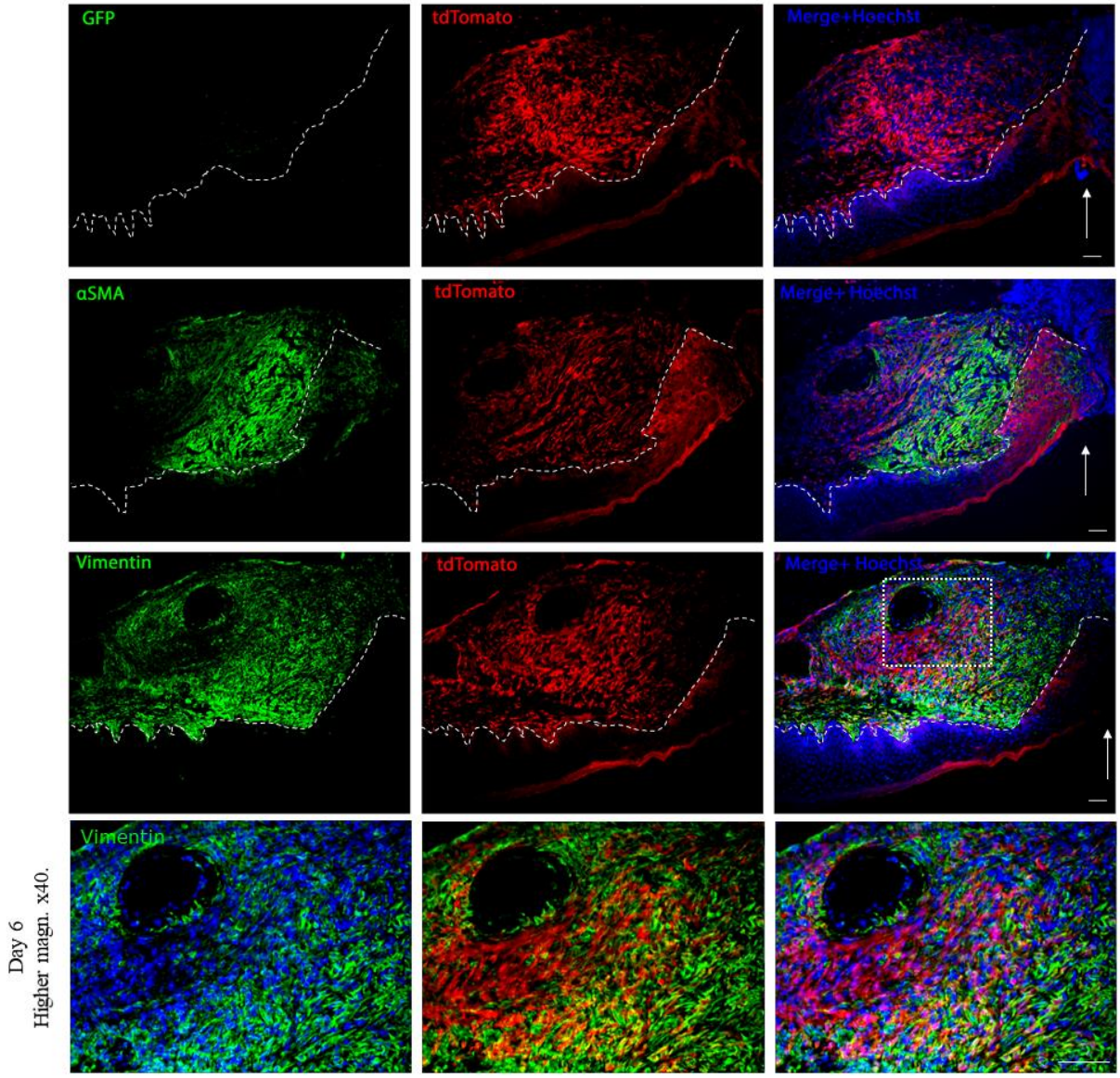

Day 6
Higher magn. x40.

Figure 4-24 NG2-lineage-positive cells contribute to mesenchymal and myofibroblast cell populations within the wounded palatal mucoperiosteum

Upon wounding, GFP-positive cells are absent from granulation tissue at day 6 post-wounding NG2-lineage-positive cells appear throughout the palate and granulation tissue, where partial overlap was observed between NG2-lineage-positve cells and Vimentin and α-SMA markers. Merged images show tdTomato (NG2-lineage-positive) cells in red and nuclei are labelled with Hoechst in blue. White dashed lines indicate the border between the epithelium and the granulation tissue. White arrows indicate the leading edge of the wound. Scale bar= 100 μm. (N=2)

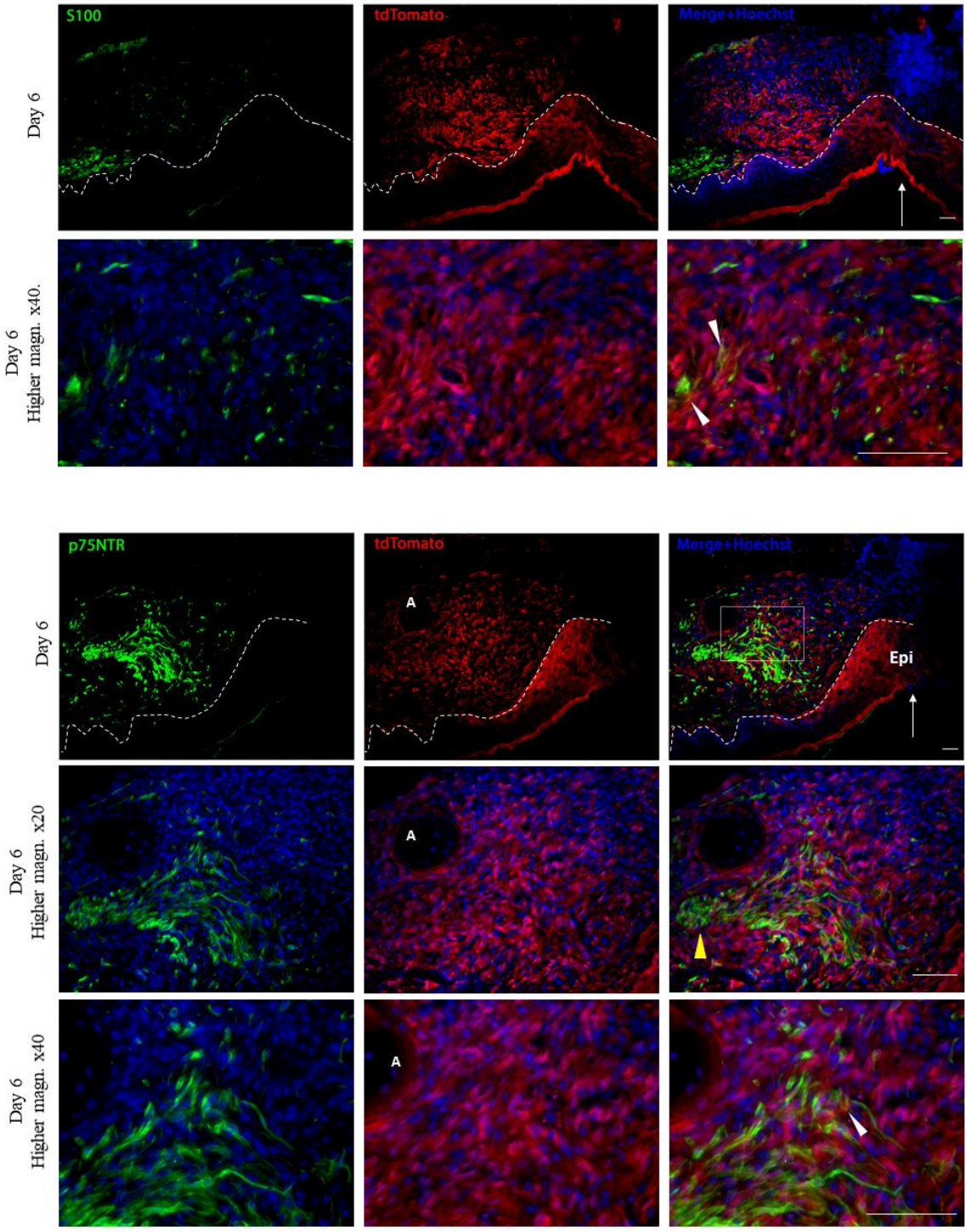
S100
tdTomato
Merge+Hoechst
Day 6
Day 6
Higher magn. x40.
p75NTR
tdTomato
Merge+Hoechst
A
Epi
Day 6
Day 6
Higher magn. x20
Day 6
Higher magn. x40

Figure 4-25 NG2-lineage-positive cells contribute minimally to peripheral nerve populations within the wounded palatal mucoperiosteum

White arrowheads indicate representative cells with dual labeling between NG2-lineage-positive cells and S100β- or p75NTR-positive cells. Merged images show tdTomato (NG2-lineage-positive) cells in red and nuclei are labelled with Hoechst in blue. White dashed lines indicate the border between the epithelium and the granulation tissue. Yellow arrowhead indicates the nerve bundle adjacent to the major palatine artery. White arrows indicate the leading edge of the wound **Epi**= oral/palatal epithelium, **A**= Major Palatine Artery. Scale bar= 100 μm. (N=2)

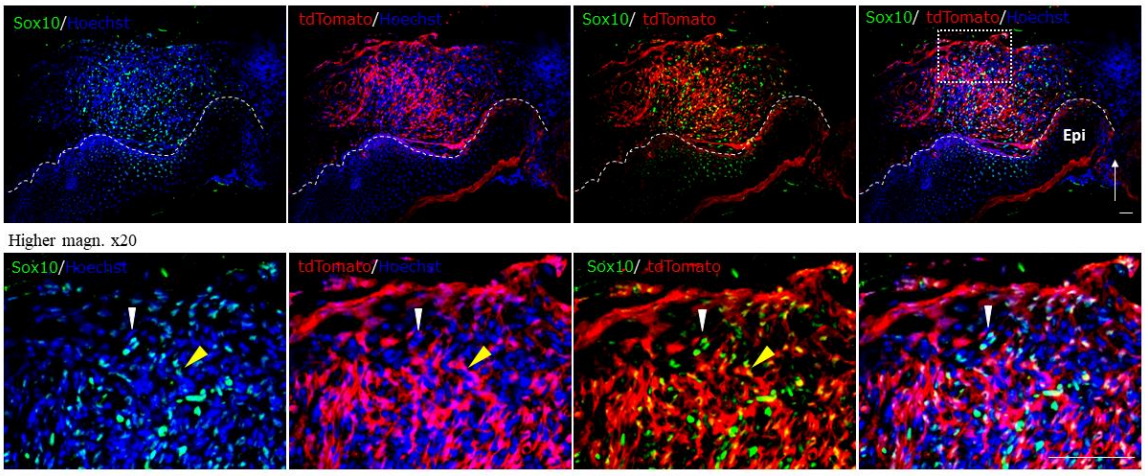

Figure 4-26 NG2-lineage-positive cells are not of neural-crest origin.

Yellow arrowheads indicate representative cells with dual labeling between NG2-lineage-positve cells and Sox10-positive cells. Merged images show tdTomato (NG2-lineage-positive) cells in red and nuclei are labelled with Hoechst in blue. White dashed lines indicate the border between the epithelium and the granulation tissue. White arrowheads indicate representative Sox10-positive, NG2-negative cells. White arrows indicate the leading edge of the wound. Scale bar= 100 μm. (N=2)

4.3.10 NG2-lineage-positive cell populations in adult palate and granulation tissue were not derived from de novo Ng2 expression in postnatal tissue.

To determine if postnatal expression of Ng2 was contributing to the positive populations observed in these tissues, recombination in a tamoxifen inducible Cre model was investigated by crossing the *Ng2GCE* line with the *Ai14* reporter (NG2-CreERT2-GFP). Tamoxifen was delivered to postnatal mice (*Ng2-ERT-CRE/Rosa*) immediately after wounding and a histological assessment of recombination was performed in 3 mice at day 6 post wounding (Fig. 4.26). Tamoxifen injection into postnatal tissue resulted in a low level of recombination, resulting in few tdTomato positive cells in the palate and the granulation, which were primarily associated with blood vessels (N=3). Experimental control conditions were also performed, as seen in Figure 4.27 (N=1 animal/control condition)**.**

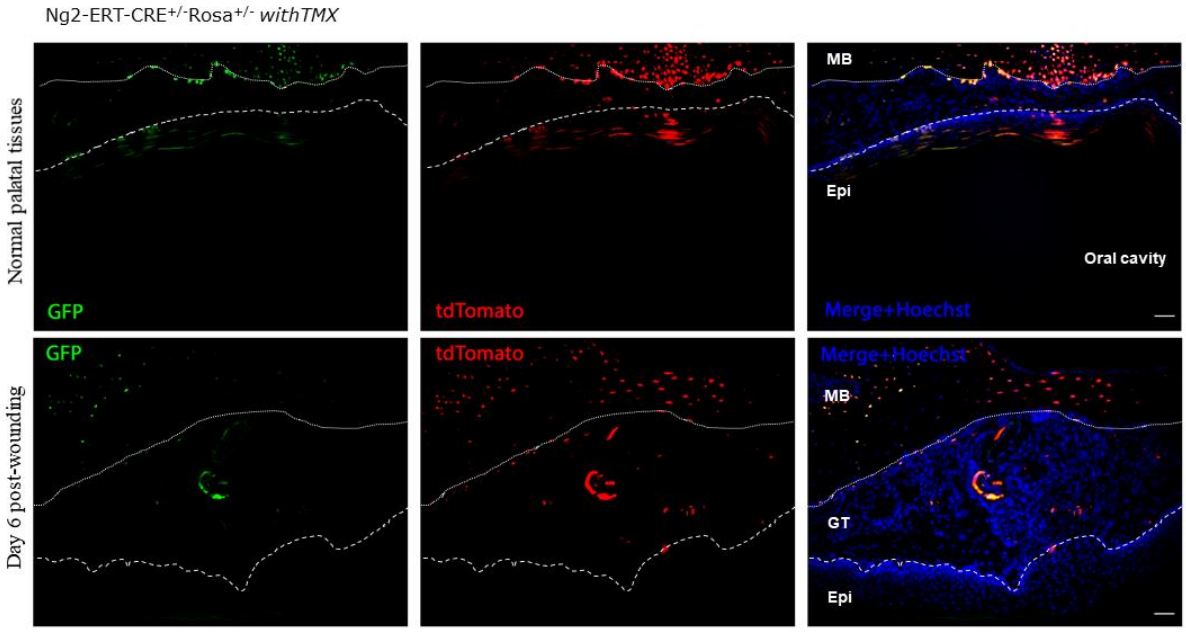

Figure 4-27 NG2 expressing cells exhibit minimal contribution in healing of adult palatal tissues

Tamoxifen was delivered to postnatal mice (*Ng2-ERT-CRE/Rosa*) right after wounding and a histological assessment of recombination was performed in 3 mice at day 6 post wounding. Merged images show tdTomato (NG2-lineage-positive) cells in red and nuclei are labelled with Hoechst in blue. White dashed lines indicate the border between the epithelium and the granulation tissue. White dotted lines indicate the border between the palatal bone and the granulation tissue. Scale bar= 100 μm.

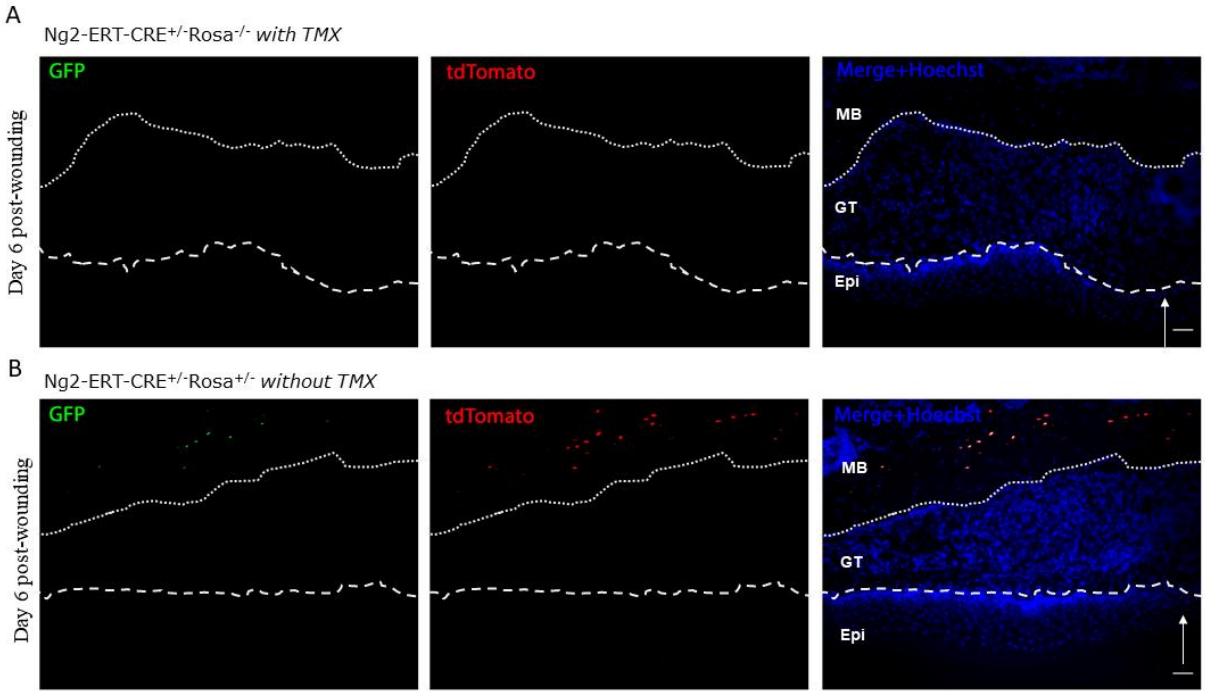

Figure 4-28 Control experimental conditions

(A) Tamoxifen was delivered to postnatal mice (*Ng2-ERT-CRE$^{+/-}$/Rosa$^{-/-}$*) right after wounding. Histological assessment 6 days post-wounding did not reveal any recombination. **(B)** *Ng2-ERT-CRE$^{+/-}$/Rosa$^{+/-}$* mouse was injected with sterile saline (instead of tamoxifen) right after wounding and histological assessment of recombination was performed at day 6 post-wounding. White dashed lines indicate the border between the epithelium and the granulation tissue. White dotted lines indicate the border between the palatal bone and the granulation tissue. **MB**= maxillary bone, **GT**= granulation tissue, **Epi**= epithelium. Scale bar= 100 μm.

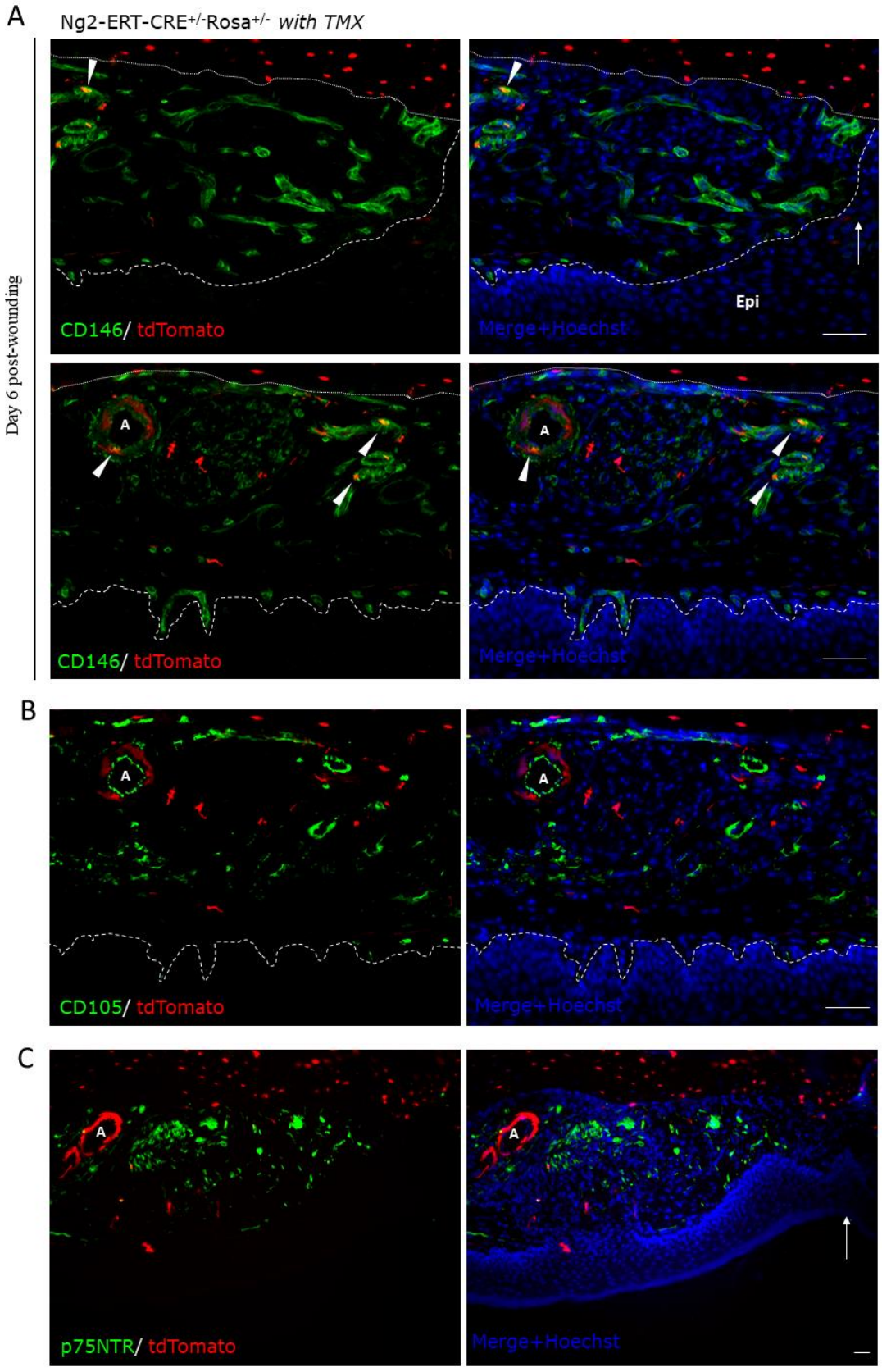
A
Ng2-ERT-CRE+/-Rosa+/- with TMX
Day 6 post-wounding
CD146/ tdTomato
Merge+Hoechst
Epi
A
CD146/ tdTomato
Merge+Hoechst
B
A
CD105/ tdTomato
Merge+Hoechst
C
A
p75NTR/ tdTomato
Merge+Hoechst

Figure 4-29 NG2-expressing cells contribute endothelial cells during repair.

Immunofluorescent staining for CD146 (**A**), CD105 (**B**) and p75NTR (**C**) was performed at day 6 post-wounding. White arrowheads indicate representative cells with dual labeling between tdTomato+ cells and CD146-positive cells. A= artery Scale bar: 100 μm.

4.4 Discussion

Using a lineage tracing approach, embryonic progenitors that differentially expressed Foxd1 or NG2 were investigated in a murine model. In our study we identified two distinct lineages of cells that are committed to different cell types in adult palate, uniquely contributing to palatal mucoperiosteum homeostasis and wound repair: The Foxd1-lineage progeny expanded after injury and contributed to the formation of neovascular structures, while the NG2-lineage progeny contributed to most of the fibrotic cells present in the wounded tissues. Interestingly, the Foxd1-lineage progeny and NG2-lineage progeny populations described here do not directly overlap with distinct embryonic lineages that have been previously identified within different organs in murine models, such as in skin, kidney, lung, liver (Chen et al., 2011; Humphreys et al., 2010b; Hung et al., 2013; Rock et al., 2011; Walker et al., 2021).

Due to the different healing patterns evident when comparing the oral cavity and the skin, here we investigated the embryonic origin of cells that contribute to palatal mucoperiosteum wound healing. Evidence suggests that identification of fibroblast lineages could be used to a degree as a predictor of cell function, but that this is likely only true within a specific tissue location. In fact, lineage itself may simply predict a cell's location, which in turn defines its phenotype (Walker et al., 2021). In the palatal mucoperiosteum palatal soft tissue is a rigid mucoperiosteum; mucosa and the periosteum are merged and tightly attached to the palatal bone, leading to excessive scarring upon wounding (Nanci, 2013). Here, we explored whether binary expression of *Foxd1* during embryogenesis could be used as a new potential marker of fibroblasts within the oral cavity and the repair process in the palatal mucoperiosteum, and to compare our findings with evidence from murine skin healing. We investigated the contribution of Foxd1 lineage to cell populations during early maxillofacial development, and we found that FLP cells are not of neural crest origin and are a major contributor to pericytes and endothelial cells for the neovascularization of the developing palatal tissues. Further, the contribution of Foxd1- and NG2-lineage cells was also assessed in homeostasis and would healing of the adult

murine palatal mucoperiosteum, where we identified that they give rise to distinct lineages of cells that are committed to different cell types.

Our group has previously shown that in skin Foxd1-derived progeny account for a subset of dermal fibroblasts and myofibroblasts during wound healing (Walker et al., 2021). In excisional wounds in skin FLP and FLN fibroblasts were both found to produce α-SMA contributing to activated myofibroblasts during tissue repair. Interestingly, these cell populations appeared to have unique expression profiles, with FLP cells showing enhanced expression of genes associated with ECM synthesis and remodelling, while FLN populations are associated with signalling/microenvironment, indicating that they have unique specializations and potentially work together in concert during homeostasis and repair (Walker et al., 2021)

The hard palate is an area of the mouth which results from the fusion of different embryonic facial processes: the palatal shelves (arising from the maxillary processes) grow vertically down the sides of the tongue, at E12. They begin as vertical (dorsoventral) projections down the sides of the developing tongue and around E14 elevate to a horizontal position above the tongue and continue to grow horizontally, until they contact and fuse along the midline. A transient epithelial seam is formed which is gradually replaced by continuous mesenchyme (Vaziri Sani et al., 2005). The secondary palate fuses with the primary palate and the nasal septum, thereby creating the separation between the oral cavity and the two nostrils (Paiva et al., 2019). Here, we showed that Foxd1-lineage positive cells contribute to various mesenchymal and ectomesenchymal tissues within the developing orofacial tissues, such as mesenchyme within meninges, nasal process of the secondary palate, whisker follicles, nasal cartilage, cells within the dental mesenchyme, the dental papilla and dental follicle of developing teeth, the eye retina and fiber bundles in the extraocular muscles, and the tongue, all of which are of neural crest- or mesodermal origin.

More detailed analysis of this cell population revealed that Foxd1-lineage positive cells were also sparsely distributed in lateral maxillary processes contributing to cells of the neovasculature. It is of interest that angioblasts are the only cells of mesodermal origin so far identified that move into the stream of migrating neural crest cells, apparently as soon

as the neural crest cells have formed as a mesenchymal population lateral and rostral to the mesodermal mesenchyme. This early incursion of mesodermal angioblasts into an apparently otherwise pure neural crest cell population enables blood vessels to form equally quickly within the neural crest-derived and mesoderm-derived mesenchyme of the head (Yoshida et al., 2008). Evidence from lineage tracing studies suggest that in the craniofacial region of mouse embryos the endothelial cells of blood vessels are of mesodermal origin and the muscular components of the vessel walls (pericytes) are derived from neural crest (Yoshida et al., 2008). Our findings further support this evidence, as here we show that within the developing palate, the vasculature structures arise from the Foxd-1 embryonic lineage and do not express neural-crest markers SOX10 and p75NTR.

In the adult mouse, the cell populations arising from Foxd1-lineage positive cells contribute to a relatively small proportion of cells in the quiescent adult palatal mucoperiosteum, mainly associated with blood vessels, where they give rise to some smooth muscle cells of peripheral veni, pericytes and some endothelial cells. FLP cells also constituted to cells of the perineurium of nerves as well as some cell populations within the endoneurium (endoneural fibroblasts/pericytes). However, our data shows that upon experimental wounding, this population is activated contributing to cells mainly associated with neovascularization of the wound. While $CD31^{+}$FLP cells were sparse in the unwounded tissues, upon wounding more than 40% of FLP cells were $CD31^{+}$. In contrast, no significant overlap with any fibroblast or myofibroblast markers was identified. This finding is in direct contrast with evidence of the Foxd1-lineage positive cell population in dermal wound healing. In skin the Foxd1 lineage represented 50%-70% of the dermal fibroblasts and contributed to myofibroblast progenitors, and only minimally to vascular cells (Rinkevich 2015, Walker et al., 2021), providing further evidence about differences between oral and skin healing characteristics. Revascularization of the wound is essential for the repair and regeneration of the tissue. Functional and persistent neoangiogenic activity has been shown to result in favorable wound healing outcomes across different tissues, such as the myocardium (Broughton et al., 2018) and skin (Moreira & Marques, 2022). Among other factors described in Chapter 1, this evidence of the distinct roles of Foxd1 progeny in skin

and palatal tissues could also be considered a contributing factor of the oral mucosa to heal without scarring.

Foxd1-derived populations in skin have been shown to display enhanced fibrogenic potential compared to their lineage-negative counterparts, as shown by FACS sorting, gene expression and functionality assays (Walker et al., 2021). Our data show that in the palate Foxd1-derived populations do not contribute to the population of myofibroblasts that populate the granulation tissue of the wound. These marked differences could point to unique healing potential between the two tissues: Foxd1-derived populations are present and expand at different extent in both skin and the palatal mucoperiosteum, but they contribute to different cells upon wounding, suggesting that tissue specificity and cell-extrinsic factors within their unique location are likely to influence their lineage determination.

We utilized the NG2 embryonic marker to investigate the contribution of perivascular cells in the wound healing process, as the blood supply in the soft and hard tissues of the palate is provided by the major palatine arteries, and surrounding branches and capillaries. Thus, we hypothesized that these arteries and associated microcirculation could be a potential source for activated and migrating cells that contribute to wound healing. In our study we found that NG2-lineage progeny cells are present in adult palatal tissues, and they expand upon wounding contributing to the mesenchymal cells and myofibroblasts within the granulation tissue. Based on our observations in the palate, it appears that the NG2-progeny marks a distinct cell population with more fibrotic profile, while the Foxd1-progeny is restricted to cells with vascular role. Our findings could lead to the development of model system that allows separation of vascular entities and pro-fibrotic myofibroblast behaviors in the same healing model. Since poor wound healing and scarring are associated with reduced vascularization and vascular stability, this model could be utilized to assess changes in vascular/fibrotic balance, and the final healing outcome.

Extensive evidence indicates that NG2 is highly expressed by pericytes (Armulik et al., 2011; Ozerdem et al., 2001; Ozerdem & Stallcup, 2004). In various different organs pericytes can differentiate into myofibroblasts and contribute extensively to tissue repair

(Chen et al., 2011, p. 201; Humphreys et al., 2010b). Pericyte function could be tissue-specific as it be influenced by the organ in which the cells reside: In lung two pericyte populations arise from the same Foxd1 progenitor, one of which co-expresses fibroblast and pericyte markers (Col1+ Pdgfrα+ Pdgfrβ+ Ng2+) (Barron et al., 2016). Type-1 pericytes (Nestin-negative, NG2-positive), produce collagen and contribute to fibrosis in skeletal muscle, but not in the kidney or the heart (Birbrair et al., 2014). In the skin, lineage tracing showed that NG2-positive cells did not give rise to any dermal fibroblast subpopulations during wound healing (Goss et al., 2021), contrary to other perivascular populations (Dulauroy, Carlo, et al., 2012). NG2-positive cells remained associated only with blood vessels, restricted to forming NG2+ blood vessel associated cells, most of which express Pdgfrα and/or Pdgfrβ. (Goss et al., 2021). The same study also showed that NG2-positive perivascular cells were primarily derived from interfollicular papillary and reticular fibroblasts during skin development as well as during regeneration, supporting a potential relationship between pericyte and fibroblast lineages (Goss et al., 2021).

In recent years, a plethora of research has demonstrated that the ECM physical and chemical properties are important determinants of cell behaviours and soft tissue healing (Argentati et al., 2019; Wells et al., 2016). Building on our previous studies (Elliott et al., 2012; Kim et al., 2019; Nikoloudaki et al., 2020), the differences observed in skin, gingival and palatal healing processes suggest that the ECM of these tissues may possess different levels of stiffness. Changing the stiffness of the cell substrate is an efficient method to control cell behavior in vitro (Pakshir & Hinz, 2018; Talele et al., 2015; Tomasek et al., 2002). To first determine whether Foxd1-lineage positive cells could expand *in vitro*, a compliant collagen gel was used as a culture substrate to selectively stimulate myofibroblast activation. Here, we found that both Foxd1-lineage-positive and -negative cells from the palatal mucoperiosteum are able to expand in culture, giving rise to fibroblast-like cells. When cells of both populations were seeded on substrates of increased stiffness (GPa) they developed distinct stress fibers, in which α-SMA was incorporated, indicating myofibroblast differentiation, while when they were seeded on very soft (0.2 kPa) substrates the cells were characterized by poor spreading and exhibited no contractile bundles. Even though these are preliminary data, these findings point to the importance of

the cell microenvironment, among other extrinsic factors, as determinants of cell differentiation and lineage commitment. To determine the functional characteristics of the FLP and FNL cells, as well as the interactions between the two populations, cell isolation via FACS analysis and gene expression analysis is required.

In the present study, Foxd1 expression by embryonic progenitors enabled the tracking of distinct cells that contribute to the vasculature of the developing palatal tissues and that maintained their spatial differences into adulthood and regeneration. NG2 progeny tracking allowed the identification of different cell populations that contribute to healing, that are not only restricted to blood vessel formation unlikely to the skin. Our findings further support that cell populations across different tissues, although they originate from common embryonic lineages, they present different phenotypes in mature and wounded tissues. This observation points to the significance of cell-extrinsic factors (extracellular environment, from tissue-specificity perspective, ECM composition and microenvironment biomechanical properties) as determinants of cell fate and behaviour across different tissues, and that could further explain the different healing patterns among them.

4.5 References

Argentati, C., Morena, F., Tortorella, I., Bazzucchi, M., Porcellati, S., Emiliani, C., & Martino, S. (2019). Insight into Mechanobiology: How Stem Cells Feel Mechanical Forces and Orchestrate Biological Functions. *International Journal of Molecular Sciences*, *20*(21), 5337. https://doi.org/10.3390/ijms20215337

Armulik, A., Genové, G., & Betsholtz, C. (2011). Pericytes: Developmental, Physiological, and Pathological Perspectives, Problems, and Promises. *Developmental Cell*, *21*(2), 193–215. https://doi.org/10.1016/j.devcel.2011.07.001

Barron, L., Gharib, S. A., & Duffield, J. S. (2016). Lung Pericytes and Resident Fibroblasts: Busy Multitaskers. *The American Journal of Pathology*, *186*(10), 2519–2531. https://doi.org/10.1016/j.ajpath.2016.07.004

Bergers, G., & Song, S. (2005). The role of pericytes in blood-vessel formation and maintenance. *Neuro-Oncology*, *7*(4), 452–464. https://doi.org/10.1215/s1152851705000232

Birbrair, A., Zhang, T., Files, D. C., Mannava, S., Smith, T., Wang, Z.-M., Messi, M. L., Mintz, A., & Delbono, O. (2014). Type-1 pericytes accumulate after tissue injury and produce collagen in an organ-dependent manner. *Stem Cell Research & Therapy*, *5*(6), 122. https://doi.org/10.1186/scrt512

Broughton, K. M., Wang, B. J., Firouzi, F., Khalafalla, F., Dimmeler, S., Fernandez-Aviles, F., & Sussman, M. A. (2018). Mechanisms of Cardiac Repair and Regeneration. *Circulation Research*, *122*(8), 1151–1163. https://doi.org/10.1161/CIRCRESAHA.117.312586

Cathery, W., Faulkner, A., Maselli, D., & Madeddu, P. (2018). Concise Review: The Regenerative Journey of Pericytes Toward Clinical Translation. *Stem Cells (Dayton, Ohio)*, *36*(9), 1295–1310. https://doi.org/10.1002/stem.2846

Chen, Y.-T., Chang, F.-C., Wu, C.-F., Chou, Y.-H., Hsu, H.-L., Chiang, W.-C., Shen, J., Chen, Y.-M., Wu, K.-D., Tsai, T.-J., Duffield, J. S., & Lin, S.-L. (2011). Platelet-derived growth factor receptor signaling activates pericyte-myofibroblast transition in obstructive and post-ischemic kidney fibrosis. *Kidney International*, *80*(11), 1170–1181. https://doi.org/10.1038/ki.2011.208

Cooke, V. G., LeBleu, V. S., Keskin, D., Khan, Z., O'Connell, J. T., Teng, Y., Duncan, M. B., Xie, L., Maeda, G., Vong, S., Sugimoto, H., Rocha, R. M., Damascena, A., Brentani, R. R., & Kalluri, R. (2012). Pericyte depletion results in hypoxia-associated epithelial-to-mesenchymal transition and metastasis mediated by met signaling pathway. *Cancer Cell*, *21*(1), 66–81. https://doi.org/10.1016/j.ccr.2011.11.024

Crisan, M., Yap, S., Casteilla, L., Chen, C.-W., Corselli, M., Park, T. S., Andriolo, G., Sun, B., Zheng, B., Zhang, L., Norotte, C., Teng, P.-N., Traas, J., Schugar, R., Deasy, B. M., Badylak, S., Bűhring, H.-J., Giacobino, J.-P., Lazzari, L., … Péault, B. (2008). A Perivascular Origin for Mesenchymal Stem Cells in Multiple Human Organs. *Cell Stem Cell*, *3*(3), 301–313. https://doi.org/10.1016/j.stem.2008.07.003

Di Carlo, S. E., & Peduto, L. (2018). The perivascular origin of pathological fibroblasts. *Journal of Clinical Investigation*, *128*(1), 54–63. https://doi.org/10.1172/JCI93558

Driskell, R. R., Lichtenberger, B. M., Hoste, E., Kretzschmar, K., Simons, B. D., Charalambous, M., Ferron, S. R., Herault, Y., Pavlovic, G., Ferguson-Smith, A. C., & Watt, F. M. (2013). Distinct fibroblast lineages determine dermal architecture in skin development and repair. *Nature*, *504*(7479), 277–281. https://doi.org/10.1038/nature12783

Driskell, R. R., & Watt, F. M. (2015). Understanding fibroblast heterogeneity in the skin. *Trends in Cell Biology*, *25*(2), 92–99. https://doi.org/10.1016/j.tcb.2014.10.001

Dulauroy, S., Carlo, S. E. D., Langa, F., Eberl, G., & Peduto, L. (2012). Lineage tracing and genetic ablation of ADAM12 + perivascular cells identify a major source of

profibrotic cells during acute tissue injury. *Nature Medicine*. https://doi.org/10.1038/nm.2848

Dulauroy, S., Di Carlo, S. E., Langa, F., Eberl, G., & Peduto, L. (2012). Lineage tracing and genetic ablation of ADAM12 + perivascular cells identify a major source of profibrotic cells during acute tissue injury. *Nature Medicine*. https://doi.org/10.1038/nm.2848

Elliott, C. G., Wang, J., Guo, X., Xu, S. -w., Eastwood, M., Guan, J., Leask, A., Conway, S. J., & Hamilton, D. W. (2012). Periostin modulates myofibroblast differentiation during full-thickness cutaneous wound repair. *Journal of Cell Science*, *125*(1), 121–132. https://doi.org/10.1242/jcs.087841

Gabbiani, G., Ryan, G. B., & Majne, G. (1971). Presence of modified fibroblasts in granulation tissue and their possible role in wound contraction. *Experientia*, *27*(5), 549–550.

Gomes, R. N., Manuel, F., & Nascimento, D. S. (2021). The bright side of fibroblasts: Molecular signature and regenerative cues in major organs. *Npj Regenerative Medicine*, *6*(1), 43. https://doi.org/10.1038/s41536-021-00153-z

Gonçalves, N. P., Mohseni, S., El Soury, M., Ulrichsen, M., Richner, M., Xiao, J., Wood, R. J., Andersen, O. M., Coulson, E. J., Raimondo, S., Murray, S. S., & Vægter, C. B. (2019). Peripheral Nerve Regeneration Is Independent From Schwann Cell p75NTR Expression. *Frontiers in Cellular Neuroscience*, *13*, 235. https://doi.org/10.3389/fncel.2019.00235

Goss, G., Rognoni, E., Salameti, V., & Watt, F. M. (2021). Distinct Fibroblast Lineages Give Rise to NG2+ Pericyte Populations in Mouse Skin Development and Repair. *Frontiers in Cell and Developmental Biology*, *9*, 1240. https://doi.org/10.3389/fcell.2021.675080

Greenhalgh, S. N., Iredale, J. P., & Henderson, N. C. (2013). Origins of fibrosis: Pericytes take centre stage. *F1000Prime Reports*. https://doi.org/10.12703/p5-37

Guillaume, R., Bressan, M., & Herzlinger, D. (2009). Paraxial mesoderm contributes stromal cells to the developing kidney. *Developmental Biology*. https://doi.org/10.1016/j.ydbio.2009.02.034

Guimarães-Camboa, N., Cattaneo, P., Sun, Y., Moore-Morris, T., Gu, Y., Dalton, N. D., Rockenstein, E., Masliah, E., Peterson, K. L., Stallcup, W. B., Chen, J., & Evans, S. M. (2017). Pericytes of Multiple Organs Do Not Behave as Mesenchymal Stem Cells In Vivo. *Cell Stem Cell*. https://doi.org/10.1016/j.stem.2016.12.006

Hinz, B. (2010). The myofibroblast: Paradigm for a mechanically active cell. *Journal of Biomechanics*, *43*(1), 146–155. https://doi.org/10.1016/j.jbiomech.2009.09.020

Hinz, B. (2015). Myofibroblasts. *Experimental Eye Research*, *142*, 56–70. https://doi.org/10.1016/j.exer.2015.07.009

Humphreys, B. D., Lin, S. L., Kobayashi, A., Hudson, T. E., Nowlin, B. T., Bonventre, J. V., Valerius, M. T., McMahon, A. P., & Duffield, J. S. (2010a). Fate tracing reveals the pericyte and not epithelial origin of myofibroblasts in kidney fibrosis. *American Journal of Pathology*, *176*(1), 85–97. https://doi.org/10.2353/ajpath.2010.090517

Humphreys, B. D., Lin, S. L., Kobayashi, A., Hudson, T. E., Nowlin, B. T., Bonventre, J. V., Valerius, M. T., McMahon, A. P., & Duffield, J. S. (2010b). Fate tracing reveals the pericyte and not epithelial origin of myofibroblasts in kidney fibrosis. *American Journal of Pathology*, *176*(1), 85–97. https://doi.org/10.2353/ajpath.2010.090517

Hung, C., Linn, G., Chow, Y. H., Kobayashi, A., Mittelsteadt, K., Altemeier, W. A., Gharib, S. A., Schnapp, L. M., & Duffield, J. S. (2013). Role of lung Pericytes and resident fibroblasts in the pathogenesis of pulmonary fibrosis. *American Journal*

of Respiratory and Critical Care Medicine, *188*(7), 820–830. https://doi.org/10.1164/rccm.201212-2297OC

Jessen, K. R., & Mirsky, R. (2005). The origin and development of glial cells in peripheral nerves. *Nature Reviews. Neuroscience*, *6*(9), 671–682. https://doi.org/10.1038/nrn1746

Kalluri, R., & Weinberg, R. A. (2009). The basics of epithelial-mesenchymal transition. *Journal of Clinical Investigation*, *119*(6), 1420–1428. https://doi.org/10.1172/JCI39104

Keswani, S. G., Balaji, S., Le, L. D., Leung, A., Parvadia, J. K., Frischer, J., Yamano, S., Taichman, N., & Crombleholme, T. M. (2013). Role of salivary vascular endothelial growth factor (VEGF) in palatal mucosal wound healing. *Wound Repair and Regeneration : Official Publication of the Wound Healing Society [and] the European Tissue Repair Society*, *21*(4), 554–562. https://doi.org/10.1111/wrr.12065

Kim, S. S., Nikoloudaki, G. E., Michelsons, S., Creber, K., & Hamilton, D. W. (2019). Fibronectin synthesis, but not α-smooth muscle expression, is regulated by periostin in gingival healing through FAK/JNK signaling. *Scientific Reports*, *9*(1), 2708. https://doi.org/10.1038/s41598-018-35805-6

Kramann, R., DiRocco, D. P., & Humphreys, B. D. (2013). Understanding the origin, activation and regulation of matrix-producing myofibroblasts for treatment of fibrotic disease: Matrix-producing myofibroblasts for treatment of fibrotic disease. *The Journal of Pathology*, *231*(3), 273–289. https://doi.org/10.1002/path.4253

LeBleu, V. S., & Neilson, E. G. (2020). Origin and functional heterogeneity of fibroblasts. *The FASEB Journal*, *34*(3), 3519–3536. https://doi.org/10.1096/fj.201903188R

LeBleu, V. S., Taduri, G., O'Connell, J., Teng, Y., Cooke, V. G., Woda, C., Sugimoto, H., & Kalluri, R. (2013). Origin and function of myofibroblasts in kidney fibrosis. *Nature Medicine*, *19*(8), 1047–1053. PubMed. https://doi.org/10.1038/nm.3218

Lemos, D. R., & Duffield, J. S. (2018). Tissue-resident mesenchymal stromal cells: Implications for tissue-specific antifibrotic therapies. *Science Translational Medicine*, *10*(426), eaan5174. https://doi.org/10.1126/scitranslmed.aan5174

Mederacke, I., Hsu, C. C., Troeger, J. S., Huebener, P., Mu, X., Dapito, D. H., Pradere, J.-P., & Schwabe, R. F. (2013). Fate-tracing reveals hepatic stellate cells as dominant contributors to liver fibrosis independent of its etiology. *Nature Communications*, *4*, 2823. https://doi.org/10.1038/ncomms3823

Metzger, D., & Chambon, P. (2001). Site- and Time-Specific Gene Targeting in the Mouse. *Methods*, *24*(1), 71–80. https://doi.org/10.1006/meth.2001.1159

Moreira, H. R., & Marques, A. P. (2022). Vascularization in skin wound healing: Where do we stand and where do we go? *Current Opinion in Biotechnology*, *73*, 253–262. https://doi.org/10.1016/j.copbio.2021.08.019

Nanci, A. (2013). Ten Cate's Oral Histology. In *Elsevier: Vol. 8th ed* (p. 166). Elsevier.

Nikoloudaki, G., Snider, P., Simmons, O., Conway, S. J., & Hamilton, D. W. (2020). Periostin and matrix stiffness combine to regulate myofibroblast differentiation and fibronectin synthesis during palatal healing. *Matrix Biology*, *94*, 31–56. https://doi.org/10.1016/j.matbio.2020.07.002

Ozerdem, U., Grako, K. A., Dahlin-Huppe, K., Monosov, E., & Stallcup, W. B. (2001). NG2 proteoglycan is expressed exclusively by mural cells during vascular morphogenesis. *Developmental Dynamics*, *222*(2), 218–227. https://doi.org/10.1002/dvdy.1200

Ozerdem, U., & Stallcup, W. B. (2004). Pathological angiogenesis is reduced by targeting pericytes via the NG2 proteoglycan. *Angiogenesis*, *7*(3), 269–276. https://doi.org/10.1007/s10456-004-4182-6

Paiva, K. B. S., Maas, C. S., Santos, P. M. dos, Granjeiro, J. M., & Letra, A. (2019). Extracellular Matrix Composition and Remodeling: Current Perspectives on Secondary Palate Formation, Cleft Lip/Palate, and Palatal Reconstruction. *Frontiers in Cell and Developmental Biology*, *7*. https://www.frontiersin.org/article/10.3389/fcell.2019.00340

Pakshir, P., & Hinz, B. (2018). The big five in fibrosis: Macrophages, myofibroblasts, matrix, mechanics, and miscommunication. *Matrix Biology*, *68–69*, 81–93. https://doi.org/10.1016/j.matbio.2018.01.019

Rinkevich, Y., Walmsley, G. G., Hu, M. S., Maan, Z. N., Newman, A. M., Drukker, M., Januszyk, M., Krampitz, G. W., Gurtner, G. C., Lorenz, H. P., Weissman, I. L., & Longaker, M. T. (2015). Identification and isolation of a dermal lineage with intrinsic fibrogenic potential. *Science*, *348*(6232). https://doi.org/10.1126/science.aaa2151

Rock, J. R., Barkauskas, C. E., Cronce, M. J., Xue, Y., Harris, J. R., Liang, J., Noble, P. W., & Hogan, B. L. M. (2011). Multiple stromal populations contribute to pulmonary fibrosis without evidence for epithelial to mesenchymal transition. *Proceedings of the National Academy of Sciences*, *108*(52), E1475–E1483. https://doi.org/10.1073/pnas.1117988108

Talele, N. P., Fradette, J., Davies, J. E., Kapus, A., & Hinz, B. (2015). Expression of α-Smooth Muscle Actin Determines the Fate of Mesenchymal Stromal Cells. *Stem Cell Reports*, *4*(6), 1016–1030. https://doi.org/10.1016/j.stemcr.2015.05.004

Tomasek, J. J., Gabbiani, G., Hinz, B., Chaponnier, C., & Brown, R. a. (2002). Myofibroblasts and mechano-regulation of connective tissue remodelling. *Nature Reviews. Molecular Cell Biology*, *3*(5), 349–363. https://doi.org/10.1038/nrm809

Vaziri Sani, F., Hallberg, K., Harfe, B. D., McMahon, A. P., Linde, A., & Gritli-Linde, A. (2005). Fate-mapping of the epithelial seam during palatal fusion rules out epithelial–mesenchymal transformation. *Developmental Biology*, *285*(2), 490–495. https://doi.org/10.1016/j.ydbio.2005.07.027

Walker, J. T., Flynn, L. E., & Hamilton, D. W. (2021). Lineage tracing of Foxd1-expressing embryonic progenitors to assess the role of divergent embryonic lineages on adult dermal fibroblast function. *FASEB BioAdvances*, *3*(7), 541–557. https://doi.org/10.1096/fba.2020-00110

Wells, A., Nuschke, A., & Yates, C. C. (2016). Skin tissue repair: Matrix microenvironmental influences. *Matrix Biology : Journal of the International Society for Matrix Biology*, *49*, 25–36. https://doi.org/10.1016/j.matbio.2015.08.001

Yamazaki, T., & Mukouyama, Y. (2018). Tissue Specific Origin, Development, and Pathological Perspectives of Pericytes. *Frontiers in Cardiovascular Medicine*, *5*, 78. https://doi.org/10.3389/fcvm.2018.00078

Yoshida, T., Vivatbutsiri, P., Morriss-Kay, G., Saga, Y., & Iseki, S. (2008). Cell lineage in mammalian craniofacial mesenchyme. *Mechanisms of Development*, *125*(9–10), 797–808. https://doi.org/10.1016/j.mod.2008.06.007

You, W.-K., Yotsumoto, F., Sakimura, K., Adams, R. H., & Stallcup, W. B. (2014). NG2 proteoglycan promotes tumor vascularization via integrin-dependent effects on pericyte function. *Angiogenesis*, *17*(1), 61–76. https://doi.org/10.1007/s10456-013-9378-1

Zeisberg, E. M., Tarnavski, O., Zeisberg, M., Dorfman, A. L., McMullen, J. R., Gustafsson, E., Chandraker, A., Yuan, X., Pu, W. T., Roberts, A. B., Neilson, E. G., Sayegh, M. H., Izumo, S., & Kalluri, R. (2007). Endothelial-to-mesenchymal transition contributes to cardiac fibrosis. *Nature Medicine*, *13*(8), 952–961. https://doi.org/10.1038/nm1613

Chapter 5

5.1 Summary of the thesis

In this thesis, I investigated how cell origin/lineage and the composition of the extracellular matrix influences processes required for tissue homeostasis and repair. While considerable research has focused on skin, less has been directed towards the oral tissues, and specifically the palatal mucoperiosteum and the periodontal ligament. My goal was to investigate how both cell-intrinsic and extrinsic factors influence processes underlying successful wound repair (palatal mucoperiosteum) and maintenance of tissue homeostasis (periodontal ligament). Using a novel palatal repair model in 6 different strains of genetically modified mice (*Postn*$^{-/-}$ *peri*^{lacZ} null mice, *Foxd1-Cre-GFP*/ *ROSA26-mTmG/þ Foxd1GC/ Ai14*, *Foxd1GCE/ Ai14*, *NG2-cre-GFP/ Ai14* and *NG2-CreER-GFP/ Ai14*), I showed that 1) the influence of periostin on cell behaviour is tissue-specific, 2) periostin is involved in maintenance of PDL matrix stability, but can also enhance PDL fibroblast mineralization under osteogenic conditions, and 3) in the palate there are two distinct cell populations of different embryonic origin with minimal overlap, one expanded after injury and contributed to the formation of neovascular structures, while the other appeared more fibrogenic and contributed to most of the cells present on the wounded tissues.

My work shows that both cell-intrinsic and cell-extrinsic factors influence healing in the palatal mucoperiosteum, information that furthers our understanding of how differences in the cellular and molecular composition of tissues combine with specific physical properties in defining healing outcomes. I also demonstrated specific cell populations and extracellular matrix (ECM) constituents involved in wound repair in palatal tissues. These findings could lead to the development of an experimental system that allows separation of the distinct cell lineages so that vascular and pro-fibrotic behaviors can be studied in the same mice, while allowing us to alter the vascular/fibrotic balance, and ultimately guide the final healing outcome.

As will be discussed below, my thesis increases our understanding of how cells and ECM composition influence repair processes in the oral cavity. This knowledge can then be

applied in the rationale development of novel biomaterials with specific biochemical and biomechanical properties targeted to accelerate and enhance the healing process, while suppressing scarring and fibrosis, after dental and maxillofacial surgical procedures.

5.2 Key findings and knowledge contribution

5.2.1 Periostin and Matrix Stiffness Combine to Regulate Myofibroblast Differentiation and Fibronectin Synthesis During Palatal Healing

Matricellular proteins are temporally regulated throughout the wound repair process, and their expression has been linked to a range of important functional outcomes, including the regulation of inflammation, angiogenesis, and fibrogenesis (Walker et al., 2015). The first aim of this thesis focused on the matricellular protein periostin as a possible extrinsic mediator of cell behavior in the repair of the palatal mucoperiosteum.

Periostin is a secreted ECM protein that our research group has shown is transiently expressed during normal cutaneous (Elliott et al., 2012a) and gingival wound repair (Kim et al., 2019). However, it persists and is overexpressed in abnormal scar tissue and other benign fibroses that are characterized by fibroblast proliferation and myofibroblast differentiation (Crawford et al., 2015; Elliott & Hamilton, 2011; Zhou et al., 2010). Using the *Postn*$^{-/-}$ mouse model (H. Rios et al., 2005), I demonstrated that periostin is required for normal healing of the palatal mucoperiosteum; loss of periostin results in delayed palatal wound-closure kinetics. In agreement with cutaneous healing, the myofibroblast marker α-SMA/Acta2 was significantly reduced in the granulation tissue of *Postn*$^{-/-}$ mice at day 6 when compared with that in WT controls. However, although reduced, α-SMA was still expressed and myofibroblasts were present which suggested that stiffness of the microenvironment in the palate is sufficient to drive myofibroblast differentiation. Similarly, in cutaneous wounds in murine skin, deletion of periostin did not affect α-SMA expression in high-tension areas at the wound edge, but α-SMA is completely absent in the relatively low-tension granulation tissue, suggesting that the stiffness of the cellular

microenvironment is a key driver for myofibroblast differentiation and contraction (Elliott et al., 2012b).

In the palate, specific structural features are present that can alter the wound healing process that are not present in skin, specifically the underlying bone. Since the role of periostin in fibrosis is well-established, in this thesis I focused on the extracellular effects of periostin in palatal healing taking into account the stiffness of the microenvironment as a driving factor for cellular responses. The palatal soft tissue is a rigid mucoperiosteum that is attached to the palatal bone and it much stiffer than buccal mucosa and contains less elastin fibers (Bourke et al., 2000). Defining the mechanical characterisation of living human oral tissues has been difficult, and due to the lack of standardisation in the methodology the reported compressive modulus data is variable (J. J. E. Choi et al., 2020; Gasik et al., 2021). Understanding further the mechanical environment and how it impacts on periostin expression upstream of α-SMA expression could provide a means to alter wound healing and reduce scarring.

Although the free gingival graft palatal wound will usually heal within 2–4 weeks (Farnoush, 1978; Keskiner et al., 2016), despite the presence of denuded palate, problems persist with repair that directly influence the microenvironment of the cells. In cleft-palate reconstructive surgeries, mucoperiosteal flaps are created on the palate close to the cleft, leaving areas of denuded bone. However, a specific feature associated with the healing of open wounds in palatal mucoperiosteum is the deposition of callus-like cancellous bone on the palate. The granulation tissue and collagen fibers of palatal bone acquires an osteogenic potential and new bone is formed (Wijdeveld et al., 1987). Most of the collagen fibers of the forming scar are oriented in a transverse direction but many fibers also show a vertical orientation. These vertical fibers become embedded in cancellous palatal bone as Sharpeys' fibers, generating a strong attachment of scar tissue to the underlying palatal bone. The transverse fibers appear to be continuous with the cervical periodontal ligament providing mechanical connection between scar and teeth, which results in palatal tipping of erupting of the teeth and restriction of maxillary growth (Berkowitz, 1977; Kuijpers-Jagtman & Long, 2000; Von Den Hoff et al., 2006; Wijdeveld et al., 1991). My data shows that the

stiffness of the palate is sufficient to drive myofibroblast differentiation even in the absence of periostin demonstrating that reduction of scar formation post-surgery is not a simple task. However, the further investigation and comparison of distinct healing patterns among skin, gingiva and the palatal mucoperiosteum could provide a deeper understanding of how differences in molecular composition and physical properties of these tissues lead to the different healing outcomes.

Using an *in vitro* model of palatal fibroblasts to investigate these findings further, cells from *Postn*$^{-/-}$ animals had a significant reduction in their ability to contract anchored collagen gel, although proliferation rate was similar to cells isolated from WT animals. Addition of exogenous rhPSTN, however, fully rescued the phenotype of the *Postn*$^{-/-}$ fibroblasts suggesting that extracellular localization of periostin is both necessary for, and sufficient to, induce gel contraction through induction of a contractile myofibroblast phenotype. As stated previously, palatal fibroblasts mirror observations our group has shown in dermal fibroblasts isolated from *Postn*$^{-/-}$ mice (Elliott et al., 2012a). However, in human gingival fibroblasts the exogenous addition of rhPSTN does not increase α-SMA protein nor induce gel contraction (Kim et al., 2019), further supporting the behavioral and phenotypic differences between gingival, palatal and dermal fibroblasts observed in vitro.

Increased matrix stiffness is also a trigger for fibroblast to myofibroblast transition by inducing maturation of focal adhesions (Tomasek et al., 2002a), which further supports the possibility that healing gingival tissue ECM may not possess the same level of stiffness that granulation tissue has in skin or the palatal mucoperiosteum. Interestingly, the presence of periostin in gingival tissue is not sufficient to induce α-SMA, suggesting that the maturity of focal adhesions and a lack of adhesive signaling in human gingival fibroblasts more likely results in an absence of myofibroblasts during healing (Kim et al., 2019).

This observation motivated me to investigate further the role of ECM stiffness and adhesive signaling as potential modulators of periostin-induced myofibroblast differentiation and mechanotransduction pathways in palatal fibroblasts (Hinz, 2015a; Pakshir & Hinz, 2018; Rousselle et al., 2019; Zent & Guo, 2018). Activated TGF-β1 binds to the TGF-βR complex stimulating intracellular signaling that promotes α-SMA production. In parallel, ECM-to-

cell mechanical transduction through the integrin/focal adhesion (FA) pathway activates RhoA, leading to assembly of α-SMA stress fibers. Changing the stiffness of the cell substrate is an efficient method to control myofibroblast activation *in vitro* (Pakshir & Hinz, 2018; Talele et al., 2015; Tomasek et al., 2002b). In cultured differentiated myofibroblasts, using collagen and polyacrylamide gel substrates of varying stiffness, α-SMA expression levels increases with increasing matrix rigidity (Arora et al., 1999; Hinz, 2010b). *In vivo*, mechanically preventing wound closure by splinting the edges of experimental wounds accelerates expression of α-SMA compared with normally healing wounds, while stress release by removing the splint leads to reduced α-SMA expression (Hinz et al., 2001) . Well established evidence indicates that we can mimic the stiffness of the wound environment using different *in vitro* model systems: it has been shown that the stiffness of the provisional ECM of early wounds is comparable with the elastic modulus of ∼10–100 Pa of newly polymerized collagen gels (Kaufman et al., 2005) and fibroblasts seeded into these gels are devoid of contractile fibers and organize actin filaments (Tamariz & Grinnell, 2002). On the contrary, in mechanically restrained gels, tension is gradually increasing and first induces the formation of α-SMA-negative stress fibers (Tamariz & Grinnell, 2002), which is similar to the *de novo* appearance of proto-myofibroblast in 5- to 6-day-old rat wound granulation tissue (Hinz, 2007; Hinz et al., 2001). The threshold stiffness for *de novo* expression of α-SMA in stress fibers ranges around 20 kPa as demonstrated for contractile wound granulation tissue and for myofibroblasts cultured on elastic substrates (Goffin et al., 2006).

In this work, I showed that myofibroblast differentiation of murine palatal fibroblasts is stimulated by culture on stiff culture substrates but suppressed on substrates mimicking normal tissue (8 kPa) or granulation tissue (0.2 kPa) ECM stiffness, which is in agreement with other reports (Achterberg et al., 2014). Differences of matrix stiffness also affected the expression of fibronectin; on very stiff substrates (1 GPa), fibronectin synthesis was down-regulated while on low stiffness (0.2 kPa) fibronectin synthesis was up-regulated. Loss of periostin resulted in lower expression *Acta2*/α-SMA levels suggesting impaired myofibroblast differentiation capacity when compared to WT cells. However, this was most evident on rigid, collagen-coated tissue culture plates which have a stiffness of 1 GPa.

Lastly, myofibroblast differentiation in *Postn*$^{-/-}$ cells was rescued with the addition of Rac inhibitor, suggesting that periostin modulates myofibroblast differentiation in stiff matrices via RhoA/ROCK pathway.

Our observations from the *in vivo* experiments in the palate showed that α-SMA is still present but reduced in the granulation tissue of *Postn*$^{-/-}$ wounds, indicating that the loss of periostin is partially compensated by the stiffness of ECM environment which is sufficient to drive myofibroblast differentiation in *Postn*$^{-/-}$ wounds. Loss of periostin also resulted in significantly reduced fibronectin expression compared to WT cells. This observation further supports our previous finding, where human gingival fibroblasts cultured in the presence rhPSTN had increased fibronectin production, an effect which was attenuated by pharmacological inhibition of FAK and JNK signaling (Kim et al., 2019). These observations indicate that in palatal fibroblasts periostin modulates myofibroblast differentiation and fibronectin synthesis in cases of extreme stiffness and in very compliant microenvironments.

Cells are subjected to mechanical stresses and receive and respond to stimuli from the ECM through integrins (Moore et al., 2010; Schwarz & Gardel, 2012). In this study we found that focal adhesion formation and size are increased with an increase in the stiffness of the cell microenvironment, and that the genetic deletion of periostin resulted in a significant defect in focal adhesion formation in *Postn*$^{-/-}$ cells. This finding provides a possible explanation of the reduced contractility and fibronectin synthesis in the absence of periostin. Collectively, we found that in the absence of periostin, the formation of both focal and fibrillar adhesions is defective demonstrating the direct functional role of periostin in adhesion properties of the cells.

The fist aim of this thesis provides further evidence that periostin and the stiffness of the ECM act as modulators of matrix synthesis and myofibroblast differentiation during palatal healing. These findings could provide new insights for the development of novel approaches and biomaterials with specific biochemical and biomechanical properties targeted to accelerate and enhance the healing process (Urbanczyk et al., 2020), while suppressing fibrosis, after dental and maxillofacial surgical procedures.

In summary, I provide further evidence based on previous work from our lab, that the tissue-specific expression patterns and extracellular effects of periostin in the palate represents a combination of defined effects in skin and gingiva.

5.2.2 Role of periostin in the maintenance and mineralization of the periodontal ligament

In the second aim of my thesis, I investigated the effect of periostin on PDL fibroblast phenotype and how this could contribute to observed PDL responses in orthodontic injury and wound healing. In mice, periostin deletion manifests in a loss of the architecture and functional disruption of several collagenous-based tissues, particularly those subject to constant mechanical loading (H. Rios et al., 2005). *Postn*$^{-/-}$ mice exhibited significant damage to the periodontal tissues following exposure to a masticatory force, but placing the animals on a soft diet was sufficient to reduce the mechanical strain on the PDL and could partially rescue both the enamel and periodontal disease-like phenotypes (H. F. Rios et al., 2008). On the contrary, in the absence of mechanical stress, the PDL of Wistar rats undergoes degradation concomitantly with a marked decrease in periostin and CTGF mRNA levels in the PDL (J. W. Choi et al., 2011), suggesting that periostin is essential for maintaining the integrity of the PDL under physiological occlusal and mastication forces. It has been postulated that this relates to collagen cross-linking (Merle & Garnero, 2012; Norris et al., 2007; Tanabe et al., 2010).

Here, using an *ex vivo* mineralization model, we show that genetic loss of periostin in *Postn*$^{-/-}$ murine periodontal tissues does not increase or decrease the re-mineralization of the periodontal ligament *ex vivo*, suggesting that the presence of periostin in the PDL does not act to prevent mineralization. RNAseq and pathway enrichment analysis of PDL cells isolated from adults of 28 and 31 years of age and cultured in DMEM in the presence of exogenous periostin were mainly enriched in genes associated with collagen fibril formation and extracellular matrix organization. The clinical significance of these findings has many implications for PDL regeneration and in particular highlights a potential important role for periostin in orthodontic tooth movement. This is a process in which the

application of a mechanical force induces bone resorption on the pressure side and bone apposition on the tension side (Krishnan & Davidovitch, 2006), while maintaining the presence of the PDL. During orthodontic movement, periostin is involved in the process of periodontium remodeling in response to mechanical force (Lv et al., 2014; Rangiani et al., 2016; Wilde et al., 2003). Application of orthodontic forces induces divergent changes of periostin mRNA levels between the pressure and tension sites of rat PDL, with increased levels in the compressed side of the ligament when compared to tension sites (Wilde et al., 2003). The tissue in the compressed sides require a dramatic re-organization to maintain its width for normal tooth function, thus increased expression of periostin is in response to the need for rapid ECM re-organization and collagen re-arrangement. In *Postn*$^{-/-}$ mice, during application of orthodontic forces, the distance of the tooth movement and mineral deposition rates are significantly reduced when compared to WT mice, exhibiting impaired arrangement, digestion, and integrity of collagen fibrils (Rangiani et al., 2016). In combination with the RNAseq data presented in this thesis, it is apparent that periostin is essential for the PDL in response to physiological periodontium remodeling and orthodontic tooth movement, and my findings provide evidence of periostin's role in ECM organization and collagen fiber formation.

In vitro studies in human periodontal ligament mesenchymal stem cells have shown that periostin affects key functional aspects: Periostin promotes cell motility, adhesion, survival (Matsuzawa et al., 2015), migration, proliferation, and differentiation (Wu et al., 2018). In addition to regulation of processes involved in matrix formation and stability, previous studies have shown a role for periostin in the regulation of matrix mineralization (Galli et al., 2014; F. Zhang et al., 2015). Although *in vitro* and not representing the microenvironment of the *in situ* PDL, it nevertheless suggests that in certain conditions, periostin may act to promote mineralization of osteogenic cell populations including PDL cells. This is consistent with the phenotype of the *Postn*$^{-/-}$ mouse (H. Rios et al., 2005). In this chapter we show that the exogenous addition of periostin to human PDL cell cultures results in significantly more calcium content when compared to osteogenic media alone, suggesting that exogenous periostin promotes or enhances the mineralization of hPDL cells under osteogenic conditions. Our findings are in agreement with previous reports (Tang et

al., 2017; Wu et al., 2018). The potential of exogenous periostin's role as a therapy could be applied in clinical practice to enhance osseointegration of dental implants. Using tissue engineering, stimulating cells to differentiate to the right phenotype with the purpose of regenerating lost tissue requires an environment capable to provide the same factors that govern cellular processes *in vivo*. Thus, exogenous periostin coating of dental implants or biomaterials for guided-tissue regeneration can be a viable approach to improve cell adhesion and osteogenic differentiation of PDL cells on implantable biomaterials.

In adult tissues, periostin is mainly localized in areas rich in progenitor cells, such as the basement membrane, periosteum, chondrocytes of developing bone and the PDL (Cai et al., 2019; Jackson-Boeters et al., 2009; Zhou et al., 2010). An increasing body of research also supports a role for periostin in the regulation and differentiation of stem cells (Tkatchenko et al., 2009), such as hematopoietic stem cells (Khurana & Verfaillie, 2013; Tanaka et al., 2016), adipose-derived stem cells (Qin et al., 2015), and human PDL stem cells (Tang et al., 2017; Wu et al., 2018). The periodontium is rich source of periodontal ligament stem cells (PDLSCs), that have gained great attention for guided dental tissue regeneration, bone grafting, and enamel matrix reconstruction, as they pose the capacity to differentiate into osteoblasts, cementoblasts, adipocytes and neural crest- like cells (Zhu & Liang, 2015). Human cultures of PDL cells are known to be heterogenous in nature (Morissette Martin et al., 2017), which somewhat mirrors the *in vivo* cellular composition. Understanding extrinsic factors that guide their differentiation remains of importance from a clinical standpoint.

Here, we investigated transcriptional changes in human PDL cells after exposure to exogenous periostin or/and osteogenic culture conditions using RNA sequensing analysis. One of the most striking findings of this set of analyses was the very strong patient-specific effect, as observed by the high variability between patient responses to treatment condition with minimal overlap of common genes differentially expressed among the 4 patients. Focused analysis on the youngest patient (15 years old) revealed higher mineralization potential (as shown by the Alizarin Red assay) and unique gene expression patterns, both in unsupplemented and osteogenic media conditions, which is in agreement with previous

reports (Li et al., 2020; J. Zhang et al., 2012). It has previously been shown that cell-donor age also affects stem cells, as PDLSCs obtained from aged donors (mean age 54 y.o.) had less regenerative capacity compared with those from young donors (mean age 15 y.o.) (Zheng et al., 2009). Zhang and coworkers compared biological features of PDLSCs obtained from donors at different ages and found that proliferation and migration ability and differentiation potential of PDLSCs decreased as donor age increased (J. Zhang et al., 2012). Moreover, PDLSCs in aged groups (older than 41 years) expressed less Stro-1 and CD146 than young donors and failed to form cementum-PDL-like structures *in vivo*, indicating that the number and regenerative ability of stem cells decreased with increasing donor age (J. Zhang et al., 2012). These observations are of great clinical importance, as autologous transplantation of PDLSCs from older individuals might be of limited effectiveness given the compromised regenerative capacity of aged PDLSCs.

In this thesis, we also showed that when hPDL cells were cultured in osteogenic conditions, pathway enrichment analysis of DEG by the exogenous addition of periostin revealed involvement of pathways associated with bone remodeling and osteoblast differentiation. This indicates that PDL cells can dramatically switch their phenotype dependent on the local microenvironment. Since periostin is localized in the periosteum and periodontium, which undegoes continous physiological remodeling, my results highlight another potential role: in bone alveolar bone remodeling. This process consists of bone formation by osteoblasts and bone resorption by osteoclasts, while the osteocytes serve as mechanosensors and orchestrators during the bone remodeling process (Florencio-Silva et al., 2015). The expression of periostin was first identified in the mouse osteoblastic cell line MC3T3-E1 and found in the alveolar bone surface *in vivo*, suggesting its role in regulation of osteoblasts function (Horiuchi et al., 1999). Consistent with these observations, other studies of long bone osteoblasts show that periostin mutations caused impeded attachment of osteoblasts to the bone matrix, as well as significant reduction in expression of type I collagen, osteocalcin, osteopontin, and alkaline phosphatase. These alternations result in inhibition of their differentiation into mature osteoblasts, as well as the decrease in mineralization processes *in vitro* (Bonnet et al., 2012; Litvin et al., 2004).

In summary, the findings of this thesis show that periostin has condition-specific actions: in non-osteogenic conditions it contributes to ECM maintenance through modification of PDL cell phenotype, while in osteogenic conditions periostin promotes the mineralization capacity of PDL cells and contributes to gene expression changes associated with bone remodeling. Further studies are required to confirm information identified in the sequencing results. Critically, continuation of this work will enhance our understanding of the molecular and cellular effects of periostin on PDL cells could be helpful for periodontal regeneration and stem cell-targeted therapy.

5.2.3 Myofibroblast Origin in Palatal Repair: Assessing the Contribution and the Fate of Foxd1 and NG2 Populations and Their Progeny During Palatal Development and Repair

The third aim of this thesis focused investigating cell lineages that contribute to palatal repair, with a focus on understanding which populations contribute to healing of the connective tissue underlying the mucosa. In this thesis, I used the constitutive expression of Foxd1 in palatal progenitor populations during development to examine how cells derived from Foxd1-expressing progenitors contribute to murine embryonic orofacial tissues and adult palatal wound repair. In addition, I also investigated the role of NG2-lineage progeny in homeostasis and would healing of the adult murine palatal mucoperiosteum.

Based on previous lineage tracing studies in kidney fibrosis (Humphreys et al., 2010), lung fibrosis (Hung et al., 2013) and in skin healing (Walker et al., 2021), here the *Foxd1*-gene was used as a marker of pericytes and progenitors of fibroblasts/myofibroblasts during murine embryonic facial development and in palatal healing through lineage tracing. A number of studies have suggested that multiple subpopulations of pericytes may exist within different tissues and differentially contribute to myofibroblast formation and fibrosis specific (Di Carlo & Peduto, 2018; Gomes et al., 2021; LeBleu & Neilson, 2020; Lemos & Duffield, 2018). In this thesis we explored whether binary expression of Foxd1 during

embryogenesis could be used as a new potential marker of fibroblasts within the oral cavity and the repair process in the palatal mucoperiosteum, and to compare our findings with evidence from murine skin healing.

During the early stages of maxillofacial development, I found that Foxd1-lineage positive (FLP) cells are not of neural crest origin but represent a major lineage that gives rise to pericytes and endothelial cells in the neovascularization of the developing palatal tissues. My results show that during development Foxd1-lineage positive cells that are sparsely distributed in lateral maxillary processes are mainly contributing to cells of the neovasculature. Angioblasts are the only cells of mesodermal origin so far identified that move into the stream of migrating neural crest cells, apparently as soon as the neural crest cells have formed as a mesenchymal population lateral and rostral to the mesodermal mesenchyme (Yoshida et al., 2008). This early incursion of mesodermal angioblasts into an apparently otherwise pure neural crest cell population enables blood vessels to form equally quickly within the neural crest-derived and mesoderm-derived mesenchyme of the head (Yoshida et al., 2008). Evidence from lineage tracing studies suggest that in the craniofacial region of mouse embryos the endothelial cells of blood vessels are of mesodermal origin and the muscular components of the vessel walls (pericytes) are derived from neural crest (Yoshida et al., 2008). Overall, limited information or analysis of cell populations through lineage tracing experiments has been performed in the oral cavity or the hard palate. Utilizing lineage tracing techniques in *Wnt1-Cre;Zsgreen*$^{fl/fl}$ mice it was demonstrated that all the tendons and mesenchyme embedding the soft palate muscles are neural crest-derived, proposing that the posterior attachment of the soft palate to the pharyngeal wall is an interface between the neural crest- and mesoderm-derived mesenchyme in the craniofacial region (Grimaldi et al., 2015). Although regional clonal diversity was also recently demonstrated in the cells of the epithelium that covers the hard palate in mice (Byrd et al., 2019; Jones et al., 2019; Yuan et al., 2019), there is limited analysis of the stromal cells of the palatal mucoperiosteum. Lineage tracing experiments have identified that neural crest-derived cells persist in adult tissues in some areas of the oral mucosa and that Lgr51-lineage-positive cells participate in the maintenance of the stroma (Boddupally et al., 2016). My findings not only provide further evidence about the

mesodermal origin of the vasculature structures within the developing palate- as they do not express neural-crest markers SOX10 and p75NTR, but also point to the mesodermal origin of the Foxd1- embryonic lineage.

In adult palatal tissues, Foxd1-lineage positive cells contribute to a relatively small proportion of cells, mainly associated with blood vessels, where they give rise to some smooth muscle cells of peripheral veni, pericytes and certain populations of endothelial cells. Upon wounding, the Foxd1-derived population becomes activated; shows significantexpansion with the cells mainly associated with neovascularization processes in the developing granulation tissue. In contrast to evidence from dermal would healing where Foxd1-derived progeny contributed to a significant portion of mesenchymal matrix producing cells (Walker et al., 2021), in the palate Foxd1-derived progeny show no significant overlap with any fibroblast or myofibroblast markers, providing further evidence about differences between oral and skin healing characteristics. My findings suggest that even though this population has a common embryonic signature, the functional properties of its terminally differentiated progeny is largely dependent on the physico-mechanical characteristics of the mature tissue: in skin, a tissue prone to scarring, this population accounts for almost 50% of the fibroblasts, while in the palate, a tissue that does not typically scar (unless major cleft-palate reconstruction surgery is performed), Foxd1 progeny only gives rise to vasculature-related cells advancing the healing outcome via neovascularization of the granulation tissue.

Interestingly, I found that NG2-lineage progeny cells are present in adult palatal tissues, but in contrast to Foxd1 progeny, they do expand upon wounding contributing to the mesenchymal cells and myofibroblasts within the granulation tissue. Based on our observations in the palate, it appears that the NG2-progeny marks a distinct cell population with a more fibrotic profile, while the Foxd1-progeny is restricted to cells with vascular role. For the first time, we have identified the two distinct major cell populations that orchestrate the wound healing process, and investigation into their specific characteristics, behaviour and balance can lead to a more thorough understanding of the different healing outcomes evident and how it can be altered through activation of certain cell populations.

The work presented in this thesis contributes to a growing understanding of fibroblast heterogeneity and provides insight into how divergent populations might cooperate during wound repair. Our findings further support that cell populations across different tissues, although they originate from common embryonic lineages, they present different phenotypes in mature and wounded tissues. This observation points to the significance of cell-extrinsic factors (extracellular environment, from tissue-specificity perspective, ECM composition and microenvironment biomechanical properties) as determinants of cell fate and behaviour across different tissues, and that could further explain the different healing patterns among them.

5.3 Experimental Limitations

In this thesis, an excisional wound of 1.5 mm diameter was created in the posterior area of the hard palate. The limiting factors in the size of experimental defect that could be created was the relatively small size of the palate available to wound and the presence of the greater major palatine arteries on other side of the hard palate. Injury of either of these arteries would be detrimental for the recovery of the animals. The small size of the wound resulted in rapid healing and optimal clinical outcomes, as excessive scarring could not be observed. Availability of *Postn*$^{-/-}$ rat model would permit for a larger critical defect that scarring could be observed and biomaterials to be tested on the site of injury, better replicating the clinical conditions.

In Chapter 3, the data obtained from the RNA sequencing analysis need to be interpreted with caution. When assessing variability within the dataset, it is preferable that the intergroup variability, representing differences between experimental conditions in comparison with control conditions, is greater than the intragroup variability, representing technical or biological variability. Our results show significant variability among the different patients, and minimal overlap between commonly differentially expressed genes. Further studies will focus on sample size, number of conditions to be compared, depth of sequence reads and promoter RNA sequencing analysis.

5.4 Future Directions

5.4.1 Harnessing exogenous factors to guide wound healing in palatal healing

Even though common dental procedures, such as palatal tissue harvesting for free gingival graft, result in optimal healing outcome in the palate (Keskiner et al., 2016), cleft-palate reconstructive surgeries result in excessive scarring, misalignment of erupting of the teeth and restriction of the maxillary development in transversal width when the patient is in their growing phase, leading to serious functional and aesthetic problems (Larjava, 2013).

In this thesis, we report the first description of palatal wound healing models in *Postn*$^{-/-}$ mice and the functional properties of isolated murine palatal cells from transgenic mice. Moreover, I show how the composition and mechanical tension of the ECM and surrounding microenvironment affect cellular responses. My data shows that periostin is at the forefront of granulation tissue development in the palate and the modulation of cell phenotype. With respect to extracellular matrix changes during palatal healing, we show that periostin modulates cell contractility and in combination with tissue stiffness, influences fibronectin synthesis. However, the overexpression and persistence of periostin in the ECM is associated with abnormal scars and other benign fibroses (Crawford et al., 2015; Elliott & Hamilton, 2011; Zhou et al., 2010). Therefore, any approach using periostin to facilitate repair would need to be tightly controlled in a spatiotemporal manner, taking into account the mechanical properties not only of the native tissue environment, but also of the proposed biomaterial.

Exogenous delivery of periostin in palatal wounds, in an environment of high tension, could have adverse effects on the healing outcome, as it would enhance the profibrotic response of the cells, leading to increased myofibroblast activity and matrix synthesis. Our lab has previously shown that delivery of recombinant periostin in an electrospun form is viable in murine skin healing, where it stimulated α-SMA expression in the granulation tissue of *Postn*$^{-/-}$ wounds (Elliot et al.,2012). More recently, we also demonstrated, in a murine model of diabetic wounds, that the addition of periostin and CCN2 in a scaffold form

increases closure rates of full-thickness skin wounds in diabetic mice, concomitant with enhanced angiogenesis (Elliott et al., 2019). The results of this thesis provide evidence of the significance not only of the chemical composition of the wound microenvironment, but also its mechanical properties in the cellular responses. Thus, when designing biomaterials it is necessary to take into account the mechanical properties of the wound microenvironment, as a major contributor to the final healing outcome.

The palatal mucoperiosteum is tightly attached to the underlying bone, leading to excessive stress forces during wound healing. During cleft palate reconstruction surgeries, flaps of palatal tissues are raised to close the oro-nasal communication, resulting in areas of denuded maxillary bone, and subsequent the deposition of callus-like cancellous bone on the palate, where most of the collagen fibers of palatal bone acquires an osteogenic potential and new bone is formed (Wijdeveld et al., 1987). The collagen fibers become embedded in cancellous palatal bone, generating a strong attachment of scar tissue to the underlying palatal bone. The mechanical stress exerted by the stiffness of ECM due to this attachment positively feedbacks on the development and progression of fibrotic conditions by directly promoting myofibroblast activation and persistence through various mechanotransduction pathways (Achterberg et al., 2014; Goffin et al., 2006; Hinz, 2015b; Pakshir & Hinz, 2018; Rousselle et al., 2019). In this thesis we showed that changing the stiffness of the cell substrate is an efficient method to control palatal myofibroblast activation and fibronectin synthesis in vitro. Thus, design of novel biomaterials for cases of cleft-palate surgeries should aim to reduce stresses developed within the wounded area, and, as a result, to create an environment that is not conducive to scarring. This can be achieved by designing a material that is able to reduce the stiffness of the area that it is applied, and that it can maintain its mechanical properties after its application on to the wounded area for a prolonged period of time, sufficient to allow the formation of a granulation tissue that is not in direct contact with the denuded bone or the callus-like osteogenic bone. Alternatively, using this current evidence, biomaterials can be designed in a way that they block the physical contact between the granulation tissue and the bone surface, preventing the collagen fibers to be embedded in the cancellus bone, thus reducing the stress of the wounded tissues and scarring.

Taking into account the totality of this knowledge, efforts should focus on improving biomaterial design, in terms not only of their chemical composition and delivery of matricellular proteins/growth factors, but also their mechanical properties with the aim to guide the cellular response towards an optimal healing outcome. Such an approach could help reduce the problems associated with maxillary growth and teeth eruption prevalent in children following cleft palate repair.

5.4.2 Investigating the functional relevance of Foxd1- and Ng2-progeny in palatal tissues

Our work has revealed two distinct embryonic-progeny populations that contribute to palatal wound healing in mice: Foxd1- expressing cells and their progeny expand and form the neovascular structures of the wounded tissues, while NG2-progeny are more fibrogenic and contributed to most of the contractile cells present in the granulation tissue of the wounds. To further investigate the functional differences of Foxd1- and NG2-lineage, palatal cells isolation and gene expression assays are needed. The isolated cells can be sorted into Foxd1-lineage positive and negative, an NG2-lineage positive and negative and assess differential gene expression profiles among these populations. In skin, Foxd1 lineage-positive and lineage-negative dermal fibroblasts were identified to have divergent gene expression patterns, with FLP cells showing more fibrotic gene expression patterns (Walker et al., 2021).

Future studies should focus on further probing how these genetic differences impact cell function. Functional differences between FACS-sorted cells should be assessed *in vitro* and *in vivo*. In vitro experiments could focus on assessing functional differences of the sorted cell populations, such as gel contraction, migration and invasion assays as well as vasculogenesis assays. In vivo, an effective strategy to assess cell function is through transplantation studies using FACS-sorted populations. Using this strategy, Driskell *et al.* identified a role of papillary fibroblasts in hair follicle formation (Driskell et al., 2013). Additionally, Rinkevich *et al.* and Jiang *et al.* provided evidence of scarring potential in the *engrailed-1* lineage of fibroblasts over the lineage-negative population using

transplantation studies (Jiang et al., 2018; Jiang & Rinkevich, 2021; Rinkevich et al., 2015). However, with cell transplantation studies, the lineages are not assessed in isolation of each other due to the contribution of cells endogenous to the recipient. Nevertheless, such experiments can provide important information on cell function.

Another method that allows for the assessment of specific lineages *in vivo* is cell ablation using a diphtheria toxin (DT)/ DT receptor (DTR) approach (Dulauroy et al., 2012; Rinkevich et al., 2015). This method results in the selective ablation of cells, controlled by Cre/Lox recombination or cell-specific promoters, inducing cell death through inhibition of protein synthesis (Saito et al., 2001). However, because the *Foxd1 and NG2* lineages are not specific to only one cell population, using this approach could have severe health consequences for the animal if not controlled by additional cell-type specific promoters, or localized DT delivery. However, results from cell ablation studies should be interpreted with caution as the effects of it could be due to a loss in total fibroblast number and not specifically the cells of interest. Exploring further the use of lineage tracing technology, how well this would work in practice is uncertain. To my knowledge, such an approach has not been explored. Overall, with the current state of available methods, cell transplantation studies offer a more robust model for *in vivo* exploration of functional differences between fibroblast lineages.

My results show for the first time that two distinct embryonic-progeny populations contribute to palatal wound healing in separate and unique ways: one involving vascular regeneration and the other associated with fibrotic processes. This points to a new technology where we can investigate these aspects of healing individually and/or combined together, opening the possibility to explore the influence of the one over the other. Such experimental model would allow us to finetune the balance between neovasculogenesis and matrix production, to examine the inverse correlation between scarring and vascularization, and ultimately determine the parameters for optimal healing outcome. For this model, a multicolor reporter system that combines two or more recombination systems for genetic targeting of more than one cell population (usually two) could be used to trace simultaneously Foxd1- and NG2-progeny. Intersectional dual-reporter systems, such as

RC::Fela, R26::FLAP, RC::RLTG, and R26NZG, can be used to label two distinct cell populations (Plummer et al., 2015; Yamamoto et al., 2009). In addition, sequential and exclusive double-reporter systems are also explored for labeling specific cell types more precisely (Zhao & Zhou, 2019). However, because of the exclusive nature of recombination design, these genetic tools only allow simultaneous labeling of two (sub)populations in tissue. Development of a multicolor reporter system capable of labeling three distinct cell populations by noninterfering recombination is useful for studying the behavior of more diverse cell types simultaneously in vivo (Liu et al., 2020).

Further exploration of functional differences could help to identify underlying cell- intrinsic mechanisms that regulate palatal repair and shed more light on the differences between oral and skin healing. Moreover, a better understanding of how diverse fibroblast populations interact, and the major mechanisms coordinating their interactions could potentially identify important targets for future investigation in the context of guided tissue regeneration in the oral environment.

5.5 Conclusions

First, the role of the matricellular protein periostin in the context of palatal healing was investigated and it was determined to be associated with fibronectin production, myofibroblast differentiation and infiltration of macrophages in wounded palatal tissues. Our findings provide further evidence that periostin and the stiffness of the ECM act as modulators of matrix synthesis and myofibroblast differentiation during palatal healing. Next, progress is made to determine the role of periostin in the homeostasis of the periodontal ligament under normal and osteogenic conditions, highlighting the diverse and tissue-specific bioactivity of periostin. Finally, a cell lineage tracing strategy was utilized and provided evidence for the presence of two distinct populations contributing to palatal wound healing, one predominately vasculogenic and one more fibrotic, providing further evidence about the intrinsic differences of cell populations that lead to distinct healing patterns among different tissues.

Through these diverse studies, insights into effects of the ECM microenvironment in the context of palatal repair and the intrinsic cell differences of populations contributing to the healing process have been made. Application of this translatable knowledge could be utilized in the future for development of biomaterials that can be targeted and guided to enhance healing outcomes while inhibiting undesired effects, such as scarring and fibrosis in a tissue-specific manner.

5.5 References

Achterberg, V. F., Buscemi, L., Diekmann, H., Smith-Clerc, J., Schwengler, H., Meister, J. J., Wenck, H., Gallinat, S., & Hinz, B. (2014). The nano-scale mechanical properties of the extracellular matrix regulate dermal fibroblast function. *Journal of Investigative Dermatology*, *134*(7), 1862–1872. https://doi.org/10.1038/jid.2014.90

Arora, P. D., Narani, N., & McCulloch, C. A. G. (1999). The compliance of collagen gels regulates transforming growth factor-β induction of α-smooth muscle actin in fibroblasts. *American Journal of Pathology*, *154*(3), 871–882. https://doi.org/10.1016/S0002-9440(10)65334-5

Berkowitz, S. (1977). Cleft lip and palate research: An updated state of the art. Section III. Orofacial growth and dentistry. *The Cleft Palate Journal*, *14*(4), 288–301.

Boddupally, K., Wang, G., Chen, Y., & Kobielak, A. (2016). Lgr5 Marks Neural Crest Derived Multipotent Oral Stromal Stem Cells: Lgr5 positive oral stromal stem cells. *STEM CELLS*, *34*(3), 720–731. https://doi.org/10.1002/stem.2314

Bonnet, N., Conway, S. J., & Ferrari, S. L. (2012). Regulation of beta catenin signaling and parathyroid hormone anabolic effects in bone by the matricellular protein periostin. *Proceedings of the National Academy of Sciences*, *109*(37), 15048–15053. https://doi.org/10.1073/pnas.1203085109

Bourke, K. A., Haase, H., Li, H., Daley, T., & Bartold, P. M. (2000). Distribution and synthesis of elastin in porcine gingiva and alveolar mucosa. *Journal of Periodontal Research*, *35*(6), 361–368. https://doi.org/10.1034/j.1600-0765.2000.035006361.x

Byrd, K. M., Piehl, N. C., Patel, J. H., Huh, W. J., Sequeira, I., Lough, K. J., Wagner, B. L., Marangoni, P., Watt, F. M., Klein, O. D., Coffey, R. J., & Williams, S. E. (2019). Heterogeneity within Stratified Epithelial Stem Cell Populations

Maintains the Oral Mucosa in Response to Physiological Stress. *Cell Stem Cell*, *25*(6), 814-829.e6. https://doi.org/10.1016/j.stem.2019.11.005

Cai, L., Brophy, R. H., Tycksen, E. D., Duan, X., Nunley, R. M., & Rai, M. F. (2019). Distinct expression pattern of periostin splice variants in chondrocytes and ligament progenitor cells. *FASEB Journal : Official Publication of the Federation of American Societies for Experimental Biology*, *33*(7), 8386–8405. https://doi.org/10.1096/fj.201802281R

Choi, J. J. E., Zwirner, J., Ramani, R. S., Ma, S., Hussaini, H. M., Waddell, J. N., & Hammer, N. (2020). Mechanical properties of human oral mucosa tissues are site dependent: A combined biomechanical, histological and ultrastructural approach. *Clinical and Experimental Dental Research*, *6*(6), 602–611. https://doi.org/10.1002/cre2.305

Choi, J. W., Arai, C., Ishikawa, M., Shimoda, S., & Nakamura, Y. (2011). Fiber system degradation, and periostin and connective tissue growth factor level reduction, in the periodontal ligament of teeth in the absence of masticatory load. *Journal of Periodontal Research*, *46*(5), 513–521. https://doi.org/10.1111/j.1600-0765.2011.01351.x

Crawford, J., Nygard, K., Gan, B. S., & O'Gorman, D. B. (2015). Periostin induces fibroblast proliferation and myofibroblast persistence in hypertrophic scarring. *Experimental Dermatology*, *24*(2), 120–126. https://doi.org/10.1111/exd.12601

Di Carlo, S. E., & Peduto, L. (2018). The perivascular origin of pathological fibroblasts. *Journal of Clinical Investigation*, *128*(1), 54–63. https://doi.org/10.1172/JCI93558

Driskell, R. R., Lichtenberger, B. M., Hoste, E., Kretzschmar, K., Simons, B. D., Charalambous, M., Ferron, S. R., Herault, Y., Pavlovic, G., Ferguson-Smith, A. C., & Watt, F. M. (2013). Distinct fibroblast lineages determine dermal architecture in skin development and repair. *Nature*, *504*(7479), 277–281. https://doi.org/10.1038/nature12783

Dulauroy, S., Carlo, S. E. D., Langa, F., Eberl, G., & Peduto, L. (2012). Lineage tracing and genetic ablation of ADAM12 + perivascular cells identify a major source of profibrotic cells during acute tissue injury. *Nature Medicine*. https://doi.org/10.1038/nm.2848

Elliott, C. G., & Hamilton, D. W. (2011). Deconstructing fibrosis research: Do pro-fibrotic signals point the way for chronic dermal wound regeneration? *Journal of Cell Communication and Signaling*, *5*(4), 301–315. https://doi.org/10.1007/s12079-011-0131-5

Elliott, C. G., Wang, J., Guo, X., Xu, S. -w., Eastwood, M., Guan, J., Leask, A., Conway, S. J., & Hamilton, D. W. (2012a). Periostin modulates myofibroblast differentiation during full-thickness cutaneous wound repair. *Journal of Cell Science*, *125*(1), 121–132. https://doi.org/10.1242/jcs.087841

Elliott, C. G., Wang, J., Guo, X., Xu, S. -w, Eastwood, M., Guan, J., Leask, A., Conway, S. J., & Hamilton, D. W. (2012b). Periostin modulates myofibroblast differentiation during full-thickness cutaneous wound repair. *Journal of Cell Science*, *125*(1), 121–132. https://doi.org/10.1242/jcs.087841

Elliott, C. G., Wang, J., Walker, J. T., Michelsons, S., Dunmore-Buyze, J., Drangova, M., Leask, A., & Hamilton, D. W. (2019). Periostin and CCN2 Scaffolds Promote the Wound Healing Response in the Skin of Diabetic Mice. *Tissue Engineering - Part A*, *25*(17–18), 1326–1339. https://doi.org/10.1089/ten.tea.2018.0268

Farnoush, A. (1978). Techniques for the Protection and Coverage of the Donor Sites in Free Soft Tissue Grafts. *Journal of Periodontology*, *49*(8), 403–405. https://doi.org/10.1902/jop.1978.49.8.403

Florencio-Silva, R., Sasso, G. R. da S., Sasso-Cerri, E., Simões, M. J., & Cerri, P. S. (2015). Biology of Bone Tissue: Structure, Function, and Factors That Influence Bone Cells. *BioMed Research International*, *2015*, 421746. https://doi.org/10.1155/2015/421746

Galli, C., Piergianni, M., Piemontese, M., Lumetti, S., Ravanetti, F., Cacchioli, A., Macaluso, G. M., & Passeri, G. (2014). Periostin improves cell adhesion to implantable biomaterials and osteoblastic differentiation on implant titanium surfaces in a topography-dependent fashion. *Journal of Biomedical Materials Research - Part A*, *102*(11), 3855–3861. https://doi.org/10.1002/jbm.a.35056

Gasik, M., Lambert, F., & Bacevic, M. (2021). Biomechanical Properties of Bone and Mucosa for Design and Application of Dental Implants. *Materials*, *14*(11), 2845. https://doi.org/10.3390/ma14112845

Goffin, J. M., Pittet, P., Csucs, G., Lussi, J. W., Meister, J. J., & Hinz, B. (2006). Focal adhesion size controls tension-dependent recruitment of α-smooth muscle actin to stress fibers. *Journal of Cell Biology*, *172*(2), 259–268. https://doi.org/10.1083/jcb.200506179

Gomes, R. N., Manuel, F., & Nascimento, D. S. (2021). The bright side of fibroblasts: Molecular signature and regenerative cues in major organs. *Npj Regenerative Medicine*, *6*(1), 43. https://doi.org/10.1038/s41536-021-00153-z

Grimaldi, A., Parada, C., & Chai, Y. (2015). A Comprehensive Study of Soft Palate Development in Mice. *PLOS ONE*, *10*(12), e0145018. https://doi.org/10.1371/journal.pone.0145018

Hinz, B. (2007). Formation and Function of the Myofibroblast during Tissue Repair. *Journal of Investigative Dermatology*, *127*(3), 526–537. https://doi.org/10.1038/sj.jid.5700613

Hinz, B. (2010a). The myofibroblast: Paradigm for a mechanically active cell. *Journal of Biomechanics*, *43*(1), 146–155. https://doi.org/10.1016/j.jbiomech.2009.09.020

Hinz, B. (2010b). The myofibroblast: Paradigm for a mechanically active cell. *Journal of Biomechanics*, *43*(1), 146–155. https://doi.org/10.1016/j.jbiomech.2009.09.020

Hinz, B. (2015a). The extracellular matrix and transforming growth factor-β1: Tale of a strained relationship. *Matrix Biology*, *47*, 54–65. https://doi.org/10.1016/j.matbio.2015.05.006

Hinz, B. (2015b). The extracellular matrix and transforming growth factor-β1: Tale of a strained relationship. *Matrix Biology*, *47*, 54–65. https://doi.org/10.1016/j.matbio.2015.05.006

Hinz, B., Celetta, G., Tomasek, J. J., Gabbiani, G., & Chaponnier, C. (2001). *Alpha-Smooth Muscle Actin Expression Upregulates Fibroblast Contractile Activity*. *12*(September), 2730–2741.

Horiuchi, K., Amizuka, N., Takeshita, S., Takamatsu, H., Katsuura, M., Ozawa, H., Toyama, Y., Bonewald, L. F., & Kudo, A. (1999). Identification and characterization of a novel protein, periostin, with restricted expression to periosteum and periodontal ligament and increased expression by transforming growth factor beta. *Journal of Bone and Mineral Research : The Official Journal of the American Society for Bone and Mineral Research*, *14*(7), 1239–1249. https://doi.org/10.1359/jbmr.1999.14.7.1239

Humphreys, B. D., Lin, S. L., Kobayashi, A., Hudson, T. E., Nowlin, B. T., Bonventre, J. V., Valerius, M. T., McMahon, A. P., & Duffield, J. S. (2010). Fate tracing reveals the pericyte and not epithelial origin of myofibroblasts in kidney fibrosis. *American Journal of Pathology*, *176*(1), 85–97. https://doi.org/10.2353/ajpath.2010.090517

Hung, C., Linn, G., Chow, Y. H., Kobayashi, A., Mittelsteadt, K., Altemeier, W. A., Gharib, S. A., Schnapp, L. M., & Duffield, J. S. (2013). Role of lung Pericytes and resident fibroblasts in the pathogenesis of pulmonary fibrosis. *American Journal of Respiratory and Critical Care Medicine*, *188*(7), 820–830. https://doi.org/10.1164/rccm.201212-2297OC

Jackson-Boeters, L., Wen, W., & Hamilton, D. W. (2009). Periostin localizes to cells in normal skin, but is associated with the extracellular matrix during wound repair. *Journal of Cell Communication and Signaling*, *3*(2), 125–133. https://doi.org/10.1007/s12079-009-0057-3

Jiang, D., Correa-Gallegos, D., Christ, S., Stefanska, A., Liu, J., Ramesh, P., Rajendran, V., De Santis, M. M., Wagner, D. E., & Rinkevich, Y. (2018). Two succeeding fibroblastic lineages drive dermal development and the transition from regeneration to scarring. *Nature Cell Biology*, *20*(4), 422–431. https://doi.org/10.1038/s41556-018-0073-8

Jiang, D., & Rinkevich, Y. (2021). Distinct fibroblasts in scars and regeneration. *Current Opinion in Genetics & Development*, *70*, 7–14. https://doi.org/10.1016/j.gde.2021.04.005

Jones, K. B., Furukawa, S., Marangoni, P., Ma, H., Pinkard, H., D'Urso, R., Zilionis, R., Klein, A. M., & Klein, O. D. (2019). Quantitative Clonal Analysis and Single-Cell Transcriptomics Reveal Division Kinetics, Hierarchy, and Fate of Oral Epithelial Progenitor Cells. *Cell Stem Cell*, *24*(1), 183-192.e8. https://doi.org/10.1016/j.stem.2018.10.015

Kaufman, L. J., Brangwynne, C. P., Kasza, K. E., Filippidi, E., Gordon, V. D., Deisboeck, T. S., & Weitz, D. A. (2005). Glioma expansion in collagen I matrices: Analyzing collagen concentration-dependent growth and motility patterns. *Biophysical Journal*, *89*(1), 635–650. https://doi.org/10.1529/biophysj.105.061994

Keskiner, I., Aydogdu, A., Balli, U., & Kaleli, A. E. (2016). Quantitative changes in palatal donor site thickness after free gingival graft harvesting: A pilot study. *Journal of Clinical Periodontology*, *43*(11), 976–984. https://doi.org/10.1111/jcpe.12592

Khurana, S., & Verfaillie, C. M. (2013). Periostin Acts As An Important Cell Cycle Regulator Of Adult Hematopoietic Stem Cells Via Binding To Integrin-αvβ3. *Blood*, *122*(21), 341. https://doi.org/10.1182/blood.V122.21.341.341

Kim, S. S., Nikoloudaki, G. E., Michelsons, S., Creber, K., & Hamilton, D. W. (2019). Fibronectin synthesis, but not α-smooth muscle expression, is regulated by periostin in gingival healing through FAK/JNK signaling. *Scientific Reports*, *9*(1), 2708. https://doi.org/10.1038/s41598-018-35805-6

Krishnan, V., & Davidovitch, Z. (2006). Cellular, molecular, and tissue-level reactions to orthodontic force. *American Journal of Orthodontics and Dentofacial Orthopedics*, *129*(4), 469.e1-469.e32. https://doi.org/10.1016/j.ajodo.2005.10.007

Kuijpers-Jagtman, A. M., & Long, R. E. (2000). The Influence of Surgery and Orthopedic Treatment on Maxillofacial Growth and Maxillary Arch Development in Patients Treated for Orofacial Clefts. *The Cleft Palate-Craniofacial Journal*, *37*(6), 1–12. https://doi.org/10.1597/1545-1569_2000_037_0527_tiosao_2.0.co_2

Larjava, H. (2013). Oral Wound Healing: Cell Biology and Clinical Management. In *Oral Wound Healing: Cell Biology and Clinical Management*. https://doi.org/10.1002/9781118704509

LeBleu, V. S., & Neilson, E. G. (2020). Origin and functional heterogeneity of fibroblasts. *The FASEB Journal*, *34*(3), 3519–3536. https://doi.org/10.1096/fj.201903188R

Lemos, D. R., & Duffield, J. S. (2018). Tissue-resident mesenchymal stromal cells: Implications for tissue-specific antifibrotic therapies. *Science Translational Medicine*, *10*(426), eaan5174. https://doi.org/10.1126/scitranslmed.aan5174

Li, X., Zhang, B., Wang, H., Zhao, X., Zhang, Z., Ding, G., & Wei, F. (2020). The effect of aging on the biological and immunological characteristics of periodontal

ligament stem cells. *Stem Cell Research & Therapy*, *11*(1), 326. https://doi.org/10.1186/s13287-020-01846-w

Litvin, J., Selim, A.-H., Montgomery, M. O., Lehmann, K., Rico, M. C., Devlin, H., Bednarik, D. P., & Safadi, F. F. (2004). Expression and function of periostin-isoforms in bone. *Journal of Cellular Biochemistry*, *92*(5), 1044–1061. https://doi.org/10.1002/jcb.20115

Liu, K., Tang, M., Jin, H., Liu, Q., He, L., Zhu, H., Liu, X., Han, X., Li, Y., Zhang, L., Tang, J., Pu, W., Lv, Z., Wang, H., Ji, H., & Zhou, B. (2020). Triple-cell lineage tracing by a dual reporter on a single allele. *The Journal of Biological Chemistry*, *295*(3), 690–700. https://doi.org/10.1074/jbc.RA119.011349

Lv, S., Liu, H., Cui, J., Hasegawa, T., Hongo, H., Feng, W., Li, J., Sun, B., Kudo, A., Amizuka, N., & Li, M. (2014). Histochemical examination of cathepsin K, MMP1 and MMP2 in compressed periodontal ligament during orthodontic tooth movement in periostin deficient mice. *Journal of Molecular Histology*, *45*(3), 303–309. https://doi.org/10.1007/s10735-013-9548-x

Martin, P., & Nunan, R. (2015). Cellular and molecular mechanisms of repair in acute and chronic wound healing. *The British Journal of Dermatology*, *173*(2), 370–378. https://doi.org/10.1111/bjd.13954

Matsuzawa, M., Arai, C., Nomura, Y., Murata, T., Yamakoshi, Y., Oida, S., Hanada, N., & Nakamura, Y. (2015). Periostin of human periodontal ligament fibroblasts promotes migration of human mesenchymal stem cell through the αvβ3 integrin/FAK/PI3K/Akt pathway. *Journal of Periodontal Research*, *50*(6), 855–863. https://doi.org/10.1111/jre.12277

Merle, B., & Garnero, P. (2012). The multiple facets of periostin in bone metabolism. *Osteoporosis International*, *23*(4), 1199–1212. https://doi.org/10.1007/s00198-011-1892-7

Moore, S. W., Roca-Cusachs, P., & Sheetz, M. P. (2010). Stretchy proteins on stretchy substrates: The important elements of integrin-mediated rigidity sensing. *Developmental Cell*, *19*(2), 194–206. https://doi.org/10.1016/j.devcel.2010.07.018

Morissette Martin, P., Creber, K., & Hamilton, D. W. (2017). 6—Measuring gene expression changes on biomaterial surfaces. In R. J. Narayan (Ed.), *Monitoring and Evaluation of Biomaterials and their Performance In Vivo* (pp. 111–131). Woodhead Publishing. https://doi.org/10.1016/B978-0-08-100603-0.00006-7

Norris, R. A., Damon, B., Kern, C. B., Wen, X., Forgacs, G., Hoffman, S., Trusk, T., Molkentin, J. D., Goodwin, R. L., Conway, S. J., Norris, R. A., Kasyanov, V., Potts, J. D., Mjaatvedt, C. H., Oka, T., Moreno-Rodriguez, R., Markwald, R. R., Sugi, Y., Davis, J., … Mironov, V. (2007). Periostin regulates collagen fibrillogenesis and the biomechanical properties of connective tissues. *Journal of Cellular Biochemistry*, *101*(3), 695–711. https://doi.org/10.1002/jcb.21224

Pakshir, P., & Hinz, B. (2018). The big five in fibrosis: Macrophages, myofibroblasts, matrix, mechanics, and miscommunication. *Matrix Biology*, *68–69*, 81–93. https://doi.org/10.1016/j.matbio.2018.01.019

Plummer, N. W., Evsyukova, I. Y., Robertson, S. D., de Marchena, J., Tucker, C. J., & Jensen, P. (2015). Expanding the power of recombinase-based labeling to uncover cellular diversity. *Development (Cambridge, England)*, *142*(24), 4385–4393. https://doi.org/10.1242/dev.129981

Qin, J., Yuan, F., Peng, Z., Ye, K., Yang, X., Huang, L., Jiang, M., & Lu, X. (2015). Periostin enhances adipose-derived stem cell adhesion, migration, and therapeutic efficiency in Apo E deficient mice with hind limb ischemia. *Stem Cell Research & Therapy*, *6*(1), 138. https://doi.org/10.1186/s13287-015-0126-x

Rangiani, A., Jing, Y., Ren, Y., Yadav, S., Taylor, R., & Feng, J. Q. (2016). Critical roles of periostin in the process of orthodontic tooth movement. *European Journal of Orthodontics*, *38*(4), 373–378. https://doi.org/10.1093/ejo/cjv071

Rinkevich, Y., Walmsley, G. G., Hu, M. S., Maan, Z. N., Newman, A. M., Drukker, M., Januszyk, M., Krampitz, G. W., Gurtner, G. C., Lorenz, H. P., Weissman, I. L., & Longaker, M. T. (2015). Identification and isolation of a dermal lineage with intrinsic fibrogenic potential. *Science*, *348*(6232). https://doi.org/10.1126/science.aaa2151

Rios, H. F., Ma, D., Xie, Y., Giannobile, W. V, Bonewald, L. F., Conway, S. J., & Feng, J. Q. (2008). Periostin Is Essential for the Integrity and Function of the Periodontal Ligament During Occlusal Loading in Mice. *Journal of Periodontology*, *79*(8), 1480–1490. https://doi.org/doi:10.1902/jop.2008.070624

Rios, H., Koushik, S. V, Wang, H., Wang, J., Zhou, H.-M., Lindsley, A., Rogers, R., Chen, Z., Maeda, M., Kruzynska-Frejtag, A., Feng, J. Q., & Conway, S. J. (2005). Periostin Null Mice Exhibit Dwarfism, Incisor Enamel Defects, and an Early-Onset Periodontal Disease-Like Phenotype. *Molecular and Cellular Biology*, *25*(24), 11131–11144. https://doi.org/10.1128/MCB.25.24.11131-11144.2005

Rognoni, E., Pisco, A. O., Hiratsuka, T., Sipilä, K. H., Belmonte, J. M., Mobasseri, S. A., Philippeos, C., Dilão, R., & Watt, F. M. (2018). Fibroblast state switching orchestrates dermal maturation and wound healing. *Molecular Systems Biology*, *14*(8), e8174. https://doi.org/10.15252/msb.20178174

Rousselle, P., Montmasson, M., & Garnier, C. (2019). Extracellular matrix contribution to skin wound re-epithelialization. *Matrix Biology : Journal of the International Society for Matrix Biology*, *75–76*, 12–26. https://doi.org/10.1016/j.matbio.2018.01.002

Saito, M., Iwawaki, T., Taya, C., Yonekawa, H., Noda, M., Inui, Y., Mekada, E., Kimata, Y., Tsuru, A., & Kohno, K. (2001). Diphtheria toxin receptor-mediated conditional and targeted cell ablation in transgenic mice. *Nature Biotechnology*, *19*(8), 746–750. https://doi.org/10.1038/90795

Schwarz, U. S., & Gardel, M. L. (2012). United we stand – integrating the actin cytoskeleton and cell–matrix adhesions in cellular mechanotransduction. *Journal of Cell Science*, *125*(13), 3051–3060. https://doi.org/10.1242/jcs.093716

Talele, N. P., Fradette, J., Davies, J. E., Kapus, A., & Hinz, B. (2015). Expression of α-Smooth Muscle Actin Determines the Fate of Mesenchymal Stromal Cells. *Stem Cell Reports*, *4*(6), 1016–1030. https://doi.org/10.1016/j.stemcr.2015.05.004

Tamariz, E., & Grinnell, F. (2002). Modulation of fibroblast morphology and adhesion during collagen matrix remodeling. *Molecular Biology of the Cell*, *13*(11), 3915–3929. https://doi.org/10.1091/mbc.e02-05-0291

Tanabe, H., Takayama, I., Nishiyama, T., Shimazaki, M., Kii, I., Li, M., Amizuka, N., Katsube, K., & Kudo, A. (2010). Periostin associates with Notch1 precursor to maintain Notch1 expression under a stress condition in mouse cells. *PloS One*, *5*(8), e12234. https://doi.org/10.1371/journal.pone.0012234

Tanaka, S., Maekawa, A., Matsubara, L., Imanishi, A., Yano, M., Roeder, R. G., Hasegawa, N., Asano, S., & Ito, M. (2016). Periostin supports hematopoietic progenitor cells and niche-dependent myeloblastoma cells in vitro. *Biochemical and Biophysical Research Communications*, *478*(4), 1706–1712. https://doi.org/10.1016/j.bbrc.2016.09.008

Tang, Y., Liu, L., Wang, P., Chen, D., Wu, Z., & Tang, C. (2017). Periostin promotes migration and osteogenic differentiation of human periodontal ligament mesenchymal stem cells via the Jun amino-terminal kinases (JNK) pathway under inflammatory conditions. *Cell Proliferation*, *50*(6), 1–11. https://doi.org/10.1111/cpr.12369

Tkatchenko, T. V., Moreno-Rodriguez, R. A., Conway, S. J., Molkentin, J. D., Markwald, R. R., & Tkatchenko, A. V. (2009). Lack of periostin leads to suppression of Notch1 signaling and calcific aortic valve disease. *Physiological Genomics*, *39*(3), 160–168. https://doi.org/10.1152/physiolgenomics.00078.2009

Tomasek, J. J., Gabbiani, G., Hinz, B., Chaponnier, C., & Brown, R. a. (2002a). Myofibroblasts and mechano-regulation of connective tissue remodelling. *Nature Reviews. Molecular Cell Biology*, *3*(5), 349–363. https://doi.org/10.1038/nrm809

Tomasek, J. J., Gabbiani, G., Hinz, B., Chaponnier, C., & Brown, R. a. (2002b). Myofibroblasts and mechano-regulation of connective tissue remodelling. *Nature Reviews. Molecular Cell Biology*, *3*(5), 349–363. https://doi.org/10.1038/nrm809

Urbanczyk, M., Layland, S. L., & Schenke-Layland, K. (2020). The role of extracellular matrix in biomechanics and its impact on bioengineering of cells and 3D tissues. *Matrix Biology*, *85–86*, 1–14. https://doi.org/10.1016/j.matbio.2019.11.005

Von Den Hoff, J. W., Maltha, J. C., & Kuijpers-Jagtman, A. M. (2006). Palatal Wound Healing:The Effects of Scarring on Growth. In S. Berkowitz (Ed.), *Cleft Lip and Palate* (pp. 301–313). Springer. https://doi.org/10.1007/3-540-30020-1_20

Walker, J. T., Flynn, L. E., & Hamilton, D. W. (2021). Lineage tracing of Foxd1-expressing embryonic progenitors to assess the role of divergent embryonic lineages on adult dermal fibroblast function. *FASEB BioAdvances*, *3*(7), 541–557. https://doi.org/10.1096/fba.2020-00110

Walker, J. T., Kim, S. S., Michelsons, S., Creber, K., Elliott, C. G., Leask, A., & Hamilton, D. W. (2015). *Cell – matrix interactions governing skin repair: Matricellular proteins as diverse modulators of cell function*. 73–88.

Wijdeveld, M. G. M. M., Grupping, E. M., Kuijpers-Jagtman, A. M., & Maltha, J. C. (1987). Wound healing of the palatal mucoperiosteum in beagle dogs after surgery at different ages. *Journal of Cranio-Maxillofacial Surgery*, *15*, 51–57. https://doi.org/10.1016/S1010-5182(87)80018-5

Wijdeveld, M. G. M. M., Maltha, J. C., Grupping, E. M., Dejonge, J., & Kuijpersjagtman, A. M. (1991). A Histological Study of Tissue-Response to Simulated Cleft-Palate

Surgery at Different Ages in Beagle Dogs. *Archives of Oral Biology*, *36*(11), 837–843.

Wilde, J., Yokozeki, M., Terai, K., Kudo, A., & Moriyama, K. (2003). The divergent expression of periostin mRNA in the periodontal ligament during experimental tooth movement. *Cell and Tissue Research*, *312*(3), 345–351. https://doi.org/10.1007/s00441-002-0664-2

Wu, Z., Dai, W., Wang, P., Zhang, X., Tang, Y., Liu, L., Wang, Q., Li, M., & Tang, C. (2018). Periostin promotes migration, proliferation, and differentiation of human periodontal ligament mesenchymal stem cells. *Connective Tissue Research*, *59*(2), 108–119. https://doi.org/10.1080/03008207.2017.1306060

Yamamoto, M., Shook, N. A., Kanisicak, O., Yamamoto, S., Wosczyna, M. N., Camp, J. R., & Goldhamer, D. J. (2009). A Multifunctional Reporter Mouse Line for Cre- and FLP-Dependent Lineage Analysis. *Genesis (New York, N.Y. : 2000)*, *47*(2), 107–114. https://doi.org/10.1002/dvg.20474

Yoshida, T., Vivatbutsiri, P., Morriss-Kay, G., Saga, Y., & Iseki, S. (2008). Cell lineage in mammalian craniofacial mesenchyme. *Mechanisms of Development*, *125*(9–10), 797–808. https://doi.org/10.1016/j.mod.2008.06.007

Yuan, X., Xu, Q., Zhang, X., Van Brunt, L. A., Ticha, P., & Helms, J. A. (2019). Wnt-Responsive Stem Cell Fates in the Oral Mucosa. *IScience*, *21*, 84–94. https://doi.org/10.1016/j.isci.2019.10.016

Zent, J., & Guo, L. W. (2018). Signaling mechanisms of myofibroblastic activation: Outside-in and inside-out. *Cellular Physiology and Biochemistry*, *49*(3), 848–868. https://doi.org/10.1159/000493217

Zhang, F., Zhang, Z., Sun, D., Dong, S., Xu, J., & Dai, F. (2015). Periostin: A Downstream Mediator of EphB4-Induced Osteogenic Differentiation of Human

Bone Marrow-Derived Mesenchymal Stem Cells. *Stem Cells International, 2016*, e7241829. https://doi.org/10.1155/2016/7241829

Zhang, J., An, Y., Gao, L.-N., Zhang, Y.-J., Jin, Y., & Chen, F.-M. (2012). The effect of aging on the pluripotential capacity and regenerative potential of human periodontal ligament stem cells. *Biomaterials*, *33*(29), 6974–6986. https://doi.org/10.1016/j.biomaterials.2012.06.032

Zhao, H., & Zhou, B. (2019). Dual genetic approaches for deciphering cell fate plasticity in vivo: More than double. *Current Opinion in Cell Biology*, *61*, 101–109. https://doi.org/10.1016/j.ceb.2019.07.004

Zheng, W., Wang, S., Ma, D., Tang, L., Duan, Y., & Jin, Y. (2009). Loss of proliferation and differentiation capacity of aged human periodontal ligament stem cells and rejuvenation by exposure to the young extrinsic environment. *Tissue Engineering. Part A*, *15*(9), 2363–2371. https://doi.org/10.1089/ten.tea.2008.0562

Zhou, H.-M., Wang, J., Elliott, C., Wen, W., Hamilton, D. W., & Conway, S. J. (2010). Spatiotemporal expression of periostin during skin development and incisional wound healing: Lessons for human fibrotic scar formation. *Journal of Cell Communication and Signaling*, *4*(2), 99–107. https://doi.org/10.1007/s12079-010-0090-2

Zhu, W., & Liang, M. (2015). Periodontal Ligament Stem Cells: Current Status, Concerns, and Future Prospects. *Stem Cells International, 2015*, 972313. https://doi.org/10.1155/2015/972313

Appendix A: Supplemental Figures and Tables

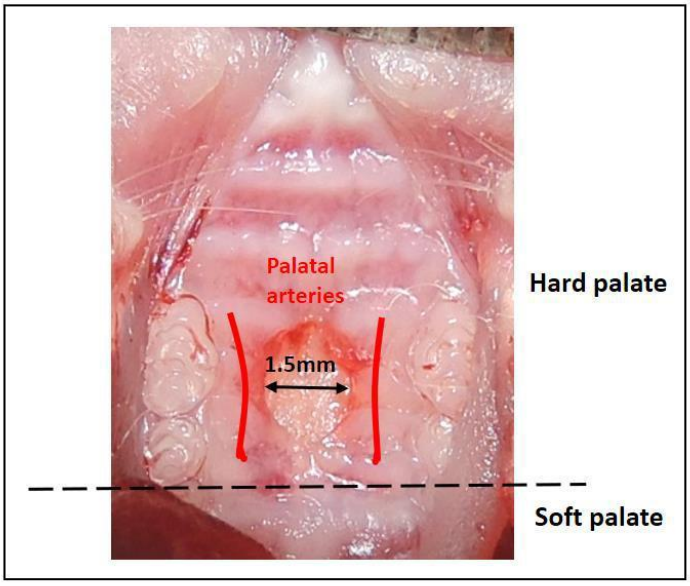

Figure A–1: Excisional Palatal Wound- One full-thickness excisional wound was made with a 1.5 mm disposable biopsy punch (Integra™ Miltex®, Integra York PA, Inc.) on the hard palate. The localization of the palatal punch biopsy was standardized with the anterior edge of the wound to be aligned with the first molar to avoid traumatizing the palatal arteries which run on either side of the wound as shown in red.

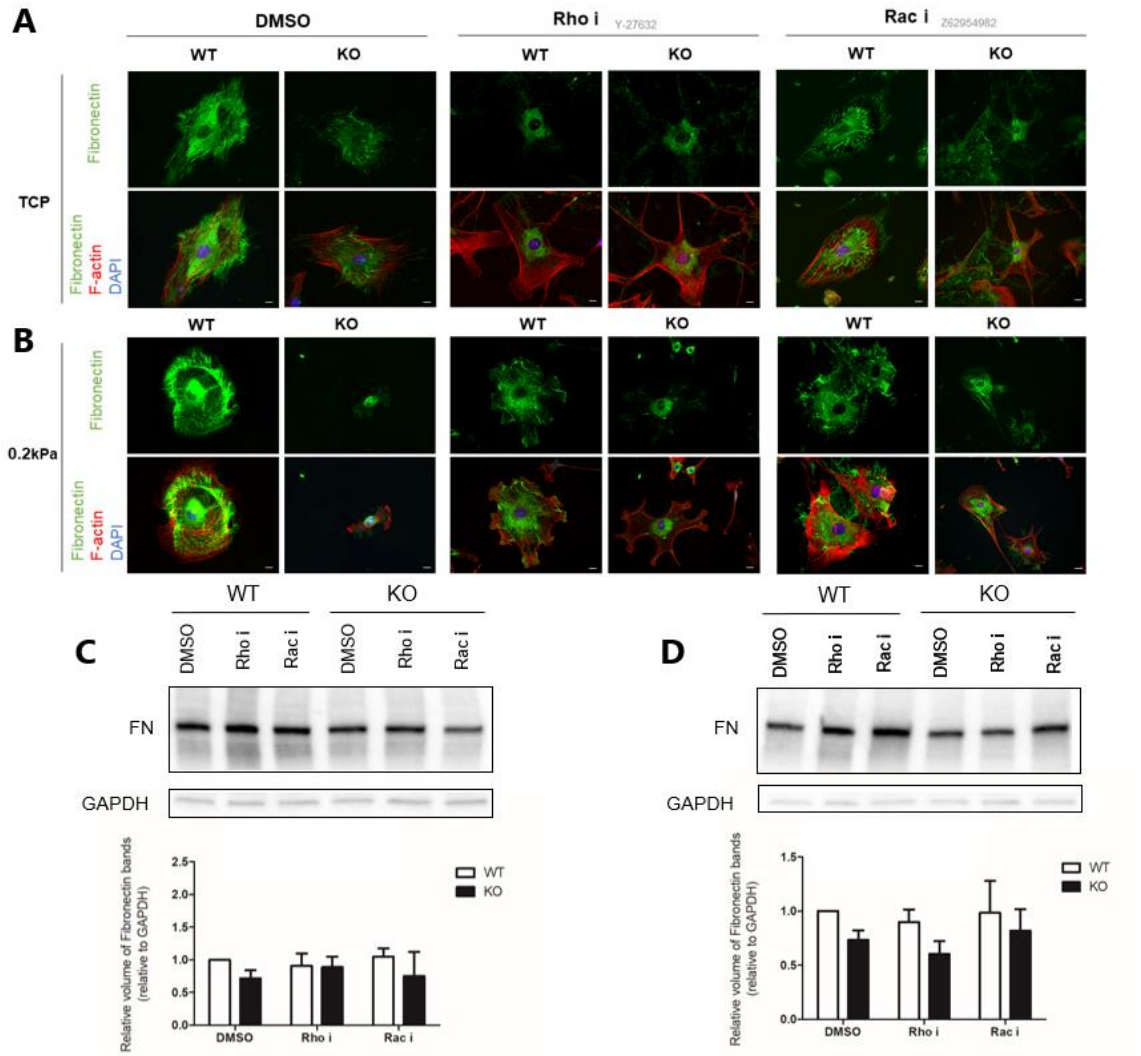

Figure A- 2: **Fibronectin matrix assembly requires RhoA pathway**. **(A)** mPFBs were cultured on TCP **(A, C)** or silicon substrates with 0.2 kPa Young's modulus of elasticity **(B, D)**, treated with pharmacological inhibitors for RhoA, Y-27632 (10µM), and Rac1, Z62954982 (50µM), and analysed for Fibronectin synthesis using immunofluorescence and Western Blotting. Western blot was used to assess Fibronectin protein level of WT and *Postn*$^{-/-}$- mPFBs on TCP **(C)** and 0.2 kPa substrate **(D)**, respectively. GAPDH was used as a loading control. Values are given as mean±SD from 3 independent experiments. Data was analyzed using ANOVA. Scale bar: 20µm.

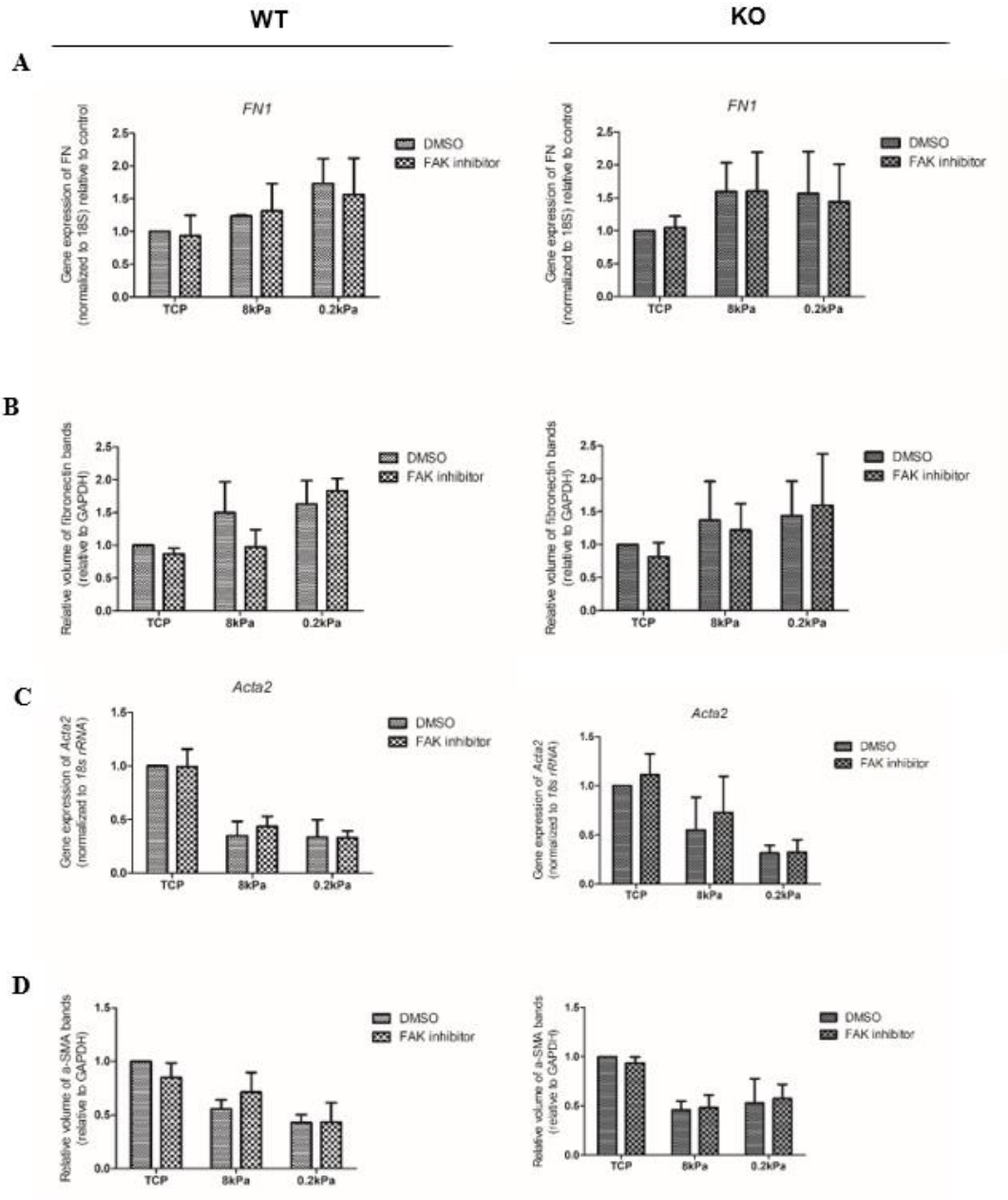

Figure A-3: WT (*Left*) and KO (*Right*) mPFBs were seeded on silicone substrates of different stiffness and treated with FAK inhibitor PF-573,228 (10 mM), or DMSO (1:1000) which served as a control. Fibronectin expression was quantified using RTqPCR **(A)** and Western Blotting **(B)** Acta2/αSMA expression was quantified using RTqPCR **(C)** and Western Blotting **(D)** Values are given as mean±SD from 3 independent experiments. Data was analyzed using ANOVA .

RNA quality analysis was performed using electrophoresis (Related to 3.2.8)

Assay Class: Eukaryote Total RNA Nano
Data Path: C:\Bioanalyzer\2020-10-20\bio_03145_2020-10-20_001.xad

Created: 10/20/2020 12:12:17 PM
Modified: 10/20/2020 12:36:10 PM

Electropherogram Summary

Ladder

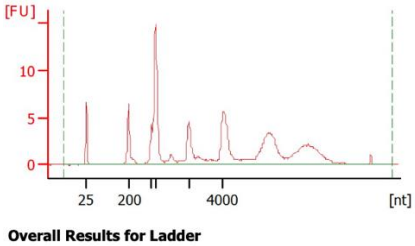

Overall Results for Ladder

RNA Area:	108.7
RNA Concentration:	150 ng/µl
Result Flagging Color:	
Result Flagging Label:	All Other Samples

F38 DMEM 1

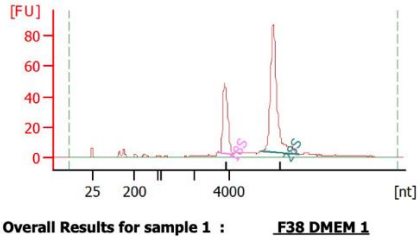

Overall Results for sample 1 : F38 DMEM 1

RNA Area:	413.1
RNA Concentration:	570 ng/µl
rRNA Ratio [28s / 18s]:	2.1
RNA Integrity Number (RIN):	10 (B.02.10)
Result Flagging Color:	
Result Flagging Label:	RIN:10

Fragment table for sample 1 : F38 DMEM 1

Name	Start Size [nt]	End Size [nt]	Area	% of total Area
18S	3,448	4,195	91.3	22.1
28S	5,784	8,005	195.3	47.3

F38 DMEM 2

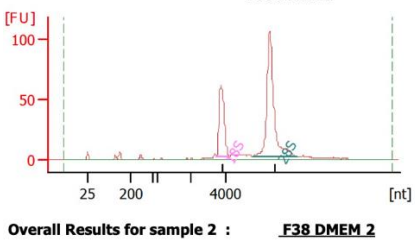

Overall Results for sample 2 : F38 DMEM 2

RNA Area:	511.7
RNA Concentration:	706 ng/µl
rRNA Ratio [28s / 18s]:	2.1
RNA Integrity Number (RIN):	10 (B.02.10)
Result Flagging Color:	
Result Flagging Label:	RIN:10

Fragment table for sample 2 : F38 DMEM 2

Name	Start Size [nt]	End Size [nt]	Area	% of total Area
18S	3,473	4,217	118.1	23.1
28S	5,532	8,087	246.9	48.2

F38 DMEM 3

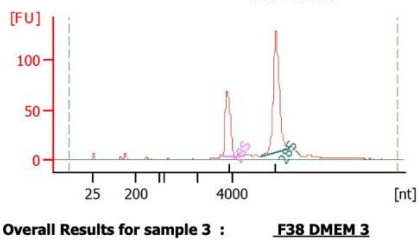

Overall Results for sample 3 : F38 DMEM 3

RNA Area:	586.3
RNA Concentration:	809 ng/µl
rRNA Ratio [28s / 18s]:	1.9
RNA Integrity Number (RIN):	10 (B.02.10)
Result Flagging Color:	
Result Flagging Label:	RIN:10

Fragment table for sample 3 : F38 DMEM 3

Name	Start Size [nt]	End Size [nt]	Area	% of total Area
18S	3,460	4,201	131.4	22.4
28S	5,605	7,257	246.5	42.0

Electropherogram Summary Continued ...

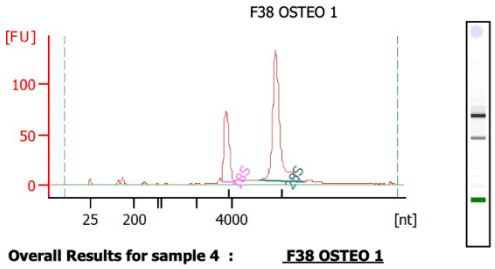

Overall Results for sample 4 : F38 OSTEO 1

RNA Area:	621.4
RNA Concentration:	858 ng/µl
rRNA Ratio [28s / 18s]:	2.2
RNA Integrity Number (RIN):	10 (B.02.10)
Result Flagging Color:	
Result Flagging Label:	RIN:10

Fragment table for sample 4 : F38 OSTEO 1

Name	Start Size [nt]	End Size [nt]	Area	% of total Area
18S	3,448	4,166	140.6	22.6
28S	5,546	8,078	311.3	50.1

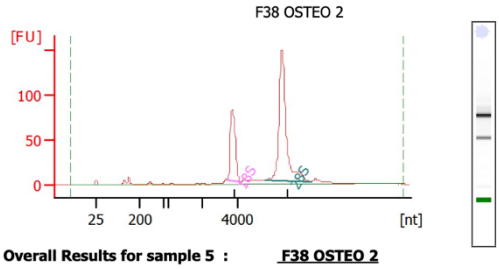

Overall Results for sample 5 : F38 OSTEO 2

RNA Area:	704.7
RNA Concentration:	973 ng/µl
rRNA Ratio [28s / 18s]:	2.2
RNA Integrity Number (RIN):	10 (B.02.10)
Result Flagging Color:	
Result Flagging Label:	RIN:10

Fragment table for sample 5 : F38 OSTEO 2

Name	Start Size [nt]	End Size [nt]	Area	% of total Area
18S	3,451	4,167	161.4	22.9
28S	5,544	8,128	355.9	50.5

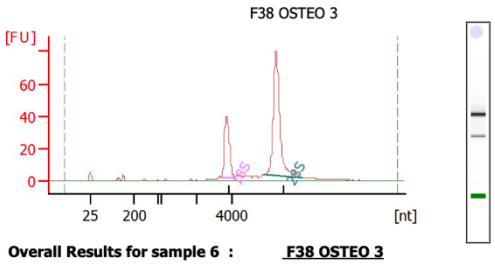

Overall Results for sample 6 : F38 OSTEO 3

RNA Area:	357.5
RNA Concentration:	494 ng/µl
rRNA Ratio [28s / 18s]:	2.4
RNA Integrity Number (RIN):	9.8 (B.02.10)
Result Flagging Color:	
Result Flagging Label:	RIN: 9.80

Fragment table for sample 6 : F38 OSTEO 3

Name	Start Size [nt]	End Size [nt]	Area	% of total Area
18S	3,467	4,185	73.4	20.5
28S	5,848	8,003	174.4	48.8

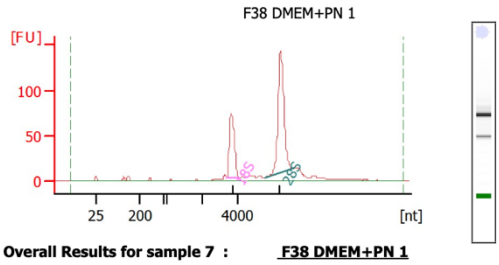

Overall Results for sample 7 : F38 DMEM+PN 1

RNA Area:	651.9
RNA Concentration:	900 ng/µl
rRNA Ratio [28s / 18s]:	2.0
RNA Integrity Number (RIN):	9.9 (B.02.10)
Result Flagging Color:	
Result Flagging Label:	RIN: 9.90

Fragment table for sample 7 : F38 DMEM+PN 1

Name	Start Size [nt]	End Size [nt]	Area	% of total Area
18S	3,429	4,147	140.4	21.5
28S	5,546	7,228	274.7	42.1

Electropherogram Summary Continued ...

F38 DMEM+PN 2

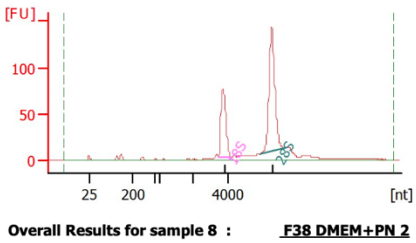

Overall Results for sample 8 : F38 DMEM+PN 2

RNA Area:	663.0
RNA Concentration:	915 ng/µl
rRNA Ratio [28s / 18s]:	1.9
RNA Integrity Number (RIN):	9.9 (B.02.10)
Result Flagging Color:	
Result Flagging Label:	RIN: 9.90

Fragment table for sample 8 : F38 DMEM+PN 2

Name	Start Size [nt]	End Size [nt]	Area	% of total Area
18S	3,426	4,145	145.1	21.9
28S	5,755	7,233	271.1	40.9

F38 DMEM+PN 3

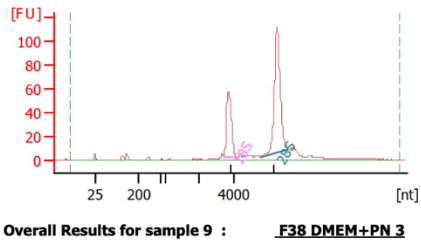

Overall Results for sample 9 : F38 DMEM+PN 3

RNA Area:	502.0
RNA Concentration:	693 ng/µl
rRNA Ratio [28s / 18s]:	1.9
RNA Integrity Number (RIN):	9.9 (B.02.10)
Result Flagging Color:	
Result Flagging Label:	RIN: 9.90

Fragment table for sample 9 : F38 DMEM+PN 3

Name	Start Size [nt]	End Size [nt]	Area	% of total Area
18S	3,407	4,126	110.4	22.0
28S	5,490	7,081	214.5	42.7

F38 OSTEO+PN 1

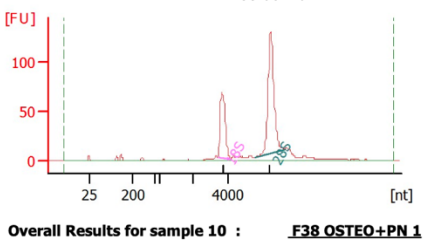

Overall Results for sample 10 : F38 OSTEO+PN 1

RNA Area:	592.3
RNA Concentration:	818 ng/µl
rRNA Ratio [28s / 18s]:	1.9
RNA Integrity Number (RIN):	10 (B.02.10)
Result Flagging Color:	
Result Flagging Label:	RIN:10

Fragment table for sample 10 : F38 OSTEO+PN 1

Name	Start Size [nt]	End Size [nt]	Area	% of total Area
18S	3,407	4,108	134.7	22.7
28S	5,490	7,214	253.3	42.8

F38 OSTEO+PN 2

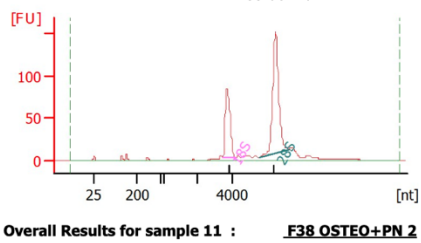

Overall Results for sample 11 : F38 OSTEO+PN 2

RNA Area:	716.8
RNA Concentration:	990 ng/µl
rRNA Ratio [28s / 18s]:	1.8
RNA Integrity Number (RIN):	10 (B.02.10)
Result Flagging Color:	
Result Flagging Label:	RIN:10

Fragment table for sample 11 : F38 OSTEO+PN 2

Name	Start Size [nt]	End Size [nt]	Area	% of total Area
18S	3,419	4,142	159.7	22.3
28S	5,512	7,186	293.6	41.0

Electropherogram Summary Continued ...

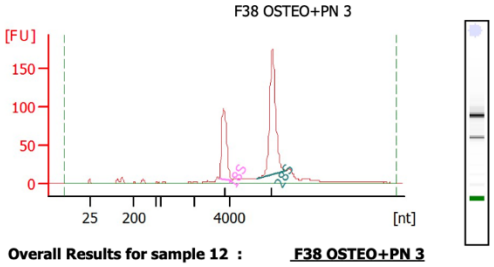

Overall Results for sample 12 : F38 OSTEO+PN 3

RNA Area:	834.1
RNA Concentration:	1,152 ng/µl
rRNA Ratio [28s / 18s]:	1.8
RNA Integrity Number (RIN):	10 (B.02.10)
Result Flagging Color:	
Result Flagging Label:	RIN:10

Fragment table for sample 12 : F38 OSTEO+PN 3

Name	Start Size [nt]	End Size [nt]	Area	% of total Area
18S	3,388	4,108	183.8	22.0
28S	5,490	7,157	334.9	40.2

Assay Class: Eukaryote Total RNA Nano
Data Path: C:\Bioanalyzer\2020-10-20\bio_03146_2020-10-20_001.xad

Created: 10/20/2020 12:55:26 PM
Modified: 10/20/2020 1:19:37 PM

Electropherogram Summary

Ladder

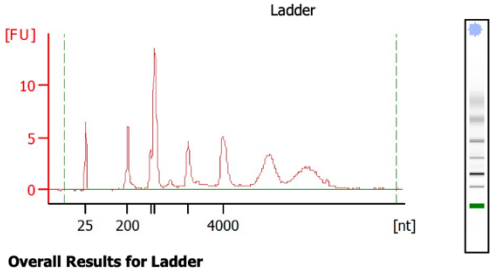

Overall Results for Ladder

RNA Area:	103.0
RNA Concentration:	150 ng/µl
Result Flagging Color:	
Result Flagging Label:	All Other Samples

F15 DMEM 1

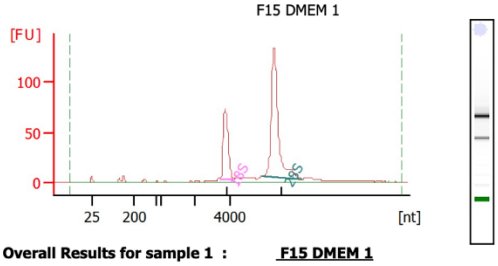

Overall Results for sample 1 : F15 DMEM 1

RNA Area:	628.9
RNA Concentration:	915 ng/µl
rRNA Ratio [28s / 18s]:	2.2
RNA Integrity Number (RIN):	10 (B.02.10)
Result Flagging Color:	
Result Flagging Label:	RIN:10

Fragment table for sample 1 : F15 DMEM 1

Name	Start Size [nt]	End Size [nt]	Area	% of total Area
18S	3,470	4,196	138.9	22.1
28S	5,839	8,112	304.1	48.4

F15 DMEM 2

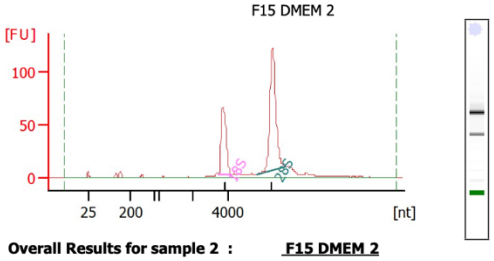

Overall Results for sample 2 : F15 DMEM 2

RNA Area:	558.4
RNA Concentration:	813 ng/µl
rRNA Ratio [28s / 18s]:	1.9
RNA Integrity Number (RIN):	10 (B.02.10)
Result Flagging Color:	
Result Flagging Label:	RIN:10

Fragment table for sample 2 : F15 DMEM 2

Name	Start Size [nt]	End Size [nt]	Area	% of total Area
18S	3,466	4,203	128.5	23.0
28S	5,602	7,264	239.2	42.8

F15 DMEM 3

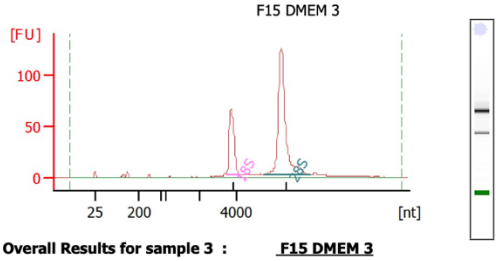

Overall Results for sample 3 : F15 DMEM 3

RNA Area:	567.7
RNA Concentration:	826 ng/µl
rRNA Ratio [28s / 18s]:	2.4
RNA Integrity Number (RIN):	10 (B.02.10)
Result Flagging Color:	
Result Flagging Label:	RIN:10

Fragment table for sample 3 : F15 DMEM 3

Name	Start Size [nt]	End Size [nt]	Area	% of total Area
18S	3,497	4,227	125.2	22.1
28S	5,595	8,180	297.5	52.4

Electropherogram Summary Continued ...

F15 OSTEO 1

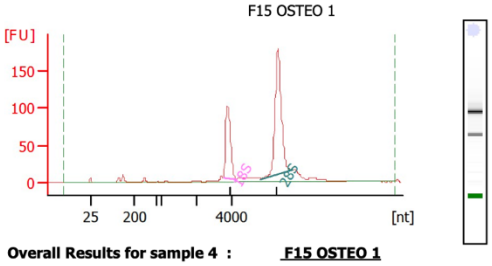

Overall Results for sample 4 : F15 OSTEO 1

RNA Area:	836.4
RNA Concentration:	1,218 ng/µl
rRNA Ratio [28s / 18s]:	1.8
RNA Integrity Number (RIN):	10 (B.02.10)
Result Flagging Color:	
Result Flagging Label:	RIN:10

Fragment table for sample 4 : F15 OSTEO 1

Name	Start Size [nt]	End Size [nt]	Area	% of total Area
18S	3,508	4,233	194.2	23.2
28S	5,607	7,316	349.2	41.8

F15 OSTEO 2

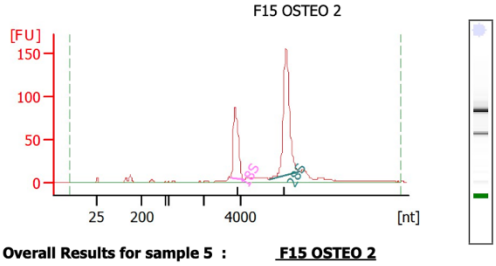

Overall Results for sample 5 : F15 OSTEO 2

RNA Area:	705.4
RNA Concentration:	1,027 ng/µl
rRNA Ratio [28s / 18s]:	1.8
RNA Integrity Number (RIN):	10 (B.02.10)
Result Flagging Color:	
Result Flagging Label:	RIN:10

Fragment table for sample 5 : F15 OSTEO 2

Name	Start Size [nt]	End Size [nt]	Area	% of total Area
18S	3,483	4,201	163.4	23.2
28S	5,564	7,258	299.5	42.5

F15 OSTEO 3

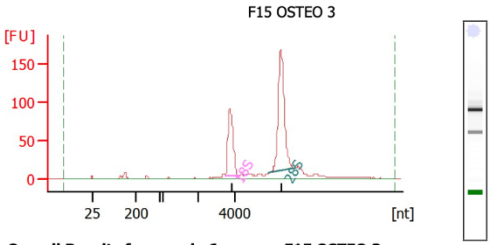

Overall Results for sample 6 : F15 OSTEO 3

RNA Area:	768.4
RNA Concentration:	1,119 ng/µl
rRNA Ratio [28s / 18s]:	1.8
RNA Integrity Number (RIN):	10 (B.02.10)
Result Flagging Color:	
Result Flagging Label:	RIN:10

Fragment table for sample 6 : F15 OSTEO 3

Name	Start Size [nt]	End Size [nt]	Area	% of total Area
18S	3,467	4,202	174.7	22.7
28S	5,838	7,290	319.9	41.6

F15 DMEM+PN 1

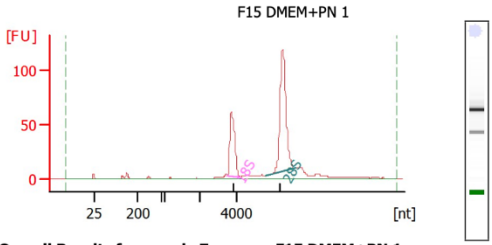

Overall Results for sample 7 : F15 DMEM+PN 1

RNA Area:	506.5
RNA Concentration:	737 ng/µl
rRNA Ratio [28s / 18s]:	2.0
RNA Integrity Number (RIN):	10 (B.02.10)
Result Flagging Color:	
Result Flagging Label:	RIN:10

Fragment table for sample 7 : F15 DMEM+PN 1

Name	Start Size [nt]	End Size [nt]	Area	% of total Area
18S	3,467	4,184	112.6	22.2
28S	5,562	7,217	224.1	44.2

Electropherogram Summary Continued ...

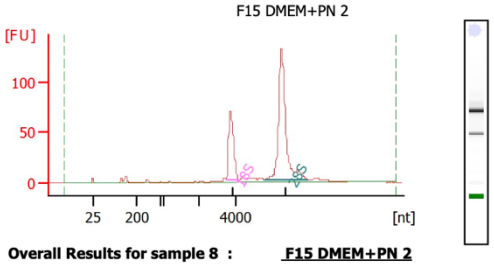

Overall Results for sample 8 : F15 DMEM+PN 2

RNA Area:	576.8
RNA Concentration:	840 ng/µl
rRNA Ratio [28s / 18s]:	2.4
RNA Integrity Number (RIN):	10 (B.02.10)
Result Flagging Color:	
Result Flagging Label:	RIN:10

Fragment table for sample 8 : F15 DMEM+PN 2

Name	Start Size [nt]	End Size [nt]	Area	% of total Area
18S	3,449	4,184	130.8	22.7
28S	5,526	7,952	309.2	53.6

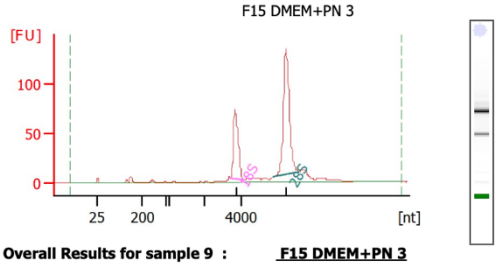

Overall Results for sample 9 : F15 DMEM+PN 3

RNA Area:	594.0
RNA Concentration:	865 ng/µl
rRNA Ratio [28s / 18s]:	1.9
RNA Integrity Number (RIN):	10 (B.02.10)
Result Flagging Color:	
Result Flagging Label:	RIN:10

Fragment table for sample 9 : F15 DMEM+PN 3

Name	Start Size [nt]	End Size [nt]	Area	% of total Area
18S	3,446	4,164	132.9	22.4
28S	5,803	7,203	250.7	42.2

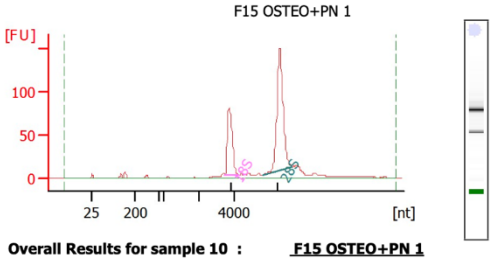

Overall Results for sample 10 : F15 OSTEO+PN 1

RNA Area:	692.5
RNA Concentration:	1,008 ng/µl
rRNA Ratio [28s / 18s]:	1.9
RNA Integrity Number (RIN):	10 (B.02.10)
Result Flagging Color:	
Result Flagging Label:	RIN:10

Fragment table for sample 10 : F15 OSTEO+PN 1

Name	Start Size [nt]	End Size [nt]	Area	% of total Area
18S	3,461	4,200	153.4	22.1
28S	5,584	7,153	287.8	41.6

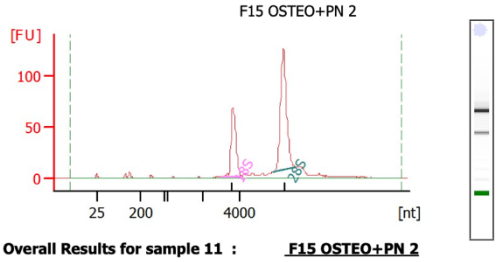

Overall Results for sample 11 : F15 OSTEO+PN 2

RNA Area:	560.3
RNA Concentration:	816 ng/µl
rRNA Ratio [28s / 18s]:	1.8
RNA Integrity Number (RIN):	10 (B.02.10)
Result Flagging Color:	
Result Flagging Label:	RIN:10

Fragment table for sample 11 : F15 OSTEO+PN 2

Name	Start Size [nt]	End Size [nt]	Area	% of total Area
18S	3,085	4,160	132.1	23.6
28S	5,921	7,107	235.7	42.1

Assay Class: Eukaryote Total RNA Nano
Data Path: C:\Bioanalyzer\2020-10-20\bio_03146_2020-10-20_001.xad

Created: 10/20/2020 12:55:26 PM
Modified: 10/20/2020 1:19:37 PM

Electropherogram Summary Continued ...

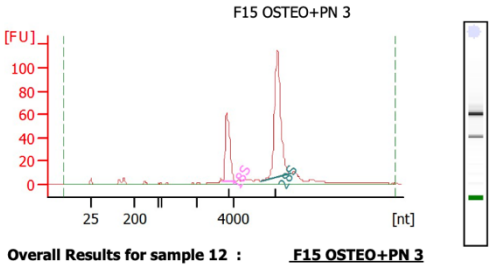

Overall Results for sample 12 : F15 OSTEO+PN 3

RNA Area:	505.9
RNA Concentration:	736 ng/µl
rRNA Ratio [28s / 18s]:	2.0
RNA Integrity Number (RIN):	10 (B.02.10)
Result Flagging Color:	
Result Flagging Label:	RIN:10

Fragment table for sample 12 : F15 OSTEO+PN 3

Name	Start Size [nt]	End Size [nt]	Area	% of total Area
18S	3,437	4,160	109.7	21.7
28S	5,550	7,218	220.4	43.6

Assay Class: Eukaryote Total RNA Nano
Data Path: C:\Bioanalyzer\2020-10-20\bio_03147_2020-10-20_001.xad

Created: 10/20/2020 1:46:34 PM
Modified: 10/20/2020 2:20:16 PM

Electropherogram Summary

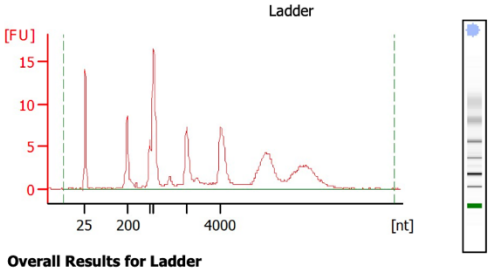

Overall Results for Ladder

RNA Area:	146.4
RNA Concentration:	150 ng/µl
Result Flagging Color:	
Result Flagging Label:	All Other Samples

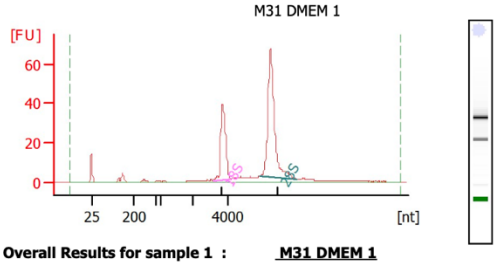

Overall Results for sample 1 : M31 DMEM 1

RNA Area:	323.7
RNA Concentration:	332 ng/µl
rRNA Ratio [28s / 18s]:	1.9
RNA Integrity Number (RIN):	10 (B.02.10)
Result Flagging Color:	
Result Flagging Label:	RIN:10

Fragment table for sample 1 : M31 DMEM 1

Name	Start Size [nt]	End Size [nt]	Area	% of total Area
18S	3,172	4,219	75.6	23.4
28S	5,918	8,052	147.4	45.5

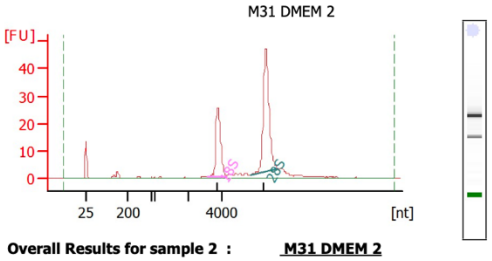

Overall Results for sample 2 : M31 DMEM 2

RNA Area:	213.1
RNA Concentration:	218 ng/µl
rRNA Ratio [28s / 18s]:	1.8
RNA Integrity Number (RIN):	10 (B.02.10)
Result Flagging Color:	
Result Flagging Label:	RIN:10

Fragment table for sample 2 : M31 DMEM 2

Name	Start Size [nt]	End Size [nt]	Area	% of total Area
18S	3,140	4,222	49.1	23.0
28S	5,698	7,212	88.8	41.7

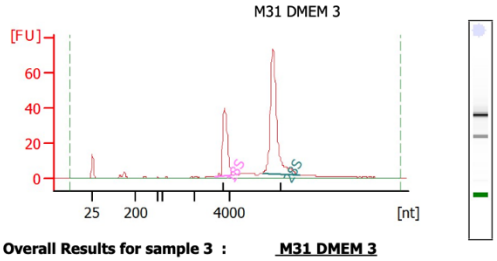

Overall Results for sample 3 : M31 DMEM 3

RNA Area:	334.3
RNA Concentration:	342 ng/µl
rRNA Ratio [28s / 18s]:	2.1
RNA Integrity Number (RIN):	10 (B.02.10)
Result Flagging Color:	
Result Flagging Label:	RIN:10

Fragment table for sample 3 : M31 DMEM 3

Name	Start Size [nt]	End Size [nt]	Area	% of total Area
18S	3,184	4,224	74.2	22.2
28S	5,991	8,169	158.1	47.3

Electropherogram Summary Continued ...

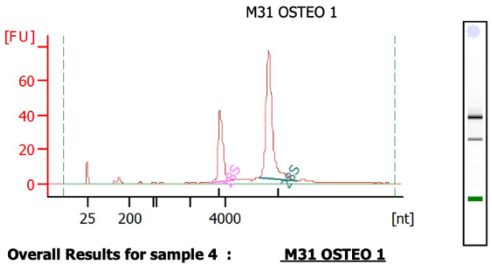

Overall Results for sample 4 : M31 OSTEO 1

RNA Area:	342.1
RNA Concentration:	350 ng/µl
rRNA Ratio [28s / 18s]:	2.1
RNA Integrity Number (RIN):	10 (B.02.10)
Result Flagging Color:	
Result Flagging Label:	RIN:10

Fragment table for sample 4 : M31 OSTEO 1

Name	Start Size [nt]	End Size [nt]	Area	% of total Area
18S	3,211	4,247	79.6	23.3
28S	6,006	8,234	164.5	48.1

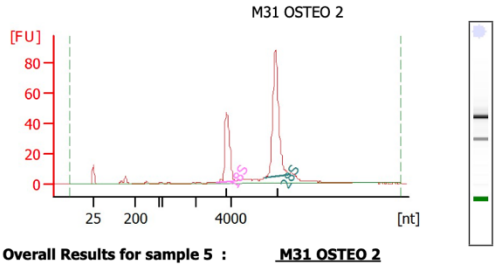

Overall Results for sample 5 : M31 OSTEO 2

RNA Area:	378.7
RNA Concentration:	388 ng/µl
rRNA Ratio [28s / 18s]:	1.8
RNA Integrity Number (RIN):	10 (B.02.10)
Result Flagging Color:	
Result Flagging Label:	RIN:10

Fragment table for sample 5 : M31 OSTEO 2

Name	Start Size [nt]	End Size [nt]	Area	% of total Area
18S	3,156	4,248	91.5	24.2
28S	6,003	7,427	168.1	44.4

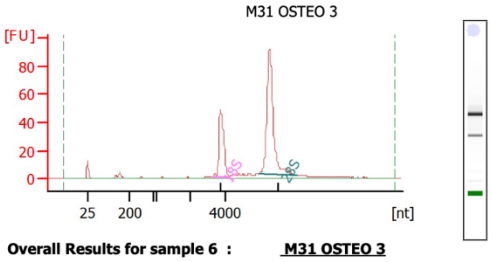

Overall Results for sample 6 : M31 OSTEO 3

RNA Area:	398.5
RNA Concentration:	408 ng/µl
rRNA Ratio [28s / 18s]:	2.1
RNA Integrity Number (RIN):	10 (B.02.10)
Result Flagging Color:	
Result Flagging Label:	RIN:10

Fragment table for sample 6 : M31 OSTEO 3

Name	Start Size [nt]	End Size [nt]	Area	% of total Area
18S	3,215	4,248	93.7	23.5
28S	5,964	8,188	198.9	49.9

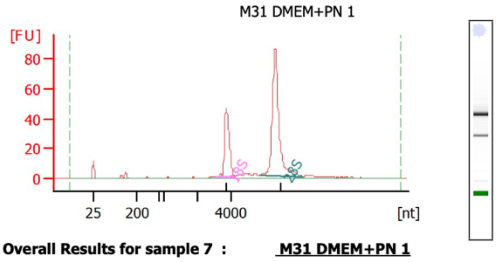

Overall Results for sample 7 : M31 DMEM+PN 1

RNA Area:	375.0
RNA Concentration:	384 ng/µl
rRNA Ratio [28s / 18s]:	2.2
RNA Integrity Number (RIN):	10 (B.02.10)
Result Flagging Color:	
Result Flagging Label:	RIN:10

Fragment table for sample 7 : M31 DMEM+PN 1

Name	Start Size [nt]	End Size [nt]	Area	% of total Area
18S	3,160	4,211	87.9	23.4
28S	5,592	8,122	194.0	51.7

Electropherogram Summary Continued ...

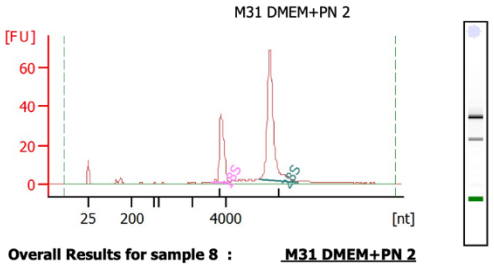

Overall Results for sample 8 : M31 DMEM+PN 2

RNA Area:	284.4
RNA Concentration:	291 ng/µl
rRNA Ratio [28s / 18s]:	2.2
RNA Integrity Number (RIN):	10 (B.02.10)
Result Flagging Color:	
Result Flagging Label:	RIN:10

Fragment table for sample 8 : M31 DMEM+PN 2

Name	Start Size [nt]	End Size [nt]	Area	% of total Area
18S	3,160	4,191	66.8	23.5
28S	5,884	8,103	144.4	50.8

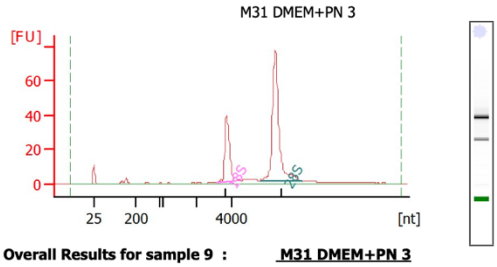

Overall Results for sample 9 : M31 DMEM+PN 3

RNA Area:	318.5
RNA Concentration:	326 ng/µl
rRNA Ratio [28s / 18s]:	2.3
RNA Integrity Number (RIN):	10 (B.02.10, Anomaly Threshold(s) manually adapted)
Result Flagging Color:	
Result Flagging Label:	RIN:10

Fragment table for sample 9 : M31 DMEM+PN 3

Name	Start Size [nt]	End Size [nt]	Area	% of total Area
18S	3,195	4,209	74.1	23.3
28S	5,633	8,090	172.6	54.2

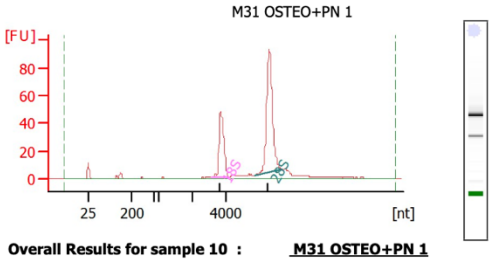

Overall Results for sample 10 : M31 OSTEO+PN 1

RNA Area:	399.2
RNA Concentration:	409 ng/µl
rRNA Ratio [28s / 18s]:	1.9
RNA Integrity Number (RIN):	10 (B.02.10)
Result Flagging Color:	
Result Flagging Label:	RIN:10

Fragment table for sample 10 : M31 OSTEO+PN 1

Name	Start Size [nt]	End Size [nt]	Area	% of total Area
18S	3,141	4,172	93.5	23.4
28S	5,592	7,227	179.4	44.9

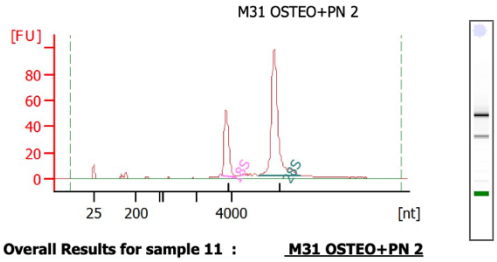

Overall Results for sample 11 : M31 OSTEO+PN 2

RNA Area:	428.8
RNA Concentration:	439 ng/µl
rRNA Ratio [28s / 18s]:	2.4
RNA Integrity Number (RIN):	10 (B.02.10)
Result Flagging Color:	
Result Flagging Label:	RIN:10

Fragment table for sample 11 : M31 OSTEO+PN 2

Name	Start Size [nt]	End Size [nt]	Area	% of total Area
18S	3,429	4,151	92.6	21.6
28S	5,555	8,051	222.3	51.8

Electropherogram Summary Continued ...

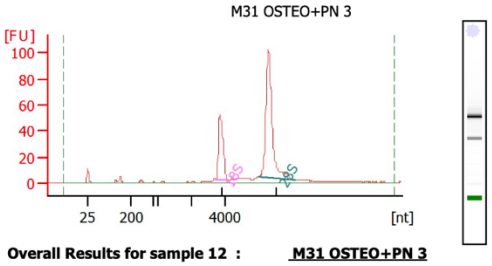

Overall Results for sample 12 : M31 OSTEO+PN 3

RNA Area:	435.3
RNA Concentration:	446 ng/µl
rRNA Ratio [28s / 18s]:	2.3
RNA Integrity Number (RIN):	10 (B.02.10)
Result Flagging Color:	
Result Flagging Label:	RIN:10

Fragment table for sample 12 : M31 OSTEO+PN 3

Name	Start Size [nt]	End Size [nt]	Area	% of total Area
18S	3,452	4,172	93.7	21.5
28S	5,904	8,044	215.7	49.6

Assay Class: Eukaryote Total RNA Nano
Data Path: C:\Bioanalyzer\2020-10-20\bio_03148_2020-10-20_001.xad

Created: 10/20/2020 2:31:44 PM
Modified: 10/20/2020 2:54:53 PM

Electropherogram Summary

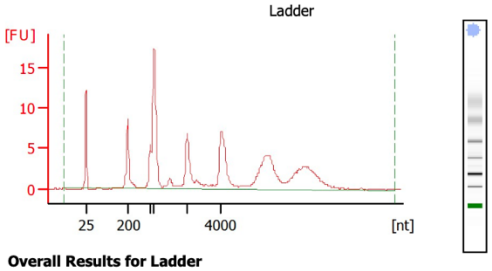

Overall Results for Ladder

RNA Area:	141.6
RNA Concentration:	150 ng/µl
Result Flagging Color:	
Result Flagging Label:	All Other Samples

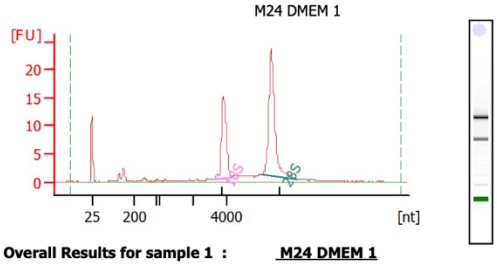

Overall Results for sample 1 : M24 DMEM 1

RNA Area:	119.3
RNA Concentration:	126 ng/µl
rRNA Ratio [28s / 18s]:	1.6
RNA Integrity Number (RIN):	10 (B.02.10)
Result Flagging Color:	
Result Flagging Label:	RIN:10

Fragment table for sample 1 : M24 DMEM 1

Name	Start Size [nt]	End Size [nt]	Area	% of total Area
18S	3,235	4,254	29.0	24.4
28S	6,019	8,058	47.9	40.2

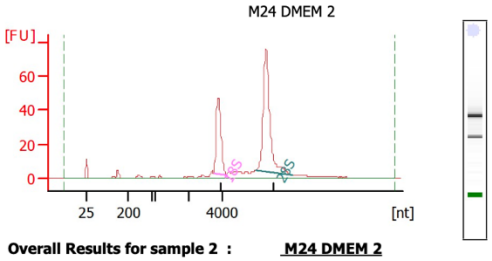

Overall Results for sample 2 : M24 DMEM 2

RNA Area:	399.7
RNA Concentration:	423 ng/µl
rRNA Ratio [28s / 18s]:	1.9
RNA Integrity Number (RIN):	10 (B.02.10)
Result Flagging Color:	
Result Flagging Label:	RIN:10

Fragment table for sample 2 : M24 DMEM 2

Name	Start Size [nt]	End Size [nt]	Area	% of total Area
18S	3,496	4,219	86.7	21.7
28S	5,936	8,123	167.4	41.9

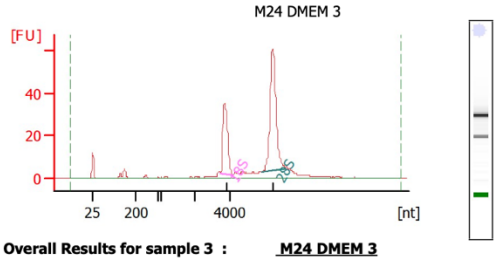

Overall Results for sample 3 : M24 DMEM 3

RNA Area:	300.1
RNA Concentration:	318 ng/µl
rRNA Ratio [28s / 18s]:	1.8
RNA Integrity Number (RIN):	9.9 (B.02.10)
Result Flagging Color:	
Result Flagging Label:	RIN: 9.90

Fragment table for sample 3 : M24 DMEM 3

Name	Start Size [nt]	End Size [nt]	Area	% of total Area
18S	3,499	4,201	64.4	21.4
28S	5,876	7,298	118.1	39.4

Electropherogram Summary Continued ...

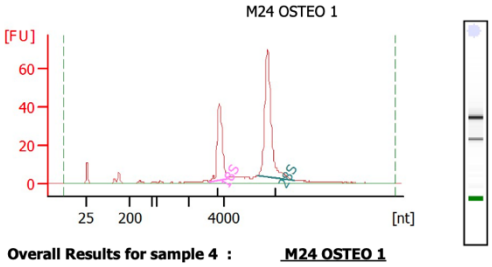

Overall Results for sample 4 : M24 OSTEO 1

RNA Area:	343.2
RNA Concentration:	364 ng/µl
rRNA Ratio [28s / 18s]:	1.8
RNA Integrity Number (RIN):	10 (B.02.10)
Result Flagging Color:	
Result Flagging Label:	RIN:10

Fragment table for sample 4 : M24 OSTEO 1

Name	Start Size [nt]	End Size [nt]	Area	% of total Area
18S	3,153	4,202	82.0	23.9
28S	5,991	8,109	148.3	43.2

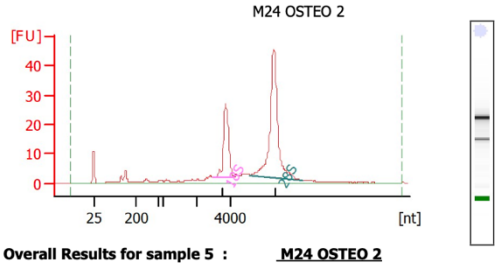

Overall Results for sample 5 : M24 OSTEO 2

RNA Area:	280.7
RNA Concentration:	297 ng/µl
rRNA Ratio [28s / 18s]:	2.3
RNA Integrity Number (RIN):	9.7 (B.02.10)
Result Flagging Color:	
Result Flagging Label:	RIN: 9.70

Fragment table for sample 5 : M24 OSTEO 2

Name	Start Size [nt]	End Size [nt]	Area	% of total Area
18S	2,943	4,165	51.7	18.4
28S	5,077	8,102	119.0	42.4

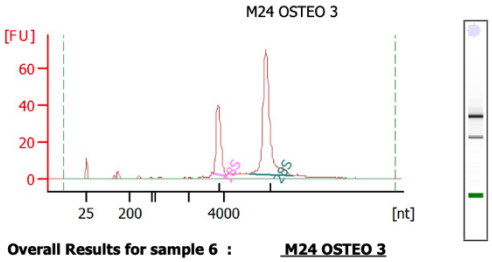

Overall Results for sample 6 : M24 OSTEO 3

RNA Area:	348.6
RNA Concentration:	369 ng/µl
rRNA Ratio [28s / 18s]:	2.3
RNA Integrity Number (RIN):	10 (B.02.10)
Result Flagging Color:	
Result Flagging Label:	RIN:10

Fragment table for sample 6 : M24 OSTEO 3

Name	Start Size [nt]	End Size [nt]	Area	% of total Area
18S	3,441	4,162	72.1	20.7
28S	5,525	7,999	162.9	46.7

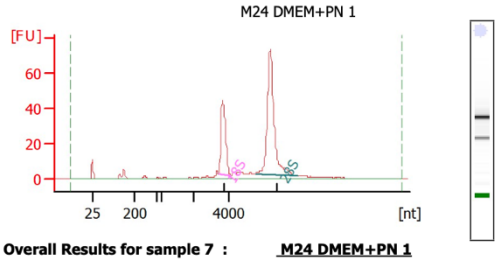

Overall Results for sample 7 : M24 DMEM+PN 1

RNA Area:	372.5
RNA Concentration:	395 ng/µl
rRNA Ratio [28s / 18s]:	2.1
RNA Integrity Number (RIN):	10 (B.02.10)
Result Flagging Color:	
Result Flagging Label:	RIN:10

Fragment table for sample 7 : M24 DMEM+PN 1

Name	Start Size [nt]	End Size [nt]	Area	% of total Area
18S	3,434	4,139	80.2	21.5
28S	5,567	7,993	169.2	45.4

Electropherogram Summary Continued ...

M24 DMEM+PN 2

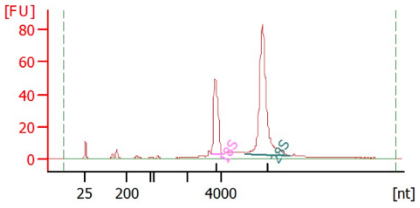

Overall Results for sample 8 : M24 DMEM+PN 2

RNA Area:	410.2
RNA Concentration:	435 ng/µl
rRNA Ratio [28s / 18s]:	2.2
RNA Integrity Number (RIN):	10 (B.02.10)
Result Flagging Color:	
Result Flagging Label:	RIN:10

Fragment table for sample 8 : M24 DMEM+PN 2

Name	Start Size [nt]	End Size [nt]	Area	% of total Area
18S	3,427	4,135	88.3	21.5
28S	5,452	8,006	193.0	47.1

M24 DMEM+PN 3

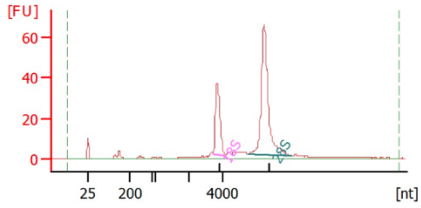

Overall Results for sample 9 : M24 DMEM+PN 3

RNA Area:	324.1
RNA Concentration:	343 ng/µl
rRNA Ratio [28s / 18s]:	2.4
RNA Integrity Number (RIN):	10 (B.02.10)
Result Flagging Color:	
Result Flagging Label:	RIN:10

Fragment table for sample 9 : M24 DMEM+PN 3

Name	Start Size [nt]	End Size [nt]	Area	% of total Area
18S	3,421	4,131	65.4	20.2
28S	5,493	8,020	154.7	47.7

M24 OSTEO+PN 1

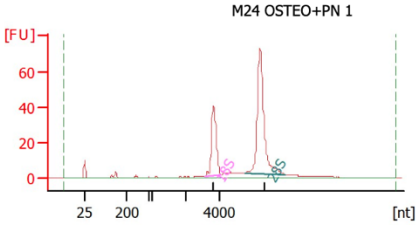

Overall Results for sample 10 : M24 OSTEO+PN 1

RNA Area:	346.6
RNA Concentration:	367 ng/µl
rRNA Ratio [28s / 18s]:	2.2
RNA Integrity Number (RIN):	10 (B.02.10)
Result Flagging Color:	
Result Flagging Label:	RIN:10

Fragment table for sample 10 : M24 OSTEO+PN 1

Name	Start Size [nt]	End Size [nt]	Area	% of total Area
18S	3,105	4,092	77.8	22.5
28S	5,473	7,881	168.2	48.5

M24 OSTEO+PN 2

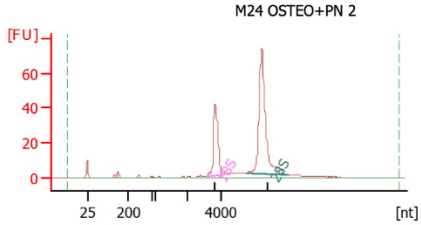

Overall Results for sample 11 : M24 OSTEO+PN 2

RNA Area:	347.4
RNA Concentration:	368 ng/µl
rRNA Ratio [28s / 18s]:	2.2
RNA Integrity Number (RIN):	10 (B.02.10)
Result Flagging Color:	
Result Flagging Label:	RIN:10

Fragment table for sample 11 : M24 OSTEO+PN 2

Name	Start Size [nt]	End Size [nt]	Area	% of total Area
18S	3,116	4,088	76.8	22.1
28S	5,436	7,934	168.5	48.5

Assay Class: Eukaryote Total RNA Nano
Data Path: C:\Bioanalyzer\2020-10-20\bio_03148_2020-10-20_001.xad

Created: 10/20/2020 2:31:44 PM
Modified: 10/20/2020 2:54:53 PM

Electropherogram Summary Continued ...

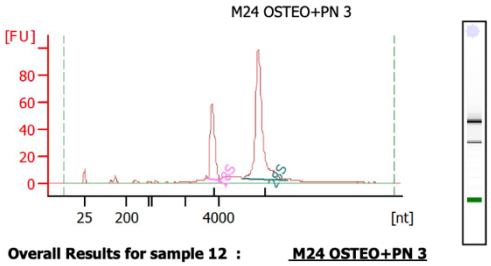

Overall Results for sample 12 : M24 OSTEO+PN 3

RNA Area:	486.8
RNA Concentration:	516 ng/µl
rRNA Ratio [28s / 18s]:	2.3
RNA Integrity Number (RIN):	10 (B.02.10)
Result Flagging Color:	
Result Flagging Label:	RIN:10

Fragment table for sample 12 : M24 OSTEO+PN 3

Name	Start Size [nt]	End Size [nt]	Area	% of total Area
18S	3,378	4,070	102.7	21.1
28S	5,395	8,046	233.9	48.0

Figure A-4: RNA quality analysis was performed using electrophoresis for all samples submitted for RNAsequencing.

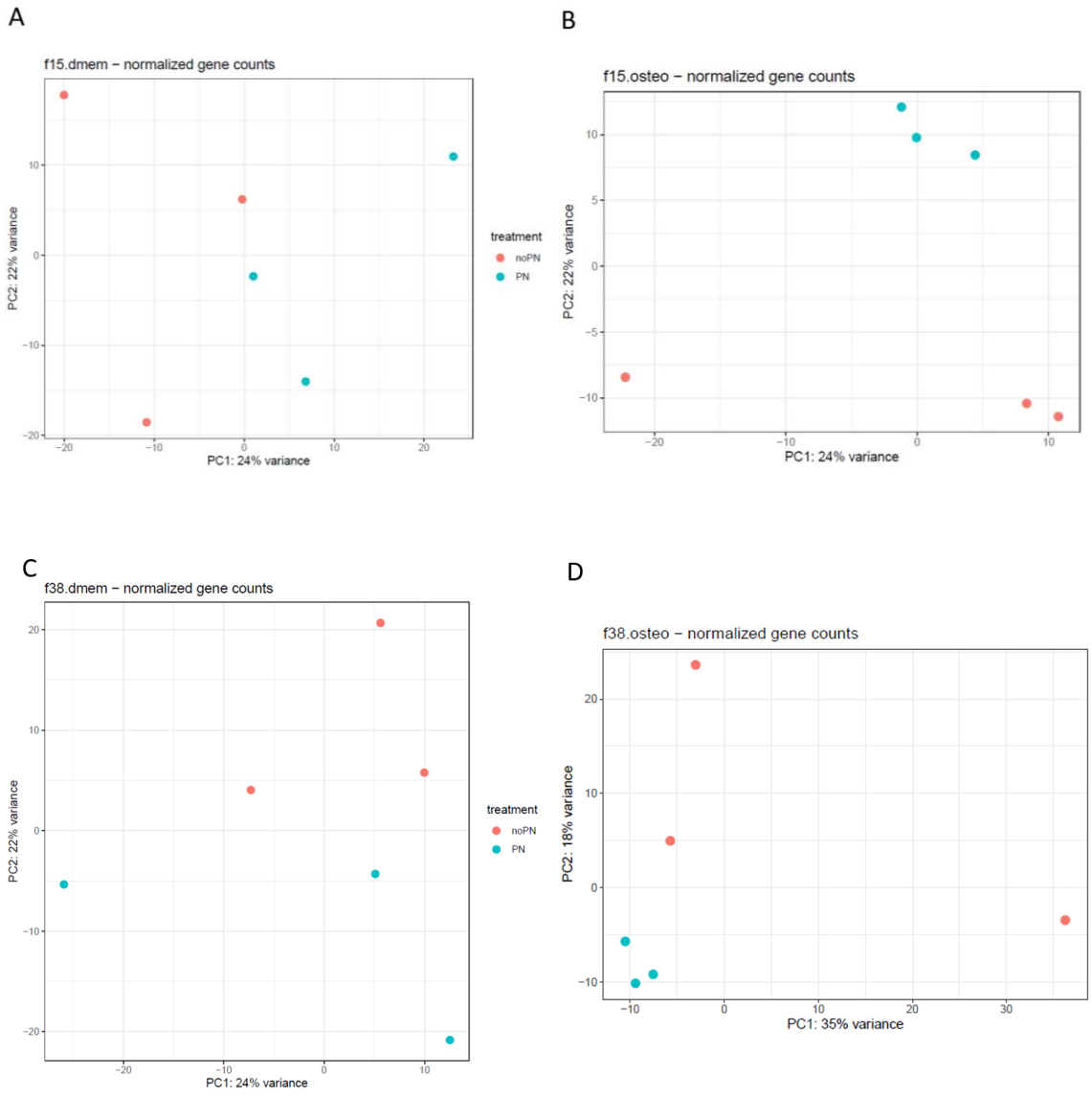
A
f15.dmem – normalized gene counts
PC2: 22% variance
PC1: 24% variance
treatment
noPN
PN
B
f15.osteo – normalized gene counts
PC2: 22% variance
PC1: 24% variance
C
f38.dmem – normalized gene counts
PC2: 22% variance
PC1: 24% variance
treatment
noPN
PN
D
f38.osteo – normalized gene counts
PC2: 18% variance
PC1: 35% variance

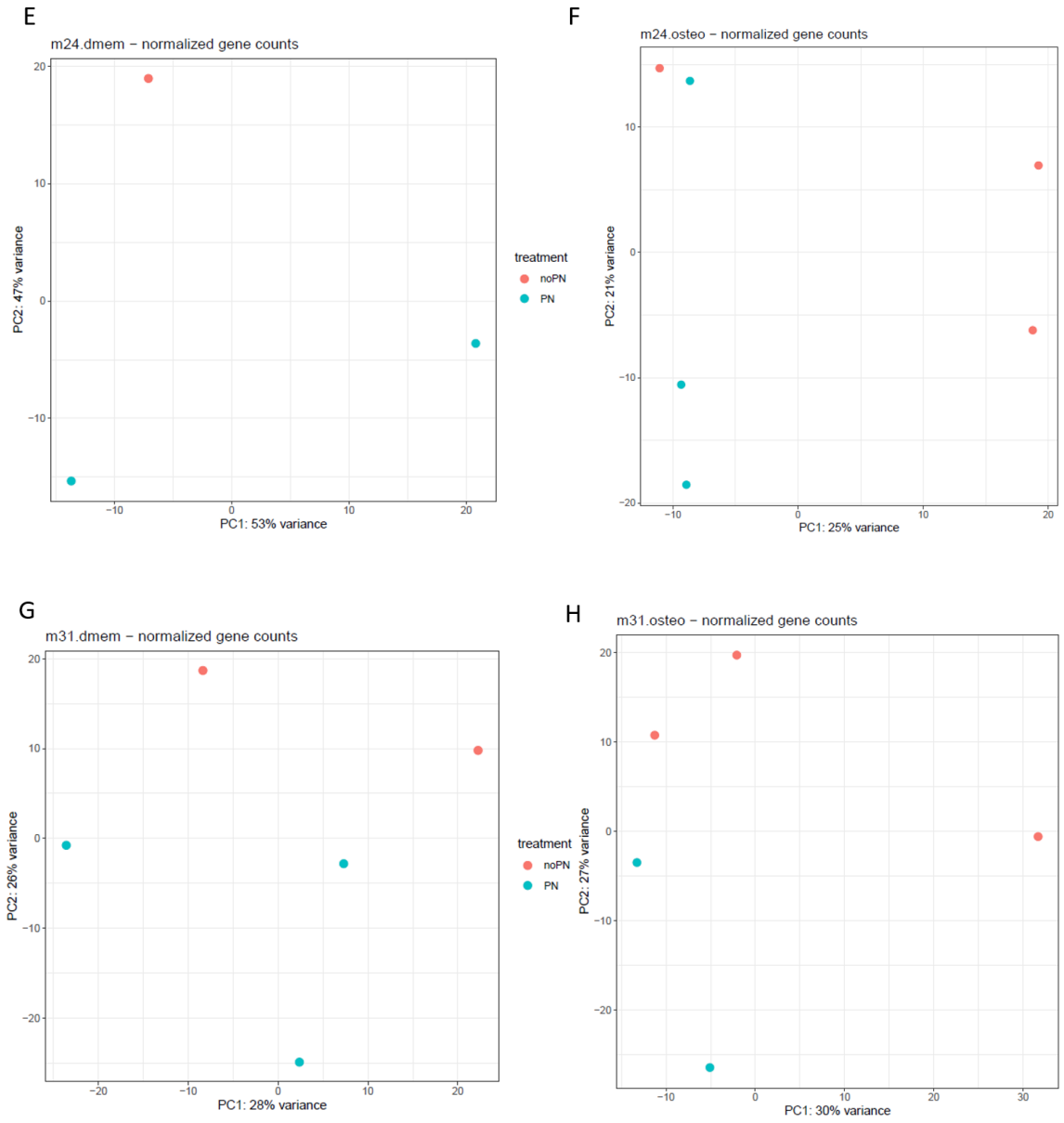

Figure A- 5: PCA plots stratified from patientID and osteogenic/non- osteogenic conditions showing strong effect of patient ID

Tables

Table A- 1: Top100 GO enrichment results of Pathway enrichment analysis in DMEM media

GO.ID	Term	Annotated	Significant	Expected	classicFisher	weight01Fisher	common
GO:0030199	collagen fibril organization	55	8	0.33	1.30E-09	1.31E-09	COL11A1 COL5A2 ADAMTS2 TNXB COL12A1 COL1A2 COL5A1 GREM1
GO:0030198	extracellular matrix organization	395	25	2.39	9.00E-19	1.01E-07	COL11A1 COL16A1 NTNG1 COL5A2 ABI3BP COL7A1 NDNF PDGFRA ADAMTS2 TNXB COL12A1 COL1A2 ELN SULF1 TNFRSF11B COL5A1 ADAMTSL1 HTRA1 MMP14 GREM1 ITGA11 THSD4 SMAD3 SULF2 ADAMTS1
GO:0071230	cellular response to amino acid stimulus	69	6	0.42	3.70E-06	3.71E-06	COL16A1 SH3BP4 COL5A2 PDGFRA COL1A2 ZEB1
GO:0110111	negative regulation of animal	35	4	0.21	5.70E-05	5.71E-05	SULF1 TNFRSF11B ASPSTN GREM1

	organ morphogenesis						
GO:0035987	endodermal cell differentiation	46	6	0.28	3.30E-07	1.00E-04	COL11A1 COL5A2 COL7A1 COL12A1 COL5A1 MMP14
GO:0051014	actin filament severing	16	3	0.1	0.00011	0.00011	SVIL DSTN MYH9
GO:0030512	negative regulation of transforming growth factor beta receptor signaling pathway	87	5	0.53	0.00018	0.00018	SPRY1 PEG10 ASPSTN HTRA1 SMAD3
GO:1903224	regulation of endodermal cell differentiation	5	2	0.03	0.00036	0.00036	COL5A2 COL5A1
GO:0030324	lung development	177	8	1.07	1.20E-05	0.00041	WNT2B MME PDGFRA SPRY1 RBPJ ADAMTS2 MMP14 CCBE1
GO:0010954	positive regulation	25	3	0.15	0.00045	0.00045	MMP14 CCBE1 MYH9

	of protein processing						
GO:0040037	negative regulation of fibroblast growth factor receptor signaling pathway	26	3	0.16	0.0005	5.00E-04	SPRY1 SULF1 SULF2
GO:2000542	negative regulation of gastrulation	6	2	0.04	0.00053	0.00053	COL5A2 COL5A1
GO:0010575	positive regulation of vascular endothelial growth factor production	28	3	0.17	0.00063	0.00063	SULF1 CCBE1 SULF2
GO:0031032	actomyosin structure organization	200	8	1.21	2.90E-05	7.00E-04	PDGFRA ELN CSRP2 CIT TPM1 SMAD3 EPB41L3 MYH9
GO:0003256	regulation of transcription from RNA polymerase II promoter involved in	7	2	0.04	0.00075	0.00075	RBPJ GREM1

	myocardial precursor cell differentiation						
GO:0035989	tendon development	7	2	0.04	0.00075	0.00075	COL11A1 COL5A1
GO:0008217	regulation of blood pressure	187	10	1.13	2.00E-07	0.00079	MME F2R COL1A2 AOPEP ADM ACTA2 TPM1 ANPEP SMAD3 HMOX1
GO:0002063	chondrocyte development	32	3	0.19	0.00094	0.00094	COL11A1 SULF1 SULF2
GO:0001657	ureteric bud development	98	6	0.59	2.90E-05	0.00096	KIF26B WNT2B SPRY1 BMPER GREM1 SMAD3
GO:0001501	skeletal system development	517	13	3.12	1.50E-05	0.00129	COL11A1 PRELP WNT2B COL5A2 PDGFRA COL1A2 SULF1 TNFRSF11B ZEB1 MMP14 GREM1 SMAD3 SULF2
GO:0001568	blood vessel development	793	22	4.79	1.80E-09	0.00148	SP100 MYLK NDNF PDGFRA RBPJ THBS2 AHR BMPER COL1A2 SULF1 ANGPT1 COL5A1 ADM ACTA2 MMP14 GREM1

							ANPEP CCBE1 PTGIS MYH9 HMOX1 ADAMTS1
GO:0032836	glomerular basement membrane development	10	2	0.06	0.00158	0.00158	SULF1 SULF2
GO:0035860	glial cell-derived neurotrophic factor receptor signaling pathway	10	2	0.06	0.00158	0.00158	SULF1 SULF2
GO:0048251	elastic fiber assembly	10	2	0.06	0.00158	0.00158	TNXB THSD4
GO:0043588	skin development	425	8	2.57	0.00428	0.00181	COL5A2 FLNB PALLD RBPJ ADAMTS2 COL1A2 COL5A1 PPL
GO:0032060	bleb assembly	11	2	0.07	0.00192	0.00192	MYLK EMP1
GO:0002003	angiotensin maturation	12	2	0.07	0.0023	0.0023	MME AOPEP
GO:0003334	keratinocyte development	12	2	0.07	0.0023	0.0023	FLNB PALLD
GO:0014831	gastro-intestinal system	12	2	0.07	0.0023	0.0023	SULF1 SULF2

	smooth muscle contraction						
GO:0032963	collagen metabolic process	113	6	0.68	6.40E-05	0.00255	F2R ADAMTS2 TNXB COL1A2 COL5A1 MMP14
GO:0003094	glomerular filtration	24	3	0.15	0.0004	0.00266	F2R SULF1 SULF2
GO:0007171	activation of transmembrane receptor protein tyrosine kinase activity	13	2	0.08	0.0027	0.0027	ANGPT1 GREM1
GO:0048701	embryonic cranial skeleton morphogenesis	48	3	0.29	0.00305	0.00305	PDGFRA MMP14 SMAD3
GO:0033689	negative regulation of osteoblast proliferation	15	2	0.09	0.00361	0.00361	GREM1 SMAD3
GO:0030514	negative regulation of BMP signaling pathway	52	3	0.31	0.00383	0.00383	BMPER HTRA1 GREM1

GO:0043116	negative regulation of vascular permeability	16	2	0.1	0.00411	0.00411	ANGPT1 ADM
GO:0007229	integrin-mediated signaling pathway	108	4	0.65	0.00418	0.00418	COL16A1 ITGA11 MYH9 ADAMTS1
GO:0097190	apoptotic signaling pathway	612	10	3.7	0.00397	0.00451	IVNS1ABP SP100 ARL6IP5 PAWR TMBIM6 UACA SMAD3 PTGIS TIMP3 HMOX1
GO:0090190	positive regulation of branching involved in ureteric bud morphogenesis	18	2	0.11	0.0052	0.0052	WNT2B GREM1
GO:0002246	wound healing involved in inflammatory response	8	2	0.05	0.00099	0.00599	F2R HMOX1
GO:0034341	response to interferon-gamma	202	4	1.22	0.03425	0.00631	KYNU SP100 FLNB IFITM2

GO:0023019	signal transduction involved in regulation of gene expression	20	2	0.12	0.0064	0.0064	PDGFRA SMAD3
GO:0009615	response to virus	349	7	2.11	0.00531	0.00647	IVNS1ABP CHRM2 PENK IFITM2 ACTA2 HTRA1 SAMHD1
GO:0051893	regulation of focal adhesion assembly	63	5	0.38	3.90E-05	0.00673	COL16A1 SLK MMP14 GREM1 SMAD3
GO:0010811	positive regulation of cell-substrate adhesion	122	5	0.74	0.00087	0.00747	COL16A1 ABI3BP NDNF EDIL3 SMAD3
GO:0048592	eye morphogenesis	156	4	0.94	0.01488	0.00757	WNT2B COL5A2 COL5A1 ZEB1
GO:0007155	cell adhesion	1474	26	8.91	5.30E-07	0.00811	KIF26B HMCN1 COL16A1 NTNG1 CLDN11 ABI3BP COL7A1 NDNF PDGFRA PALLD EDIL3 SPOCK1 TNXB COL12A1 THBS2 NT5E ANGPT1 COL5A1 SLK PAWR MMP14

							GREM1 ITGA11 TPM1 SMAD3 MYH9
GO:0007517	muscle organ development	407	13	2.46	1.10E-06	0.00834	COL11A1 KCNK2 MYLK FLNB RBPJ ETV1 ELN TAGLN SVIL GREM1 ITGA11 TPM1 SMAD3
GO:0001759	organ induction	24	2	0.15	0.00916	0.00916	WNT2B SPRY1
GO:0030325	adrenal gland development	24	2	0.15	0.00916	0.00916	PDGFRA SMAD3
GO:0002092	positive regulation of receptor internalization	25	2	0.15	0.00992	0.00992	ANGPT1 GREM1
GO:0051894	positive regulation of focal adhesion assembly	25	2	0.15	0.00992	0.00992	COL16A1 SMAD3
GO:0045766	positive regulation of angiogenesis	208	6	1.26	0.00166	0.01009	BMPER ADM GREM1 CCBE1 PTGIS HMOX1
GO:0043627	response to estrogen	75	3	0.45	0.01058	0.01058	TNFRSF11B MMP14 HMOX1

GO:0060384	innervation	26	2	0.16	0.0107	0.0107	SULF1 SULF2
GO:0002040	sprouting angiogenesis	196	5	1.18	0.00678	0.01113	BMPER ANGPT1 GREM1 CCBE1 HMOX1
GO:0008285	negative regulation of cell population proliferation	786	14	4.75	0.00028	0.01146	KCNK2 SH3BP4 SPRY1 RBPJ F2R SULF1 ADM ZEB1 PAWR GREM1 TPM1 SMAD3 HMOX1 ADAMTS1
GO:0001666	response to hypoxia	359	10	2.17	6.50E-05	0.01154	KCNK2 NDNF RBPJ PENK ADM TMBIM6 MMP14 SMAD3 PTGIS HMOX1
GO:0006915	apoptotic process	1996	24	12.06	0.00074	0.01159	IVNS1ABP SP100 ARL6IP5 NDNF F2R AHR PEG10 SULF1 TNFRSF11B ANGPT1 TNFSF15 ADM SLK PAWR TMBIM6 CIT PHLDA1 GREM1 UACA SMAD3 EPB41L3 PTGIS TIMP3 HMOX1
GO:0030335	positive regulation of cell migration	567	10	3.43	0.00231	0.01182	MYLK LRRC15 PDGFRA F2R ANGPT1 MMP14 SMAD3 CCBE1 HMOX1 ADAMTS1

GO:0046851	negative regulation of bone remodeling	17	2	0.1	0.00464	0.01195	TNFRSF11B GREM1
GO:0008366	axon ensheathment	139	2	0.84	0.20522	0.01203	CLDN11 EPB41L3
GO:0001525	angiogenesis	610	17	3.69	1.50E-07	0.01243	SP100 NDNF PDGFRA RBPJ THBS2 BMPER SULF1 ANGPT1 ADM MMP14 GREM1 ANPEP CCBE1 PTGIS MYH9 HMOX1 ADAMTS1
GO:0043524	negative regulation of neuron apoptotic process	149	4	0.9	0.01276	0.01276	NDNF F2R ANGPT1 HMOX1
GO:2000727	positive regulation of cardiac muscle cell differentiation	29	2	0.18	0.01321	0.01321	RBPJ GREM1
GO:0001890	placenta development	156	5	0.94	0.00258	0.01445	MME RBPJ ADM HTRA1 PTGIS
GO:0006919	activation of cysteine-	86	3	0.52	0.0153	0.0153	F2R TNFSF15 SMAD3

	type endopeptidase activity involved in apoptotic process						
GO:0048706	embryonic skeletal system development	130	7	0.79	1.40E-05	0.01569	COL11A1 PDGFRA SULF1 ZEB1 MMP14 SMAD3 SULF2
GO:0055010	ventricular cardiac muscle tissue morphogenesis	48	3	0.29	0.00305	0.01571	COL11A1 RBPJ TPM1
GO:0030201	heparan sulfate proteoglycan metabolic process	32	2	0.19	0.01595	0.01595	SULF1 SULF2
GO:0097421	liver regeneration	32	2	0.19	0.01595	0.01595	SULF2 HMOX1
GO:0014068	positive regulation of phosphatidylinositol 3-kinase signaling	88	3	0.53	0.01626	0.01626	PDGFRA F2R ANGPT1

GO:0060537	muscle tissue development	409	12	2.47	6.90E-06	0.01665	COL11A1 KCNK2 MYLK FLNB PDGFRA RBPJ ELN SVIL CSRP2 GREM1 TPM1 SMAD3
GO:0072283	metanephric renal vesicle morphogenesis	16	2	0.1	0.00411	0.01787	KIF26B GREM1
GO:2000352	negative regulation of endothelial cell apoptotic process	34	2	0.21	0.0179	0.0179	NDNF ANGPT1
GO:0030036	actin cytoskeleton organization	707	14	4.27	9.30E-05	0.01802	FLNB PDGFRA PALLD TNXB ELN SVIL PAWR CSRP2 CIT TPM1 SMAD3 EPB41L3 DSTN MYH9
GO:0050776	regulation of immune response	1027	6	6.21	0.59258	0.01838	COL1A2 PAWR SMAD3 COLEC12 SAMHD1 HMOX1
GO:0030513	positive regulation of BMP signaling pathway	35	2	0.21	0.01891	0.01891	RBPJ SULF1

GO:0003382	epithelial cell morphogenesis	36	2	0.22	0.01995	0.01995	FLNB PALLD
GO:0030282	bone mineralization	117	4	0.71	0.00555	0.02048	COL1A2 ASPSTN GREM1 SMAD3
GO:0061458	reproductive system development	447	11	2.7	8.40E-05	0.02239	WNT2B MME PDGFRA RBPJ SULF1 ADM HTRA1 PLEKHA5 MMP14 PTGIS ADAMTS1
GO:0009611	response to wounding	656	15	3.96	9.60E-06	0.02261	KCNK2 TFPI MYLK NDNF PDGFRA F2R COL1A2 COL5A1 ADM TPM1 SMAD3 PPL SULF2 MYH9 HMOX1
GO:1904706	negative regulation of vascular associated smooth muscle cell proliferation	39	2	0.24	0.02319	0.02319	TPM1 HMOX1
GO:0003176	aortic valve development	32	2	0.19	0.01595	0.02378	RBPJ ELN
GO:0032467	positive regulation	40	2	0.24	0.02431	0.02431	SVIL CIT

	of cytokinesis						
GO:0043280	positive regulation of cysteine-type endopeptidase activity involved in apoptotic process	134	5	0.81	0.00133	0.02558	ARL6IP5 F2R TNFSF15 UACA SMAD3
GO:0030308	negative regulation of cell growth	190	4	1.15	0.02825	0.02825	SH3BP4 MEG3 GREM1 SMAD3
GO:0045785	positive regulation of cell adhesion	428	8	2.59	0.00447	0.02845	KIF26B COL16A1 ABI3BP NDNF EDIL3 ANGPT1 TPM1 SMAD3
GO:0072012	glomerulus vasculature development	26	3	0.16	0.0005	0.02937	PDGFRA ANGPT1 ACTA2
GO:0002175	protein localization to paranode region of axon	5	1	0.03	0.02985	0.02985	EPB41L3
GO:0006172	ADP biosynthetic process	5	1	0.03	0.02985	0.02985	AK5

GO:0009153	purine deoxyribonucleotide biosynthetic process	5	1	0.03	0.02985	0.02985	AK5
GO:0009217	purine deoxyribonucleoside triphosphate catabolic process	5	1	0.03	0.02985	0.02985	SAMHD1
GO:0009912	auditory receptor cell fate commitment	5	1	0.03	0.02985	0.02985	RBPJ
GO:0014805	smooth muscle adaptation	5	1	0.03	0.02985	0.02985	HMOX1
GO:0014900	muscle hyperplasia	5	1	0.03	0.02985	0.02985	HMOX1
GO:0019441	tryptophan catabolic process to kynurenine	5	1	0.03	0.02985	0.02985	KYNU
GO:0032763	regulation of mast cell cytokine production	5	1	0.03	0.02985	0.02985	HMOX1
GO:0032910	regulation of	5	1	0.03	0.02985	0.02985	SMAD3

	transformin g growth factor beta3 production						
GO:00 36337	Fas signaling pathway	5	1	0.03	0.02985	0.02985	SP100

Table A-2: Top100 GO enrichment results of Pathway enrichment analysis in osteogenic media

GO.ID	Term	Annotated	Significant	Expected	classic Fisher	weight01 Fisher	common
GO:1900084	regulation of peptidyl-tyrosine autophosphorylation	5	3	0.02	8.50E-07	8.51E-07	VEGFA CAV1 GREM1
GO:0046851	negative regulation of bone remodeling	17	3	0.08	5.50E-05	1.91E-05	SFRP1 TMEM119 GREM1
GO:0002092	positive regulation of receptor internalization	25	3	0.11	0.00018	0.00018	VEGFA ANGPT1 GREM1
GO:0051894	positive regulation of focal adhesion assembly	25	3	0.11	0.00018	0.00018	S100A10 VEGFA SFRP1
GO:0051016	barbed-end actin filament capping	26	3	0.12	0.00021	0.00021	CAPG SVIL TRIOBP
GO:1902035	positive regulation of hematopoietic stem cell proliferation	6	2	0.03	0.00029	0.00029	KITLG N4BP2L2

GO:0060346	bone trabecula formation	10	2	0.04	0.00086	0.00086	SFRP1 GREM1
GO:0007156	homophilic cell adhesion via plasma membrane adhesion molecules	168	5	0.75	0.00092	0.00092	HMCN1 PALLD FAT1 PCDHGC3 CDH11
GO:0009629	response to gravity	11	2	0.05	0.00105	0.00105	FOSL1 PKM
GO:0032060	bleb assembly	11	2	0.05	0.00105	0.00105	MYLK EMP3
GO:0007171	activation of transmembrane receptor protein tyrosine kinase activity	13	2	0.06	0.00148	0.00148	ANGPT1 GREM1
GO:0051496	positive regulation of stress fiber assembly	52	3	0.23	0.00161	0.00161	S100A10 SFRP1 TPM1
GO:0045668	negative regulation of osteoblast differentiation	53	3	0.24	0.0017	0.0017	TWIST2 SFRP1 GREM1
GO:0033689	negative regulation of osteoblast proliferation	15	2	0.07	0.00198	0.00198	SFRP1 GREM1

GO:0007155	cell adhesion	1474	22	6.56	3.10E-07	0.00199	HMCN1 S100A10 ALCAM PALLD FAT1 EDIL3 PCDHGC3 VEGFA THBS2 CAV1 SFRP1 ANGPT1 PLAU KITLG NTN4 GREM1 TPM1 CDH11 ADGRE5 TRIOBP COL6A2 COL6A1
GO:0043116	negative regulation of vascular permeability	16	2	0.07	0.00226	0.00226	VEGFA ANGPT1
GO:0051014	actin filament severing	16	2	0.07	0.00226	0.00226	CAPG SVIL
GO:0071456	cellular response to hypoxia	208	5	0.93	0.00237	0.00271	LMNA VEGFA AQP1 SFRP1 PTGIS
GO:0090190	positive regulation of branching involved in ureteric bud morphogenesis	18	2	0.08	0.00286	0.00286	VEGFA GREM1
GO:0032793	positive regulation of CREB transcription factor activity	20	2	0.09	0.00353	0.00353	VEGFA CAMK1D

GO:0045019	negative regulation of nitric oxide biosynthetic process	20	2	0.09	0.00353	0.00353	CAV1 PTGIS
GO:0001666	response to hypoxia	359	9	1.6	3.10E-05	0.00387	LMNA VEGFA CAV1 AQP1 SFRP1 PLAU PKM PTGIS CST3
GO:0000281	mitotic cytokinesis	72	3	0.32	0.00407	0.00407	SPTBN1 SNX18 CIT
GO:1903019	negative regulation of glycoprotein metabolic process	22	2	0.1	0.00427	0.00427	PTX3 CST3
GO:0045765	regulation of angiogenesis	403	10	1.79	1.20E-05	0.00508	VEGFA THBS2 AQP1 ADGRA2 SFRP1 NIBAN2 GREM1 PKM PTGIS ADAMTS1
GO:0008360	regulation of cell shape	156	4	0.69	0.0052	0.0052	VEGFA SYNE3 TPM1 CDC42EP4
GO:0043312	neutrophil degranulation	487	7	2.17	0.00599	0.00599	QSOX1 PTX3 TUBB4B PLAU PKM CST3 ADGRE5
GO:0002040	sprouting angiogenesis	196	5	0.87	0.00183	0.00607	VEGFA ADGRA2 ANGPT1 GREM1 PKM

GO:0031954	positive regulation of protein autophosphorylation	27	2	0.12	0.0064	0.0064	VEGFA GREM1
GO:0030512	negative regulation of transforming growth factor beta receptor signaling pathway	87	3	0.39	0.0069	0.0069	SPRY1 PEG10 CAV1
GO:0009615	response to virus	349	4	1.55	0.07037	0.00784	HMGA1 CHRM2 FOSL1 SAMHD1
GO:1905603	regulation of blood-brain barrier permeability	7	2	0.03	0.00041	0.00878	VEGFA ANGPT1
GO:0001657	ureteric bud development	98	4	0.44	0.00096	0.00909	SPRY1 VEGFA SFRP1 GREM1
GO:0007411	axon guidance	284	6	1.26	0.00168	0.01033	SPTBN1 ALCAM PALLD VEGFA NIBAN2 NTN4
GO:0008285	negative regulation of cell population proliferation	786	11	3.5	0.00071	0.01101	LMNA SPRY1 HMGA1 CAV1 SFRP1 NIBAN2 FOSL1 GREM1 TPM1 KANK2 ADAMTS1

GO:0030198	extracellular matrix organization	395	10	1.76	1.00E-05	0.01104	QSOX1 PTX3 CAV1 NTN4 GREM1 LOXL1 CST3 COL6A2 ADAMTS1 COL6A1
GO:0003382	epithelial cell morphogenesis	36	2	0.16	0.01119	0.01119	PALLD FAT1
GO:0030224	monocyte differentiation	38	2	0.17	0.01241	0.01241	VEGFA FASN
GO:1900026	positive regulation of substrate adhesion-dependent cell spreading	38	2	0.17	0.01241	0.01241	S100A10 TRIOBP
GO:0033138	positive regulation of peptidyl-serine phosphorylation	109	3	0.49	0.01274	0.01274	VEGFA CAV1 ANGPT1
GO:0090343	positive regulation of cell aging	23	2	0.1	0.00466	0.01315	LMNA HMGA1
GO:0051169	nuclear transport	357	3	1.59	0.21266	0.01323	LMNA HMGA1 ANGPT1
GO:0010719	negative regulation of epithelial to mesenchymal transition	40	2	0.18	0.01369	0.01369	SPRY1 SFRP1

GO:0032467	positive regulation of cytokinesis	40	2	0.18	0.01369	0.01369	SVIL CIT
GO:0042060	wound healing	536	8	2.39	0.00265	0.01387	MYLK VEGFA CAV1 DGKI PLEC PLAU TPM1 PPL
GO:0007566	embryo implantation	58	3	0.26	0.0022	0.01472	VEGFA PTGIS CST3
GO:0030335	positive regulation of cell migration	567	10	2.52	0.00021	0.0148	TWIST2 MYLK VEGFA CAV1 ADGRA2 ANGPT1 PLAU CAMK1D KITLG ADAMTS1
GO:0045785	positive regulation of cell adhesion	428	8	1.91	0.00064	0.01548	S100A10 EDIL3 VEGFA CAV1 SFRP1 ANGPT1 TPM1 TRIOBP
GO:0015701	bicarbonate transport	43	2	0.19	0.01572	0.01572	SLC4A2 AQP1
GO:0016339	calcium-dependent cell-cell adhesion via plasma membrane cell adhesion molecules	43	2	0.19	0.01572	0.01572	PCDHGC3 CDH11
GO:0043067	regulation of programmed cell death	1617	16	7.2	0.00187	0.0159	LMNA TWIST2 VEGFA CAV1 AQP1 SFRP1

							ANGPT1 NIBAN2 FOSL1 CAMK1D KITLG PHLDA1 GREM1 PTGIS CST3 KANK2
GO:0007044	cell-substrate junction assembly	99	6	0.44	5.20E-06	0.01673	S100A10 TNS1 VEGFA SFRP1 PLEC GREM1
GO:0006935	chemotaxis	655	12	2.92	3.20E-05	0.01685	SPTBN1 ALCAM PALLD VEGFA ADGRA2 ANGPT1 NIBAN2 FOSL1 PLAU CAMK1D NTN4 GREM1
GO:0030952	establishment or maintenance of cytoskeleton polarity	9	2	0.04	0.00069	0.01749	LMNA AQP1
GO:0007431	salivary gland development	39	2	0.17	0.01305	0.01752	NTN4 CST3
GO:0032570	response to progesterone	46	2	0.2	0.01786	0.01786	CAV1 FOSL1
GO:0007157	heterophilic cell-cell adhesion via plasma membrane cell adhesion molecules	47	2	0.21	0.0186	0.0186	HMCN1 ALCAM

GO:0001541	ovarian follicle development	57	3	0.25	0.00209	0.01969	PTX3 VEGFA KITLG
GO:0007595	lactation	49	2	0.22	0.02012	0.02012	VEGFA CAV1
GO:0034260	negative regulation of GTPase activity	49	2	0.22	0.02012	0.02012	SPRY1 DGKI
GO:0045104	intermediate filament cytoskeleton organization	50	2	0.22	0.0209	0.0209	PLEC PPL
GO:0045540	regulation of cholesterol biosynthetic process	50	2	0.22	0.0209	0.0209	FASN LSS
GO:0072073	kidney epithelium development	142	5	0.63	0.00043	0.02118	SPRY1 VEGFA SFRP1 GREM1 KANK2
GO:0034104	negative regulation of tissue remodeling	22	4	0.1	2.50E-06	0.0213	SFRP1 TMEM119 GREM1 CST3
GO:0014910	regulation of smooth muscle cell migration	86	3	0.38	0.00668	0.02164	PLAU TPM1 ADAMTS1
GO:0001765	membrane raft assembly	12	2	0.05	0.00126	0.02181	S100A10 CAV1

GO:0048846	axon extension involved in axon guidance	37	2	0.16	0.01179	0.02184	ALCAM VEGFA
GO:0050731	positive regulation of peptidyl-tyrosine phosphorylation	195	4	0.87	0.01123	0.02191	VEGFA ANGPT1 KITLG GREM1
GO:0009217	purine deoxyribonucleoside triphosphate catabolic process	5	1	0.02	0.02207	0.02207	SAMHD1
GO:0010716	negative regulation of extracellular matrix disassembly	5	1	0.02	0.02207	0.02207	CST3
GO:0015670	carbon dioxide transport	5	1	0.02	0.02207	0.02207	AQP1
GO:0018057	peptidyl-lysine oxidation	5	1	0.02	0.02207	0.02207	LOXL1
GO:0030047	actin modification	5	1	0.02	0.02207	0.02207	TRIOBP
GO:0030950	establishment or maintenance of actin cytoskeleton polarity	5	1	0.02	0.02207	0.02207	AQP1

GO:0035426	extracellular matrix-cell signaling	5	1	0.02	0.02207	0.02207	NTN4
GO:0036324	vascular endothelial growth factor receptor-2 signaling pathway	5	1	0.02	0.02207	0.02207	VEGFA
GO:0038033	positive regulation of endothelial cell chemotaxis by VEGF-activated vascular endothelial growth factor receptor signaling pathway	5	1	0.02	0.02207	0.02207	VEGFA
GO:0045578	negative regulation of B cell differentiation	5	1	0.02	0.02207	0.02207	SFRP1
GO:0045636	positive regulation of melanocyte differentiation	5	1	0.02	0.02207	0.02207	KITLG
GO:0046060	dATP metabolic process	5	1	0.02	0.02207	0.02207	SAMHD1

GO:0048550	negative regulation of pinocytosis	5	1	0.02	0.02207	0.02207	CAV1
GO:0052405	negative regulation by host of symbiont molecular function	5	1	0.02	0.02207	0.02207	PTX3
GO:0060414	aorta smooth muscle tissue morphogenesis	5	1	0.02	0.02207	0.02207	MYLK
GO:0061302	smooth muscle cell-matrix adhesion	5	1	0.02	0.02207	0.02207	PLAU
GO:0070662	mast cell proliferation	5	1	0.02	0.02207	0.02207	KITLG
GO:0071504	cellular response to heparin	5	1	0.02	0.02207	0.02207	SFRP1
GO:0090245	axis elongation involved in somitogenesis	5	1	0.02	0.02207	0.02207	SFRP1
GO:0090259	regulation of retinal ganglion cell axon guidance	5	1	0.02	0.02207	0.02207	VEGFA
GO:0090289	regulation of osteoclast proliferation	5	1	0.02	0.02207	0.02207	GREM1

GO:1900158	negative regulation of bone mineralization involved in bone maturation	5	1	0.02	0.02207	0.02207	GREM1
GO:1901228	positive regulation of transcription from RNA polymerase II promoter involved in heart development	5	1	0.02	0.02207	0.02207	GREM1
GO:1901534	positive regulation of hematopoietic progenitor cell differentiation	5	1	0.02	0.02207	0.02207	KITLG
GO:1903391	regulation of adherens junction organization	5	1	0.02	0.02207	0.02207	VEGFA
GO:1903596	regulation of gap junction assembly	5	1	0.02	0.02207	0.02207	CAV1
GO:1904956	regulation of midbrain dopaminergic	5	1	0.02	0.02207	0.02207	SFRP1

	neuron differentiation						
GO:1905605	positive regulation of blood-brain barrier permeability	5	1	0.02	0.02207	0.02207	ANGPT1
GO:0030514	negative regulation of BMP signaling pathway	52	2	0.23	0.02249	0.02249	SFRP1 GREM1
GO:0045766	positive regulation of angiogenesis	208	5	0.93	0.00237	0.02379	VEGFA AQP1 GREM1 PKM PTGIS
GO:0048699	generation of neurons	1570	13	6.99	0.02107	0.02471	CRABP2 SPTBN1 ALCAM PALLD MAN2A1 VEGFA SFRP1 NIBAN2 CAMK1D NTN4 CIT CDH11 TRIOBP
GO:0030199	collagen fibril organization	55	2	0.24	0.02498	0.02498	GREM1 LOXL1

Table A-3. Top100 GO enrichment results of Pathway enrichment analysis in DMEM for patient F15

GO.ID	Term	Annotated	Significant	Expected	classicFisher	weight01Fisher	common
GO:0051973	positive regulation of telomerase activity	36	4	0.15	1.70E-05	1.71E-05	XRCC5 HNRNPD HNRNPA2B1 GREM1
GO:0014912	negative regulation of smooth muscle cell migration	38	4	0.16	2.10E-05	4.01E-05	SERPINE1 IGFBP3 PRKG1 LRP1
GO:0001649	osteoblast differentiation	231	7	0.99	6.10E-05	6.51E-05	IL6ST GPNMB IGFBP3 PENK GREM1 FASN RPS15
GO:0042493	response to drug	397	9	1.7	5.10E-05	7.41E-05	TXNIP CENPF XRCC5 HMGB2 FYN ABCA1 GAS6 TIMP2 SREBF1
GO:0000028	ribosomal small subunit assembly	21	3	0.09	9.60E-05	9.61E-05	XRCC5 RPS19 RPS15
GO:0046813	receptor-mediated virion attachment to host cell	5	2	0.02	0.00018	0.00018	LRRC15 GAS6
GO:004	axon	5	2	0.02	0.00018	0.00018	LAMB2 LRP1

8677	extension involved in regeneration						
GO:0060266	negative regulation of respiratory burst involved in inflammatory response	5	2	0.02	0.00018	0.00018	GRN RPS19
GO:1900158	negative regulation of bone mineralization involved in bone maturation	5	2	0.02	0.00018	0.00018	GREM1 RFLNB
GO:0007568	aging	319	9	1.37	9.00E-06	0.00019	YBX1 MME PDGFRB SERPINE1 PENK GSN LRP1 TIMP2 SREBF1
GO:0050918	positive chemotaxis	67	4	0.29	0.0002	2.00E-04	HMGB2 GPNMB LRP1 HMGB1
GO:0061304	retinal blood vessel morphogenesis	6	2	0.03	0.00027	0.00027	CYP1B1 COL4A1
GO:0006335	DNA replication-dependent nucleosome	32	3	0.14	0.00035	0.00035	H3C2 H4C3 H4C8

	assembly						
GO:0032392	DNA geometric change	116	4	0.5	0.00157	0.00036	XRCC5 HMGB2 HNRNPA2B1 HMGB1
GO:0150094	amyloid-beta clearance by cellular catabolic process	7	2	0.03	0.00038	0.00038	MME LRP1
GO:0044267	cellular protein metabolic process	5350	40	22.97	4.90E-05	0.00042	PLPP3 LEPR YBX1 CTSK MGAT5 XRCC5 NCL CBLB LAMB2 HNRNPD IL6ST PDGFRB STC2 FYN H3C2 H4C3 H4C8 SERPINE1 GPNMB IGFBP3 PENK PAPPA GSN ABCA1 CFL1 PSAP LRP1 HSP90B1 HMGB1 GAS6 TNFRSF19 GREM1 CEMIP TIMP2 GRN SREBF1 RPS19 RPS15 FBLN1 TIMP3
GO:1905049	negative regulation of metallopeptidase activity	18	3	0.08	5.90E-05	0.00049	LRP1 TIMP2 TIMP3
GO:000	Notch	195	6	0.84	0.00019	5.00E-04	YBX1 IL6ST CDH6

7219	signaling pathway						S1PR3 POSTN RPS19
GO:0051045	negative regulation of membrane protein ectodomain proteolysis	8	2	0.03	0.0005	5.00E-04	TIMP2 TIMP3
GO:0051103	DNA ligation involved in DNA repair	8	2	0.03	0.0005	5.00E-04	HMGB2 HMGB1
GO:0071295	cellular response to vitamin	32	3	0.14	0.00035	0.00063	PENK POSTN GAS6
GO:0006265	DNA topological change	9	2	0.04	0.00064	0.00064	HMGB2 HMGB1
GO:0048263	determination of dorsal identity	9	2	0.04	0.00064	0.00064	GREM2 GREM1
GO:0000183	rDNA heterochromatin assembly	40	3	0.17	0.00067	0.00067	H3C2 H4C3 H4C8
GO:0035581	sequestering of extracellular ligand from receptor	10	2	0.04	0.0008	8.00E-04	GREM2 GREM1
GO:0032355	response to estradiol	141	6	0.61	3.20E-05	0.00093	TXNIP HNRNPD H2AZ1 PDGFRB PENK POSTN

GO:0071310	cellular response to organic substance	2756	36	11.83	1.00E-10	0.00097	LEPR YBX1 GREM2 CYP1B1 XRCC5 NCL MME HNRNPD H2AZ1 HMGB2 IL6ST PDGFRB SLIT3 STC2 FYN H3C2 HLA-C SERPINE1 HNRNPA2B1 PENK GSN ABCA1 CFL1 PSAP LRP1 HSP90B1 HMGB1 POSTN COL4A1 GAS6 TNFRSF19 GREM1 NFAT5 FASN SREBF1 TIMP3
GO:0048680	positive regulation of axon regeneration	11	2	0.05	0.00098	0.00098	LRP1 GRN
GO:0045814	negative regulation of gene expression, epigenetic	126	5	0.54	0.00021	0.00115	H2AZ1 H3C2 H4C3 H4C8 HMGB1
GO:0043312	neutrophil degranulation	487	8	2.09	0.00115	0.00115	XRCC5 MME HLA-C GSN PSAP HMGB1 TIMP2 GRN
GO:0033629	negative regulation of	12	2	0.05	0.00117	0.00117	CYP1B1 SERPINE1

	cell adhesion mediated by integrin						
GO:1900025	negative regulation of substrate adhesion-dependent cell spreading	13	2	0.06	0.00138	0.00138	POSTN FBLN1
GO:0090399	replicative senescence	14	2	0.06	0.0016	0.0016	MME SERPINE1
GO:0033151	V(D)J recombination	15	2	0.06	0.00184	0.00184	HMGB2 HMGB1
GO:0043410	positive regulation of MAPK cascade	554	9	2.38	0.00061	0.00208	PDGFRB GPNMB IGFBP3 PSAP LRP1 HMGB1 GAS6 TNFRSF19 TIMP2
GO:0051014	actin filament severing	16	2	0.07	0.0021	0.0021	GSN CFL1
GO:0002576	platelet degranulation	129	4	0.55	0.00231	0.00231	SERPINE1 PSAP GAS6 TIMP3
GO:0070374	positive regulation of ERK1 and ERK2 cascade	215	5	0.92	0.00233	0.00233	PDGFRB GPNMB LRP1 HMGB1 GAS6
GO:0070293	renal absorption	17	2	0.07	0.00237	0.00237	GSN GAS6
GO:002	extracellular	82	4	0.35	0.00043	0.00266	CTSK LRP1 TIMP2

2617	matrix disassembly						ADAMTS5
GO:0045653	negative regulation of megakaryocyte differentiation	18	2	0.08	0.00266	0.00266	H4C3 H4C8
GO:0051895	negative regulation of focal adhesion assembly	18	2	0.08	0.00266	0.00266	PHLDB2 LRP1
GO:0006303	double-strand break repair via nonhomologous end joining	96	4	0.41	0.00078	0.00291	XRCC5 DEK H4C3 H4C8
GO:0032956	regulation of actin cytoskeleton organization	360	8	1.55	0.00016	0.00296	CDC42EP3 PHLDB2 SYNPO2 RHOBTB3 PDGFRB GSN CFL1 LRP1
GO:0090026	positive regulation of monocyte chemotaxis	19	2	0.08	0.00297	0.00297	SERPINE1 HMGB1
GO:0010875	positive regulation of cholesterol efflux	20	2	0.09	0.00329	0.00329	ABCA1 LRP1
GO:0014911	positive regulation of	48	3	0.21	0.00115	0.00389	PDGFRB LRP1 POSTN

	smooth muscle cell migration						
GO:0036120	cellular response to platelet-derived growth factor stimulus	22	2	0.09	0.00398	0.00398	PDGFRB FYN
GO:0010469	regulation of signaling receptor activity	174	5	0.75	0.00092	0.00435	GREM2 CBLB SERPINE1 HMGB1 GREM1
GO:0043687	post-translational protein modification	363	6	1.56	0.00471	0.00471	LAMB2 STC2 IGFBP3 PENK HSP90B1 GAS6
GO:0032331	negative regulation of chondrocyte differentiation	24	2	0.1	0.00473	0.00473	GREM1 RFLNB
GO:0001953	negative regulation of cell-matrix adhesion	43	4	0.18	3.40E-05	0.00489	PHLDB2 SERPINE1 LRP1 POSTN
GO:1901224	positive regulation of NIK/NF-kappaB signaling	80	3	0.34	0.00494	0.00494	HMGB1 GREM1 NFAT5
GO:001	viral process	924	15	3.97	7.80E-	0.00499	XRCC5 LRRC15

6032					06		IL6ST DEK FYN HLA-C HNRNPA2B1 GSN CADM1 CFL1 HMGB1 GAS6 RPS19 RPS15 FBLN1
GO:0050829	defense response to Gram-negative bacterium	81	3	0.35	0.00511	0.00511	HMGB2 SERPINE1 RPS19
GO:0006309	apoptotic DNA fragmentation	26	2	0.11	0.00553	0.00553	HMGB2 HMGB1
GO:0045892	negative regulation of transcription, DNA-templated	1321	16	5.67	0.00013	0.00562	TXNIP CENPF YBX1 XRCC5 H2AZ1 HMGB2 TENM2 H3C2 H4C3 H4C8 HNRNPA2B1 DRAP1 HMGB1 GAS6 GREM1 SREBF1
GO:0002218	activation of innate immune response	144	3	0.62	0.02411	0.00589	XRCC5 FYN HMGB1
GO:0031954	positive regulation of protein autophosphorylation	27	2	0.12	0.00596	0.00596	GPNMB GREM1

GO:0048143	astrocyte activation	27	2	0.12	0.00596	0.00596	LRP1 GRN
GO:0042060	wound healing	536	11	2.3	1.80E-05	0.00636	PLPP3 PHLDB2 PDGFRB FYN H3C2 SERPINE1 GSN PRKG1 POSTN GAS6 FBLN1
GO:0010575	positive regulation of vascular endothelial growth factor production	28	2	0.12	0.0064	0.0064	CYP1B1 IL6ST
GO:0016233	telomere capping	55	3	0.24	0.0017	0.00671	HNRNPD H4C3 H4C8
GO:0090314	positive regulation of protein targeting to membrane	30	2	0.13	0.00733	0.00733	FYN CEMIP
GO:0002790	peptide secretion	501	7	2.15	0.00572	0.00815	STXBP5 ABCA1 CADM1 PSAP LRP1 HMGB1 SREBF1
GO:0010629	negative regulation of gene expression	2766	26	11.88	5.60E-05	0.00886	TXNIP CENPF YBX1 SERBP1 XRCC5 NCL HNRNPD H2AZ1 HMGB2 TENM2 SLIT3 STC2 FYN

							H3C2 H4C3 H4C8 SERPINE1 GPNMB HNRNPA2B1 DRAP1 HMGB1 GAS6 GREM1 SREBF1 RPS19 RPS15
GO:2000352	negative regulation of endothelial cell apoptotic process	34	2	0.15	0.00934	0.00934	SERPINE1 GAS6
GO:0035909	aorta morphogenesis	35	2	0.15	0.00988	0.00988	PDGFRB LRP1
GO:0043066	negative regulation of apoptotic process	919	12	3.95	0.00053	0.00998	PTMA HMGB2 IL6ST PDGFRB FYN SERPINE1 CFL1 LRP1 HSP90B1 GAS6 GREM1 GRN
GO:0010721	negative regulation of cell development	343	5	1.47	0.01605	0.01002	S1PR3 LRP1 POSTN RFLNB FBLN1
GO:0034097	response to cytokine	1227	22	5.27	5.90E-09	0.01009	LEPR YBX1 GREM2 XRCC5 NCL MME IL6ST SLIT3 FYN H3C2 HLA-C HNRNPA2B1 GSN CFL1 HSP90B1 POSTN GAS6

							TNFRSF19 NFAT5 TIMP2 FASN TIMP3
GO:0043277	apoptotic cell clearance	51	3	0.22	0.00137	0.01076	LRP1 HMGB1 GAS6
GO:0032689	negative regulation of interferon-gamma production	38	2	0.16	0.01158	0.01158	HMGB1 GAS6
GO:0071392	cellular response to estradiol stimulus	38	2	0.16	0.01158	0.01158	HNRNPD H2AZ1
GO:0043666	regulation of phosphoprotein phosphatase activity	117	4	0.5	0.00162	0.0117	MGAT5 PDGFRB IGFBP3 HSP90B1
GO:0007041	lysosomal transport	110	3	0.47	0.01184	0.01184	PSAP LRP1 GRN
GO:0045766	positive regulation of angiogenesis	208	4	0.89	0.01234	0.01234	CYP1B1 SERPINE1 GREM1 GRN
GO:0071222	cellular response to lipopolysaccharide	208	4	0.89	0.01234	0.01234	HMGB2 SERPINE1 ABCA1 HMGB1
GO:1904894	positive regulation of receptor signaling	93	4	0.4	0.00069	0.01241	CYP1B1 MGAT5 IL6ST FYN

	pathway via STAT						
GO:1904358	positive regulation of telomere maintenance via telomere lengthening	37	2	0.16	0.011	0.01269	XRCC5 HNRNPA2B1
GO:0046466	membrane lipid catabolic process	38	2	0.16	0.01158	0.01269	CYP1B1 PSAP
GO:0030335	positive regulation of cell migration	567	12	2.43	5.20E-06	0.01273	PLPP3 MGAT5 LRRC15 PDGFRB SERPINE1 GPNMB LRP1 HMGB1 POSTN GAS6 CEMIP GRN
GO:0051208	sequestering of calcium ion	124	2	0.53	0.09938	0.01275	HSP90B1 CEMIP
GO:0045089	positive regulation of innate immune response	213	6	0.91	0.00031	0.01296	XRCC5 HMGB2 FYN CADM1 HMGB1 RPS19
GO:0032526	response to retinoic acid	108	3	0.46	0.01127	0.01317	PDGFRB ABCA1 SREBF1
GO:0006352	DNA-templated transcription, initiation	249	3	1.07	0.09182	0.01336	H4C3 H4C8 HMGB1
GO:000	response to	905	11	3.89	0.00163	0.01339	TXNIP LEPR

9725	hormone						HMGB2 PDGFRB SLIT3 STC2 FYN PAPPA TIMP2 SREBF1 TIMP3
GO:1902042	negative regulation of extrinsic apoptotic signaling pathway via death domain receptors	41	2	0.18	0.0134	0.0134	HMGB2 SERPINE1
GO:0060964	regulation of gene silencing by miRNA	116	3	0.5	0.01365	0.01365	H3C2 H4C3 H4C8
GO:0034080	CENP-A containing nucleosome assembly	43	2	0.18	0.01467	0.01467	H4C3 H4C8
GO:0050769	positive regulation of neurogenesis	485	7	2.08	0.00481	0.01482	XRCC5 MME IL6ST FYN LRP1 TIMP2 GRN
GO:0045471	response to ethanol	122	3	0.52	0.01561	0.01561	FYN PENK GSN
GO:0042542	response to hydrogen peroxide	146	5	0.63	0.00041	0.01568	TXNIP CYP1B1 PDGFRB FYN PSAP
GO:0002263	cell activation involved in immune response	720	9	3.09	0.00367	0.01599	XRCC5 MME HLA-C GSN PSAP LRP1 HMGB1 TIMP2 GRN

GO:1904646	cellular response to amyloid-beta	45	2	0.19	0.016	0.016	FYN LRP1
GO:0009991	response to extracellular stimulus	507	8	2.18	0.00149	0.01602	STC2 PENK GSN ABCA1 POSTN GAS6 SREBF1 RPS19
GO:0061572	actin filament bundle organization	161	4	0.69	0.00511	0.01657	PHLDB2 SYNPO2 HSP90B1 RFLNB
GO:0032570	response to progesterone	46	2	0.2	0.01668	0.01668	TXNIP SREBF1
GO:0007266	Rho protein signal transduction	140	4	0.6	0.00311	0.01672	CDC42EP3 PDGFRB ABCA1 CFL1
GO:0050729	positive regulation of inflammatory response	158	4	0.68	0.00478	0.01688	IL6ST SERPINE1 GRN RPS19

Table A-4: Top100 GO enrichment results of Pathway enrichment analysis in osteogenic for patient F15

GO.ID	Term	Annotated	Significant	Expected	classicFisher	weight01Fisher	common
GO:0000184	nuclear-transcribed mRNA catabolic process, nonsense-mediated decay	120	18	1.16	1.00E-16	1.02E-16	RPL37A RPS27A RPSA RPL24 RPS12 RPL7 RPS20 RPS6 RPL35 RPL12 RPLP2 RPL27A RPLP0 RPLP1 RPS2 RPL13 RPS21 RPL3
GO:0019083	viral transcription	178	18	1.72	1.20E-13	1.21E-13	RPL37A RPS27A RPSA RPL24 RPS12 RPL7 RPS20 RPS6 RPL35 RPL12 RPLP2 RPL27A RPLP0 RPLP1 RPS2 RPL13 RPS21 RPL3
GO:0043484	regulation of RNA splicing	156	8	1.5	0.00014	6.21E-06	NCL HNRNPH1 HNRNPA2B1 AHNAK HNRNPH3 SLC38A2 AHNAK2 FUS
GO:0051973	positive regulation of telomerase activity	36	5	0.35	2.30E-05	2.31E-05	HNRNPD HNRNPA2B1 CCT2 PTGES3 HSP90AA1
GO:003	oncostatin-M-	7	3	0.07	3.00E-	3.01E-05	OSMR IL6ST

8165	mediated signaling pathway				05		IL13RA1
GO:0048861	leukemia inhibitory factor signaling pathway	8	3	0.08	4.80E-05	4.81E-05	OSMR IL6ST IL13RA1
GO:0030199	collagen fibril organization	55	6	0.53	1.50E-05	9.41E-05	DDR2 ADAMTS2 COL5A1 SERPINH1 NF1 COLGALT1
GO:0030198	extracellular matrix organization	395	25	3.81	9.00E-14	1.00E-04	QSOX1 DDR2 CCN1 COL16A1 CTSK NTNG1 ANTXR1 PHLDB2 ABI3BP COL7A1 PDGFRA ADAMTS2 LAMA4 ELN COL5A1 HSD17B12 SERPINH1 LRP1 COL4A1 FLRT2 THSD4 NF1 TIMP2 COLGALT1 FBLN1
GO:0000027	ribosomal large subunit assembly	30	4	0.29	0.00019	0.00019	RPL24 RPL12 RPLP0 RPL3
GO:0043312	neutrophil degranulation	487	14	4.7	0.00028	0.00028	QSOX1 RAB10 MME PPIA DDX3X SDCBP TUBB4B MGST1 CCT2 CKAP4 GNS HMGB1 HSP90AA1

							TIMP2
GO:0045669	positive regulation of osteoblast differentiation	66	5	0.64	0.00044	0.00044	DDR2 CCN1 IL6ST FAM20C CTHRC1
GO:0050821	protein stabilization	187	8	1.8	0.00047	0.00047	PLPP3 CCT5 H1-5 GNAQ CCT2 PTGES3 HSP90AA1 PPIB
GO:0071230	cellular response to amino acid stimulus	69	5	0.67	0.00054	0.00054	COL16A1 HNRNPD PDGFRA ZEB1 COL4A1
GO:0021987	cerebral cortex development	118	6	1.14	0.001	0.00083	GNG12 ROBO1 TACC3 SLC38A2 LRP1 NF1
GO:0035722	interleukin-12-mediated signaling pathway	47	4	0.45	0.00108	0.00108	LMNB1 PPIA HNRNPA2B1 RPLP0
GO:0051131	chaperone-mediated protein complex assembly	22	3	0.21	0.00119	0.00119	CCT2 PTGES3 HSP90AA1
GO:1905323	telomerase holoenzyme complex assembly	6	2	0.06	0.00135	0.00135	PTGES3 HSP90AA1
GO:0032496	response to lipopolysacch	334	9	3.22	0.00524	0.00137	GNG12 PTGFR HMGB2 FER

	aride						AKAP12 PENK VIM MGST1 HMGB1
GO:0032392	DNA geometric change	116	5	1.12	0.00536	0.00184	RPS27A HMGB2 HNRNPA2B1 DDX3X HMGB1
GO:0150094	amyloid-beta clearance by cellular catabolic process	7	2	0.07	0.00188	0.00188	MME LRP1
GO:1905049	negative regulation of metallopeptidase activity	18	3	0.17	0.00065	0.00247	LRP1 TIMP2 TIMP3
GO:0051045	negative regulation of membrane protein ectodomain proteolysis	8	2	0.08	0.00249	0.00249	TIMP2 TIMP3
GO:0051103	DNA ligation involved in DNA repair	8	2	0.08	0.00249	0.00249	HMGB2 HMGB1
GO:0007409	axonogenesis	482	12	4.65	0.00256	0.00279	STMN1 NTNG1 MACF1 S100A6 ZEB2 RAB10 ROBO1 MAP1B LRP1 MYCBP2 HSP90AA1 FLRT2
GO:0032964	collagen biosynthetic	53	3	0.51	0.01453	0.00317	COL5A1 SERPINH1 VIM

	process						
GO:0006265	DNA topological change	9	2	0.09	0.00319	0.00319	HMGB2 HMGB1
GO:0045762	positive regulation of adenylate cyclase activity	9	2	0.09	0.00319	0.00319	NF1 TIMP2
GO:0060087	relaxation of vascular associated smooth muscle	9	2	0.09	0.00319	0.00319	PRKG1 KCNMA1
GO:0002181	cytoplasmic translation	103	5	0.99	0.00323	0.00323	RPSA RPL24 RPLP0 RPLP1 RPS21
GO:0051592	response to calcium ion	147	5	1.42	0.01407	0.00338	TXNIP HNRNPD PENK KCNMA1 FUS
GO:0001568	blood vessel development	793	17	7.65	0.00177	0.0038	TGFBR3 PRRX1 LEPR CCN1 NCL ANTXR1 ROBO1 SEC24B PDGFRA AHR GPNMB ENPP2 COL5A1 LRP1 COL4A1 NF1 SERPINF1
GO:1904851	positive regulation of establishment of protein	10	2	0.1	0.00396	0.00396	CCT5 CCT2

	localization to telomere						
GO:0043488	regulation of mRNA stability	186	7	1.79	0.00222	0.004	RPS27A XRN1 HNRNPD SET VIM FUS PSMA7
GO:0050918	positive chemotaxis	67	4	0.65	0.004	0.004	HMGB2 GPNMB LRP1 HMGB1
GO:0033327	Leydig cell differentiation	11	2	0.11	0.00481	0.00481	PDGFRA MGST1
GO:0051574	positive regulation of histone H3-K9 methylation	11	2	0.11	0.00481	0.00481	LMNA H1-5
GO:1904871	positive regulation of protein localization to Cajal body	11	2	0.11	0.00481	0.00481	CCT5 CCT2
GO:0030335	positive regulation of cell migration	567	14	5.47	0.00124	0.00499	PLPP3 DDR2 CCN1 IL1R1 LRRC15 PDGFRA FER AKAP12 GPNMB SDCBP ENPP2 LRP1 HMGB1 CEMIP
GO:0006617	SRP-dependent cotranslational protein targeting to	12	2	0.12	0.00573	0.00573	RN7SL3 RN7SL1

	membrane, signal sequence recognition						
GO:0033690	positive regulation of osteoblast proliferation	12	2	0.12	0.00573	0.00573	CCN1 CTHRC1
GO:0038063	collagen-activated tyrosine kinase receptor signaling pathway	12	2	0.12	0.00573	0.00573	DDR2 COL4A1
GO:0090331	negative regulation of platelet aggregation	12	2	0.12	0.00573	0.00573	PRKG1 CD9
GO:0016032	viral process	924	35	8.91	2.80E-12	0.00597	EPS15 RPL37A RPS27A RPSA AP2M1 RPL24 LRRC15 PDGFRA IL6ST RPS12 PPIA HNRNPA2B1 DDX3X RPL7 RPS20 RPS6 RPL35 RPL12 SET RPLP2 RPL27A VIM RPLP0 HMGB1 HSP90AA1 RPLP1 PPIB RPS2 RPL13 KPNA2 PSMA7 RPS21 FBLN1 RPL3

							LGALS1
GO:1901998	toxin transport	41	3	0.4	0.00719	0.00719	ANTXR1 CCT5 CCT2
GO:0006935	chemotaxis	655	13	6.32	0.01117	0.00721	LYST CCN1 ROBO1 PDGFRA HMGB2 FER GPNMB ENPP2 LRP1 HMGB1 MYCBP2 FLRT2 PPIB
GO:0006334	nucleosome assembly	145	6	1.4	0.00286	0.0073	HMGB2 H4C4 H1-5 H2BC17 H4C3 SET
GO:0150011	regulation of neuron projection arborization	14	2	0.14	0.0078	0.0078	NTNG1 MACF1
GO:0031623	receptor internalization	115	5	1.11	0.00517	0.00805	EPS15 AP2M1 SDCBP LRP1 CD9
GO:0045773	positive regulation of axon extension	43	3	0.41	0.00821	0.00821	MACF1 MAP1B LRP1
GO:0071711	basement membrane organization	30	4	0.29	0.00019	0.00877	NTNG1 PHLDB2 COL4A1 FLRT2
GO:0051174	regulation of phosphorus metabolic process	1870	33	18.04	0.00046	0.00883	PLPP3 DDR2 LEPR CCN1 ZEB2 RPS27A ROBO1 PARP14 PDGFRA IL6ST FER CCNG1

							AKAP12 FAM20C GPNMB DDX3X SDCBP ENPP2 GNAQ SET LRP1 PTGES3 HMGB1 TNFRSF19 HSP90AA1 CEMIP RPLP1 NF1 TIMP2 TAOK1 PRNP FBLN1 TIMP3
GO:0000463	maturation of LSU-rRNA from tricistronic rRNA transcript (SSU-rRNA, 5.8S rRNA, LSU-rRNA)	15	2	0.14	0.00895	0.00895	RPL7 RPL35
GO:0010763	positive regulation of fibroblast migration	15	2	0.14	0.00895	0.00895	DDR2 AKAP12
GO:0033151	V(D)J recombination	15	2	0.14	0.00895	0.00895	HMGB2 HMGB1
GO:1902043	positive regulation of extrinsic apoptotic signaling pathway via death domain receptors	15	2	0.14	0.00895	0.00895	TRPS1 TIMP3

GO:1904874	positive regulation of telomerase RNA localization to Cajal body	15	2	0.14	0.00895	0.00895	CCT5 CCT2
GO:0014047	glutamate secretion	45	3	0.43	0.00931	0.00931	SLC1A3 SLC38A2 NF1
GO:0010464	regulation of mesenchymal cell proliferation	33	3	0.32	0.00389	0.00956	PRRX1 LMNA ZEB1
GO:0090177	establishment of planar polarity involved in neural tube closure	15	2	0.14	0.00895	0.0096	SEC24B CTHRC1
GO:0007004	telomere maintenance via telomerase	69	5	0.67	0.00054	0.0099	XRN1 CCT5 CCT2 PTGES3 HSP90AA1
GO:0060628	regulation of ER to Golgi vesicle-mediated transport	16	2	0.15	0.01016	0.01016	SEC24B GAS1
GO:0032956	regulation of actin cytoskeleton organization	360	8	3.47	0.02383	0.01078	STMN1 PHLDB2 PDGFRA FER RHOBTB3 ELN LRP1 TAOK1

GO:0043280	positive regulation of cysteine-type endopeptidase activity involved in apoptotic process	134	4	1.29	0.04095	0.01108	CCN1 ROBO1 DDX3X HMGB1
GO:0006895	Golgi to endosome transport	17	2	0.16	0.01144	0.01144	EPS15 VPS13C
GO:0014002	astrocyte development	45	3	0.43	0.00931	0.0127	VIM LRP1 NF1
GO:0045653	negative regulation of megakaryocyte differentiation	18	2	0.17	0.01279	0.01279	H4C4 H4C3
GO:0051895	negative regulation of focal adhesion assembly	18	2	0.17	0.01279	0.01279	PHLDB2 LRP1
GO:0048146	positive regulation of fibroblast proliferation	51	3	0.49	0.0131	0.0131	DDR2 S100A6 PDGFRA
GO:0003151	outflow tract morphogenesis	80	4	0.77	0.0075	0.01438	TGFBR3 ROBO1 SEC24B ELN
GO:003	substrate	106	4	1.02	0.01944	0.01443	NTNG1 ANTXR1

4446	adhesion-dependent cell spreading						FER FBLN1
GO:0007155	cell adhesion	1474	39	14.22	5.60E-09	0.01466	PLPP3 DDR2 CCN1 COL16A1 NTNG1 MACF1 ANTXR1 RAB10 ROBO1 RPSA PHLDB2 CLDN11 ABI3BP COL7A1 LPP PDGFRA PCDH18 MYO10 IL6ST CDH6 FER LAMA4 PTPRK DST GPNMB SVEP1 COL5A1 HSD17B12 PRKG1 LRP1 CD9 HMGB1 FLRT2 NFAT5 NF1 TGM2 PRNP FBLN1 LGALS1
GO:0071243	cellular response to arsenic-containing substance	20	2	0.19	0.01569	0.01569	DDX3X SLC38A2
GO:0006457	protein folding	230	10	2.22	8.20E-05	0.01578	QSOX1 CCT5 PPIA GANAB CCT2 PTGES3 SACS HSP90AA1 PPIB ST13
GO:0010951	negative regulation of endopeptidase	258	9	2.49	0.00092	0.01622	COL7A1 CAST DDX3X SERPINH1 ARL6IP1 TIMP2

	activity						SERPINF1 PRNP TIMP3
GO:0010955	negative regulation of protein processing	33	3	0.32	0.00389	0.01707	CAST GAS1 PRNP
GO:0042276	error-prone translesion synthesis	21	2	0.2	0.01723	0.01723	RPS27A REV3L
GO:0032355	response to estradiol	141	5	1.36	0.01192	0.01749	PTGFR TXNIP HNRNPD MAP1B PENK
GO:0035584	calcium-mediated signaling using intracellular calcium source	22	2	0.21	0.01884	0.01884	PTGFR PRNP
GO:0010632	regulation of epithelial cell migration	301	6	2.9	0.07198	0.01898	PLPP3 MACF1 ENPP2 HMGB1 NF1 SERPINF1
GO:0070570	regulation of neuron projection regeneration	32	2	0.31	0.03799	0.01913	PRRX1 LRP1
GO:0008366	axon ensheathment	139	3	1.34	0.15107	0.01913	CLDN11 CD9 NF1
GO:0003013	circulatory system process	576	7	5.56	0.32141	0.01915	MME AKAP12 ELN ASPH SVEP1 PRKG1 KCNMA1

GO:0042026	protein refolding	23	2	0.22	0.0205	0.0205	HSP90AA1 ST13
GO:1903077	negative regulation of protein localization to plasma membrane	23	2	0.22	0.0205	0.0205	AP2M1 LRRC15
GO:0030036	actin cytoskeleton organization	707	16	6.82	0.0014	0.02068	STMN1 CDC42BPA EHBP1 ANTXR1 PHLDB2 PDGFRA FER RHOBTB3 MARCKS ELN SDCBP TPM2 PRKG1 LRP1 NF1 TAOK1
GO:0030325	adrenal gland development	24	2	0.23	0.02223	0.02223	PDGFRA NF1
GO:0034123	positive regulation of toll-like receptor signaling pathway	24	2	0.23	0.02223	0.02223	DDX3X HMGB1
GO:0042776	mitochondrial ATP synthesis coupled proton transport	24	2	0.23	0.02223	0.02223	ATP5PD ATP5PO
GO:009	cochlea	24	2	0.23	0.02223	0.02223	CTHRC1 ZEB1

0103	morphogenesis						
GO:0046330	positive regulation of JNK cascade	138	5	1.33	0.01094	0.0235	ZEB2 SDCBP HMGB1 TNFRSF19 TAOK1
GO:0045104	intermediate filament cytoskeleton organization	50	3	0.48	0.01242	0.02382	MACF1 DST VIM
GO:0009615	response to virus	349	6	3.37	0.12239	0.02385	LYST STMN1 CCT5 DDX3X PENK TPT1
GO:0031532	actin cytoskeleton reorganization	105	4	1.01	0.01885	0.0257	CDC42BPA ANTXR1 PDGFRA FER
GO:0006309	apoptotic DNA fragmentation	26	2	0.25	0.02584	0.02584	HMGB2 HMGB1
GO:0060021	roof of mouth development	91	4	0.88	0.01168	0.02667	TGFBR3 PRRX1 PDGFRA ASPH
GO:0010811	positive regulation of cell-substrate adhesion	122	4	1.18	0.03057	0.02678	CCN1 COL16A1 ABI3BP HSD17B12
GO:0007026	negative regulation of microtubule depolymerization	27	2	0.26	0.02774	0.02774	MAP1B TAOK1
GO:003	positive	27	2	0.26	0.02774	0.02774	GPNMB DDX3X

1954	regulation of protein autophosphorylation						
GO:0006413	translational initiation	192	19	1.85	3.60E-14	0.19511765	RPL37A RPS27A RPSA RPL24 RPS12 DDX3X RPL7 RPS20 RPS6 RPL35 RPL12 RPLP2 RPL27A RPLP0 RPLP1 RPS2 RPL13 RPS21 RPL3
GO:0006614	SRP-dependent cotranslational protein targeting to membrane	105	20	1.01	1.30E-20	0.37994737	RPL37A RPS27A RPSA RPL24 RPS12 RPL7 RPS20 RPS6 RPL35 RPL12 RPLP2 RPL27A RPLP0 RN7SL3 RN7SL1 RPLP1 RPS2 RPL13 RPS21 RPL3

Appendix B: Human Ethics Approval

Western Research

Date: 16 February 2022

To: Douglas Hamilton

Project ID: 4988

Study Title: Physical, Biological and Pharmacological Factors Influencing human oral cell physiology

Application Type: HSREB Initial Application

Review Type: Delegated

Full Board Reporting Date: 15/March/2022

Date Approval Issued: 16/Feb/2022 07:16

REB Approval Expiry Date: 16/Feb/2023

Dear Douglas Hamilton

The Western University Health Science Research Ethics Board (HSREB) has reviewed and approved the above mentioned study as described in the WREM application form, as of the HSREB Initial Approval Date noted above. This research study is to be conducted by the investigator noted above. **All other required institutional approvals and mandated training must also be obtained prior to the conduct of the study**.

Documents Approved:

Document Name	Document Type	Document Date	Document Version
Database - oral tissues	Case Report Form	18/Nov/2021	1
Oral Cell Isolation protocol	Protocol	23/Nov/2021	1
HSREB Hamilton consent Revision	Written Consent/Assent	14/Feb/2022	3

No deviations from, or changes to, the protocol or WREM application should be initiated without prior written approval of an appropriate amendment from Western HSREB , except when necessary to eliminate immediate hazard(s) to study participants or when the change(s) involves only administrative or logistical aspects of the trial.

REB members involved in the research project do not participate in the review, discussion or decision.

The Western University HSREB operates in compliance with, and is constituted in accordance with, the requirements of the TriCouncil Policy Statement: Ethical Conduct for Research Involving Humans (TCPS 2); the International Conference on Harmonisation Good Clinical Practice Consolidated Guideline (ICH GCP); Part C, Division 5 of the Food and Drug Regulations; Part 4 of the Natural Health Products Regulations; Part 3 of the Medical Devices Regulations and the provisions of the Ontario Personal Health Information Protection Act (PHIPA 2004) and its applicable regulations. The HSREB is registered with the U.S. Department of Health & Human Services under the IRB registration number IRB 00000940.

Please do not hesitate to contact us if you have any questions. Sincerely,

Ms. Nicola Geoghegan-Morphet , Ethics Officer on behalf of Dr. Philip Jones, HSREB Chair

Note: This correspondence includes an electronic signature (validation and approval via an online system that is compliant with all regulations).

Appendix C: Animal Ethics Approval

2019-142:1:

AUP Number: 2019-142
AUP Title: Molecular Mechanisms underlying palatal healing.
Yearly Renewal Date: 07/01/2022

The **annual renewal** to Animal Use Protocol (AUP) 2019-142 has been approved by the Animal Care Committee (ACC), and will be approved through to the above review date.

Please at this time review your AUP with your research team to ensure full understanding by everyone listed within this AUP.

As per your declaration within this approved AUP, you are obligated to ensure that:

1. This Animal Use Protocol is in compliance with:
    - Western's Senate MAPP 7.12 [PDF]; and
    - Applicable Animal Care Committee policies and procedures.
2. Prior to initiating any study-related activities—as per institutional OH&S policies—all individuals listed within this AUP who will be using or potentially exposed to hazardous materials will have:
    - Completed the appropriate institutional OH&S training;
    - Completed the appropriate facility-level training; and
    - Reviewed related (M)SDS Sheets.

Submitted by: Cristancho, Martha on behalf of the Animal Care Committee

Animal Care Committee Chair

Animal Care Commitee
The University of Western Ontario
London, Ontario Canada N6A 5C1
519-661-2111 x 88792
auspc@uwo.ca | ACC Website

Curriculum Vitae

Georgia Nikoloudaki

Education:

2015- present:	PhD candidate, Anatomy and Cell Biology Schulich School of Medicine and Dentistry, Western University, Canada
2019- 2020:	DSATP Endodontics Resident, Faculty of Dentistry, University of Toronto
2012-2015:	MSc in Dentistry with Clinical Specialty in Endodontics School of Dentistry, National and Kapodistrian University of Athens, Greece
2006-2011:	Bachelor's degree in Dentistry (DDS) School of Dentistry, National and Kapodistrian University of Athens, Greece

Honours and Awards:

Dean's Scholarship for Graduate Research (2015-2019)

CADR-NCOHR Student Research Award 2017, by the Canadian Association for Dental Research (CADR) and the Network for Canadian Oral Health Research (NCOHR)

Western Graduate Research Scholarship (2015-16, 2016-17, 2017-18, 2018-19)

Related Work Experience:

Jan.2021 – present: Assistant Professor (full-time tenure track), Endodontics
Schulich Dentistry, Western University, Canada

2015- 2019: Adjunct Clinical Professor in Endodontics, Dentistry 5328, Schulich Dentistry, Western University, Canada

Publications:

1. Nikoloudaki G. Functions of Matricellular Proteins in Dental Tissues and Their Emerging Roles in Orofacial Tissue Development, Maintenance, and Disease. Int. J. Mol. Sci. 2021, 22(12), 6626; https://doi.org/10.3390/ijms22126626
2. Nikoloudaki G., Snider P., Simmons O., Conway SJ, Hamilton DW. Periostin and Matrix Stiffness Combine to Regulate Myofibroblast Differentiation and Fibronectin Synthesis During Palatal Healing Matrix Biology 2020 Aug; Online ahead of print https://doi.org/10.1016/j.matbio.2020.07.002
3. Nikoloudaki G., Kreber C., Hamilton DW. Wound Healing and Fibrosis: A Contrasting Role for Periostin in Skin and the Oral Mucosa. AJP Cell Physiology 2020 May; 318(6) -https://doi.org/10.1152/ajpcell.00035.2020
4. Nikoloudaki G., Brooks S., Peidl AP., Tinney D., Hamilton DW. JNK Signaling as a Key Modulator of Soft Connective Tissue Physiology, Pathology, and Healing. International Journal of Molecular Sciences 2020 Febr; 21(3):1015 - https://doi.org/10.3390/ijms21031015
5. Kim SS., Nikoloudaki G., Michelsons S., Creber K., Hamilton DW. Fibronectin synthesis, but not α-smooth muscle expression, is regulated by periostin in gingival healing through FAK/JNK signaling. Scientific Reports 2019 Febr; 9(1):2708
6. Kim SS., Nikoloudaki G., Darling M., Rieder MJ., and Hamilton DW. Phenytoin activates smad3 phosphorylation and periostin expression in drug-induced gingival overgrowth. Histology and histopathology 2018 Jun;33(12):18015
7. Farmakis ETR., Palamidakis F., Skondra F., Nikoloudaki G., Pantazis N. Emergency care provided in a Greek Dental School: A prospective study. Int Dent J.2016 Oct;66(5):280-6.

8. Nikoloudaki G., Meliou E., Kerezoudis N.P. MTA dissolution following successful endodontic periapical surgery after 7-years recall: A unique case report. ENDO-Endodontic Practice Today, Quintessence Publishing, 2016; 10(1):35-40.
9. Nikoloudaki G., Diomataris M., Spiropoulos S., Papazoglou S. Endodontic and aesthetic management of a fused maxillary central incisor with a supernumerary tooth. ENDO-Endodontic Practice Today, Quintessence Publishing, 2015; 9(3):219-224.
10. Nikoloudaki G., Kontogiannis T.G., Kerezoudis N.P., Mastoris M. Evaluation of the root and canal morphology of maxillary permanent molars and the incidence of the second mesiobuccal root canal in Greek population using cone-beam computed tomography. Invited paper to The Open Dentistry Journal, Oro-Maxillofacial Radiology and Imaging, Special Thematic Issue, 2015; 9 (Suppl 2: M3): 267-272.
11. Nikoloudaki G., Kontogiannis T., Meliou H., Kerezoudis NP. A comparative in-vitro study of sealing ability of four different materials used in furcation perforation. Open Journal of Stomatology, 2014; 4, 402-411.

PRESENTATIONS AND POSTERS

- Nikoloudaki G., Hamilton DW (2019, July) Effect of periostin on the profibrotic phenotype of palatal fibroblasts, FASEB 2019, Lisbon, Portugal
- Nikoloudaki G., Hamilton DW (2019, June) Effect of periostin on the profibrotic phenotype of palatal fibroblasts, IADR 2019, Vancouver, BC, Canada
- Nikoloudaki G., Snider P., Simmons O, Conway SJ, Hamilton DW (2018, May) Periostin regulates a-SMA and fibronectin synthesis in palatal wound healing, CCTC 2018, Toronto, ON, Canada
- Nikoloudaki G., Snider P., Simmons O, Conway SJ, Hamilton DW (2018, March) Characterizing the Effect of Periostin Deletion on Palatal Wound Healing, AADR/CARD Annual Meeting, Florida, USA

- Nikoloudaki G., Snider P., Simmons O, Conway SJ, Hamilton DW (2017, October) Characterization of the effect of periostin deletion on palatal wound healing, Anatomy and Cell Biology Research Day, Western University, Canada
- Kim SS., Nikoloudaki G., Michelsons S., Creber K., Hamilton DW. (2016, October) Role of periostin in the regulation of gingival healing. Dental Research Day, Schulich Dentistry, Western University, London, ON, Canada